

**Gelled Polymer Systems for Permeability Modification  
in Petroleum Reservoirs**

**Final Report**

**By  
G. Paul Willhite  
Don W. Green  
John L. Thiele  
C. Stanley McCool  
Kristin B. Mertes**

**September 1991**

**Performed Under Contract No. DE-FG07-89ID12846**

**The University of Kansas  
Lawrence, Kansas**

---

**Bartlesville Project Office  
U. S. DEPARTMENT OF ENERGY  
Bartlesville, Oklahoma**



## **DISCLAIMER**

This report was prepared as an account of work sponsored by an agency of the United States Government. Neither the United States Government nor any agency thereof, nor any of their employees, makes any warranty, express or implied, or assumes any legal liability or responsibility for the accuracy, completeness, or usefulness of any information, apparatus, product, or process disclosed, or represents that its use would not infringe privately owned rights. Reference herein to any specific commercial product, process, or service by trade name, trademark, manufacturer, or otherwise does not necessarily constitute or imply its endorsement, recommendation, or favoring by the United States Government or any agency thereof. The views and opinions of authors expressed herein do not necessarily state or reflect those of the United States Government or any agency thereof.

This report has been reproduced directly from the best available copy.

Available to DOE and DOE contractors from the Office of Scientific and Technical Information, P.O. Box 62, Oak Ridge, TN 37831; prices available from (615)576-8401, FTS 626-8401.

Available to the public from the National Technical Information Service, U.S. Department of Commerce, 5285 Port Royal Rd., Springfield, VA 22161.

Gelled Polymer Systems for Permeability Modification in  
Petroleum Reservoirs

Final Report

By  
G. Paul Willhite  
Don W. Green  
John L. Thiele  
C. Stanley McCool  
Kristin B. Mertes

September 1991

Work Performed Under Contract No. DE-FG07-89ID12846

Prepared for  
U.S. Department of Energy  
Assistant Secretary for Fossil Energy

Jerry Casteel, Project Manager  
Bartlesville Project Office  
P. O. Box 1398  
Bartlesville, OK 74005

I. Aoki, Project Manager  
Idaho Operations Office  
785 DOE Place  
Idaho Falls, ID 83402

Prepared by  
The University of Kansas  
Lawrence, Kansas



## ABSTRACT

The research program described in this report was conducted to improve the performance and predictability of in situ gelation processes designed to increase volumetric sweep efficiency of fluid displacement processes. A principal objective of this research was to develop procedures for design and evaluation of permeability modification processes. Research was conducted in three broad areas: 1) Physical and Chemical Characterization of Gelling Systems, 2) In Situ Gelation and 3) Mathematical Modeling of In Situ Gelation. Gelling systems used chromium as the crosslinking agent. Polyacrylamide and polysaccharides gelling systems were studied.

Research was conducted on the chemical structure of polymer/metal ion complexes, kinetics of the reduction of Cr(VI) to Cr(III) by thiourea, kinetics of oligomerization and uptake of chromium by polyacrylamide and rheology of chromium/polysaccharide gelling systems. Studies of polymer/metal ion complexes were conducted using solutions of pure monomer, dimer and trimer forms of chromium. Gelation results suggest that the gelation of Cr(III)/polymer systems is dependent on the formation of the trimer species which can react rapidly with hydrolyzed portions of the polyacrylamide. Several chromium(III) salts and complexes were studied to design and characterize a system which could form gel with polyacrylamide in the pH range 6.0 to 8.0. A bis-ethylenediamine monomer complex was found to have satisfactory gelation properties in this pH range. A mathematical model was developed to examine the kinetics of Cr(III) oligomerization and uptake of chromium by polyacrylamide. A reaction rate model for the reduction of

chromium(VI) by thiourea in the 4.0 to 5.0 pH range was developed using experimental data from chromium reduction experiments.

Rheological studies were completed on chromium/polysaccharide gels. Under zero net shear, polysaccharide gels are formed that are significantly stiffer than similar polyacrylamide gels. The initial pH of the solution has the most significant effect on the rate of crosslinking of polysaccharide gels. Formation of permanent crosslinks in the polysaccharide system appears to be completely inhibited by shear. Crosslink formation occurs in some systems after shear is stopped.

In situ gelation experiments were conducted using a bis-ethylenediamine chromium complex and chromium(III) polyacrylamide gelling systems in sandpacks. As observed in previous in situ gelation experiments, in situ gelation occurred much earlier than gelation in beaker tests where gel solutions were maintained under conditions of no shear.

A numerical model of in situ gelation of chromium/polyacrylamide systems was developed for linear displacement in a sandpack. The numerical model is based on filtration mechanisms and is consistent with experimental data and models developed in this research program. The linear model was converted to radial coordinates and scaled to reservoir size. Critical process variables were studied with the radial model and guidelines were developed for the design of field applications.

## TABLE OF CONTENTS

	PAGE
ABSTRACT . . . . .	ii
TABLE OF CONTENTS . . . . .	iv
LIST OF TABLES . . . . .	vii
LIST OF FIGURES . . . . .	ix
CHAPTER 1	
INTRODUCTION . . . . .	1-1
1.1 Background . . . . .	1-1
1.2 Current State of Technology . . . . .	1-2
1.3 Objectives of the Research Program . . . . .	1-4
1.4 Research Requirements to Improve Process Efficiency and Predictability . . . . .	1-4
1.5 Report Format . . . . .	1-4
1.6 Project Personnel . . . . .	1-4
1.7 Publications . . . . .	1-5
CHAPTER 2	
CHEMICAL STRUCTURE OF POLYMER/METAL ION COMPLEXES . . . . .	2-1
2.1 Chemical Structure of Polymer/Metal Ion Complex . . . . .	2-1
2.5 References . . . . .	2-4
CHAPTER 3	
REDUCTION OF CHROMIUM(VI) TO CHROMIUM(III) BY THIOUREA IN THE 4.0 TO 5.0 pH RANGE . . . . .	3-1
3.1 Introduction . . . . .	3-1
3.2 Experimental Section . . . . .	3-2
3.3 Reaction Rate Model . . . . .	3-5

3.4	Conclusions . . . . .	3-14
CHAPTER 4		
	KINETICS OF Cr(III) SPECIES FORMATION AND UPTAKE BY POLYACRYLAMIDE(PAam) . . . . .	4-1
4.1	Introduction . . . . .	4-1
4.2	Model Development . . . . .	4-3
4.3	Results and Discussion . . . . .	4-9
CHAPTER 5		
	COMPLEX STUDIES . . . . .	5-1
5.1	Introduction . . . . .	5-1
5.2	Chromium Complex Studies . . . . .	5-1
5.3	PAam - Dien Monomer System . . . . .	5-2
5.4	Displacement Experiments with the Dien Complex . . . . .	5-3
5.5	Experimental Results . . . . .	5-4
5.6	Summary and Discussion of Results . . . . .	5-5
CHAPTER 6		
	RHEOLOGY OF POLYSACCHARIDE-CHROMIUM(III) GELLING SOLUTION . . . . .	6-1
6.1	Introduction . . . . .	6-1
6.2	Summary of Previous Work . . . . .	6-1
6.3	Experimental Approach . . . . .	6-2
6.4	Zero Net Shear Results . . . . .	6-3
6.5	Shear Results . . . . .	6-3
6.6	Sandpack Effluent Results . . . . .	6-4
6.7	Conclusions . . . . .	6-4

CHAPTER 7	
IN SITU GELATION OF A POLYACRYLAMIDE/Cr(III) SYSTEM IN UNCONSOLIDATED POROUS MEDIA . . . . .	7-1
7.1 Introduction and Objectives . . . . .	7-1
7.2 Experimental Program . . . . .	7-1
7.3 Results and Discussion . . . . .	7-5
7.4 Conclusions . . . . .	7-6
CHAPTER 8	
MATHEMATICAL MODELING OF IN SITU GELATION IN POROUS MEDIA . . . . .	8-1
8.1 Introduction and Objective . . . . .	8-1
8.2 Background . . . . .	8-2
8.3 Model Formulation . . . . .	8-2
8.4 Results: Simulation of Marty et al., System . . . . .	8-2
8.5 Results: Simulation of McCool's Polyacrylamide/Redox System . . . . .	8-9
8.6 Results: Simulation of Hejri's Biopolymer/Cr <sup>+3</sup> System . . . . .	8-15
8.7 Radial Modeling of In Situ Gelation . . . . .	8-30
8.8 Conclusions and Recommendations . . . . .	8-40

## LIST OF TABLES

		PAGE
2.1	Gel time and Observations for Mixtures of Metal Complexes and Polyacrylamide . . . . .	2-2
2.2	Reaction of Cr(III) with Polyacrylamide Analogs . . . . .	2-3
3.1	Reaction of Initial Reagent Concentrations . . . . .	3-17
4.1	Overall Cr(III) Oligomer Reactions in the Cr(III)-PAam Gelation System Assuming that only Cr(III) Monomer (C1), Dimer (C2) and Trimer (C3) Exist in Significant Amounts . . . . .	4-2
4.2	Rates of Gelation of Different Cr(III) Species <sup>2</sup> . . . . .	4-3
4.3	Cr(III) Species Reactions and Rate Constraints Used in Modeling Rotzinger's Cr(III) Species Data with Initial Cr(III) at .04 M and pH 4.5 . . . . .	4-7
4.4	Simulated Cr(III) Species Results for [Cr(III)] = 100 ppm, 1M NaClO <sub>4</sub> and different pH's . . . . .	4-10
4.5	The Simulated Rates of Reaction and Fractions of Total Cr(III) for Oligomers Attached and in Solution as a Function of Time for [Cr(III)] = 100 ppm, pH = 4.5 and [PAam] = 5000 ppm . . . . .	4-11
4.6	The Simulated Rates of Reactions and Fractions of Total Cr(III) for Oligomers Attached and in Solution as a Function of Time for [Cr(III)] = 100 ppm, pH = 4.0, and [PAam] = 5000 ppm . . . . .	4-12
5.1	Gel Displacement SPB . . . . .	5-6
5.2	Details of Sandpack SPB . . . . .	5-7
7.1	Gel Displacement Conditions . . . . .	7-8
8.1	Parameters used in Marty et al. Gelation Simulations . . . . .	8-48
8.2	Location and Extent of McCool's Zones of Flow Resistance . . . . .	8-48
8.3	Comparison of Simulated and Actual Zones of Flow Resistance for McCool's System . . . . .	8-48

8.4	Parameters used in Gelation Simulations . . . . .	8-49
8.5	Scaling Relationships for Chromium Species Rate Constants . . . . .	8-49
8.6	pH Trends for Chromium Oligomerization Simulations . . . . .	8-49
8.7	Essential Features of Hejri's Biopolymer Displacements . . . . .	8-50
8.8	Comparison of Parameters used in Polyacrylamide/Redox and Biopolymer/Cr <sup>+3</sup> Simulations . . . . .	8-50
8.9	Porous Media Properties for the Multiple-Layer Reservoir Simulation . . . . .	8-50

## LIST OF FIGURES

		PAGE
2.1	pH of Polyacrylamide Solutions vs. Time, Cr(III) Monomer and PAAM . . . . .	2-5
2.2	pH of Polyacrylamide Solutions vs. Time Cr(III) Dimer and PAAM . . . . .	2-6
2.3	pH of Polyacrylamide Solutions vs. Time, Cr(III) Trimer and PAAM . . . . .	2-7
3.1	Reaction Rate Versus Surface to Mass Ratio for New Pyrex Bottles and Beads . . . . .	3-18
3.2	Reaction Rate Versus Surface to Mass Ratio for New and Used Pyrex Bottles and Beads . . . . .	3-19
3.3	Three Pairs of Sets of Experimental Chromium(VI) Concentration Versus Time Data . . . . .	3-20
3.4	Three Pairs of Sets of Experimental Hydrogen Ion Concentration Versus Time Data . . . . .	3-21
3.5	Equation 7 Fit to Sample Hydrogen Ion Versus Time Data . . . . .	3-22
3.6	The Prediction of the Reaction Rate Model and Sample Chromium(VI) Versus Time Data . . . . .	3-23
3.7	The Prediction of the Reaction Rate Model and Sample Chromium(VI) Versus Time Data . . . . .	3-24
3.8	The Prediction of the Reaction Rate Model and Sample Chromium(VI) Versus Time Data . . . . .	3-25
3.9	The Contribution of Reactions A and B to the Overall Rate of a Sample Reaction . . . . .	3-26
3.10	The Concentrations of the Thiourea, Disulfide and Sulfate in a Sample Reaction Mixture . . . . .	3-27
4.1	Percent Monomer and Dimer vs. Time for an Initial [Cr(III)] = .04 M and pH = 4.5 . . . . .	4-14
4.2	Percent Trimer vs. Time for an Initial [Cr(III)] = .04 M and pH = 4.5 . . . . .	4-15

4.3	Percent Tetramer vs. Time for an Initial [Cr(III)] = .04 M and pH = 4.5 . . . . .	4-16
4.4	Percent Oligomers Larger than Tetramer vs. Time for an Initial [Cr(III)] = .04 M and pH = 4.5 . . . . .	4-17
4.5	Comparison of Cr(III) Uptake by PAam to Cr(III) Oligomerization at [Cr(III)] = .002 M, pH = 4.5 . . . . .	4-18
5.1	Viscosity - Time Plot for [Cr(en) <sub>2</sub> Cl <sub>2</sub> ] <sup>+1</sup> Gel System at 35°C . . . . .	5-8
5.2	pH - Time Plot for [Cr(en) <sub>2</sub> Cl <sub>2</sub> ] <sup>+1</sup> Gel System at 35°C . . . . .	5-9
5.3	Sandpack SPB . . . . .	5-10
5.4	Total Flow Resistance of Sandpack for Gel Displacement SPB . . . . .	5-11
5.5	Flow Resistance of Section 2 for Gel Displacement SPB . . . . .	5-11
5.6	Flow Resistance of Section 3 for Gel Displacement SPB . . . . .	5-12
5.7	Flow Resistance of Section 4 for Gel Displacement SPB . . . . .	5-12
5.8	Flow Resistance of Section 5 for Gel Displacement SPB . . . . .	5-13
5.9	Flow Resistance of Section 6 for Gel Displacement SPB . . . . .	5-13
5.10	Effluent pH for Gel Displacement SPB . . . . .	5-14
5.11	Flow Rate for Gel Displacement SPB . . . . .	5-14
5.12	Effluent Viscosity for Gel Displacement SPB . . . . .	5-15
5.13	Effluent Chromium Concentration for Gel Displacement SPB . . . . .	5-15
6.1	Rheograms of (1500 ppm filtered) Biopolymer Solutions Used in Gelation Studies . . . . .	6-7

6.2	Development of Storage Modulus at pH 6 for the Xanthan Gel Solution Using Different Polymer Batches . . . . .	6-8
6.3	Effect of Initial pH on the Development of the Storage Modulus of the Gel Solution . . . . .	6-9
6.4	Correlation of the Initial Rate of Gelation with Hydrogen Ion Concentration . . . . .	6-10
6.5	Correlation of Initial Rate of Gelation with Inverse Hydrogen Ion Concentration . . . . .	6-11
6.6	Effect of Continuous Shear on the Development of the Storage Modulus at pH 6.0 . . . . .	6-12
6.7	Development of the Storage Modulus with Time for Feed and Effluent Samples Used in Sandpack Experiments . . . . .	6-13
7.1	Gel Time Experimental Setup . . . . .	7-9
7.2	Schematic Diagram of the Apparatus for the Gel Displacement Experiments . . . . .	7-10
7.3	Rheolog Viscometer Gel Time and Ph 5000 ppm PAam (lot TV), 75 ppm Cr <sup>3+</sup> System . . . . .	7-11
7.4	Viscosity-Time Behavior for a Typical 5000 ppm PAam (lot TV), 75 ppm Cr <sup>3+</sup> System . . . . .	7-12
7.5	Gel Solution Displacement in Sandpack LSPG3-90 5000 ppm PAam (lot TV), 75 ppm Cr <sup>3+</sup> System . . . . .	7-13
7.6	Gel Solution Displacement in Sandpack LSPG4-90 5000 ppm PAam (lot TV), 75 ppm Cr <sup>3+</sup> System . . . . .	7-14
7.7	Gel Solution Displacement in Sandpack LSPG5-90 5000 ppm PAam (lot TV), 75 ppm Cr <sup>3+</sup> System . . . . .	7-15
8.1	Representative Displacement Data by Marty [see Reference 3] . . . . .	8-51
8.2	Area Under the Apparent Viscosity Profile of Marty Run #6 after 53 hours [see Reference 3] . . . . .	8-52
8.3	Area Under the Simulated Apparent Viscosity Profile of Marty Run #6 after 53 hours [see Reference 3] . . . . .	8-53

8.4	Effluent Plots from Figures 8.2 and 8.3 . . . . .	8-54
8.5	Comparison of Marty Displacement Data with Numerically Simulated In Situ Gelation Runs [see Reference 3] . . . . .	8-55
8.6A	Simulated Gelation Run (0.88 ft/day) . . . . .	8-56
8.6B	Marty Gelation Data (0.88 ft/day) [see Reference 3] . . . . .	8-57
8.7A	Simulated Gelation Run (1.37 ft/day) . . . . .	8-58
8.7B	Marty Gelation Data (1.37 ft/day) [see Reference 3] . . . . .	8-59
8.8A	Simulated Gelation Run (1.61 ft/day) . . . . .	8-60
8.8B	Marty Gelation Data (1.61 ft/day) [see Reference 3] . . . . .	8-61
8.9A	Simulated Gelation Run (2.25 ft/day) . . . . .	8-62
8.9B	Marty Gelation Data (2.25 ft/day) [see Reference 3] . . . . .	8-63
8.10A	Simulated Gelation Run (2.64 ft/day) . . . . .	8-64
8.10B	Marty Gelation Data (2.64 ft/day) [see Reference 3] . . . . .	8-65
8.11	Comparison of Simulated and Actual Polymer Effluent Data (2.64 ft/day) . . . . .	8-66
8.12	Storage Modulus Growth for Fast-Gelling Solutions Containing CatAn-160 Polyacrylamide . . . . .	8-67
8.13	Viscosity Growth for Fast-Gelling Solutions Containing CatAn-160 Polyacrylamide . . . . .	8-68
8.14	Representative Hydrogen Ion Concentration Data . . . . .	8-69
8.15	Hydrogen Ion Concentration Model for McCool Gelation Displacements [see Reference 1] . . . . .	8-70
8.16	Simulation of McCool Gelation Displacements SP7, SP8, SP10 [see Reference 1] . . . . .	8-71
8.17a	Apparent Viscosity Profiles for McCool Gel Solution Displacement SP7 [see Reference 1] . . . . .	8-72
8.17b	Apparent Viscosity Profiles for McCool Gel Solution Displacement SP8 [see Reference 1] . . . . .	8-73

8.17c	Apparent Viscosity Profiles for McCool Gel Solution Displacement SP10 [see Reference 1]	8-74
8.18	Simulated Polymer Effluent Profiles for McCool Gelation Displacements SP7, SP8 and SP10 [see Reference 1]	8-75
8.19	Cr <sup>+3</sup> Uptake Versus Time for Solutions of Biopolymer and Cr <sup>+3</sup>	8-76
8.20	Storage Modulus Evolution for 1500 ppm FLOCON 4800 and 50 ppm Cr <sup>+3</sup>	8-77
8.21	Viscosity versus Time for 1500 ppm Biopolymer and 50 ppm Cr <sup>+3</sup> Under Zero Shear	8-78
8.22	Rate of Conversion of Monomer as a Function of pH	8-79
8.23	Comparison of Rotzinger et al. Table Ia with Dimerization Model Results [see Reference 27]	8-80
8.24	Comparison of Rotzinger et al. Table Ib with Dimerization Model Results [see Reference 27]	8-81
8.25	Comparison of Stünzi et al. Table II with Dimerization Model Results [see Reference 26]	8-82
8.26	Chromium Dimerization Rate as a Function of Chromium Concentration at Different pH's	8-83
8.27	Simulated Chromium Oligomer Concentrations for Hejri's Gelling System [see Reference 4]	8-84
8.28	Storage Modulus Evolution of Biopolymer/Cr <sup>+3</sup> Solutions Under Variable Shear Rates	8-85
8.29	Spherical Approximation of a Biopolymer Molecule	8-86
8.30	Hejri's Displacement Data [see Reference 4] (Sandpack 4, V <sub>D</sub> = 1.10 ft/day)	8-87
8.31	Simulated Biopolymer Gelation Run (Sandpack 4, V <sub>D</sub> = 1.10 ft/day)	8-88
8.32	Simulated Polymer Effluent Viscosity (Sandpack 4, V <sub>D</sub> = 1.10 ft/day)	8-89
8.33	Hejri Displacement Data [see Reference 4] (Sandpack 6, V <sub>D</sub> = 2.26 ft/day)	8-90

8.34	Simulated Biopolymer Gelation Run (Sandpack 6, $V_D = 2.26$ ft/day) . . . . .	8-91
8.35	Simulated Polymer Effluent Viscosity (Sandpack 6, $V_D = 2.26$ ft/day) . . . . .	8-92
8.36	Hejri Displacement Data [see Reference 4] (Sandpack 7, $V_D = 1.38$ ft/day) . . . . .	8-93
8.37	Simulated Biopolymer Gelation Run (Sandpack 7, $V_D = 1.38$ ft/day) . . . . .	8-94
8.38	Simulated Polymer Effluent Viscosity (Sandpack 7, $V_D = 1.38$ ft/day) . . . . .	8-95
8.39	Logarithmically Distributed Grid Nodes in Radial Coordinates . . . . .	8-96
8.40	Linearly Distributed Grid Nodes in Radial Coordinates . . . . .	8-96
8.41	Comparison of Reservoir Pressures Near the Wellbore Calculated with Logarithmic and Linear Grid Spacing . . . . .	8-97
8.42	pH Trends for Simulation of Radial Reservoir Test Cases . . . . .	8-98
8.43	Simulated Gelation Run in Radial Geometry (Case 1 : pH from 4.5 to 5.7) . . . . .	8-99
8.44	Storage Modulus Growth During the Shutin Period (Case 1 : pH from 4.5 to 5.7) . . . . .	8-100
8.45	Simulated Gelation Run in Radial Geometry (Case 2 : pH from 4.5 to 6.7) . . . . .	8-101
8.46	Storage Modulus Growth During the Shutin Period (Case 2 : pH from 4.5 to 6.7) . . . . .	8-102
8.47	Simulated Gelation Run in Radial Geometry (Case 3 : pH from 4.5 to 7.7) . . . . .	8-103
8.48	Storage Modulus Growth During the Shutin Period (Case 3 : pH from 4.5 to 7.7) . . . . .	8-104
8.49	Simulated Gelation Run in Radial Geometry (Case 4 : pH from 4.5 to 7.7, 15,000 ppm Thiourea) . . . . .	8-105

8.50	Concentrations of Attached and Ionic $\text{Cr}^{+3}$ after 72 Hours : Case 4 . . . . .	8-106
8.51	Concentrations of Attached and Ionic $\text{Cr}^{+3}$ after 72 Hours : Case 2 . . . . .	8-107
8.52	Storage Modulus Growth During the Shutin Period (Case 4 : pH from 4.5 to 7.7, 15,000 ppm Thiourea) . . . . .	8-108
8.53	Simulated Gelation Run in Radial Geometry (Case 5 : pH from 5.5 to 7.7, 15,000 ppm Thiourea) . . . . .	8-109
8.54	Storage Modulus Growth During the Shutin Period (Case 5 : pH from 5.5 to 7.7, 15,000 ppm Thiourea) . . . . .	8-110
8.55	Water Injection Well in a Three-Layer Reservoir with Varying Permeability . . . . .	8-111
8.56	Simulated Displacement into a High Permeability Zone (3.5 Darcies) in Radial Geometry . . . . .	8-112
8.57	Simulated Displacement into a Medium Permeability Zone (0.35 Darcies) in Radial Geometry . . . . .	8-113
8.58	Simulated Displacement into a Low Permeability Zone (0.035 Darcies) in Radial Geometry . . . . .	8-114

## CHAPTER 1

### INTRODUCTION

#### 1.1 BACKGROUND

A major problem in waterflooding and application of enhanced oil recovery processes is low volumetric sweep efficiency resulting from channeling of injected fluids through fractures or high permeability streaks. When channeling occurs, oil in the tighter parts of a reservoir is bypassed. Several metal ion/polymer systems have been developed for improving volumetric sweep efficiency in fluid displacement processes. When properly formulated, these systems form gels in the pore structure or in fractures, reducing rock permeability. Water or other fluids injected subsequent to a gel treatment are diverted to other, tighter parts of the reservoir displacing oil that was previously unswept.

##### 1.1.1 Types of Gel Systems

Several metal ion/polymer systems have been developed for improving volumetric sweep efficiency in fluid displacement processes. Most of these systems are being field tested in injection wells to modify the injection profile, redirecting injected fluids from well swept regions of the reservoir where permeability is high, to poorly swept regions of low permeability which usually contain significant amounts of mobile oil. Systems being field-tested have gelation times of a few hours to a day or so and the treatment is usually limited to the region in the immediate vicinity of the wellbore when the gelling solution is injected into the porous matrix. In fractured reservoirs, these gelling systems can be propagated substantial distances from the wellbore. In-depth treatment of the porous matrix has not received significant field testing.

Permeability modification methods can be subdivided into three categories based on the nature of the gelling reaction and method of placement. Categories are listed below:

1. Fast Gelling Systems
2. Timed Gelling Systems
3. Slug Systems

A brief description of each approach follows.

**Fast Gelling Systems.** In fast gelling systems, the metal ion, usually Cr(III), is added directly to the polymer solution. The reaction between Cr(III) and polymer begins immediately and is completed within minutes to a day or so. Both polyacrylamides and polysaccharides react with Cr(III) over certain composition ranges to form viscous solutions and gels. Polysaccharide gels can be sheared after formation and may be pumped into a formation where they reheel when the shear ceases.

**Timed Gelling Systems.** Gelation rate can be controlled in some systems through chemical reaction. In the chrome/redox system, Cr(III) is produced by the reduction of Cr(VI) using reducing agents such as bisulfite, thiosulfate or thiourea. By selection of concentrations and pH, gelation time may be controlled from hours to months at room temperature by the kinetics of the chromium reduction process. Gelation occurs in situ and in-depth penetration is believed to be possible with long gelling times. Many polyacrylamides can be gelled with this process. The gelation rate of biopolymers can also be controlled through redox reactions.

Gelation can also be controlled by complexing the metal ion with a chelating agent such as citrate, propionate or acetate. The rate of gelation is believed to be controlled by the reaction between the polymer and the metal ion complex. Recent papers report successful field tests using chrome propionate and chrome acetate systems. Research in our current DOE program has shown that ethylenediamine and diethylene triamine complexes with Cr(III) delay gelation of polyacrylamides. Chrome citrates have been introduced on the market but there is little information about their effectiveness. It is known that partially hydrolyzed polyacrylamides react with aluminum in aluminum citrate solutions at pH values of 6-7 to form viscous solutions and rigid gels.<sup>1</sup>

**Slug Systems.** The process involves alternate injection of aluminum citrate and partially hydrolyzed polyacrylamide separated by a small water spacer. Permeability reduction occurs when the polymer and aluminum citrate solutions interact in situ. Although this process is described as a construction of a layered gel structure, recent studies suggest that permeability reduction is most likely the result of formation of a gel structure similar to those observed when aluminum citrate and polymer are mixed.

## 1.2 CURRENT STATE OF TECHNOLOGY

Metal ion crosslinking based on chromium chemistry remains the principal technology being applied in the field although other options are under development. Chromium (III) is used exclusively as the crosslinker for xanthan biopolymers. Polyacrylamide gels are created in situ by reducing Cr(VI) to Cr(III) or by the reaction of a Cr(III) complex with the polymer. The redox reaction is of interest because the gelation rate can be controlled by controlling the rate that Cr(III) is produced in the redox reaction.<sup>1</sup> Gelation times on the order of days to months at room temperature can be

obtained by selection of the redox agent and compositions. In some applications, the presence of hydrogen sulfide in the available water precludes the use of a redox system because hydrogen sulfide is a strong reducing agent. This situation led to the development of complexes such as Cr-acetate<sup>2</sup> and Cr-propionate<sup>3</sup> that are stable in the pH range typical of field brine and will gel polyacrylamide at a controlled rate in the presence of hydrogen sulfide. There is increased interest in using Cr(III) complexes, due to concerns over the toxicity of Cr(VI). There is also some interest in developing gelling systems that do not involve a metal ion. Several systems have been introduced commercially based on organic crosslinkers. One of these systems is based on the gelation of polyvinyl alcohol using glutaraldehyde<sup>4</sup>. Another system is a variant of silica gel chemistry.

Design of permeability modification treatments is done primarily by running a series of static bottle tests at reservoir temperature to determine the polymer and crosslinking ion concentrations required in order to form a stable gel. In some cases, rheological measurements during gelation and post gelation experiments are used to assess the strength of the developed gel. This is of particular interest for gels to be used to treat fractured reservoirs and production wells. If tests are done in porous media, the tests are usually done on short cores which are often dominated by end effects.

Research during the past several years has increased the general understanding of the gelation process and the behavior of gelling solutions as they flow through porous media<sup>5-8</sup>. Ranges of compositions where gels are formed have been determined for several systems as well as procedures for screening systems. The effects of key variables such as polymer and metal ion concentrations on gelation rate are known. Hydrogen ion concentration (pH) is a dominant variable in metal ion gelation processes that was not recognized in early studies. The effect of pH on the gelation of a polyacrylamide of low degree of hydrolysis has been quantified by an empirical correlation<sup>9</sup>. Studies of developed gels indicate that most gels will not be stable when they are exposed to brine after gelation. Gels either swell or synerese depending on pH and composition of the brine. The impact of this characteristic on in situ behavior is under study. It was noted earlier that gelation studies are typically done in a series of static bottle tests. However, in practice, the gelling solution experiences a widely ranging shear environment as it moves away from the injection well. Rheological measurements show that gelation is a strong function of the applied shear rate and that gel times determined in static bottle tests are not representative of the gel time of a gelling solution that has been subjected to prolonged shear<sup>10</sup>.

### 1.3 OBJECTIVES OF THE RESEARCH PROGRAM

The research program described in this report was conducted to improve the performance and predictability of in situ gelation processes designed to increase volumetric sweep efficiency of fluid displacement processes. A principal objective of the research was to develop procedures for design and evaluation of permeability modification processes by coupling results of laboratory experiments with mathematical models. Another objective was to develop gelling systems which have the potential for in-depth permeability modification. The research is a continuation of research initiated under DOE Contract AC19-85BC10843, "Investigation of the Application of Gelled Polymer Systems for Permeability Modification in Petroleum Reservoirs", October 1, 1985-September 30, 1988.<sup>10</sup>

### 1.4 RESEARCH REQUIREMENTS TO IMPROVE PROCESS EFFICIENCY AND PREDICTABILITY

Further research was needed to complete research tasks that were more difficult than anticipated as well as to investigate important problems that have been encountered during the course of our research.

### 1.5 REPORT FORMAT

The research covered in this report has a broad scope. The report has been organized into an "Introduction" plus eight chapters covering the different specific research projects. Chapters 2 - 4 and 6 are concerned with gel chemistry, kinetics of the gelation reaction and rheological characterization of gel systems. Chapters 5, 7-8 describe research related to the behavior of gel systems in porous media. Chapter 9 describes a mathematical model that has been developed to simulate the gelation process in porous media.

### 1.6 PROJECT PERSONNEL

Project personnel responsible for the research work are identified in the different chapters. There were eight faculty/professional staff involved. These were from the participating units of the University; the Department of Chemical and Petroleum Engineering, the Tertiary Oil Recovery Project (TORP) and the Department of Chemistry. In addition, several graduate students participated in conjunction with studies leading to M.S. or Ph.D. degrees. In addition Messrs. E. Clark and H. Kroeger of TORP assisted in development and maintenance of laboratory equipment and provided assistance in analytical work. Mrs. R. Sleeper and Ms. N. Davis-Lockwood provided secretarial assistance.

## 1.7 PUBLICATIONS

The following publications and presentations have resulted from this research project.

### **Presentations**

Rocha, C. A., Green, D. W., Willhite, G. P. and Michnick, M. J., "An Experimental Study of the Interactions of Aluminum Citrate Solutions and Silica Sand", SPE 18503 Presented at Society of Petroleum Engineers International Symposium On Oilfield Chemistry, February 8-10, 1989, Houston, Texas.

Marty, L., Green, D. W. and Willhite, G. P., "The Effect of Flow Rate on the In Situ Gelation of A Chrome/Redox/ Polyacrylamide System", SPE 18504, Presented at Society of Petroleum Engineers International Symposium on Oilfield Chemistry, February 8-10, 1989, Houston, Texas.

Hejri, S., Green, D.W. and Willhite, G.P., "In-Situ Gelation of a Xanthan/Cr(III) Gel System in Porous Media, SPE 19634, Presented at the SPE Annual Technical Conference and Exhibition, October 8-11, 1989.

Jousset, F., Green, D.W., Willhite, G.P., and McCool, C.S., "Effect of High Shear Rate on In Situ Gelation of a Xanthan/Cr(III) System", SPE/DOE 20213, Presented at SPE/DOE Seventh Symposium on Enhanced Oil Recovery, April 22-25, 1990, Tulsa, Oklahoma.

Todd, B.J., Willhite, G.P., and Green, D.W., "A Mathematical Model of In-Situ Gelation of Polyacrylamide by a Redox Process", SPE/DOE 20215, Presented at SPE/DOE Seventh Symposium on Enhanced Oil Recovery, April 22-25, 1990, Tulsa, Oklahoma.

### **Theses**

Dolan, Douglas M., "An Experimental Study of the Effects of pH and Shear on the Gelation of a Xanthan-Chromium(III) Solution", M. S. Thesis, University of Kansas, 1989.

Hejri, Shahabaldin, "An Experimental Investigation Into the Flow and Rheological Behavior of a Xanthan and Xanthan/Cr(III) Gel System in Porous Media", Ph.D. Dissertation, University of Kansas, 1989.

Todd, Burt, "Numerical Modeling of In Situ Gelation in Porous Media", Ph.D. Dissertation, University of Kansas, 1990.



## CHAPTER 2

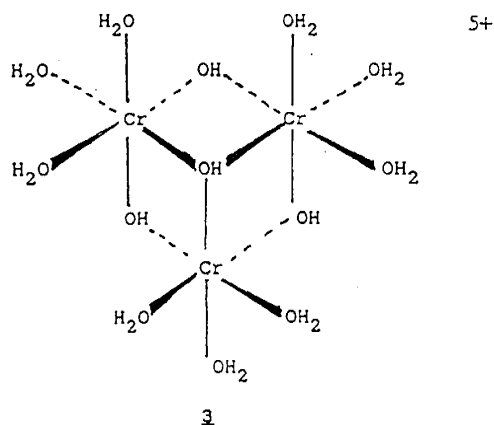
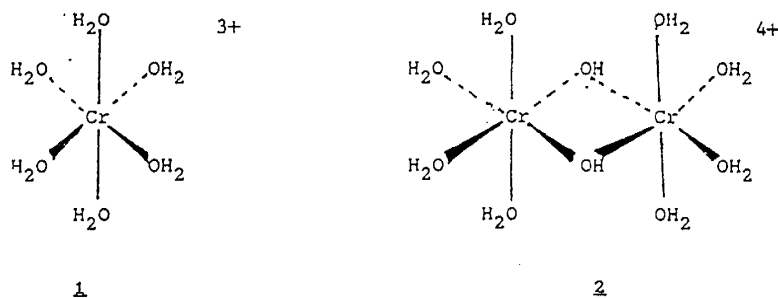
### CHEMICAL STRUCTURE OF POLYMER/METAL ION COMPLEXES

Principal Investigator: Kristin B. Mertes

Research Associate: Rongjuan Fei

This task has been involved with the investigation of the chemistry and structure of complexes formed between chromium(III) and polyacrylamide which are responsible for gelation. Aquated chromium(III) is known for its propensity to form  $\mu$ -hydroxo-bridged oligomers, and it has been proposed that these species are what is responsible for crosslinking and gelling the polyacrylamide.

Of particular relevance to this study is the work reported by Stünzi and coworkers, involving kinetic studies of the hydrolysis of chromium(III) in aqueous solution.<sup>1-4</sup> In conjunction with these studies, the Swiss group isolated in a pure form the monomeric, dimeric and trimeric chromium(III) species (1 - 3). Higher oligomers are also formed.



Solutions of pure monomer 1, dimer 2, and trimer 3 were obtained using a slightly modified procedure of the Swiss group<sup>1</sup> and were examined and compared with aqueous CrCl<sub>3</sub> with respect to gelation properties. Of particular interest are the differences in gelation times and the required concentrations for gelation among the three pure species compared to the usual aqueous CrCl<sub>3</sub> solution (Table 2.1).

TABLE 2.1

Comparison of the Gelation Tendencies of Chromium(III) Oligomers with Polyacrylamide (PAam) as a Function of Concentration (ppm) and Time (h).

Molecular Species	[Cr(III)]	[PAam]	NaCl (%)	Initial pH	Gel Time
CrCl <sub>3</sub> ·6H <sub>2</sub> O	400	5,000	2	4.5	0.4
CrCl <sub>3</sub> ·6H <sub>2</sub> O	400	10,000	4	4.4	1.7
<u>1</u>	400	5,000	2	4.5	2.5
<u>2</u>	20	5,000	2	4.4	20
<u>2</u>	10	5,000	2	4.4	22
<u>2</u>	5	5,000	2	4.4	864
<u>3</u>	20	5,000	2	4.5	0.83
<u>3</u>	10	5,000	2	4.4	3
<u>3</u>	5	5,000	2	4.4	432

Of note are the small quantities of the trimer required for gelation. Such a finding may indicate that the trimer is the species primarily responsible for the gelation, i.e. crosslinking, process.

Additional studies were performed to examine the pH dependency of the gelation process for all three species, monomer, dimer, and trimer. The results are shown in Figures 1-3. In these reactions, the initial pH of the polyacrylamide (PAam) was adjusted to the starting value shown as time = -1 days. Then the chromium solution was added. The initial pH of the chromium solution varied from 2.15 - 2.46 depending on which species was involved. The approximate gel time is marked by X on the graphs. As can be seen, the trimer gelled essentially immediately independent of the starting pH of the PAam, whereas the dimer gelled within hours at higher pH, but took days at pH 4 and below. At pH 2 the dimer did not gel. The monomer was the slowest

to gel, taking days for pH's from 5 to 9. No gelation was observed for the monomer below pH 5. Of particular interest are the gel colors. Both the monomer and dimer yielded violet gels, while that observed for the trimer was blue-green. The trimer formed very strong gels, while the monomer and dimer formed medium to strong gels.

The trimer 3 was found to be even more efficient at causing gelation than the acetate analog  $[\text{Cr}_3(\text{OH})_2(\text{CH}_3\text{COO})_6][\text{CH}_3\text{COO}] \cdot 6\text{H}_2\text{O}$ . This compound is currently being used in some oil recovery applications because it can gel at higher pH's. Nonetheless, gelation time for 40 ppm of the acetate at an initial pH of 4.5 was 8 days, compared to 50 minutes for 20 ppm of the chromium trimer at the same pH.

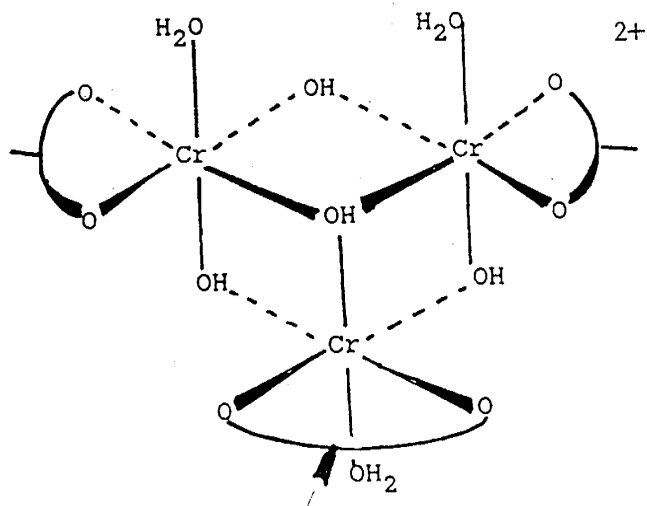
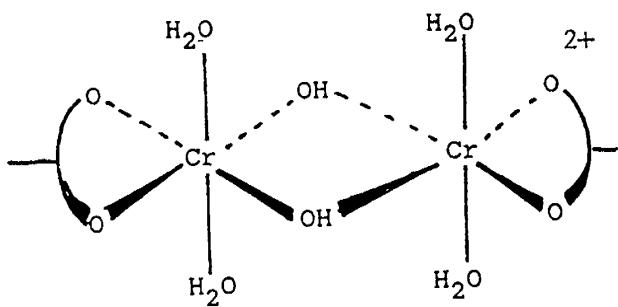
Additional studies were performed on a variety of metal ions to investigate the possibilities for other gelation species. The results are shown in Table 2.

TABLE 2.2

Gelation times as a function of pH for a variety of complexes.

Complex	[Complex] (ppm)	[PAam]	[NaCl]	gelation pH
$\text{CrCl}_6 \cdot 6\text{H}_2\text{O}$	100	5000	2%	5-8
$\text{Cr}(\text{CH}_3\text{COO})_3$	100	5000	2%	3-9
$\text{Co}(\text{en})_3\text{I}_3$	100	5000	2%	no gelation
$\text{CoCl}_2 \cdot 6\text{H}_2\text{O}$	100	5000	2%	no gelation
$\text{CuCl}_2$	100	5000	2%	slight gelation pH 7-9
$\text{FeCl}_3 \cdot 6\text{H}_2\text{O}$	100	5000	2%	immediate gelation pH 3-9

The studies performed to date indicate that the gelation process is dependent on the formation of the trimer species, which can rapidly react with the hydrolyzed carboxylate portions of the polyacrylamide. The time delay in the gelation observed for the monomer and dimer may be due to the necessity of forming trimer in sufficient concentrations to cause major crosslinking. If the trimer is responsible for gelation, it could be responsible for crosslinking three portions of the polyacrylamide polymer via chelating carboxylates, whereas the dimer would probably result in maximally two such linkages:



\* en = ethylenediamine

References:

1. Stünzi, H.; Spiccia, L.; Rotzinger, F. P.; Marty, W.; Inorg. Chem. 1989, 28, 66-71.
2. Rotzinger, F. P.; Stünzi, H.; Marty, W.; Inorg. Chem. 1986, 25, 489-495.
3. Spiccia, L.; Marty, W.; Giovanoli, R.; Inorg. Chem. 1988, 27, 2660-2666.
4. Thompson, M.; Connick, R. E.; Inorg. Chem. 1981, 20, 2279-2285.

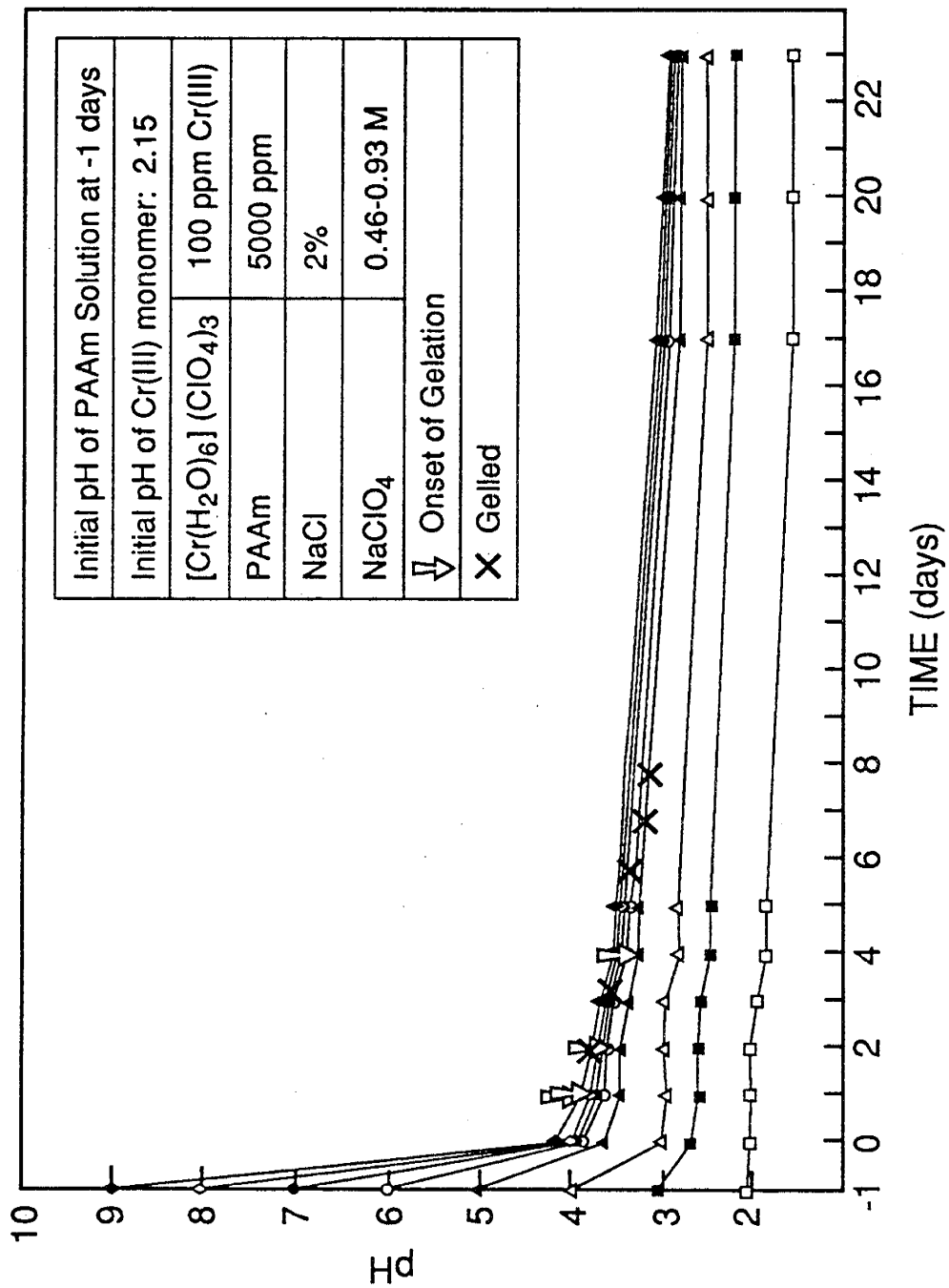


Figure 2.1. pH of Polycrylamide Solutions vs. Time, Cr(III) Monomer and PAAm

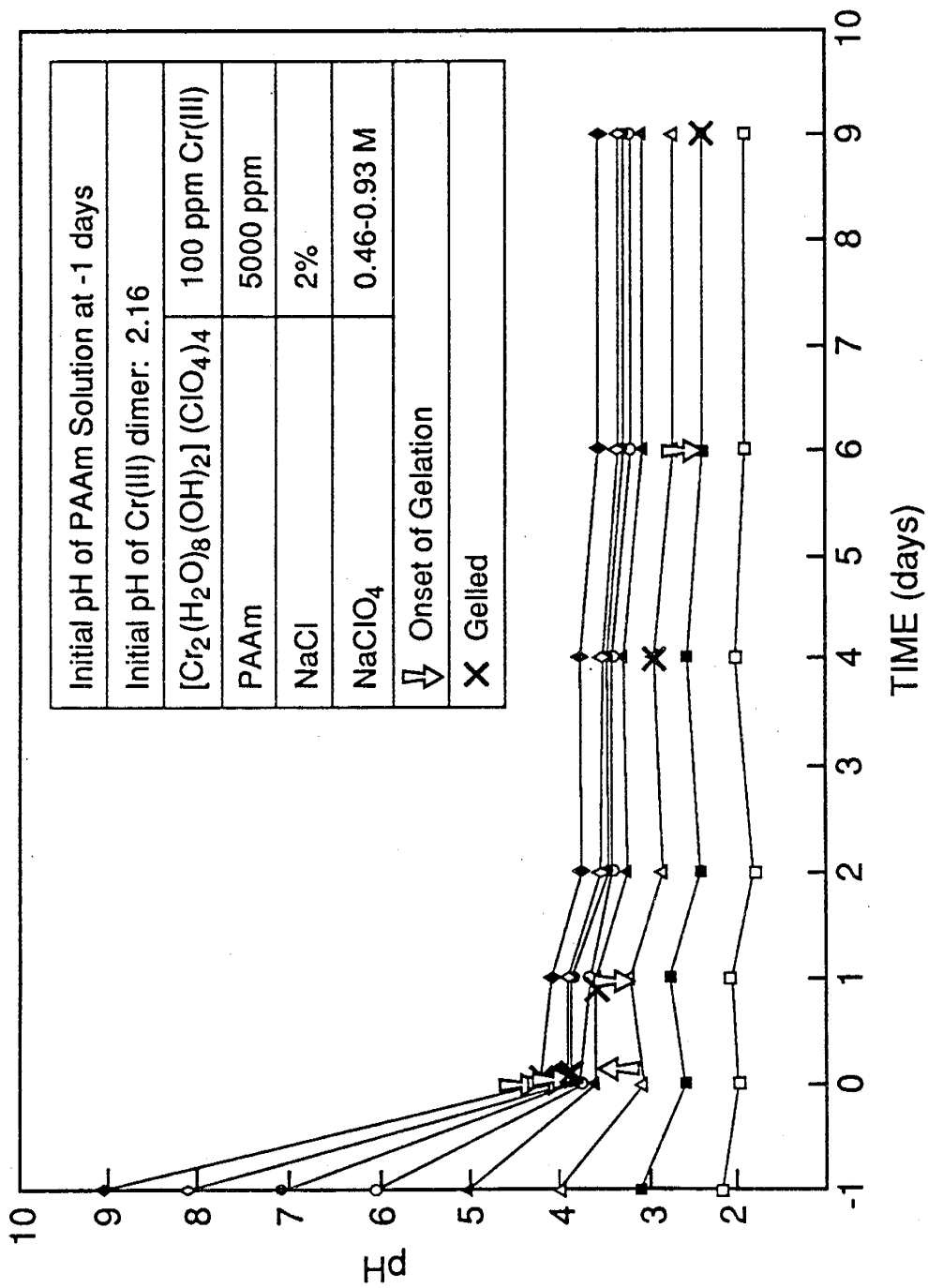


Figure 2.2. pH of Polyacrylamide Solutions vs. Time, Cr(III) Dimer and PAAm

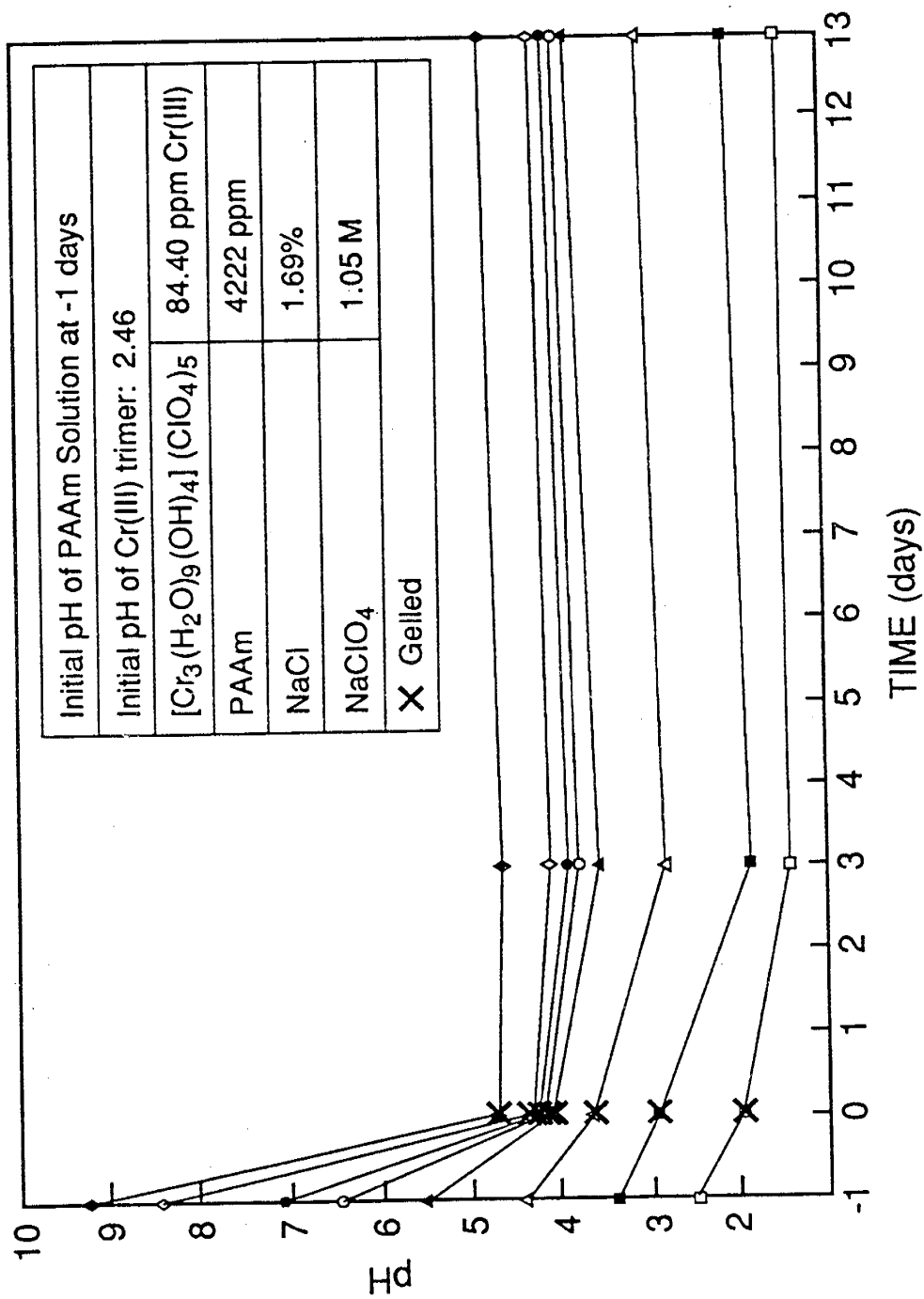


Figure 2.3. pH of Polyacrylamide Solutions vs. Time, Cr(III) Trimer and PAAm



CHAPTER 3  
REDUCTION OF CHROMIUM(VI) TO CHROMIUM(III) BY THIOUREA  
IN THE 4.0 TO 5.0 pH RANGE

Principal Investigators: G. Paul Willhite  
Don W. Green  
Kristin B. Mertes

Graduate Research Assistant: Thomas A. Maxcy

ABSTRACT

The reduction of chromium(VI) by thiourea is an important part of the chromium(VI)-thiourea-polyacrylamide gel polymer system used in enhanced oil recovery processes. Mixtures containing chromium(VI), thiourea, sodium chloride and an acetate buffer, to prevent the formation of a brown precipitate, were prepared and allowed to react at 25°C. Using previously developed analytical techniques, the chromium(VI) concentration and the hydrogen ion concentration of the reaction mixtures were determined as the reaction progressed. The reaction rate was a function of the concentrations of chromium(VI), thiourea, hydrogen ions and the acetate buffer. The reaction rate was also a function of the ratio of the surface area of the reaction container to the mass of the reaction mixture and the chemical state of the surface of the reaction container. A reaction rate model for the reduction of chromium(VI) by thiourea in the 4.0 to 5.0 pH range was developed using the experimental data and insight from the literature on the mechanisms of chromium(VI) - thiol reactions.

3.1 INTRODUCTION

A gel polymer system composed of chromium(VI), thiourea and polyacrylamide is used by the petroleum industry in enhanced oil recovery processes. This gel polymer system has been studied for a number of years at The University of Kansas and shows promise as a permeability modification process<sup>1,2</sup>. Gels are formed in the 4.0 to 5.0 pH range by a two step process. First, chromium(VI) is reduced to chromium(III) by thiourea. Second, the produced chromium(III) reacts with the carboxyl groups on the partially hydrolyzed polyacrylamide to form a crosslinked polymer gel. In order to more fully understand this gel polymer system, a reaction rate model is needed for the reduction of chromium(VI) by thiourea in the 4.0 to 5.0 pH range.

The reduction of chromium(VI) to chromium(III) has been studied by many researchers. Reviews of early work using a variety of reducing agents are available<sup>3,4</sup> as are papers on the reduction of chromium(VI) by

thiols other than thiourea<sup>5-14</sup>. Reduction of chromium(VI) by thiourea in strongly acidic solutions has been used to standardize thiourea solutions<sup>15-19</sup>. Olatunji and McAuley<sup>20</sup> studied the rate of reduction of chromium(VI) by thiourea in the 0.0 to 0.6 pH range and developed a reaction rate equation for this pH range. Kinetic studies of the reduction of chromium(VI) by thiourea in the 4.0 to 5.0 pH range have not been performed.

The objective of this work was to develop a reaction rate model for the reduction of chromium(VI) to chromium(III) by thiourea in the 4.0 to 5.0 pH range. To meet this objective, aqueous solutions containing chromium(VI) and thiourea were prepared and the chromium(VI) and hydrogen ion concentrations were measured as the reactions progressed. The experimental data along with insight into the reaction mechanisms, available from previous studies of the reduction of chromium(VI) by thiourea and other reducing agents, were used to develop the reaction rate model.

### 3.2 EXPERIMENTAL SECTION

#### 3.2.1 Chemicals and glassware

All reagents used were reagent grade and were used without further purification. Acetic acid and sodium acetate were added to each reaction mixture to prevent the formation of a brown precipitate. Formation of a brown precipitate during the course of the reduction reaction and the use of the acetic acid - sodium acetate buffer to prevent the precipitate have been described in previous reports and will be described in detail in a future dissertation<sup>21</sup>. Sodium chloride was added to each reaction mixture so the initial total ionic strength was close to 0.35 mol per kg (2.0 weight percent). Deionized water, with a resistivity of at least 10 megohm\*cm, was used to make up the reaction mixtures.

Chromium(VI) is carcinogenic and must be handled with care, plastic gloves should be used at all times when working with chromium(VI). Solutions containing chromium must be treated as hazardous waste and disposed of properly.

Wheaton Lab 45 Pyrex bottles, with an internal volume of 680 ml, were used to contain the reaction mixtures, Fisher scientific 1000 and 2000 ml Pyrex flasks were used to contain the stock solutions and Fisher 0.5 mm in diameter Pyrex beads were used to increase the glass surface area in a reaction container. All glassware was cleaned prior to use at 80 to 90°C with a cleaning solution containing 19 g of concentrated Micro cleaning solution per liter of distilled water. The following procedures were used to clean the Wheaton Pyrex bottles. One hundred grams of cleaning solution was added to two bottles, the caps were screwed onto the bottles and the bottles were shaken for 2 minutes. The bottles were

then rinsed 15 times with distilled water, rinsed once with 10 megohm cm deionized water, allowed to drain at room temperature for one minute and dried in a 70°C drying oven. Pyrex flasks and Pyrex beads were cleaned using similar procedures.

### 3.2.2 Experimental procedures and equipment.

The following procedures were used to prepare 600 g reaction mixtures. Stock solutions of chromium(VI) - sodium chloride, thiourea and acetic acid - sodium acetate were prepared. An appropriate amount, 100 to 200 g, of the chromium(VI) - sodium chloride stock solution was added to a clean Wheaton bottle and, 50 to 200 g, of the thiourea stock solution, the acetic acid - sodium acetate stock solution and deionized water were added to a second clean Wheaton bottle. Both bottles were then placed in a 25°C constant temperature water bath and left overnight to insure that the solution temperature was 25°C. On the following day the combination of stock solutions in the second bottle was poured into the bottle that contained the chromium(VI) - sodium chloride stock solution which became the container for the reaction mixture. The bottle containing the reaction mixture was capped, shaken for 30 seconds and returned to the constant temperature water bath.

The chromium(VI) concentration of the reaction mixture was determined four times during the course of each reaction. The visible absorbance of a sample of the reaction mixture was measured on a Ciba Corning Diagnostics Corporation, Gilford Response II spectrophotometer. Pairs of 2 and 10 mm path length quartz cuvetts were used with the path length for a given measurement chosen so that the absorbance of the sample was between 0.18 and 0.90 absorbance units. The chromium(VI) concentration of the sample was determined from the visible absorbance of the mixture using procedures developed previously in this laboratory<sup>21</sup>. The spectroscopic analytical technique was shown to be capable of determining the chromium(VI) concentration of similar mixtures containing chromium(VI) and chromium(III) with an average error of approximately 1%.

The hydrogen ion concentration of the reaction mixture was measured ten times during the course of each reaction using a Corning, flat surface combination electrode and a Fischer Scientific, Accumet Model 910 pH meter. Between measurements the electrode was rinsed in distilled water and after each days work the electrode was rinsed in distilled water, Micro cleaning solution, 0.1 molar hydrochloric acid and pH 7.0 buffer solution. The hydrogen ion concentration data, when expressed as pH, were normally distributed with a standard deviation of 0.012 pH units which is consistent with the data scatter observed by Silva<sup>22</sup> during the measurement of sodium cations with a sodium selective electrode.

### 3.2.3 Increased reaction rate due to the surface area of the reaction container.

The reaction rate was a function of the concentrations of chromium(VI), thiourea, hydrogen ions, and the acetate buffer. It was also found to depend on two variables previously thought to be unimportant. First, the reaction rate was a function of the ratio of the surface area of the reaction container to the mass of the reaction mixture. For example, the reaction rate increased when inert material such as Pyrex beads and Teflon chips was added to the reaction mixture. Second, the reaction rate was a function of the chemical state of the surface of the reaction container. For example, the reaction rate was higher in bottles used previously to contain a reduction reaction mixture than in bottles that had not been used to contain a reduction reaction. No difference in reaction rate was observed between new bottles and bottles that had been used to contain unreactive stock solutions. Various cleaning procedures were tried but, the increased reaction rate in bottles that had been previously used to contain a reaction mixture could not be eliminated.

To quantify the change in reaction rate with surface to mass ratio, the surface to mass ratio of reaction mixtures was varied by the addition of 0.5 mm in diameter Pyrex beads. Three reaction mixtures were prepared and each mixture was poured into 8 new 140 ml Pyrex bottles. The bottles contained from 0 to 30 grams of new Pyrex beads resulting in surface to mass ratios of 1.0, 2.5, 4.3 and 6.6 cm<sup>2</sup> per g. The reaction rates were found to increase linearly with surface to mass ratio, Figure 3.1. To quantify the surface chemical state effects, the beads and bottles used in experiment B were cleaned and reused in an otherwise identical experiment, experiment D Figure 3.2. As before the reaction rate increased with surface to volume ratio but, with used bottles and beads the slope of the reaction rate versus surface area line is twice as great as that observed using new bottles and beads.

The increase in the rate of reaction due to the surface of the reaction container could be important under some reaction conditions. For the present, it was decided to concentrate our efforts on the study of the bulk reaction rate. Two procedures were used to reduce the effects of the surface of the reaction container on the rate of the reduction reaction. First, the reduction reaction was contained in new bottles or in bottles that had been used to contain only unreactive mixtures of stock solutions. This eliminated the increase in reaction rate that was observed when the reaction was run in containers that had been previously used to contain a reduction reaction. Second, the mass of the reaction mixtures was large enough so that the surface to mass ratio of the reaction was 0.60 cm<sup>2</sup> per g. Based on the data presented in Figure 1, the increase in reaction rate due to the surface of the reaction container for a surface to mass ratio of 0.60 cm<sup>2</sup> per g is between 5 and 10 % of the total reaction rate.

### 3.2.4 Experimental results.

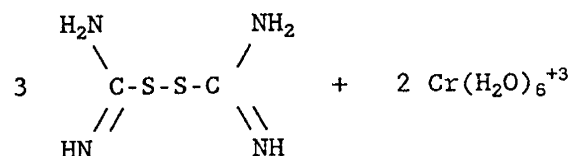
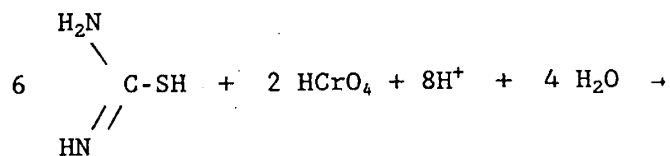
To develop a reaction rate model, chromium(VI) concentration versus time data and hydrogen ion concentration versus time data were collected from reaction mixtures with systematically varied reagent concentrations. The range of initial concentrations for each of the reagents are shown in Table 3.1. The initial chromium(VI) concentration of each reaction mixture was 0.03 mol per kg. The chromium(VI) concentration of the reaction mixtures dropped during the course of the reaction from the initial 0.03 mol per kg to from 0.025 to 0.005 mol per kg consequently, it was not necessary to vary the initial chromium(VI) concentration.

Two experiments were performed at each of twelve sets of experimental conditions to verify the reproducibility of experimental data. Chromium(VI) concentration and hydrogen ion concentrations versus time data for three of the twelve pairs of experiments are presented in this report and the remaining nine pairs of experimental data will be presented in a Ph.D. dissertation<sup>21</sup>. Chromium(VI) concentration versus time data, four data points each from three pairs of experiments, are shown in Figure 3.3. Hydrogen ion concentration versus time data, nine to eleven points each from three pairs of experiments, are shown in Figure 3.4. As can be seen from the sample results, the chromium(VI) concentration and the hydrogen ion concentration versus time data, generated using the procedures described above, are in close agreement from experiment to experiment.

A total of 318 reduction reaction experiments were performed. The initial experiments, designated data1 through data276, were performed to develop the experimental procedures. The final 40 experiments, designated data277 through data324, used the experimental procedures described above to generate sets of reproducible concentration versus time data. Sample results are presented at various points in this report and additional data will be presented in a Ph.D. dissertation<sup>21</sup>.

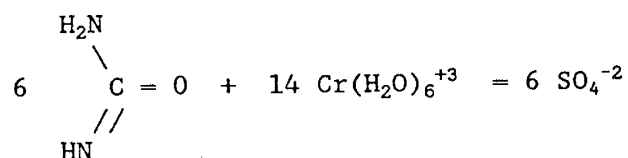
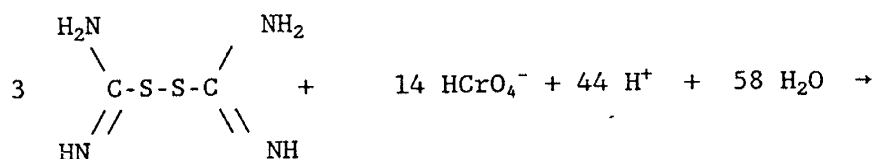
### 3.3 REACTION RATE MODEL

The oxidation of the sulfur atom in a molecule of thiourea by chromium(VI) is a two step reaction<sup>16</sup>. In the first step, the sulfur atom in thiourea is oxidized from -2 to -1 converting thiourea to a disulfide and chromium(VI) to chromium(III)<sup>9,14,18</sup>, Reaction 3-A.



(3-A)

In the second step, the two sulfur atoms in disulfide are oxidized from -1 to +6 converting the disulfide to sulfate and chromium(VI) to chromium(III)<sup>14,15</sup>, Reaction 3-B.



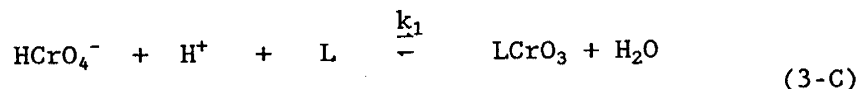
(3-B)

The overall rate of the reduction reaction is the sum of the rates of Reaction 3-A and Reaction 3-B. In the first two subsections, reaction rate equations are developed for Reactions 3-A and 3-B. In the third and fourth subsections, procedures used to determine values for the reaction rate constants are discussed. In the final subsection, chromium(VI) concentration versus time values predicted by the reaction rate model are compared to the experimental chromium(VI) concentration versus time data.

### 3.3.1 Reaction mechanism for the oxidation of thiourea to disulfide

Insight into the mechanism of Reaction 3-A is available in the literature both from studies of the reduction of chromium(VI) by thiourea<sup>20</sup> and from studies of the reduction of chromium(VI) by other

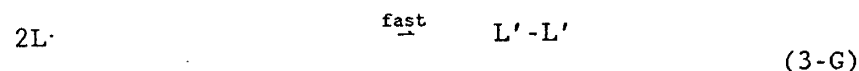
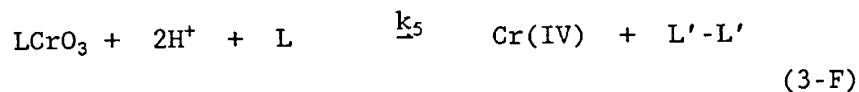
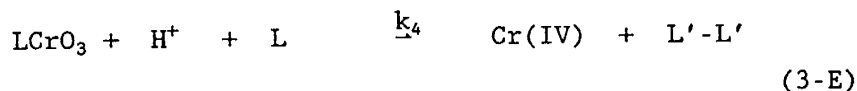
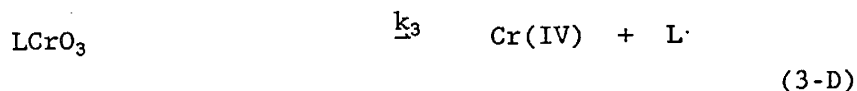
thiols<sup>5-14</sup>. The following reaction sequence for the reduction of chromium(VI) by thiourea was proposed by Olatunji and McAuley<sup>20</sup>. The first step is the reaction of the ligand L (thiourea) with chromium(VI) to form a thioester.



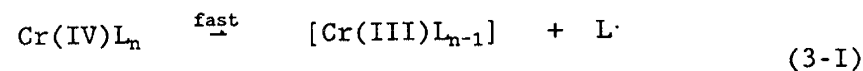
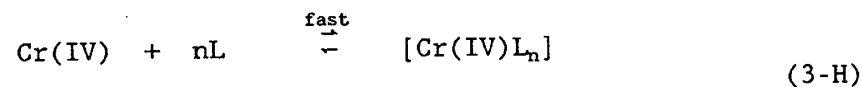
where

L = thiourea

The following steps provide three pathways for the decomposition of the thioester (LCrO<sub>3</sub>) into chromium(IV).

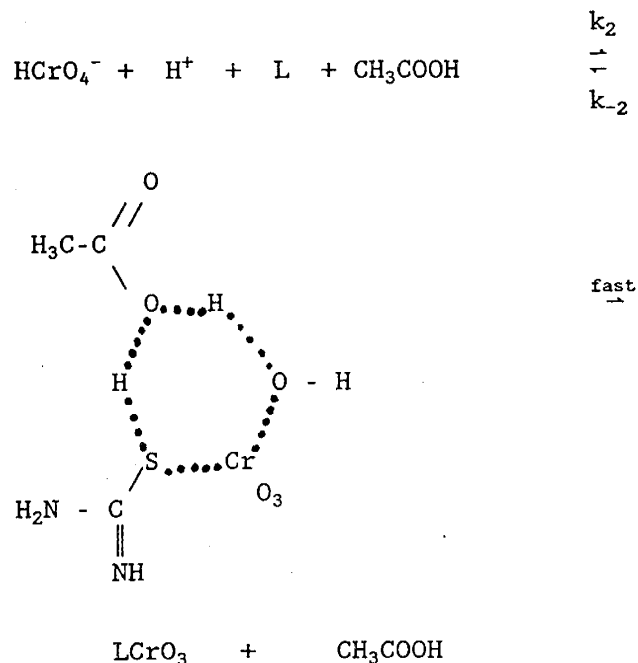


The final steps of the reaction sequence are the reaction of chromium(IV) with thiourea to form chromium(III).



The acetic acid - sodium acetate buffer increases the rate of the reduction reaction. We continued to use the buffer because it was the only way known to prevent a brown precipitate from forming during the

reduction reaction. The increase in reaction rate due to the buffer is believed to be due to acid catalysis during the formation of the thioester intermediate<sup>13</sup>, probably through the formation of a cyclic intermediate<sup>23</sup>, Reaction 3-K.



(3-K)

Acid catalysis during the formation of the thioester is a parallel reaction path to Reaction 3-C.

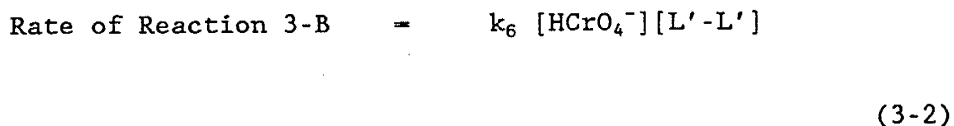
A reaction rate equation for Reaction 3-A can be derived from Reactions 3-C through 3-K, Equation 3.1.

Rate of Reaction 3-A =

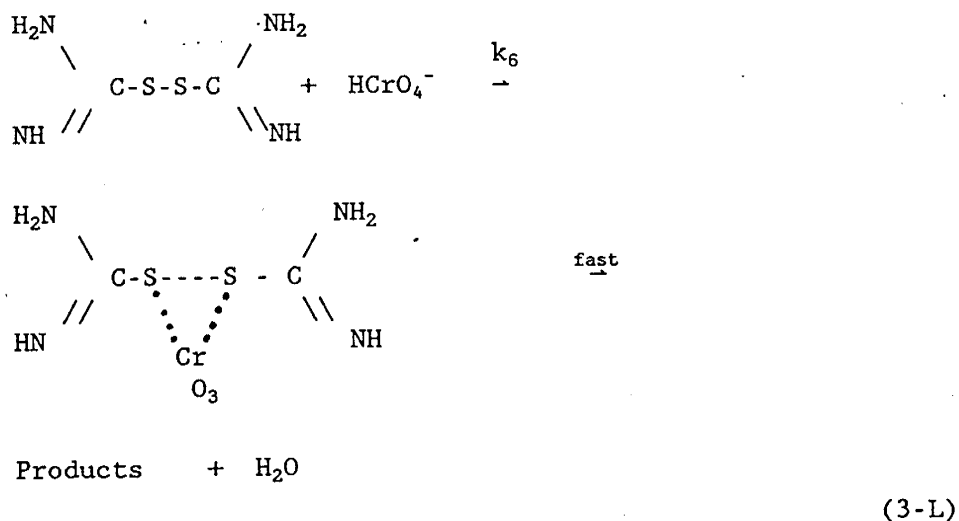
$$\frac{\frac{k_1 k_4}{(k_1 + k_3)} [\text{HCrO}_4^-] [\text{L}] [\text{L}] [\text{H}^+] [\text{H}^+] \left(1.0 + \frac{k_2 [\text{Buffer}]}{k_1}\right) \left(1.0 + \frac{k_3}{k_4 [\text{L}] [\text{H}^]} + \frac{k_5 [\text{H}^]}{k_4}\right)}{1.0 + \frac{k_1 [\text{Buffer}]}{(k_1 + k_3)} + \frac{k_4 [\text{L}] [\text{H}^]}{(k_1 + k_3)} + \frac{k_5 [\text{L}] [\text{H}^] [\text{H}^]}{(k_1 + k_3)}} \quad (3-1)$$

### 3.3.2 Reaction mechanisms for the oxidation of disulfide to sulfate.

Less is known about the mechanism of Reaction 3-B than of Reaction 3-A. For example, no reports on the rate of reduction of chromium(VI) by disulfides are available in the literature. Several reaction rate equations for Reaction 3-B, in conjunction with Equation 3-1 for Reaction 3-A, were fit to the experimental chromium(VI) concentration versus time data. The best fit of the experimental data was obtained when Equation 3-2 was used to predict the rate of Reaction 3-B.



Since Equation 3-2 gave the best fit of the reaction rate model to the experimental data we believe that the rate controlling step in the reaction of chromium(VI) with disulfide is as follows.



The disulfide chromium(VI) complex in Reaction L is reasonable because a bichromate molecule and two thiourea molecules are involved in a similar transition complex leading to the formation of the disulfide in Reaction 3-E<sup>9</sup>.

### 3.3.3 Estimation of reagent concentrations during the reaction

Some additional equations and assumptions are required in order to fit the reaction rate equations, Equations 3-1 and 3-2, to the experimental concentration versus time data. These equations and assumptions are discussed in the following paragraphs.

Three chromium(VI) species, bichromate ( $\text{HCrO}_4^-$ ), dichromate ( $\text{Cr}_2\text{O}_7^{2-}$ ) and chromate ( $\text{CrO}_4^{2-}$ ), are present in solutions containing chromium(VI) in the 3.0 to 5.5 pH range. Bichromate is the predominate species at the chromium(VI) and hydrogen ion concentrations used in this work and consequently, the reactions involving chromium(VI) were written with bichromate as the reactive species. When the reaction rate equations were fit to the experimental data, the three chromium(VI) species were assumed to be equally reactive and the bichromate concentration in Equations 3-1 and 3-2 was replaced with the total chromium(VI) concentration.

As shown in Reaction 3-M aquated chromium(III) reacts with the acetate buffer to form tris(acetato)chromium(III)<sup>24</sup>.



It was assumed that the reaction between the produced chromium(III) and the acetate buffer proceeded quickly in comparison with the reduction reaction so that all of the produced Chromium(III) was present in the reaction mixture as tris(acetato)chromium(III). This assumption is consistent with the low rate of chromium(III) production and the relatively high rate of reaction of chromium(III) with carboxyl groups. An example of the rate of reaction of chromium(III) with carboxyl groups can be found from previous work in this group on the reaction of chromium(III) with the carboxyl groups on polyacrylamide<sup>25</sup>. It was also assumed that the acetate molecules bound to the produced chromium(III) were not able to catalyze the formation of the chromium(VI) - thioester, Reaction 3-K. The concentration of acetate buffer available to catalyze the reduction reaction was found from the following equation.

$$[\text{Buffer}]_t = [\text{Buffer}]_i - 3.0([\text{Cr}(\text{VI})]_i - [\text{Cr}(\text{VI})]_t)$$

i = initial concentration  
t = concentration at time t

(3-3)

Thiourea depletion from the reaction mixtures was assumed to be due only to the oxidation of thiourea to disulfide. Under some conditions thiourea has been found to form complexes with chromium(III) offering a second mechanism for thiourea concentration reduction<sup>18</sup>. No evidence of the formation of chromium(III) - thiourea complexes was found in this study. This indicates, that under the reaction conditions used in this

study, that the value of n was 1 in Reactions 3-H and 3-I. The rate of thiourea depletion from the reaction mixtures was found from the stoichiometry of Reaction 3-A and the reaction rate of Equation 3-1, Equation 3-4.

$$\frac{d[\text{thiourea}]}{dt} = 3.0 \text{ Rate of Reaction 3-A} \quad (3-4)$$

The concentration of thiourea remaining in the reaction mixture at a given time was found by integrating Equations 3-4 and subtracting the result from the initial thiourea concentration.

The concentration of disulfide in the reaction mixture was found using a similar procedure. The rates of formation and further reaction of disulfide were found by combining the stoichiometry of Reactions 3-A and 3-B with the reaction rates predicted by Equations 3-1 and 3-2, Equation 3-5.

$$\frac{d[L'-L']}{dt} = \begin{matrix} 3/2 \text{ Rate of Reaction 3-A} \\ -3/14 \text{ Rate of Reaction 3-B} \end{matrix} \quad (3-5)$$

The concentration of disulfide remaining in the reaction mixture at a given time was found by integrating Equation 3-5.

The hydrogen ion concentration of the reaction mixtures was estimated using a correlating equation for hydrogen ion concentration versus time data developed originally by Southard<sup>26</sup>, Equation 3-6,

$$[H^+]_t = \frac{1.0}{(A + Bt)} \quad (3-6)$$

and modified by Todd<sup>27</sup>, Equation 3-7.

$$[H^+]_t = \frac{1.0}{(A + Bt^C)} \quad (3-7)$$

where A, B and C are empirical constants.

The three constants in Equation 3-7 were determined for each experiment by fitting the equation to the experimental hydrogen ion concentration versus time data. Hydrogen ion concentration values predicted by Equation 3-7 are compared to hydrogen ion concentration versus time data in Figure 3.5. Procedures are being developed to predict the hydrogen ion concentration of the reaction mixture from the stoichiometry of Reactions 3-A and 3-B and the acid - base equilibrium of the species in solution. Some progress has been made, as reported in a previous quarterly report, and it is hoped that additional progress can be made on this or an alternative approach to the prediction of hydrogen ion concentration. At this time, Equation 3-7 and the constants determined from each set of experimental data provide a more accurate estimation of the hydrogen ion concentration than the predictive methods.

### 3.3.4 Determination of reaction rate constants from experimental data.

Values of the reaction rate constants  $k_1$ ,  $k_{-1}$ ,  $k_2$ ,  $k_{-2}$ ,  $k_3$ ,  $k_4$  and  $k_5$  in Equations 3-1 cannot be determined independently but,  $k_6$  in Equation 3-2 and combinations of the rate constants in Equation 3-1 such as  $k_1k_4/(k_{-1}+k_3)$  can be determined. Equations 3-1 and 3-2 were fit to the experimental chromium(VI) versus time data to determine these values. To do this, Equations 3-1 and 3-2 were integrated numerically using a fourth order Runge-Kutta integration technique<sup>28</sup>. The concentrations of thiourea, disulfide, acetate buffer and hydrogen ions were determined using the procedures and equations discussed above. Reaction rate constants were determined using the IMSL nonlinear regression routine ZXSSQ<sup>29</sup>. A detailed description of the computational procedures used and a copy of the computer program will be included in a future Ph.D. dissertation<sup>21</sup>.

Some of the terms in Equation 3-1 did not contribute to the reaction rate models fit of the experimental data. Olatunji and McAuley found that Reaction 3-F contributed to the rate of the reduction reaction at pH levels from 0.0 to 0.6. At the pH levels in this study, 4.0 to 5.0, the contribution of Reaction 3-F compared to Reaction 3-E was reduced by four orders of magnitude. The terms due to Reaction 3-F,  $k_5[H^+]/k_4$  and  $k_5[L][H^+][H^+]/(k_{-1}+k_3)$ , in Equation 3-1 did not contribute significantly to the reaction rate at the pH levels in this study and were dropped from the reaction rate model. Reaction 3-D has been observed when chromium(VI) is reduced by some thiols but, with many thiols this reaction path does not contribute significantly to the overall reaction rate<sup>13</sup>. The term due to Reaction 3-D,  $k_3/(k_4[L][H^+])$ , in Equation 3-1 did not contribute to the fit of the reaction rate model to the experimental data and was dropped from the reaction rate model. Similarly, the term  $k_{-2}[\text{Buffer}]/(k_{-1}+k_3)$  did not contribute to the fit of the reaction rate model to the experimental data and was dropped from the model. With the above terms removed from Equation 3-1 the rate equation for Reaction 3-A is as follows.

Rate of Reaction 3-A =

$$\frac{\frac{k_1 k_4}{(k_{-1} + k_3)} [\text{HCrO}_4^-] [\text{L}] [\text{L}] [\text{H}^+] [\text{H}^+] \left(1.0 + \frac{k_2 [\text{Buffer}]}{k_1}\right)}{\left(1.0 + \frac{k_4 [\text{L}] [\text{H}^+]}{(k_{-1} + k_3)}\right)} \quad (3-8)$$

Values determined for the groups of reaction rate constants in Equation 3-8 and the rate constant in Equation 3-2 are as follows.

$$\begin{aligned} k_1 k_4 / (k_{-1} + k_3) &= 0.1750 \cdot 10^{11} \text{ kg}^4 / \text{mol}^4 \text{ hr} \\ k_2 / k_1 &= 0.1868 \cdot 10^2 \text{ kg/mol} \\ k_4 / (k_{-1} + k_3) &= 0.7184 \cdot 10^7 \text{ kg}^2 / \text{mol}^2 \\ k_6 &= 0.2149 \cdot 10^1 \text{ kg/mol hr} \end{aligned}$$

### 3.3.5 Modeling results.

The experimental concentration versus time data showed that the rate of the reduction reaction is dependent on the concentrations of chromium(VI), thiourea, hydrogen ions and the acetate buffer. Experimental reaction rates as functions of the reagent concentrations are in agreement with the mechanisms and assumptions presented in the previous subsections. Predictions of the reaction rate model are compared to sample experimental chromium(VI) concentration versus time data in Figures 3.6, 3.7, and 3.8. Predictions of the reaction rate model are compared to all of the experimental data in a future dissertation<sup>21</sup>. As can be seen from the comparison of the reaction rate model to experimental data, the fit of the model to the data is very good. The distribution of the differences between the predictions of the reaction rate model and the experimental values divided by the experimental values are normally distributed with a standard deviation of 1.56%. The small value of the standard deviation confirms that the reaction rate model fits the data well.

The contribution of Reactions 3-A and 3-B to the overall rate of the reduction reaction, as predicted by the reaction rate model, are shown in Figure 3.9. The amount of sulfur present in the reaction mixture as thiourea, disulfide and sulfate for the same reaction mixture is shown in Figure 3.10.

Partially hydrolyzed polyacrylamide contains carboxylate groups that are similar to the carboxylate groups of acetic acid and sodium acetate. We hope that when the reduction reaction is run in the presence

of polyacrylamide that the acetate groups on the polymer will contribute to the rate of the reduction reaction in the same way as the acetate groups in the acetic acid - sodium acetate buffer. This assumption will be tested by running the reduction reaction in the presence of polyacrylamide and in the presence of polyacrylamide and the acetate buffer. If the reaction rate model does not fit the data taken from solutions containing polyacrylamide, a correction term will be added to the reaction rate model to explain the reaction rate in the presence of polyacrylamide.

### 3.4 CONCLUSIONS

Experimental chromium(VI) and hydrogen ion concentration versus time data were obtained during the reduction of chromium(VI) by thiourea in the presence of an acetate buffer in the 4.0 to 5.0 pH range. The rate of the reaction depends on the concentrations of chromium(VI), thiourea, hydrogen ions, the acetate buffer and the surface area and chemical state of the reaction container. A reaction rate model was developed that fit the experimental chromium(VI) concentration versus time data.

### REFERENCES

1. Terry, R.E., Huang, C., Green, D.W., Michnick, M.J. and Willhite, G.P., "Correlation of Gelation Times for Polymer Solutions Used as Sweep Improvement Agents," Soc. Pet. Eng. J. 1981, 21, pp. 229-235.
2. McCool, C.S., "An Experimental Study of the In Situ Gelation of a Polyacrylamide/Chromium(VI)/Thiourea System in a Porous Medium," Ph.D. Dissertation, University of Kansas, Lawrence, Kansas, 1988.
3. Westheimer, F.H., "The Mechanisms of Chromic Acid Oxidations," Chem. Rev. 1949, 45, pp. 419-451.
4. Beattie, J.K. and Haight, G.P., Jr., "Chromium(VI) Oxidations of Inorganic Substances," Progr. Inorg. Chem. 1972, 17, pp. 93-145.
5. Baldea, I. and Niac, G., "The Reaction between Chromate and Thiosulfate. I. The Chromatothiosulfate Intermediate," Inorg. Chem. 1968, 7, pp. 1232-1234.
6. Edmonds, M.I., Howlett, K.E. and Wedzicha, B.L., "Kinetics and Mechanisms of Redox Reactions in Aqueous Solutions. Part III. The Reaction between Chromium(VI) and Thiosulphate," J. Chem. Soc. A: 1970, pp. 2866-2870.

7. Hojo, Y., Sugiura, Y. and Tanaka, H., "Chromium(III)-Penicillamine Complex: Some Properties and Rapid Chelation from Chromium(VI) and Penicillamine," J. Inorg. Nucl. Chem. 1977, 39, pp. 1859-1863.
8. McAuley, A. and Olatunji, M.A., "Metal-ion Oxidations in Solution. Part XVIII. Characterization, Rates, and Mechanism of Formation of the Intermediates in the Oxidation of Thiols by Chromium(VI)," Can. J. Chem. 1977, 55, pp. 3328-3334.
9. McAuley, A. and Olatunji, M.A., "Metal-ion Oxidations in Solution. Part XIX. Redox Pathways in the Oxidation of Penicillamine and Glutathione by Chromium(VI)," Can. J. Chem. 1977, 55, pp. 3335-3340.
10. McCann, J.P. and McAuley, A., "Metal Oxidations in Solution. Part XIII. The Reaction of Chromium(VI) with L-Cysteine in Perchlorate Media," J. Chem. Soc. Dalton Trans. 1975, pp. 783-790.
11. Muirhead, K.A. and Haight, G.P., Jr., "Kinetics and Mechanisms of the Oxidation of Thiocyanate Ion by Chromium(VI)," Inorg. Chem. 1973, 12, pp. 1116-1120.
12. Muirhead, K.A., Haight, G.P., Jr., Beattie, J.K., "Mechanism of Formation of Thiosulfatochromium(VI) Ion and Direct Evidence for nucleophilic Catalysis of the hydrolysis of Dichromate Ion," J. Am. Chem. Soc. 1972, 94, pp. 3006-3010.
13. Connett, P.H. and Wetterhahn, K.E., "In Vitro Reaction of the Carcinogen Chromate with Cellular Thiols and Carboxylic Acids," J. Am. Chem. Soc. 1985, 107, pp. 4282-4288.
14. Connett, P.H. and Wetterhahn, K.E., "Reaction of Chromium(VI) with Thiols: pH Dependence of Chromium(VI) Thio Ester Formation," J. Am. Chem. Soc. 1986, 108, pp. 1842-1847.
15. Cuthill, R. and Atkins, C., "The Determination of Thiourea," J. Soc. Chem Ind., London 1937, 56, pp. 5-8T.
16. Gupta, K.S., Swarup, R. and Sharma, D.N., "Oxidimetric Determination of Thiourea by Dichromate," Labdev J. Sci. Tech. 1974, 12a, pp. 84.
17. Rao, V.R.S., "Oxidation of Thiourea by Potassium Dichromate," Fresenius' Z. Anal. Chem. 1970, 249, pp. 189.
18. Singh, B. and Verma, B.C., "Thiourea and its Organic Derivatives. Part V. Oxidimetric Determination with Potassium Dichromate," Z. Anal. Chem. 1963, 196, pp. 432-433.

19. Verma, B.C., Swaminathan, K. and Kumar, S., "Thiourea as Reductimetric Standard: Standardisation of Cerium(IV), Dichromate, Bromate, Chloramine-T, and N-Bromosuccinimide Solutions," Mikrochimica Acta [Wien] 1978, II, pp. 191-196.
20. Olatunji, M.A. and McAuley, A., "Metal-ion Oxidations in Solution. Part XII. Oxidation of Thiourea and NN'-Ethylenethiourea by Chromium(VI) in Perchlorate Media," J. Chem. Soc. Dalton Trans. 1975, pp. 682-688.
21. Maxcy, T.A., Ph.D. Dissertation in progress.
22. Silva, M., "Multiphase Equilibria for a Multisolvent Electrolyte System," Ph.D. Dissertation, University of Kansas, Lawrence, Kansas, 1990.
23. Haim, A., "Acid-Catalyzed Substitution of OH<sub>-</sub> in the Hydrogen Chromate(VI) Anion by Various Ligands. Free Energy Relationships and Mechanistic Considerations," Inorg. Chem. 1972, 11, pp. 3147-3149.
24. Hamm, R.E., Johnson, R.L. and Perkins, R.H., Davis, R.E., "Complex Ions of Chromium. VIII. Mechanism of Reaction of Organic Acid Anions with Chromium(III)," J. AM. Chem. Soc. 1958, 80, pp. 4469-4471.
25. Hunt, J.A., "An Experimental Study of the Kinetics of the Crosslinking Reaction Between Chromium(III) and Polyacrylamide," Ph.D. Dissertation, University of Kansas, Lawrence, Kansas, 1987.
26. Southard, M.Z., "A Kinetic Study of the Reaction Between Chromium(VI) and Thiourea at 80°C in the Presence of Polyacrylamide," M.S. Thesis, University of Kansas, Lawrence, Kansas, 1983.
27. Todd, B.J., "Numerical Modeling of In Situ Gelation in Porous Media," Ph.D. Dissertation, University of Kansas, Lawrence, Kansas, 1990.
28. Carnahan, B., Luther, H.A. and Wilkes, J.O. Applied Numerical Methods, John Wiley & Sons, Inc. New York 1969.
29. International Mathematical and Statistical Libraries, Inc. Vol. 3, 1987

TABLE 3.1

## RANGE OF INITIAL REAGENT CONCENTRATIONS

Chromium(VI)	0.003 moles per kg 150.0 ppm
Thiourea	0.010, 0.020, 0.040 moles per kg 760, 1520, 6080 ppm
H+	0.000010, 0.000032, 0.000100 moles per kg 5.0, 4.5, 4.0 pH
Buffer	0.030, 0.050, 0.075 moles per kg 2100, 3500, 5300 ppm
NaCl	0.275 to 0.338 moles per kg 1.60 to 1.93 wt. %
Surface area of reaction container to mass of the reacting solution	0.60 cm <sup>2</sup> per gr

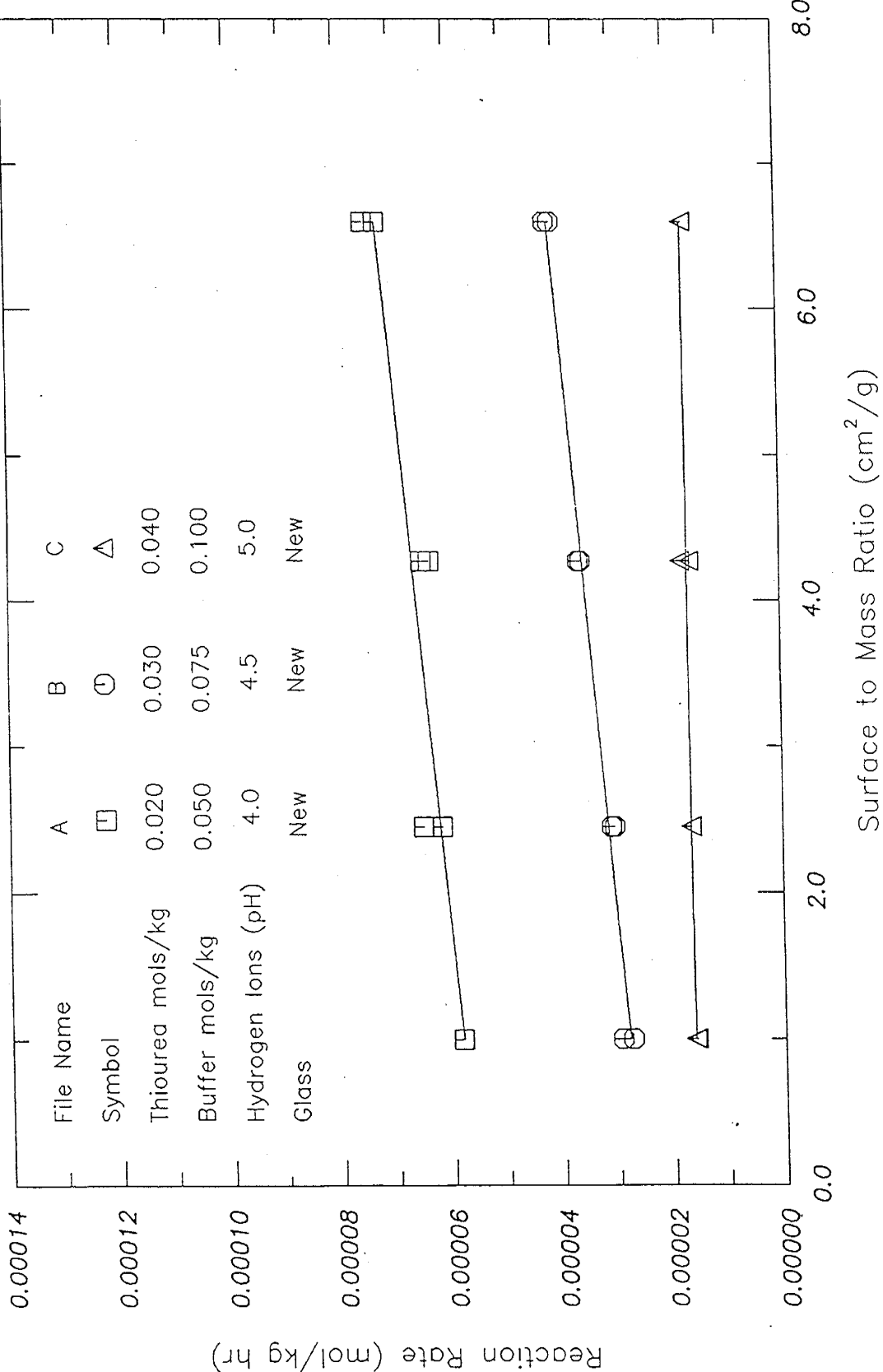


Figure 3.1 Reaction Rate Versus Surface to Mass Ratio for New Pyrex Bottles and Beads

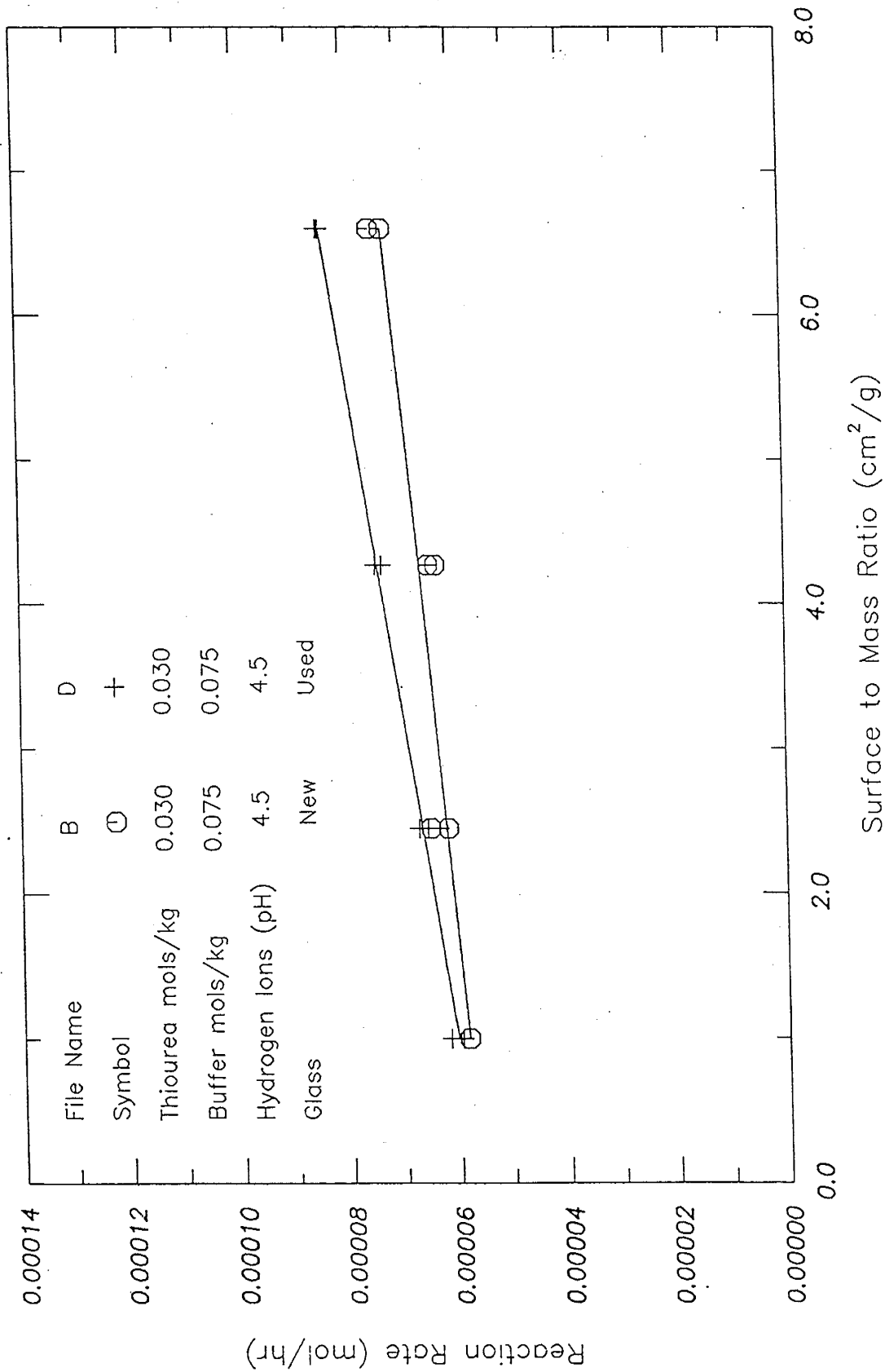


Figure 3.2 Reaction Rate Versus Surface to Mass Ratio for New and Used Pyrex Bottles and Beads.

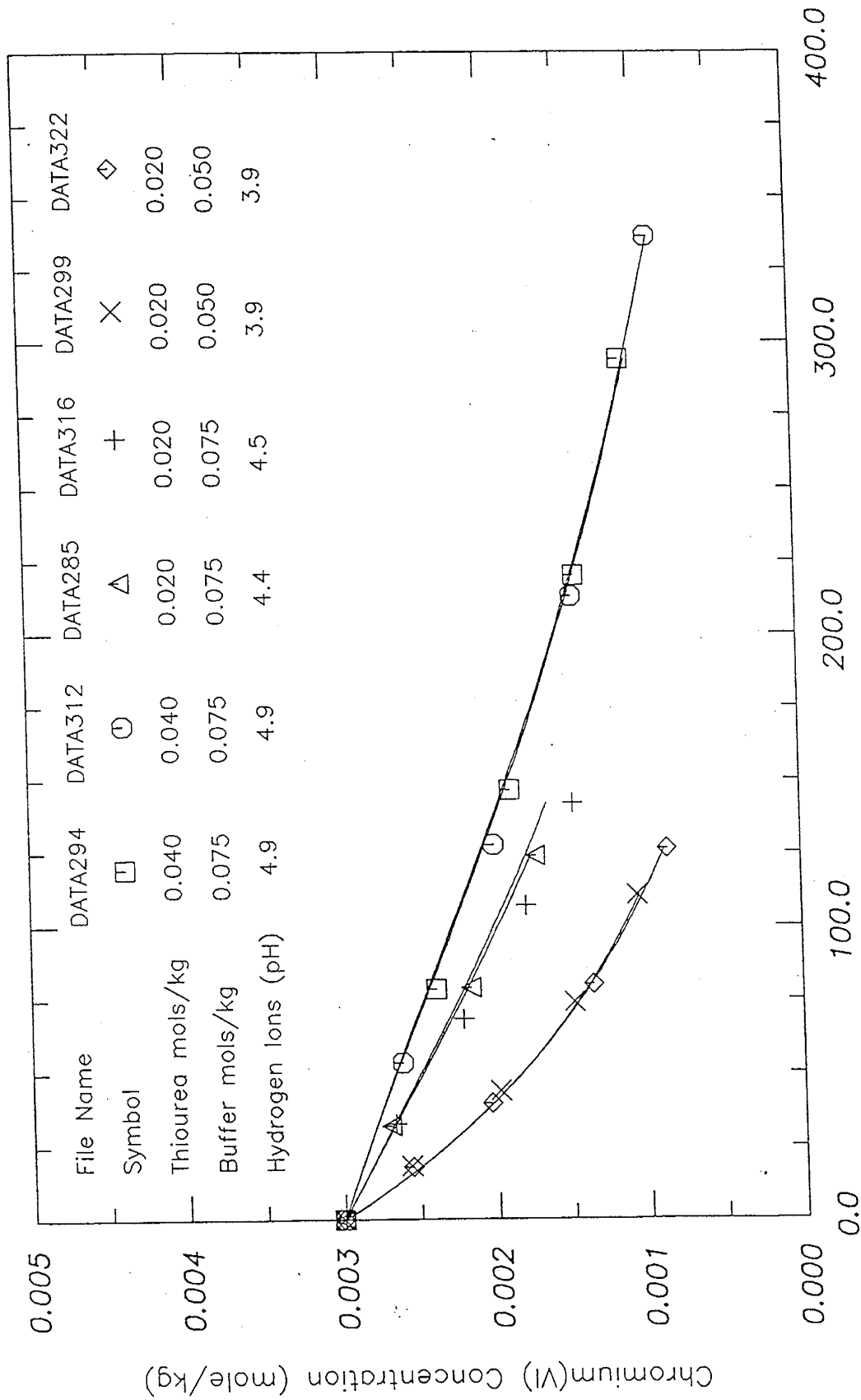


FIGURE 1.12: Sample Title

Figure 3.3 Three Pairs of Sets of Experimental Chromium(VI) Concentration Versus Time Data.

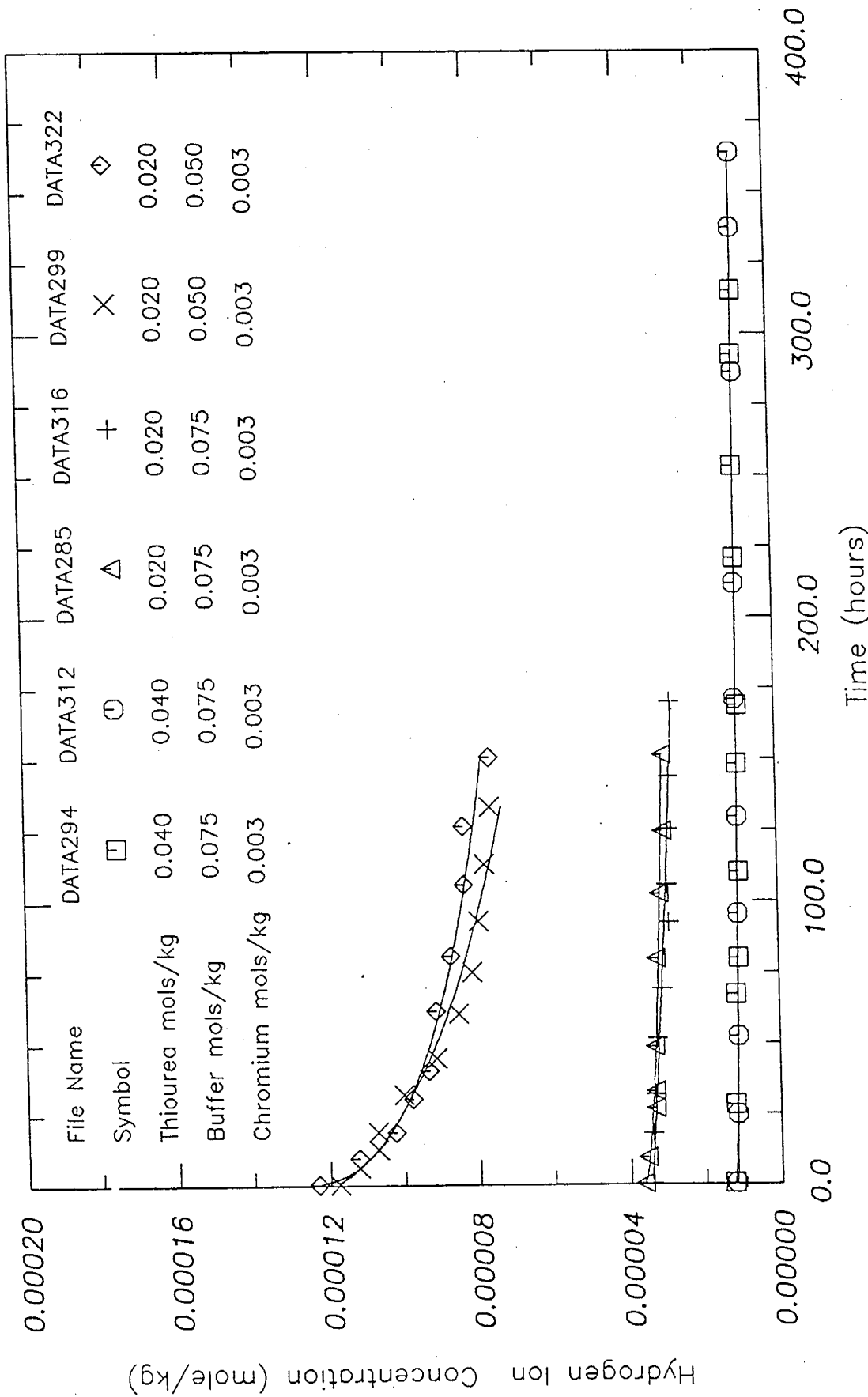
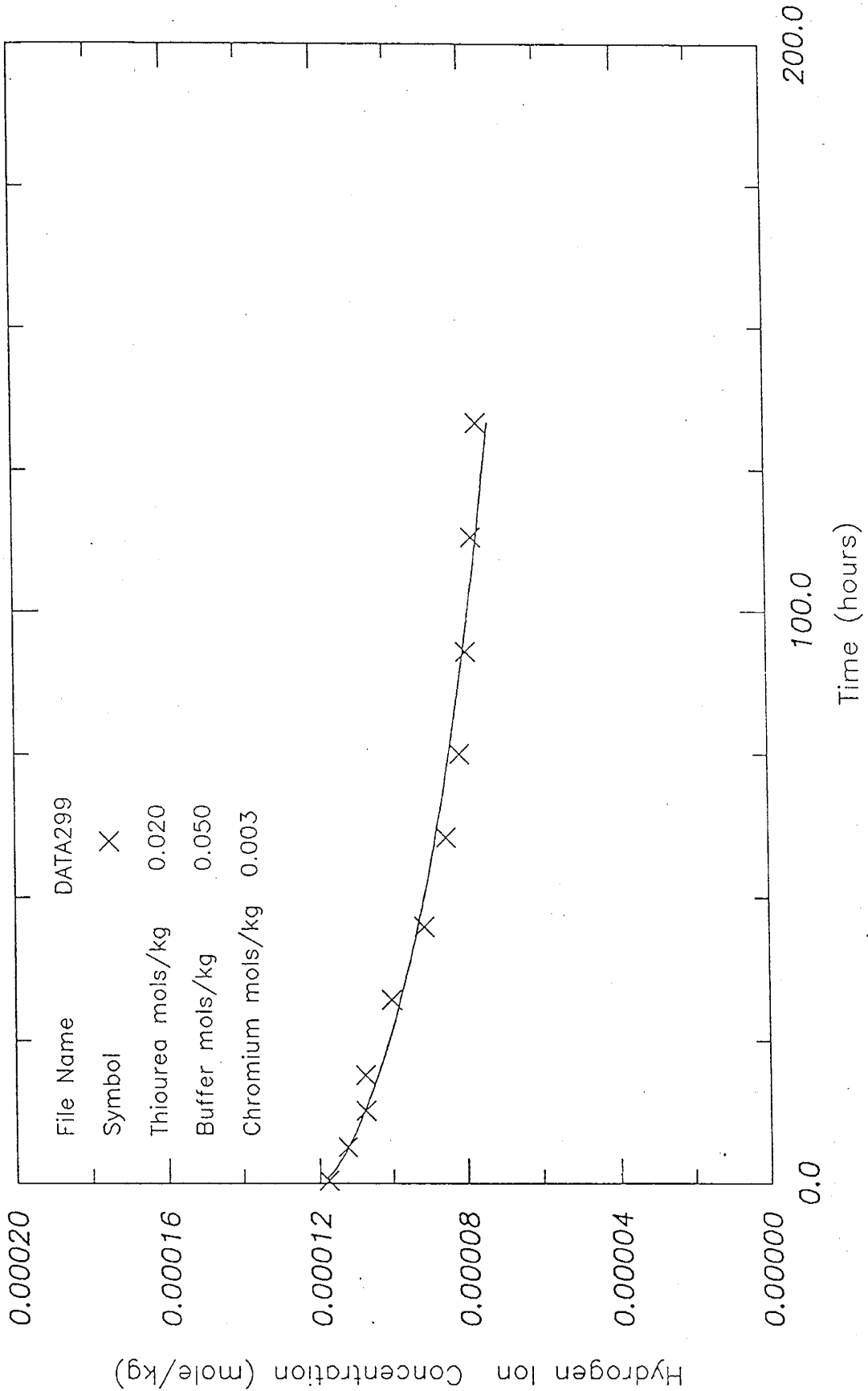


FIGURE 1.12: Sample Title

Figure 3.4 Three Pairs of Sets of Experimental Hydrogen Ion Concentration Versus Time Data.



File Name DATA299  
 Symbol X  
 Thiourea mols/kg 0.020  
 Buffer mols/kg 0.050  
 Chromium mols/kg 0.003

FIGURE 1.12: Sample Title

Figure 3.5 Equation 7 Fit to Sample Hydrogen Ion Versus Time Data.

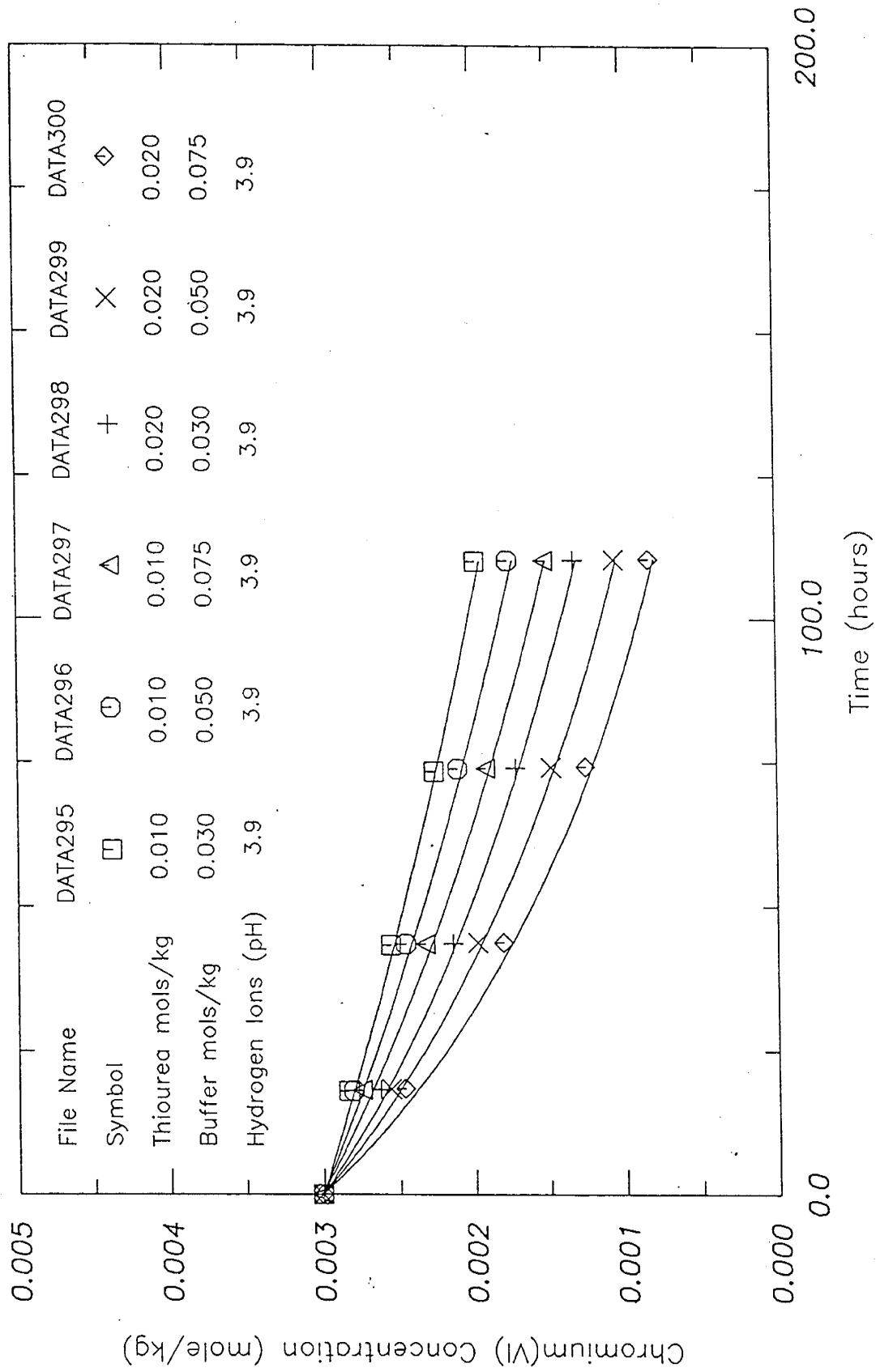


FIGURE 1.12: Sample Title

Figure 3.6 The Prediction of the Reaction Rate Model and Sample Chromium(VI) Versus Time Data.

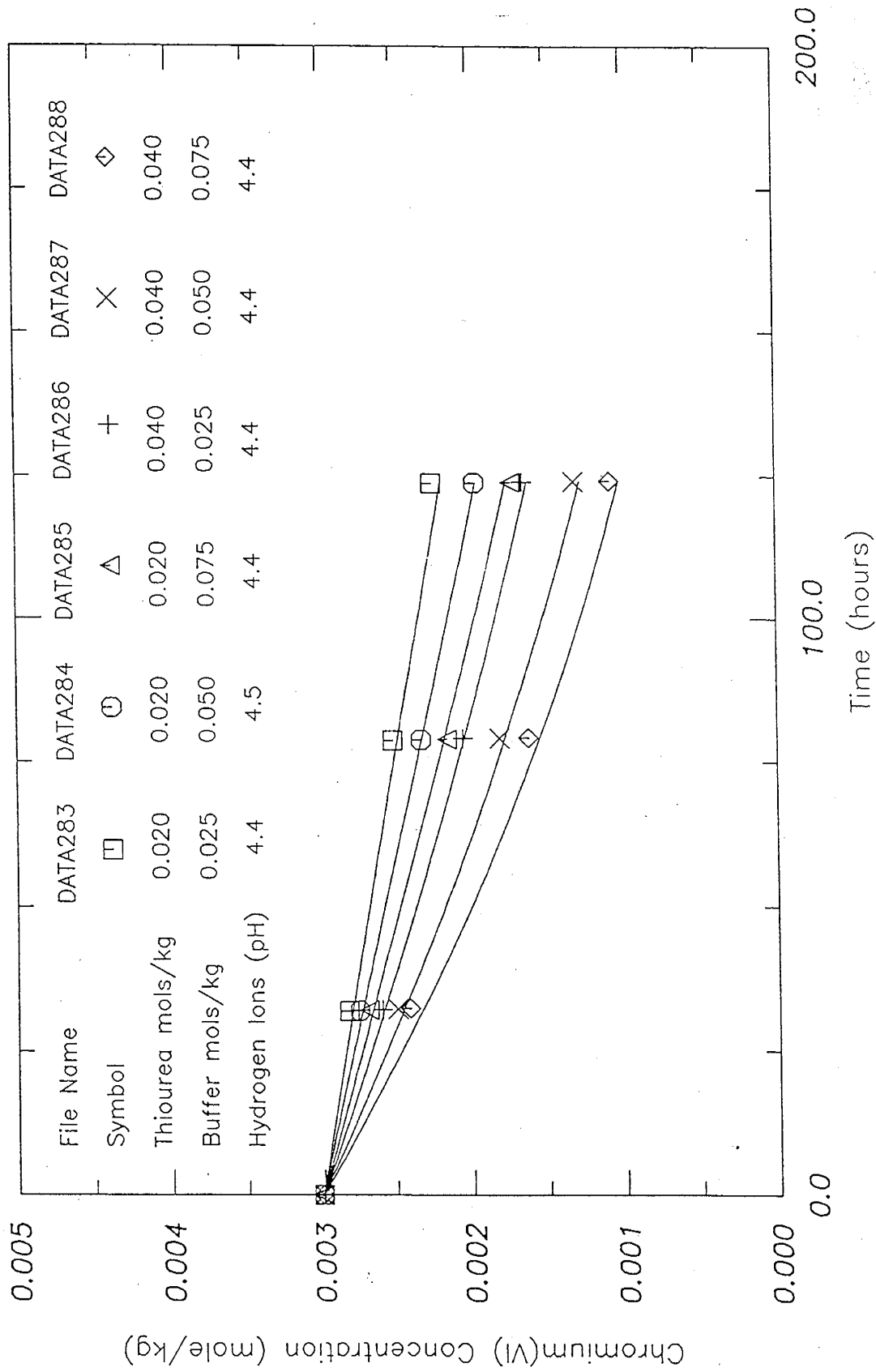


FIGURE 1.12: Sample Title

Figure 3.7 The Prediction of the Reaction Rate Model and Sample Chromium(VI) Versus Time Data.

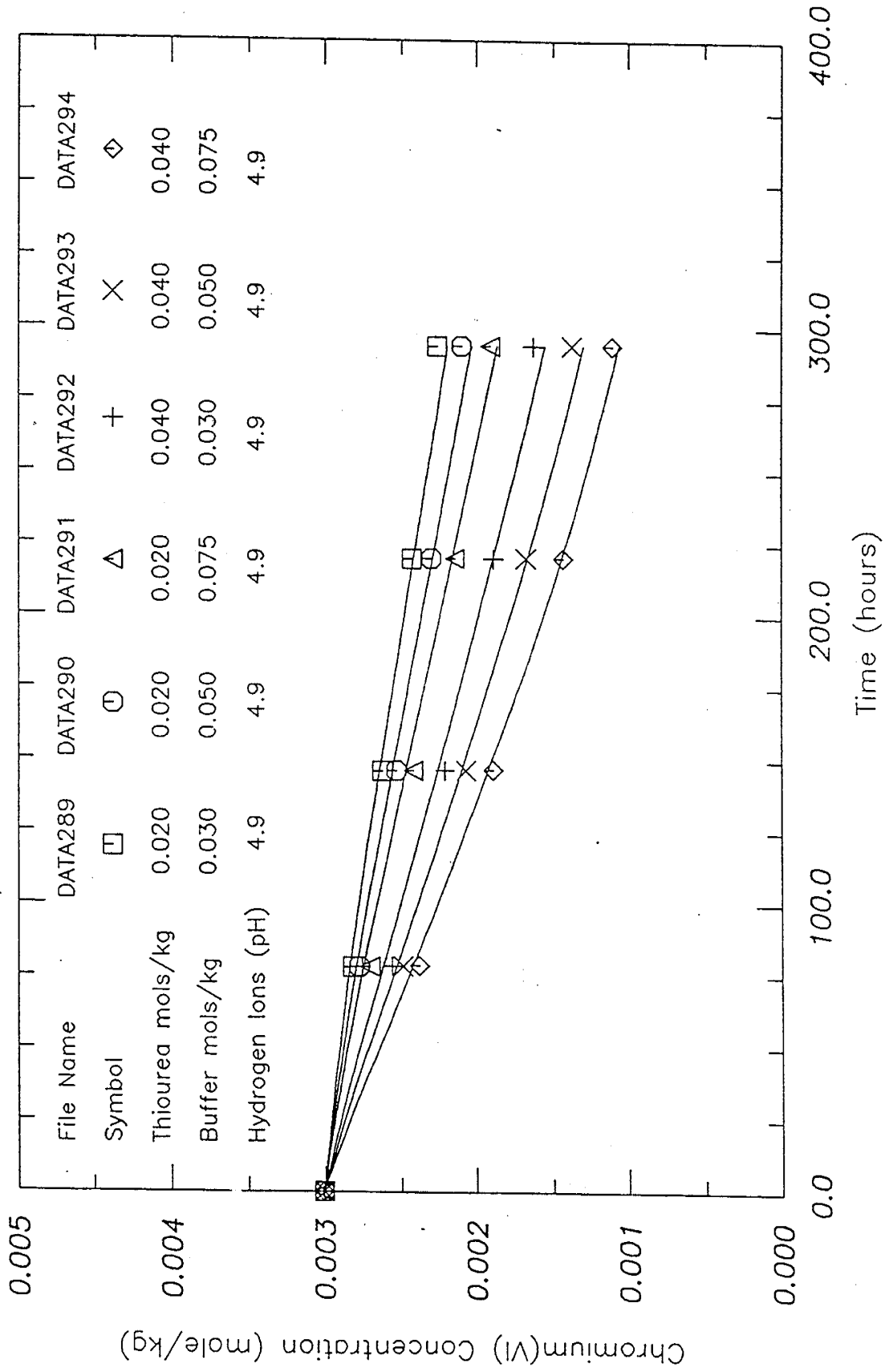


FIGURE 1.12: Sample Title

Figure 3.8 The Prediction of the Reaction Rate Model and Sample Chromium(VI) Versus Time Data.

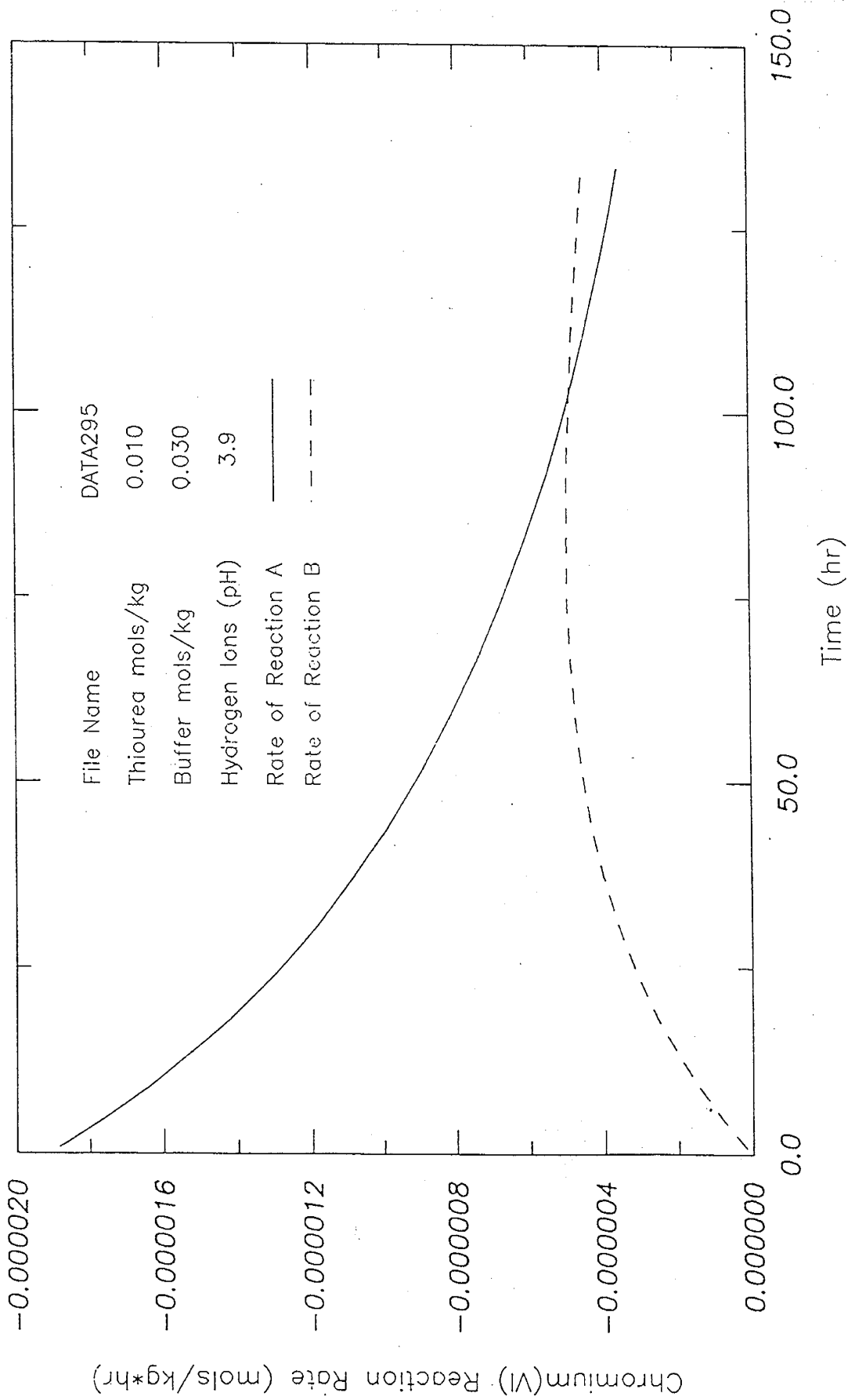


Figure 3.9 The Contribution of Reactions A and B to the Overall Rate of a Sample Reaction.

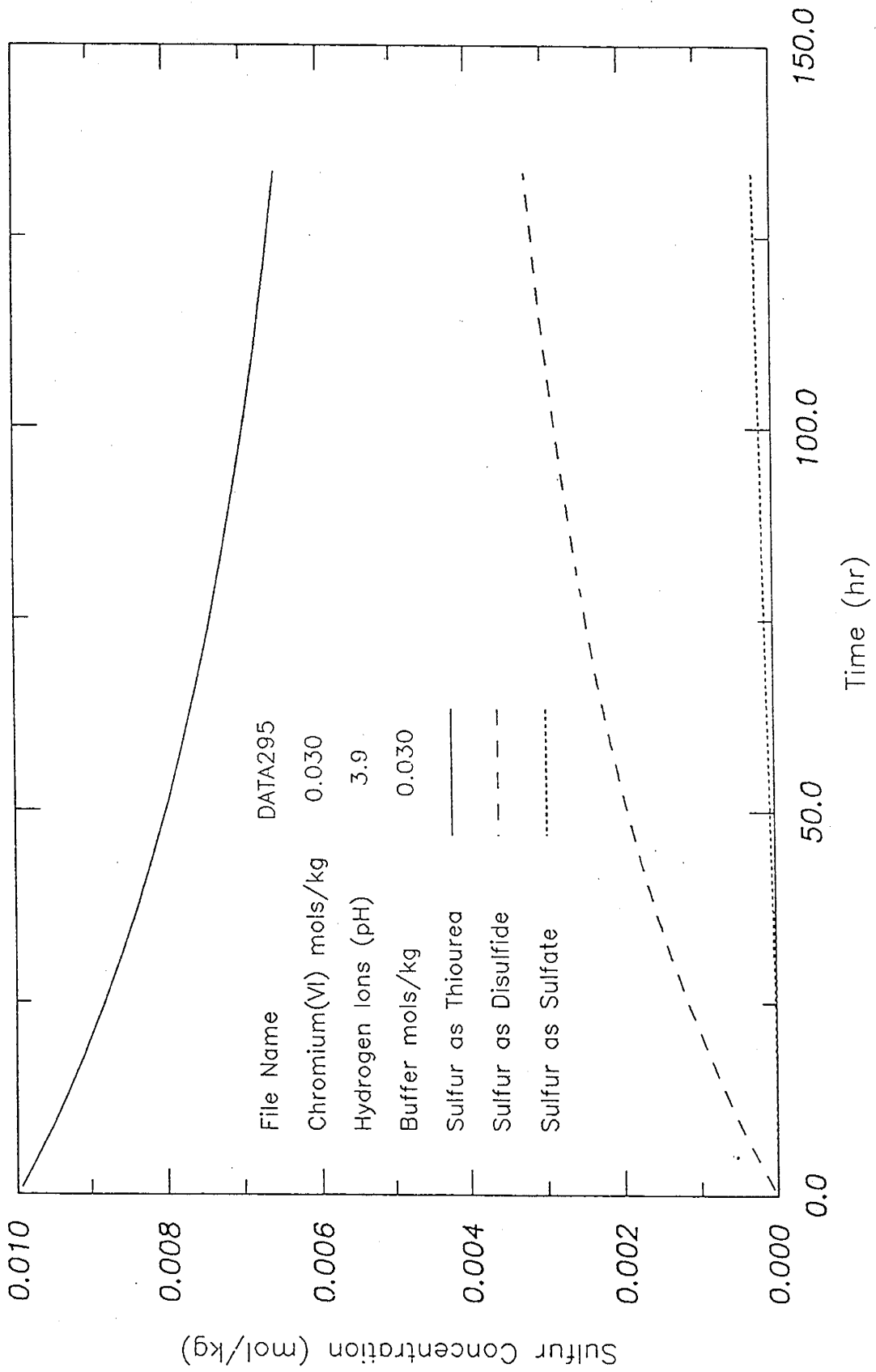


Figure 3.10 The Concentrations of the Thiourea, Disulfide and Sulfate in a Sample Reaction Mixture.



## CHAPTER 4

### KINETICS OF Cr(III) SPECIES FORMATION AND UPTAKE BY POLYACRYLAMIDE (PAam)

Principal Investigators: Don W. Green, G. Paul Willhite

Graduate Research Assistant: Carol L. G. Dona

#### 4.1 INTRODUCTION

Previous Cr(III)-PAam uptake work by Hunt<sup>1</sup> resulted in a predictive overall Cr(III) uptake rate equation,

$$\frac{d[Cr(III)]_{upt}}{dt} = \frac{k_{jh}[Cr(III)]^{1.32}}{[H^+]} \left( \frac{f[PAam] - ([Cr(III)]_o - [Cr(III)])}{f} \right)^8 \quad (4-1)$$

where  $k_{jh} = 1.7 \times 10^{-4} \text{ (hr)}^{-1} \text{ (M)}^{-1.12}$

$f$  = fraction of PAamCONH<sub>2</sub> groups which are in hydrolyzed (PAamCOOH) form.

This equation provided a good fit to the experimental data for Cr(III) concentrations ranging from 1.9- 12.0 x 10<sup>-4</sup>M (10-60 ppm), PAam concentrations from 6.9 -69 x 10<sup>-3</sup>M (500-5000 ppm) and pH values from 4.0 to 5.5\*. Development of this rate expression was based on an irreversible uptake reaction described by an equation of the form,



(4-2)

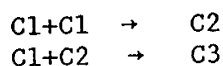
\* This experimental system used Cr(III) and PAam sources of Cr(NO<sub>3</sub>)<sub>3</sub>·9H<sub>2</sub>O and Aldrich Lot #12 non-ionic PAam. Molar concentrations of PAam represent the molar concentration of the sum of the PAamCONH<sub>2</sub> and PAamCOOH groups. The experiments were performed in 0.1M KNO<sub>3</sub>.

Further studies<sup>2,4-6</sup> have indicated that the reaction described by Equation 2 is actually a series of Cr(III)-PAam uptake and Cr(III)-Cr(III) oligomerization reactions. Assuming that the only Cr(III) oligomers which exist in solution and attached to the PAam are monomer (C1), dimer (C2), and trimer (C3), the potential reactions occurring during Cr(III) uptake by PAam are listed in Table 4.1.

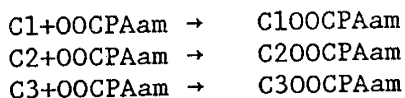
TABLE 4.1

Overall Cr(III) Oligomer Reactions in the Cr(III)-PAam Gelation System Assuming that only Cr(III) Monomer (C1), Dimer (C2) and Trimer (C3) Exist in Significant Amounts

Oligomerization in solution



Uptake of Cr(III) by PAam



Uptake of Cr(III) by attached Cr(III) (oligomerization to attached Cr(III))



Gelation by oligomerization



Gelation by secondary attachment of an attached oligomer to OOCPAam



where  $C1 \equiv Cr(H_2O)_6^{+3}$ ,  $C2 \equiv Cr_2(\mu OH)_2(H_2O)_8^{+4}$ ,  $C3 \equiv Cr_3(\mu OH)_4(H_2O)_9^{+5}$

Preliminary gelation results<sup>2</sup> have indicated that the gelation rate is very sensitive to the type of Cr(III) oligomer attached to the PAam [Table 4.2].

TABLE 4.2

Rates of Gelation of Different Cr(III) Species<sup>2</sup>

Cr(III) oligomer	Gelation time range (hrs)	pH range*	Cr(III) (ppm)	PAam (ppm)
monomer	192-48	5-9	100	5000
dimer	20-3	5-9	100	5000
trimer	immediate	5-9	84	4222

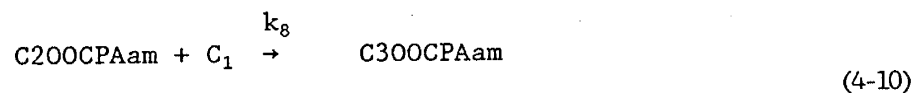
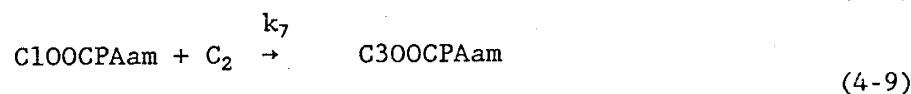
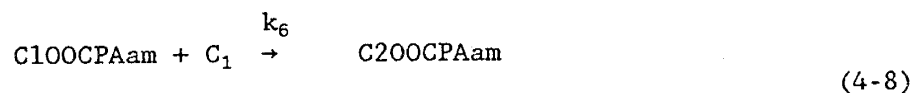
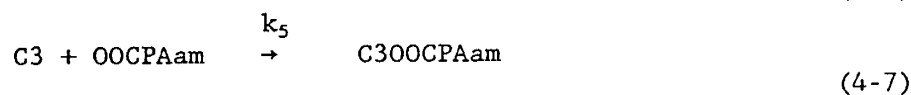
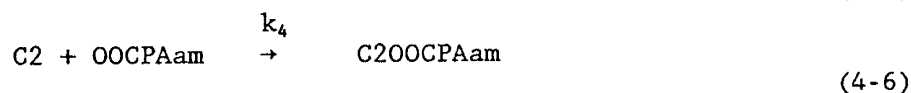
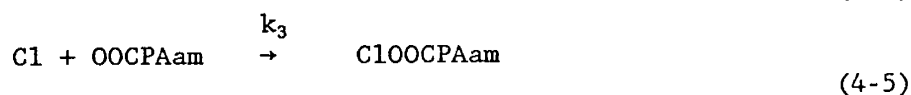
\* The pH's listed are those of the PAam solutions before mixing with the Cr(III) oligomer solutions. The final gelation solutions contained NaCl (.34 M) and NaClO<sub>4</sub> (.25-1.5M). Lot #12 Aldrich non-ionic PAam was used.

It was decided that experiments measuring the individual oligomer uptakes by PAam combined with further oligomer gelation experiments would provide more information about the roles of uptake and gelation of different oligomers in the overall gelation process. The following numerical modelling was performed to predict the rates of C2 and C3 formation in the absence of PAam and then to apply these predictions to the Cr(III) oligomerization reactions in the presence of PAam. In this way, estimates of the experimental pH, time, and concentration conditions could be obtained where the oligomer uptake due to the attachment of Cr(III) oligomers to PAamCOO(H) was isolated from the uptake reactions of Cr(III) oligomers attaching to PAam-attached Cr(III) and the oligomerization reactions of Cr(III) oligomers attaching to Cr(III) oligomers in solution.

#### 4.2 MODEL DEVELOPMENT

The gelation system which was modeled assumed that all the Cr(III) was in monomeric form initially and that, after upwards pH adjustment, the Cr(III) monomer reacted with both the PAamCOO(H) groups and with other Cr(III) molecules. Since the vigorous stirring during the proposed uptake experiments was expected to minimize gelation<sup>3</sup>, the gelation reactions were ignored. It was also assumed that with the relatively short reaction times and the relatively low Cr(III) concentrations,

formation of oligomers larger than C3 was negligible. The following reactions from Table 4.2 then remained.



The differential rate equations corresponding to Equations 4-3 through 4-10 were:

Differential rate equations - uptake

$$\begin{aligned} \frac{d [C1OOCPAam]}{dt} = & \frac{k_3 [C1]^{1_3} [OOCPAam]^{m_3}}{fn_3 [H^+]} \\ - & \frac{[k_6 [C1OOCPAam]^{1_6} [C1]^{m_6}}{fn_6 [H^+]} - \frac{k_7 [C1OOCPAam]^{1_7} [C2]^{m_7}}{fn_7 [H^+]} \end{aligned} \quad (4-11)$$

$$\begin{aligned} \frac{d[C2OOCPAam]}{dt} &= \frac{k_4 [C2]^{1_4} [OOCPAam]^{m_4}}{fn_4 [H^*]} \\ &+ \frac{k_6 [C1OOCPAam]^{1_6} [C1]^{m_6}}{fn_6 [H^*]} - \frac{k_8 [C2OOCPAam] [C1]^{m_8}}{fn_8 [H^*]} \end{aligned} \quad (4-12)$$

$$\begin{aligned} \frac{d[C3OOCPAam]}{dt} &= \frac{k_5 [C3]^{1_5} [OOCPAam]^{m_5}}{fn_5 [H^*]} \\ &+ \frac{k_7 [C1OOCPAam]^{m_7} [C2]^{1_7}}{fn_7 [H^*]} + \frac{k_8 [C2OOCPAam]^{m_8} [C1]^{1_8}}{fn_8 [H^*]} \end{aligned} \quad (4-13)$$

Cr(III) oligomerization in solution.

$$\begin{aligned} \frac{d[C1]}{dt} &= \frac{-2k_1 [C1]^{m_1}}{fn_1 [H^*]} - \frac{k_2 [C2]^{1_2} [C1]^{m_2}}{fn_2 [H^*]} - \frac{k_3 [C1]^{1_3} [OOCPAam]^{m_3}}{fn_3 [H^*]} \\ &- \frac{k_6 [C1]^{1_6} [C1OOCPAam]^{m_6}}{fn_6 [H^*]} - \frac{k_8 [C1]^{1_8} [C2OOCPAam]^{m_8}}{fn_8 [H^*]} \end{aligned} \quad (4-14)$$

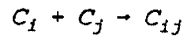
$$\begin{aligned} \frac{d[C2]}{dt} &= \frac{k_1 [C1]^{m_1}}{fn_1 [H^*]} - \frac{k_2 [C2]^{1_2} [C1]^{m_2}}{fn_2 [H^*]} \\ &- \frac{k_4 [C2]^{1_4} [OOCPAam]^{m_4}}{fn_4 [H^*]} - \frac{k_7 [C1OOCPAam]^{1_7} [C2]^{m_7}}{fn_7 [H^*]} \end{aligned} \quad (4-15)$$

$$\frac{d[C3]}{dt} = \frac{k_2 [C2]^{1_2} [C1]^{m_2}}{fn_2 [H^*]} - \frac{k_5 [C3]^{1_5} [OOCPAam]^{m_5}}{fn_5 [H^*]} \quad (4-16)$$

In order to compare the oligomerization rates of Equations 4.3 and 4.4 with the uptake rates of Equations 4.5-4.10, it was necessary to determine values for the  $l_i$ 's,  $fn_i$   $[H^+]$ 's,  $k_i$ 's, and  $m_i$ 's in equations 4.11-4.16.

#### 4.2.1 Estimation of the Oligomerization Rate Equation Parameters

A series of studies on the rates of formation of different Cr(III) hydrolytic oligomers has been performed by a Swiss group of researchers under the direction of Werner Marty<sup>4-6</sup>. These studies found that at constant pH, the oligomer reactions could be represented as elementary reactions of the form,



(4-17)

with an overall second-order differential rate expression (assuming isolated reactions) of the form,

$$\frac{d[C_{ij}]}{dt} = k_{ij}[C_i][C_j]$$

(4-18)

For the  $C_1 + C_1 \rightarrow C_2$  reaction, they determined  $k_{ij}$ 's for a pH range of 3.5-5 and a Cr(III) range of 0.005-0.09 M (250-4500 ppm) in the presence of 1 M  $NaClO_4$ <sup>4</sup>. Rate constants for the  $C_2 + C_2 \rightarrow C_4$  reaction were determined for the pH range of 4-5 and a Cr(III) range of 0.003-2500 M (125-2500 ppm) in 1 M  $NaClO_4$ <sup>5</sup>. They also followed the concentrations of  $C_1$ ,  $C_2$ ,  $C_3$ ,  $C_4$  and  $C_4^+$  (the sum of all oligomers larger than  $C_4$ ) in systems in which the pH's, after initial adjustment, were either held constant or allowed to decrease.

Using Rotzinger's data<sup>4</sup> at pH 4.5, a predictive Cr(III) oligomer formation numerical model was developed. The model allowed oligomers up to the size of octomers, assumed that all initial  $C_4^+$  was in the form of the pentamer ( $C_5$ ), ignored the volume of base added to maintain constant pH, assumed that all oligomer reactions followed general second-order reaction kinetics, used Rotzinger's  $C_1 + C_1 \rightarrow C_2$  rate constant  $k_{11}$  for pH 4.5<sup>4</sup> and multiples of Rotzinger's  $k_{11}$  for the higher oligomer formation rate constants.

Comparisons of the simulated results with Rotzinger's experimental data for an initial  $[Cr(III)]$  of 0.04 M (2000 ppm) and a constant pH of

4.5 (Figures 4.1 - 4.4) show generally good agreement. The departures of the simulated results for the monomer and dimer from the experimental results as time increases are expected since dilution of oligomer concentrations from base addition in the experimental system (approximately 10% of the total volume at 160 min.) was not taken into account in the simulations. The oligomer reactions and their respective rate constants used in the simulation are listed in Table 4.3.

TABLE 4.3

Cr(III) Species Reactions and Rate Constraints Used in Modeling Rotzinger's Cr(III) Species Data with Initial Cr(III) at .04 M and pH 4.5

Equations	Rate Constraints (M <sup>-1</sup> , hr <sup>-1</sup> )	Multiples of k <sub>11</sub> in final match
C1+C1 → C2	2.88	1
C1+C2 → C3	5.76	2
C2+C2 → C4	17.28	6
C1+C3 → C4	17.28	6
C1+C4 → C5	14.40	5
C2+C3 → C5	14.40	5
C1+C5 → C6	17.28	6
C2+C4 → C6	23.04	8
C3+C3 → C6	17.28	6
C2+C5 → C7	20.16	7
C3+C4 → C7	20.16	7
C1+C6 → C7	20.16	7
C1+C7 → C8	23.04	8
C2+C6 → C8	25.92	9
C3+C5 → C8	23.04	8
C4+C4 → C8	23.04	8

Using Rotzinger's rate constants at different pH's<sup>4</sup> for the C1+C1 → C2 reaction rate constants and the multiples of  $k_{11}$  obtained from the previous simulation for the higher oligomer rate constants, oligomer concentrations vs. time for the Cr(III) concentrations representative of our gelation system (50-100 ppm, .0095-.0019 M) were simulated for pH's of 4.0, 4.5 and 5.0 (Table 4.4). The predicted oligomer concentrations vs. time for pH 4.5 are compared against the Cr-PAam uptake concentrations predicted by the Hunt equation (Equation 4.1) in Figure 4.5. The relatively slow rates of formation for C2 and C3 at pH 4.5 gave an initial indication that the oligomerization reactions were significantly slower than the Cr(III)-PAam uptake reactions for pH's less than 4.5 and that isolation of the uptake reactions from the oligomerization reactions by means of pH and time was possible. The oligomerization simulations also predicted that minimal amounts of oligomers higher in molecular weight than C3 would form with pH's less than 4.5, [Cr(III)]'s less than 100 ppm, and times less than 10 hours.

The results of the preceding Cr(III) species simulations were then used to estimate the oligomerization kinetic parameters in Equations 4.11-4.16. Rotzinger's rate constant values<sup>4</sup> were used for predicting C2 formation and the simulated C1 + C2 → C3 rate constants,  $k_{12}$ 's, were used for predicting C3 formation. The rate of oligomerization to PAam-attached Cr(III) was assumed to be the same as the rate of oligomerization of Cr(III) to Cr(III) in solution, resulting in  $k_6=k_{11}=k_1$  and  $k_7=k_8=k_{12}=k_2$ . The oligomer reactions were assumed to be overall second order and elementary, resulting in  $m_1, m_2, l_1$  and  $l_2$  equaling 1. Since the Rotzinger experiments were performed at constant pH, the  $f_{n_1}([H^+])$ 's were automatically incorporated into his reported  $k_{11}$ 's and these values were used directly.

#### 4.2.2 Estimation of Kinetic Rate Parameters for the Cr(III)-PAam Uptake Reactions

The Hunt equation (Equation 4.1) was used as the basis for estimation of  $l_3-l_8$  and  $m_3-m_8$ . The coefficient on [PAamCOO(H)] was assumed constant for C1, C2 and C3 attachment and equal to the Hunt coefficient, resulting in  $m_3-m_8$  equally 0.8. The uptake rate constants for C1, C2 and C3,  $k_3-k_5$  were assumed to be equal to the Hunt rate constant ( $k_{jh}$ ),  $1.7 \times 10^{-4} \text{ hr}^{-1} \text{ M}^{-12}$ . The  $f_i$  ( $[H^+]$ )'s for C1, C2 and C3 PAamCOO(H) attachment were assumed to be the same and equal to the Hunt  $[H^+]$  dependence of  $[H^+]^{-1}$ . The PAamCOO(H) term was assumed to be equal to the Hunt PAam site balance term ( $f\{\text{PAam}\} - ([\text{Cr(III)}]_o - [\text{Cr(III)}])$ ) with  $f=.05$  and  $[\text{Cr(III)}] = [\text{C1}] + 2[\text{C2}] + 3[\text{C3}]$ .

### 4.3 RESULTS AND DISCUSSION

Using the estimated kinetic rate parameters from 4.2.1 and 4.2.2, Equations 4.11-4.13 were then combined and simplified to Equation 4.19.

$$\begin{aligned} \frac{d[Cr(III)]_{upt}}{dt} &= \frac{d[C100CPAam]}{dt} + \frac{2d[C200CPAam]}{dt} + \frac{3[C300CPAam]}{dt} \\ &= k_{jH}([C1]^{1.32} + (2[C2])^{1.32} + (3[C3])^{1.32}) \left( \frac{[f[PAam] - ([Cr(III)]_o - [Cr(III)])]}{f} \right)^{0.8} \\ &\quad + k_1[C100CPAam][C1] + 2k_2[C100PAam][C2] + k_2[C200CPAam][C1] \end{aligned}$$

(4-19)

Examination of Equation 4.19 shows that two uptake terms exist, the first right-hand term representing Cr(III) uptake by PAamCOO(H) sites and the remaining right-hand terms representing the Cr(III) uptake by PAam-attached Cr(III). Equation 4.19 was numerically integrated for a [Cr(III)] of .0019 M (100 ppm) and pH's of 4.0 and 4.5 to assess the relative uptake rates of Cr(III) by PAamCOO(H) and PAamCOOCr(III) and the relative rates of uptake to oligomerization. [Tables 4.5 and 4.6].

For pH 4.5, a [Cr(III)] of .019 M, and times less than 9 hours, the model predicts that the uptake rate due to PAam-attached Cr(III) is less than 5% the uptake rate of Cr(III) by PAamCOO(H) sites and that the combined rate of oligomerization due to both Cr(III) attachment to PAamCOOCr(III) and solution Cr(III) is less than 10% the uptake rate of Cr(III) by PAamCOO(H) sites (Table 4.5). Under the same concentration and time conditions, but for a pH of 4.0, the uptake rate due to PAam-attached Cr(III) is less than 1% the uptake rate due to PAamCOO(H) and the combined oligomerization rate is less than 3% the uptake rate of Cr(III) by PAamCOO(H) (Table 4.6). These results suggest that through appropriate choices of pH and time, the uptake reaction of the Cr(III) monomer by PAamCOO(H) sites can be isolated from the uptake reaction of Cr(III) monomer attaching to PAam-attached Cr(III) and from further Cr(III) monomer oligomerization reactions. Future work plans include verifying these predictions experimentally as well as using the simulated  $C2 + C2 \rightarrow C4$  and  $C3 + C3 \rightarrow C6$  rate constants to numerically predict pH and time ranges where C2 and C3 oligomerization would be expected to be minimal compared to C2 and C3 PAamCOO uptake.

TABLE 4.4  
 Simulated Cr(III) Species Results  
 for [Cr(III)] = 100 ppm, 1M NaClO<sub>4</sub>, and different pH's  
 a) pH 4.0

Time(hrs)	Fraction of Cr(III) As				
	C1	C2	C3	C4	C4 <sup>+</sup>
1	0.9989	0.0011	0.000001	0	0
2	0.9978	0.0022	0.000004	0	0
3	0.9967	0.0033	0.000008	0	0
4	0.9956	0.0043	0.000014	0	0
5	0.9946	0.0054	0.000022	0	0
6	0.9935	0.0065	0.000032	.000001	0
7	0.9924	0.0076	0.000043	.000001	0
8	0.9913	0.0086	0.000056	.000001	0
9	0.9902	0.0097	0.000071	.000002	0
10	0.9891	0.0108	0.000087	.000003	0

b) pH 4.5

Time(hrs)	Fraction of Cr(III) As				
	C1	C2	C3	C4	C4 <sup>+</sup>
1	0.9890	0.0108	0.000009	0.000003	0
2	0.9785	0.0212	0.000034	0.000020	0
3	0.9680	0.0312	0.000074	0.000064	0.000002
4	0.9576	0.0410	0.000128	0.000146	0.000006
5	0.9474	0.0503	0.000194	0.000276	0.000002
6	0.9374	0.0594	0.000272	0.000461	0.000003
7	0.9275	0.0681	0.000360	0.000708	0.000006
8	0.9178	0.0765	0.000456	0.00102	0.000009
9	0.9082	0.0846	0.000561	0.00141	0.000014
10	0.8988	0.0924	0.000674	0.00186	0.000021

c) pH 5.0

Time(hrs)	Fraction of Cr(III) As				
	C1	C2	C3	C4	C4 <sup>+</sup>
1	0.8988	0.0924	0.000674	0.00186	0.0002
2	0.8114	0.1550	0.002034	0.0106	0.0026
3	0.7351	0.1944	0.00348	0.0256	0.0102
4	0.6678	0.2165	0.00473	0.0437	0.0247
5	0.6083	0.2264	0.00571	0.0618	0.0464
6	0.5554	0.2281	0.00646	0.0780	0.0745
7	0.5083	0.2244	0.00684	0.0914	0.1075
8	0.4663	0.2173	0.00708	0.1018	0.1437
9	0.4287	0.2084	0.00717	0.1094	0.1818
10	0.3952	0.1984	0.00715	0.1145	0.2204

TABLE 4.5

The Simulated Rates of Reaction and Fractions of Total Cr(III) for Oligomers Attached and in Solution as a Function of Time for [Cr(III)] = 100 ppm, pH = 4.5, and [PAam] = 5000 ppm.

Time(hr)	Rates of Reaction (moles/hr) X 10,000				
	frac. Cr(III) Uptaken	PAamCOO(H) Uptake	Olig., Total	Olig., to PAamCr(III)	Olig., Solution
1	0.0792	1.390	0.095	.0077	0.088
2	0.1479	1.207	0.087	.0134	0.075
3	0.2082	1.059	0.081	.0176	0.065
4	0.2616	0.936	0.075	.0207	0.056
5	0.3093	0.833	0.070	.0231	0.049
6	0.3521	0.747	0.066	.0247	0.043
7	0.3907	0.672	0.062	.0259	0.038
8	0.4257	0.609	0.059	.0267	0.034
9	0.4577	0.553	0.055	.0271	0.030
10	0.4869	0.505	0.052	.0274	0.027

Time(hr)	Frac. Cr(III)					
	C1 in Solution	C2 in Solution	C3 in Solution	C1 Attached	C2 Attached	C3 Attached
1	0.9110	0.0098	0.0001	0.0786	0.0006	0.0000
2	0.8344	0.0174	0.0003	0.1457	0.0022	0.0001
3	0.7680	0.0232	0.0005	0.2034	0.0046	0.0002
4	0.7098	0.0277	0.0008	0.2537	0.0076	0.0004
5	0.6585	0.0311	0.0011	0.2976	0.0111	0.0006
6	0.6129	0.0336	0.0014	0.3364	0.0147	0.0009
7	0.5722	0.0354	0.0017	0.3707	0.0186	0.0014
8	0.5336	0.0367	0.0020	0.4014	0.0226	0.0018
9	0.5026	0.0375	0.0023	0.4288	0.0265	0.0023
10	0.4726	0.0379	0.0025	0.4535	0.0305	0.0029

TABLE 4.6

The Simulated Rates of Reactions and Fractions of Total Cr(III) for Oligomers Attached and in Solution as a Function of Time for

[Cr(III)] = 100 ppm,  
pH = 4.0, and [PAam] = 5000 ppm.

Time(hr)	Rates of Reaction (moles/hr) X 10,000				
	frac. Cr(III) Uptaken	PAamCOO(H) Uptake	Olig., Total	Olig. to PAamCr(III)	Olig. in Solution
1	0.0263	0.488	0.010	0.0003	0.010
2	0.0515	0.466	0.010	0.0005	0.009
3	0.0755	0.445	0.010	0.0007	0.009
4	0.0984	0.426	0.009	0.0009	0.008
5	0.1204	0.407	0.009	0.0011	0.008
6	0.1414	0.390	0.009	0.0013	0.008
7	0.1616	0.374	0.009	0.0014	0.007
8	0.1810	0.359	0.008	0.0016	0.007
9	0.1996	0.345	0.008	0.0017	0.007
10	0.2175	0.332	0.008	0.0018	0.006

Time(hr)	Fraction of Cr(III) As					
	C1 in Solution	C2 in Solution	C3 in Solution	C1 Attached	C2 Attached	C3 Attached
1	0.9726	0.0011	0.0000	0.0263	0.0000	0.0000
2	0.9465	0.0021	0.0000	0.0514	0.0001	0.0000
3	0.9215	0.0030	0.0000	0.0753	0.0002	0.0000
4	0.8977	0.0039	0.0000	0.0981	0.0003	0.0000
5	0.8749	0.0047	0.0000	0.1199	0.0004	0.0000
6	0.8531	0.0054	0.0000	0.1408	0.0006	0.0000
7	0.8322	0.0062	0.0000	0.1608	0.0008	0.0000
8	0.8121	0.0068	0.0000	0.1800	0.0010	0.0000
9	0.7929	0.0074	0.0001	0.1983	0.0012	0.0000
10	0.7744	0.0080	0.0001	0.2160	0.0015	0.0000

## NOMENCLATURE:

$k_{jh}$	:	The rate constant in the Hunt equation, $m^{-1}, m^{-.12}$
PAam	:	poly(acrylamide)
$[Cr(III)]_{upt}$	:	The concentration of Cr(III) uptaken by the PAam(M)
C1	:	Cr(III) monomer
C2	:	Cr(III) dimer
C3	:	Cr(III) trimer
C4	:	Cr(III) tetramer
C5	:	Cr(III) pentamer
C6	:	Cr(III) hexamer
C7	:	Cr(III) heptamer
C8	:	Cr(III) octomer
C100CPAam	:	Cr(III) monomer attached to PAam
C200CPAam	:	Cr(III) dimer attached to PAam
C300CPAam	:	Cr(III) trimer attached to PAAM
PAamCOOC100CPAam	:	PAam Cr(III) monomer crosslink
PAamCOOC200CPAam	:	PAam Cr(III) dimer crosslink
PAamCOOC300CPAam	:	PAam Cr(III) trimer crosslink
Olig., total	:	total oligomerization rate (moles/hr.) x 10,000
Olig., to PAamCr(III)	:	oligomerization rate to attached Cr(III) (moles/hr.) x 10,000
Olig., solution	:	oligomerization rate to Cr(III) in solution (moles/hr.) x 10,000

## REFERENCES

1. Hunt, J.A., Young, T-S., Green, D.W. and Willhite, G.P., "A Study of Cr(III)-Polyacrylamide Reaction Kinetics by Equilibrium Dialysis", AIChE Journal, V 35, No. 2, February, 1989, pp. 250-258.
2. Fei, R-J., Unpublished Results, University of Kansas, March, 1989.
3. Dona, C.L.D, Unpublished Results, University of Kansas, September, 1989.
4. Rotzinger, F.P., Stünzi, H., and Marty, W., Inorganic Chemistry, v 25, No. 4, 1986, pp. 489-495.
5. Besso, C., Thesis, University of Neuchatel, 1984.
6. Stünzi, H., Spiccia, L., Rotzinger, F.P., and Marty, W., Inorganic Chemistry, V 28, No. 1., 1989, pp. 66-71.

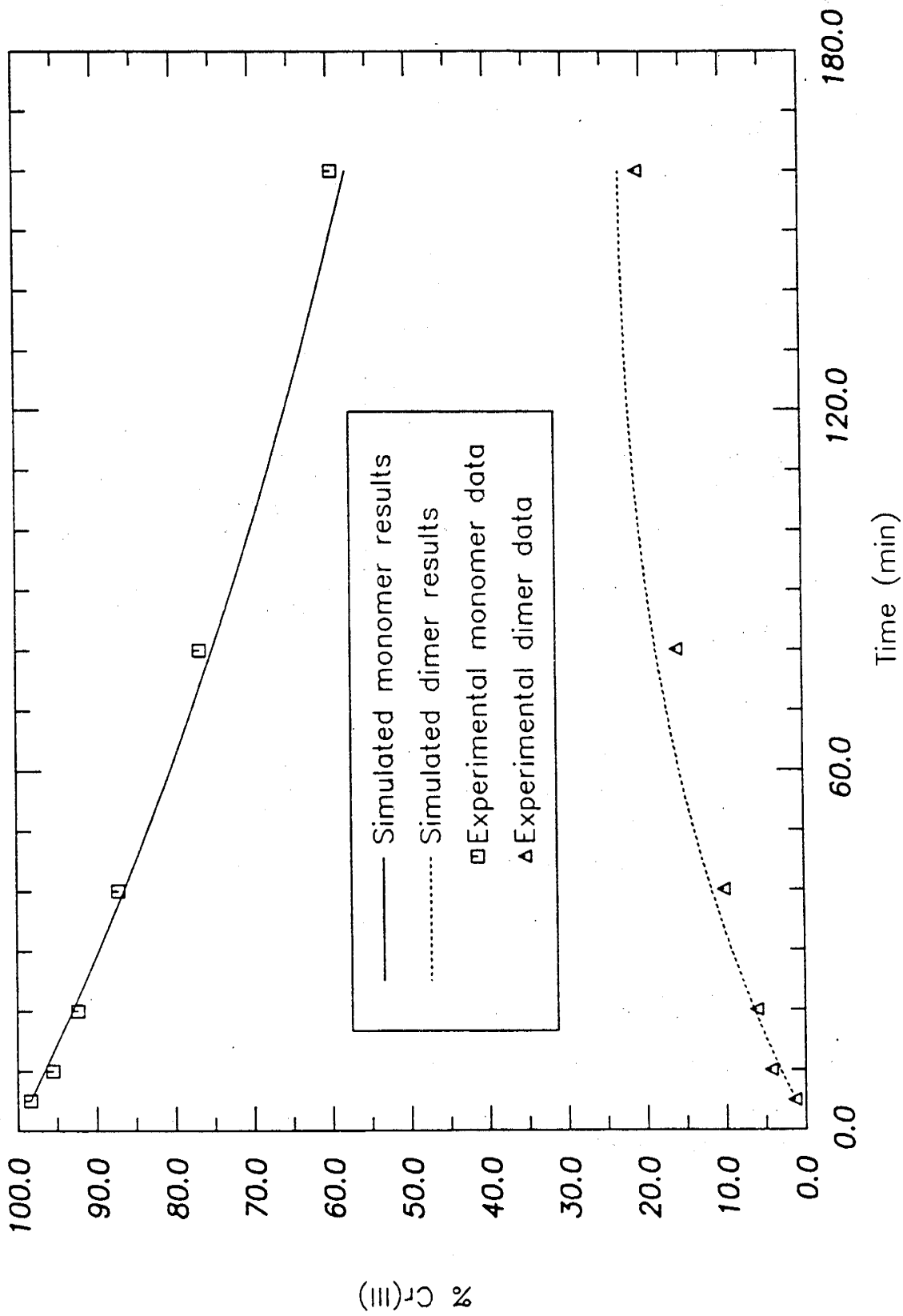


Figure 4.1 Percent monomer and dimer vs. time for an initial  $[Cr(III)] = .04 M$  and  $pH = 4.5$

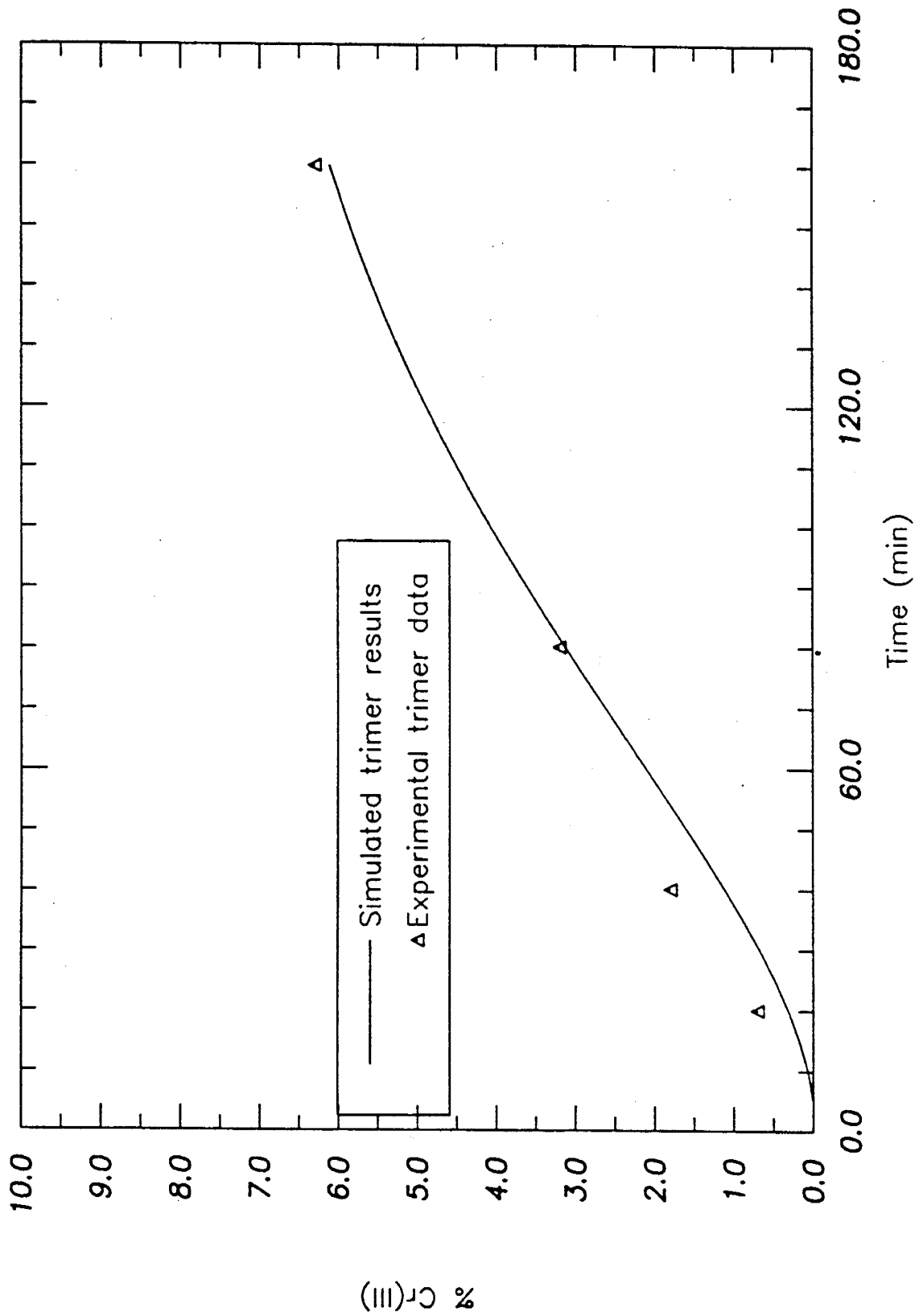


Figure 4.2 Percent trimer vs. time for an initial [Cr(III)] = .04 M and pH = 4.5

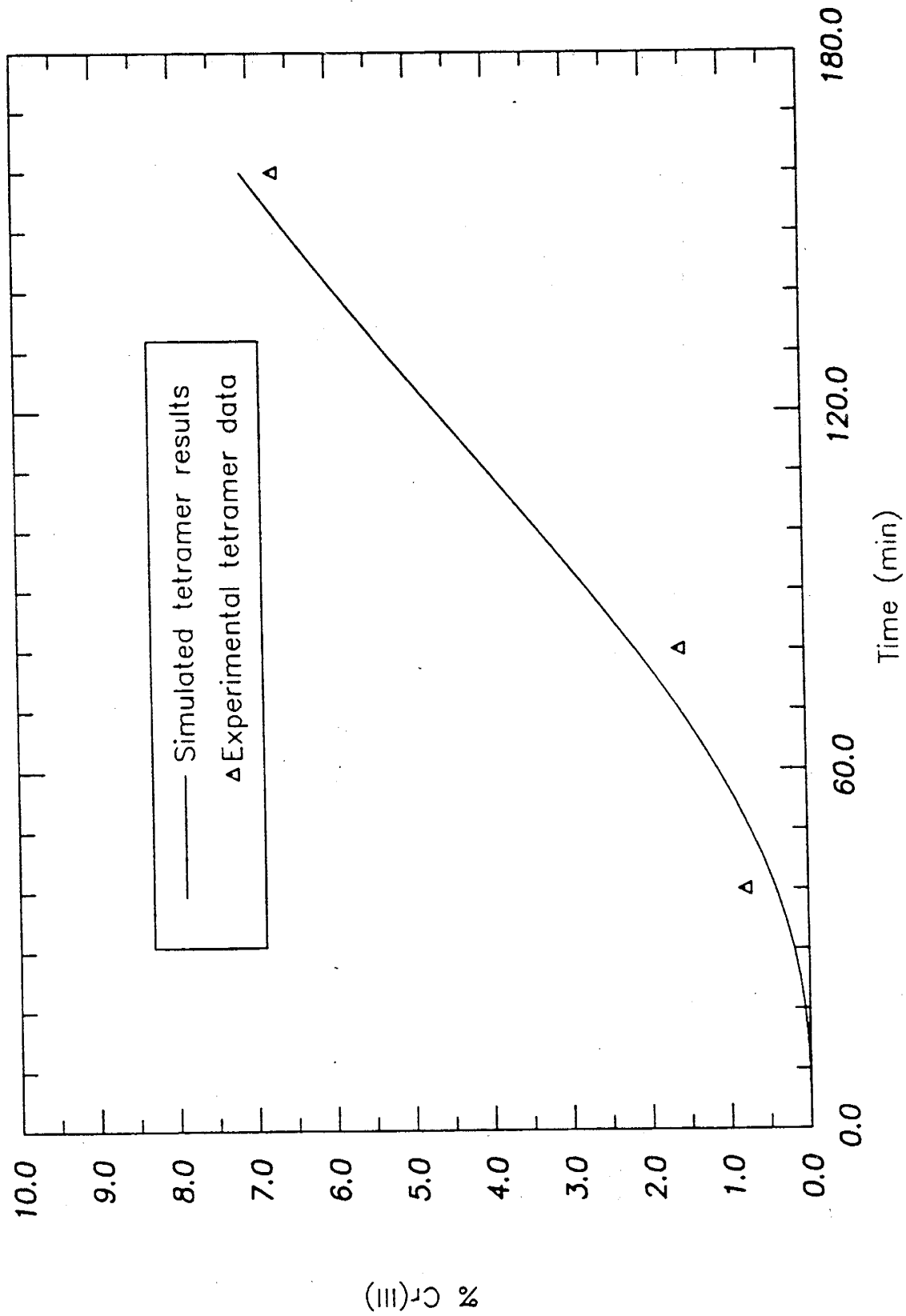


Figure 4.3 Percent tetramer vs. time for an initial  $[Cr(III)] = .04 M$  and  $pH = 4.5$

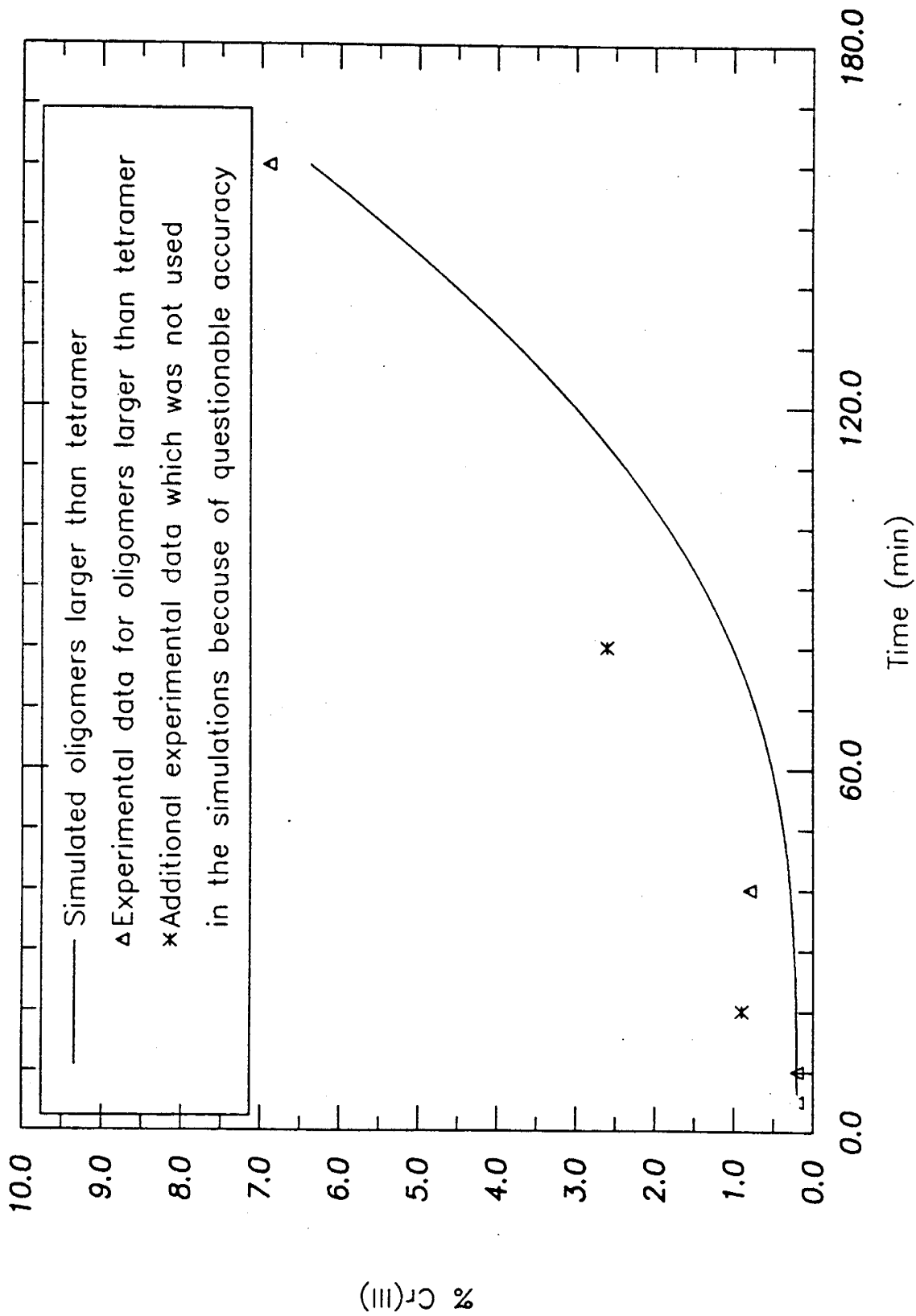


Figure 4.4 Percent oligomers larger than tetramer vs. time for an initial  $[Cr(III)] = .04 M$  and  $pH = 4.5$

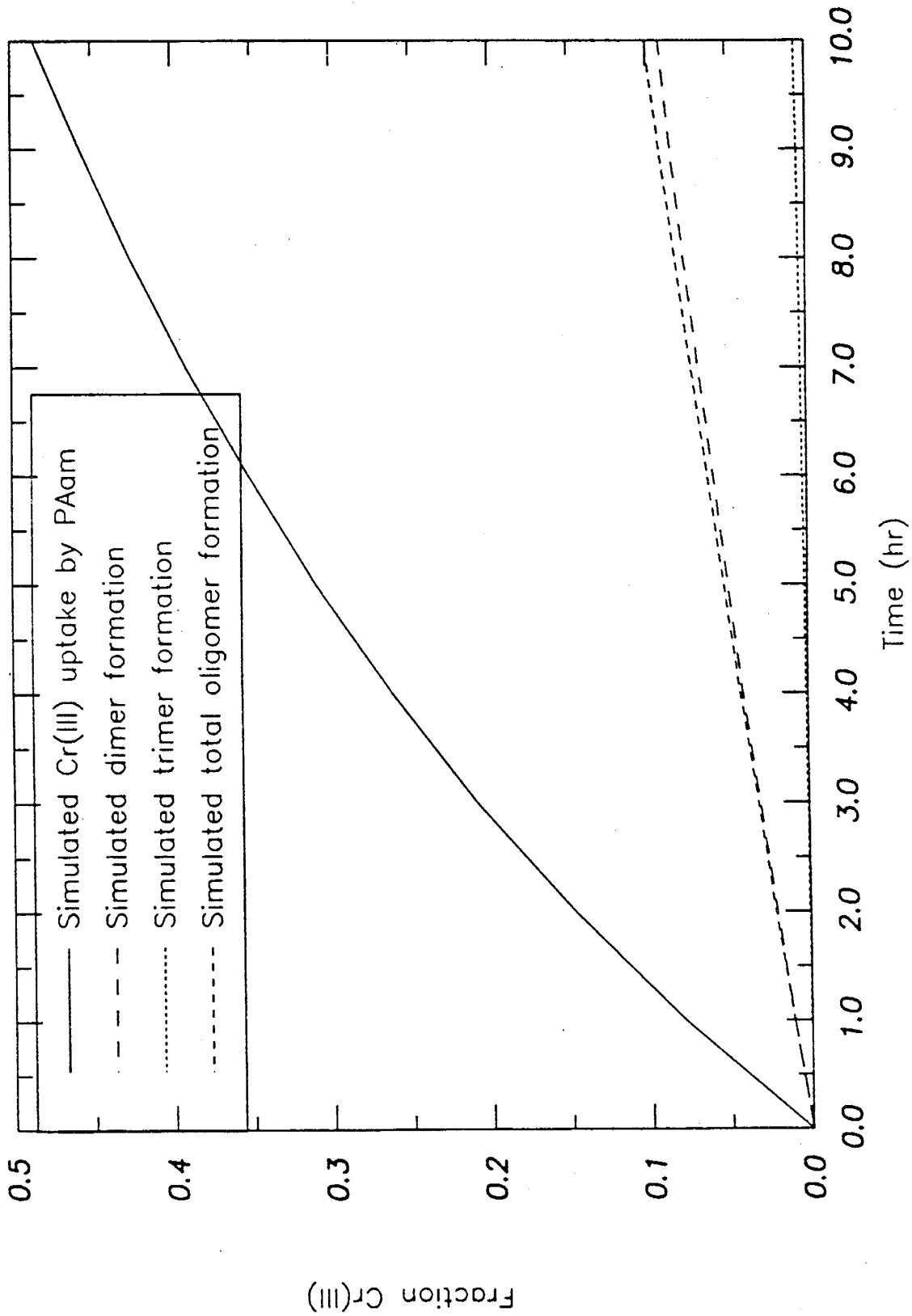


Figure 4.5 Comparison of Cr(III) uptake by PAam to Cr(III) oligomerization at  $[Cr(III)] = .002 M$ ,  $pH = 4.5$

## CHAPTER 5

### COMPLEX STUDIES

Principal Investigators: G. Paul Willhite, Don W. Green and  
C. Stanley McCool

Graduate Research Assistant: Anil Mathur

#### 5.1 Introduction

Previous work in our laboratory involving in-situ gelation studies in porous media have almost entirely been in the pH range of 4.5 to 5.5, whereas many petroleum reservoirs have resident fluids at higher pH levels, typically ranging from 5.5 to 7.0. Results of in-situ studies in the lower pH ranges may, therefore, not necessarily be applicable to such reservoirs. With this in mind, it was decided to design and pursue a system involving a metal ion i.e., chromium and a polymer such as polyacrylamide, which could gel at a higher pH level, specifically in the range 6.0 - 8.0.

#### 5.2 Chromium Complex Studies

Several chromium (III) salts and complexes were studied to design and characterize a system which could form gels with polyacrylamide in the pH range 6.0 to 8.0. Some of the chromium salts studied were:

- (i) chromium acetate
- (ii) chromium chloride
- (iii) chromium formate
- (iv) chromium acetylacetonate
- (v) chromium (trimer) acetate
- (vi) chromium (dimer) ethylenediamine complex
- (vii) chromium tris-ethylenediamine complex, and,
- (viii) chromium dichloro bis-ethylenediamine complex

Bottle tests were conducted with the above complexes and the gel solutions prepared were monitored for gelation behavior and the change in pH with time. The procedure consisted of mixing a 6,667 ppm polyacrylamide (Aldrich Lot TV) solution, which had been pre-stirred, filtered and allowed to sit for approximately five days, with a 400 ppm Cr(III) solution prepared with the above salts, in a 3:1 ratio. The resulting mixture with a polymer concentration of 5,000 ppm, a salt (generally NaCl) concentration of 20,000 ppm, and a 100 ppm Cr(III) concentration was divided into five different jars and the pH of the sample in each jar was adjusted to around 4.0, 5.0, 6.0, 7.0 and 8.0. The samples were then transferred to a water bath at 25° C. The pH of these gel solutions was checked on a daily basis and the samples were inspected visually for gel behavior by tilting the jars.

The results of this preliminary bottle testing showed that most of the complexes could form gels with polyacrylamide but with an accompanying drop in pH of the gel solution from its preadjusted pH level. The two systems which were exceptions were the ethylenediamine monomer  $[\text{Cr}(\text{en})_2\text{Cl}_2]^{+1}$  complex, and the ethylenediamine dimer  $[\text{Cr}(\text{en})_2 \cdot (\text{OH})_2 \cdot \text{Cr}(\text{en})_2]^{+4}$  complex. The ethylenediamine monomer and dimer complexes are fairly stable with respect to ligand substitution reactions and these ligands remain bound to the metal while the more labile coordination sites containing water or chloride ligands undergo substitution reactions and bind to groups on the polymer.

Ethylenediamine complexes were prepared in the laboratory. Additional testing showed that it was not possible to reproduce gelation results with the dimer species, and although samples gelled in the pH range of 6.5 - 7.5, they did so with a wide inconsistency in the gelation time. It was not possible to conclude whether any correlation existed between the preparation procedure and the gelation behavior of the dimer prepared. Also, the preparation of the dimer was an involved and complex procedure as compared to the simple one step distillation procedure for the monomer species. (It may be worth mentioning that both the monomer and the dimer of the ethylenediamine complex are not available commercially in the United States or outside). Further investigation, therefore, was entirely focussed on the cis-dichloro bis(ethylenediamine) chromium(III) chloride, the  $[\text{Cr}(\text{en})_2\text{Cl}_2]^{+1}$  complex.

### 5.3 PAam - Dien Monomer System

The bis-ethylenediamine monomer complex was prepared in the laboratory by dissolving chromium (III) chloride in dimethylformamide (DMF), distilling the mixture to approximately 148° C, and adding ethylenediamine drop by drop to the mixture cooled to 100° C. The resulting compound is then dried and purified by recrystallization in ice-cold, concentrated hydrochloric acid giving the pure complex product [2].

Additional bottle tests were conducted with this complex and polyacrylamide and the results are as shown in Figures 5.1 and 5.2. The testing procedure involved mixing an aged polymer solution (6,667 ppm, Aldrich Lot TV, pre-stirred and filtered a week in advance) and an aged chromium solution (400 ppm) in a 3:1 ratio, yielding a gel solution with a 5,000 ppm polymer concentration and a chromium (III) concentration of 100 ppm. The bottle containing this gel solution was then placed in a water bath at 35° C, under conditions of zero shear. After 24 hours, another quantity of the same polymer and chromium solutions were mixed in exactly the same proportion and placed in the water bath. This procedure was repeated after 2,3,4,5,6,8 and 11 days. The pH and viscosity of all these samples were monitored on a daily basis as is shown in Figures 5.1 and 5.2. It was determined that the gelation time of this system was  $10 \pm 1$  days, as most samples gelled within the 9 - 11 days period, at a pH of around 6.9. (Gelation time was defined as the time taken for the gel sample to reach a viscosity of 100 cp).

#### 5.4 Displacement Experiments with the Dien Complex

Using the bottle tests mentioned in Sections 5.2 and 5.3 as a basis, displacement experiments were designed to study in-situ gelation with the polyacrylamide and the ethylenediamine complex system. Table 5.1 describes the gel system used for one such displacement run, SPB.

##### 5.4.1 Displacement apparatus

The experimental apparatus for the displacement runs consisted of the polymer and chromium solutions being displaced from glass transfer cylinders by red gauge oil pumped from ISCO pumps. The whole system was enclosed in an air bath at a constant temperature to minimize fluctuations in pumping rates due to thermal expansion. Flow of polymer and the chromium solution from the transfer cylinders was directed to the inlet of a static in-line mixer, the exit of which was attached to the sandpack inlet. The in-line mixer and sandpack temperature were held constant at 35° C by a water bath. Effluent fractions from the sandpack were collected hourly using a fraction collector or collected in jars which were changed manually.

Pressure ports were installed along the sandpack length for the measurement of differential pressures. These pressures were sensed by a Validyne transducer/demodulator system. Automatic acquisition of the pressure data was accomplished with a computer equipped with an analog-to-digital converter.

##### 5.4.2 Preparation of sandpack SPB

A sandpack porous media holder was constructed from acrylic stock, as shown in Figure 5.3. The main holder was a 1.5 inch ID tube fitted with endplates and sealed with a rubber O-ring. Grooves were cut in the endplates to allow uniform distribution of entering and exiting fluids.

To stabilize the sand in the holder, TFE screens were inserted in the pressure ports and at the inlet and outlet faces. Two screens were placed at each face, a 380 mesh screen to the sand side and a 40 mesh screen to the endplate side. The fine mesh screen kept the sand in place and the coarse mesh screen provided structure between the fine mesh screen and the grooves cut in the endplate.

The sand was packed in the holder using an automatic sandpacking device. This device produces a sandpack with relatively constant permeabilities throughout the length of the pack. During the automatic packing procedure a 1 centimeter length of a relatively coarse sand (washed flint silica) was packed at the inlet and outlet faces. This coarse sand provided a buffer between the F-140 sand and the screens. After packing, the sandpicks were saturated with a 20,000 ppm NaCl solution and porosity and permeabilities were measured. (Refer Table 5.2).

Prior to conducting the displacement run using the gel solutions, it was necessary to adjust the pH of the resident brine. This was achieved by displacing many (>10) pore volumes of brine that had been adjusted to a pH of 6.9 by the addition of NaOH solution until the effluent pH stabilized at 6.9. This was done because the PAam - ethylenediamine monomer system gels at a stable pH of around 6.9.

## 5.5 Experimental Results

Figures 5.4 - 5.9 show the apparent viscosity versus time for the total sandpack and Sections 2-6. Pressure measurements in Section 5 and 7 were erratic and are not presented. Apparent viscosity is equivalent to the average viscosity of the flowing fluid in the section, assuming there is no change in the permeability of the section due to polymer adsorption/entrapment. Apparent viscosity is a measure of the flow resistance in a particular section of the sandpack.

Figure 5.4 shows the apparent viscosity versus time based on the pressure drop measured over the entire sandpack length. The apparent viscosity increased linearly with time up to 118 hours as the more viscous gelling solution displaced the resident brine. The dip in the data from 37 to 46 hours is due to temporary plugging of the first pressure port. After polymer breakthrough at 118 hours, the apparent viscosity continued to increase gradually up to 128 hours. After 128 hours, the apparent viscosity increased very rapidly indicating a much increased resistance to flow. This increase apparently reflected the onset of gelation at some point in the sandpack.

Figures 5.5 to 5.9 show the flow resistance with time in the different sections of the sandpack. A sharp and sudden increase in the flow resistance, however, occurred in Section 6 only, as shown in Figure 5.9. Here the apparent viscosity was close to 1 cp while brine was being displaced initially. It then started increasing gradually and after 125 hours there was a sudden increase up to 100 cp, indicating the onset of gelation.

Flow rate for the experiment was measured as a function of time throughout the run by measuring the weight of the effluent fractions collected on an hourly basis. Flow rate remained steady throughout the run at an average of 4.8 ml/hr., except towards the end of the run when the sandpack was plugged up. Figure 5.11 shows the flow rate versus time for the run. Effluent pH was also measured with time and is shown in Figure 5.10.

The chromium concentration and the viscosity of the effluent samples were also checked. It is evident from Figure 5.12 that the effluent viscosity remained around 1 cp till the breakthrough of the polymer/gel solution at 130 hours, after which it increased and reached 10 cp before the run was stopped. Chromium concentration before breakthrough was also zero before breakthrough around 1.1 pore volumes and the final effluent chromium concentration reached only 5 ppm, indicating retention of chromium in the porous medium.

## 5.6 Summary and Discussion of Results

Results from the displacement run SPB show that flow resistance increased significantly in a specific section in the sandpack. This increase could have been caused by an increase in the gelling solution viscosity or by a decrease in the effective permeability of the sandpack. It was not possible to effectively study the pH behavior of the gelling system in this run since the displacement was stopped only 19 hours after initial breakthrough of the polymer/gel system.

### References

1. McCool, C.S., Green, D.W. and Willhite, G.P., "Permeability Reduction Mechanisms in In-Situ Gelation of a Polyacrylamide/Chromium(VI)/Thiourea System," paper SPE/DOE 17333, presented at the SPE/DOE Enhanced Oil Recovery Symposium, Tulsa, Oklahoma, April 17-20, 1988.
2. Erik Pederson, "Preparation of Bis- and Tris(diamine)chromium(III) Complexes via Dimethyl Sulfoxide and Dimethylformamide Complexes," *Acta Chemica Scandinavica*, 24 (1970) 3362 - 3372.
3. Jordan, D.S., Green, D.W., Terry, R.E., and Willhite, G.P., "Effect of Temperature on Gelation Time for Polyacrylamide-Chromium(III) Systems," paper SPE 10059, presented at the SPE 56th Annual Technical Conference, San Antonio, Texas, October 5-7.
4. Huang, C.G., Green, D.W. and Willhite, G.P., "An Experimental Study of the In Situ Gelation of Chromium(III)-Polyacrylamide Polymer in Porous Media," *SPE Reservoir Engineering*, 583-592, (November 1986).
5. Prud'homme, R.K., Uhl, J.T., Poinsette, J.P. and Halverson, F., "Rheological Monitoring of the Formation of Polyacrylamide/Cr<sup>+3</sup> Gels." *SPEJ*, 804-808, (October 1983).
6. Hubbard, S., Roberts, L.J. and Sorbie, K.S., "Experimental and Theoretical Investigation of Time-Setting Polymer Gels in Porous Media," paper SPE/DOE 14946, presented at the SPE/DOE 5th Symposium on Enhanced Oil Recovery, Tulsa, Oklahoma, April 20-23, 1986.
7. Sorbie, K.S., Parke, A. and Clifford, P.J., "Experimental and Theoretical Study of Polymer Flow in Porous Media," paper SPE 14231, presented at the 60th SPE Annual Technical Conference, Las Vegas, NV, September 22-25, 1985.

TABLE 5.1

GEL DISPLACEMENT SPB

Gel solution composition

PAam (Lot TV)	: 5,000 ppm
NaCl	: 2.0 % (0.342 moles/liter)
Cr(III)	: 100 ppm (1.923 m.moles/l)
Cr complex used	: [Cr(en) <sub>2</sub> Cl <sub>2</sub> ]:Cl
Polymer solution pH (6,667 ppm)	: 6.65
Polymer soln. viscosity (6,667 ppm)	: 36.4 cp
pH of 400 ppm Cr(III) solution	: 4.82 (upon immediate mixing)
Initial pH of gel solution	: 5.84 (in-line mixer sample)
Initial viscosity of gel solution	: 18.48 cp (in-line mixer sample)
Final pH of gel soln. (after run)	: 6.72 (in-line mixer sample)
Initial pH of brine in sandpack	: 6.94
Gel time for inline mixer sample before run	: approx. 12 days
Gel time for inline mixer sample after run	: approx. 10 days

TABLE 5.2

DETAILS OF SANDPACK SPB

<u>SECTION</u>	<u>LENGTH, CM</u>	<u>PERM., DARCIES</u>
1	5.1	4.6
2	25.5	4.4
3	25.5	4.6
4	25.5	4.4
5	25.5	4.2
6	25.5	4.3
7	5.1	4.5
----- TOTAL -----	----- 137.7 -----	----- 4.4* -----

\* permeability for total sandpack calculated without considering the first and last sections.

PORE VOLUME : 548.3 ml.  
 POROSITY : 35.0 %  
 FLOW RATE : 4.80 ml/hr. or 0.95 ft/day  
 RESIDENCE TIME : 114.20 hours or 4.76 days  
 SAND USED : Ottawa grade F-140 (1 cm. flint silica used near end plates for support)

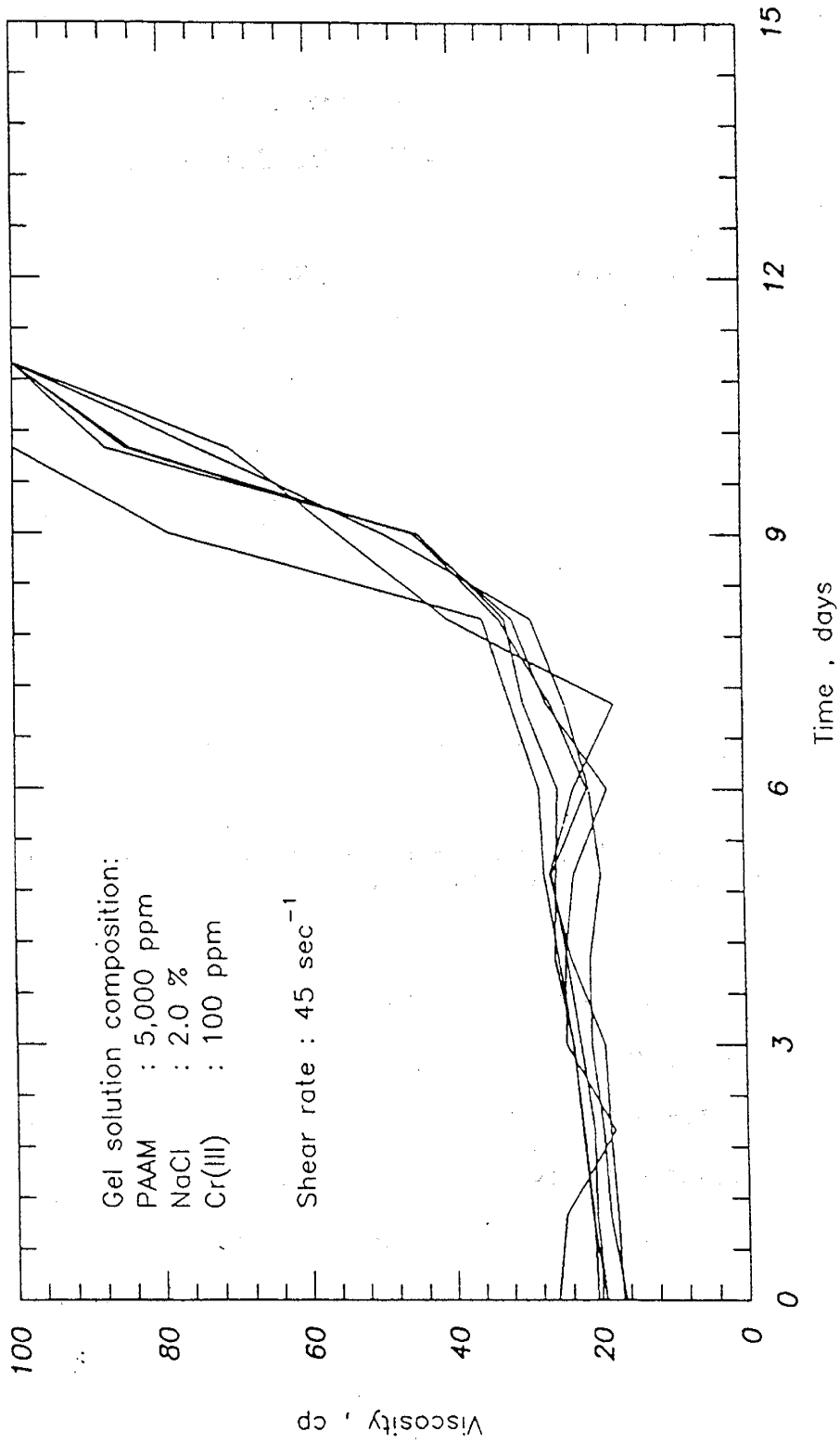


Figure 5.1 Viscosity - Time Plot for [Cr(en)<sub>2</sub>Cl<sub>2</sub>]<sup>+</sup> Gel System at 35°C

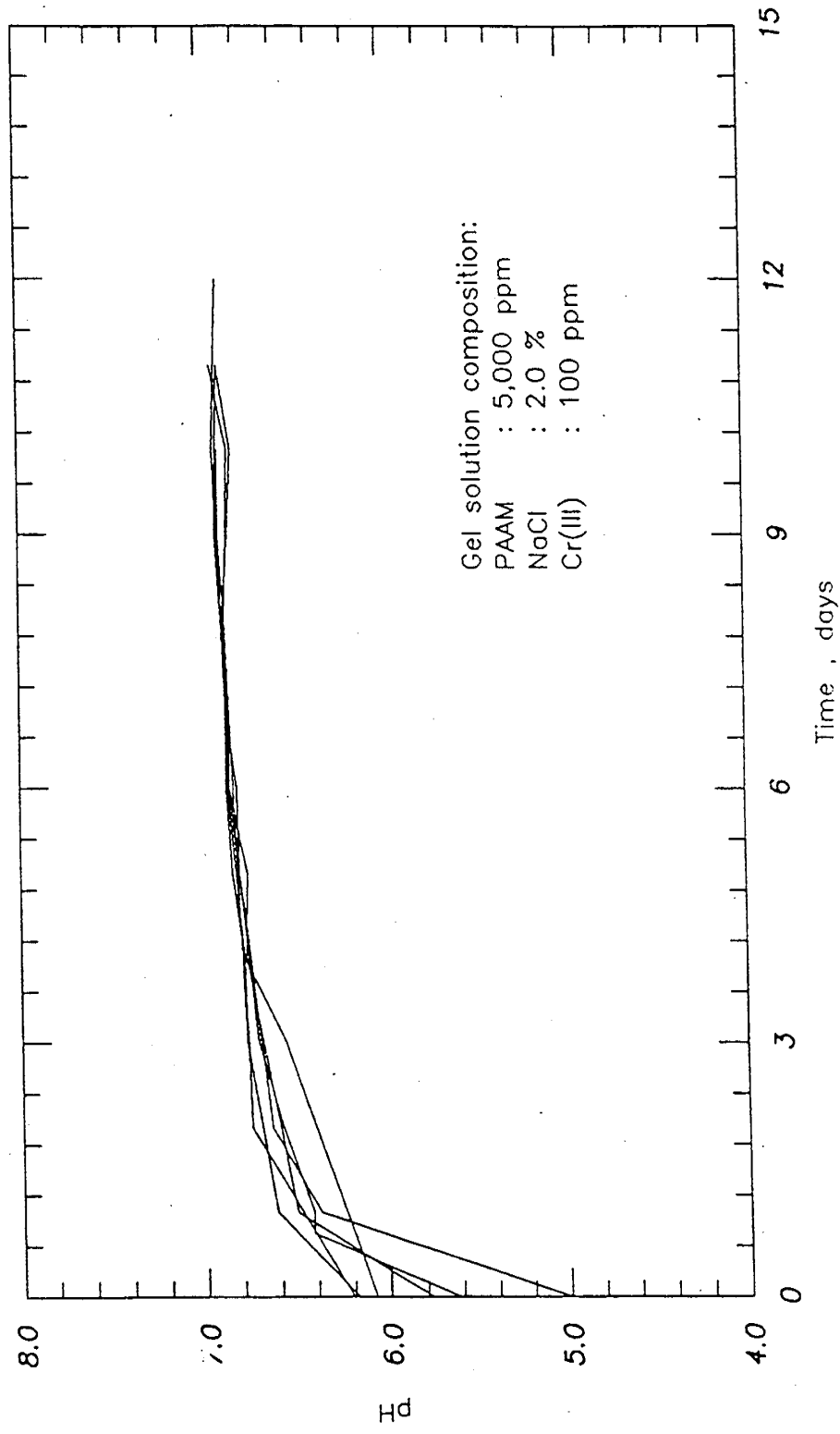


Figure 5.2 pH - Time Plot for  $[Cr(en)_2Cl_2]^+1$  Gel System at 35°C

Total Length : 54 inches  
Diameter : 1.5 inches  
Porosity : 35.0 %

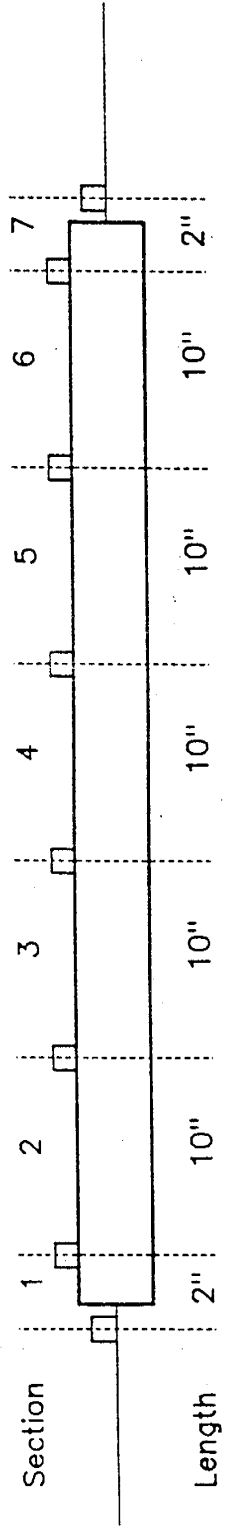


Figure 5.3 Sandpack SPB

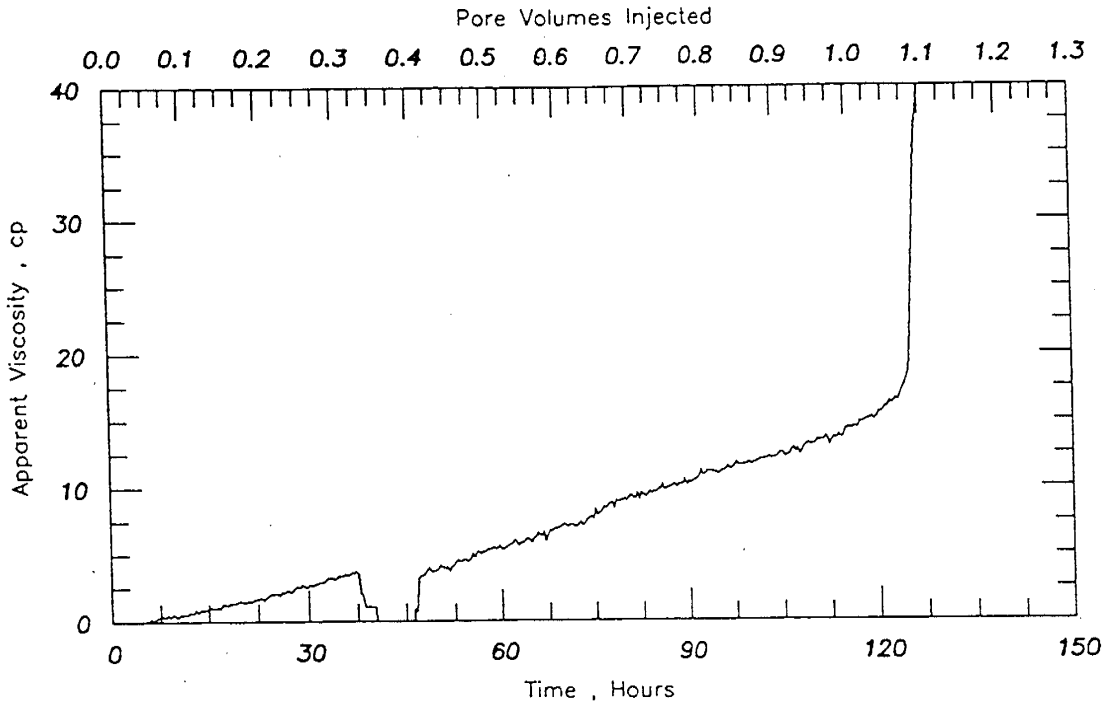


Figure 5.4 Total Flow Resistance of Sandpack for Gel Displacement SPB

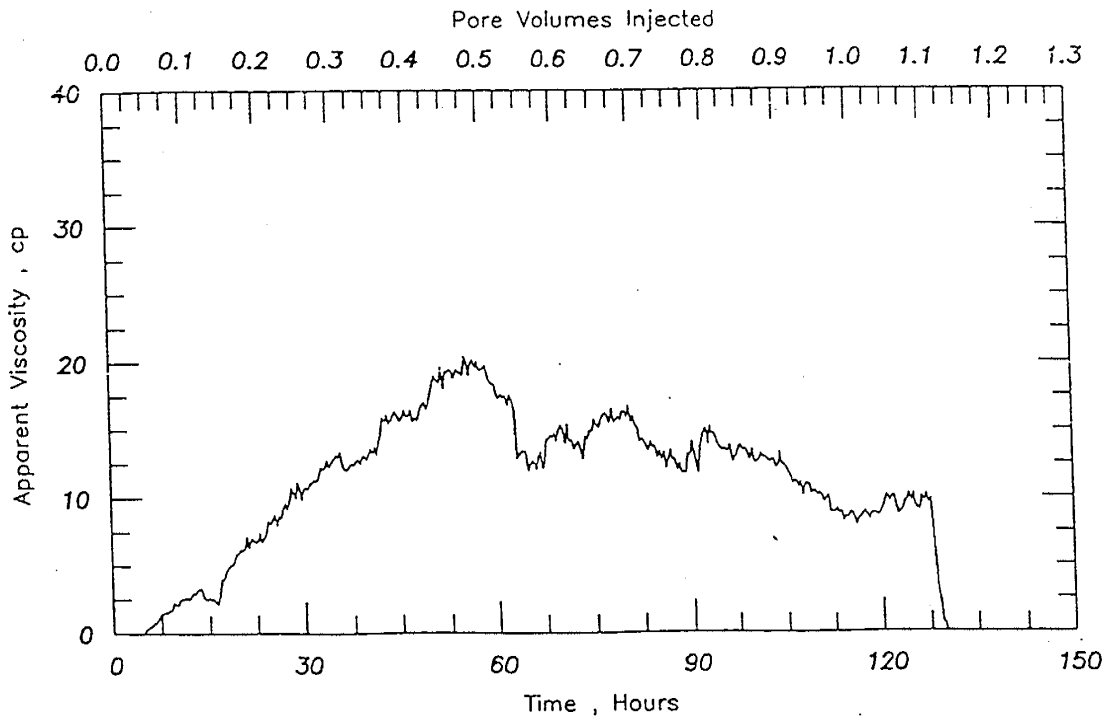


Figure 5.5 Flow Resistance of Section 2 for Gel Displacement SPB

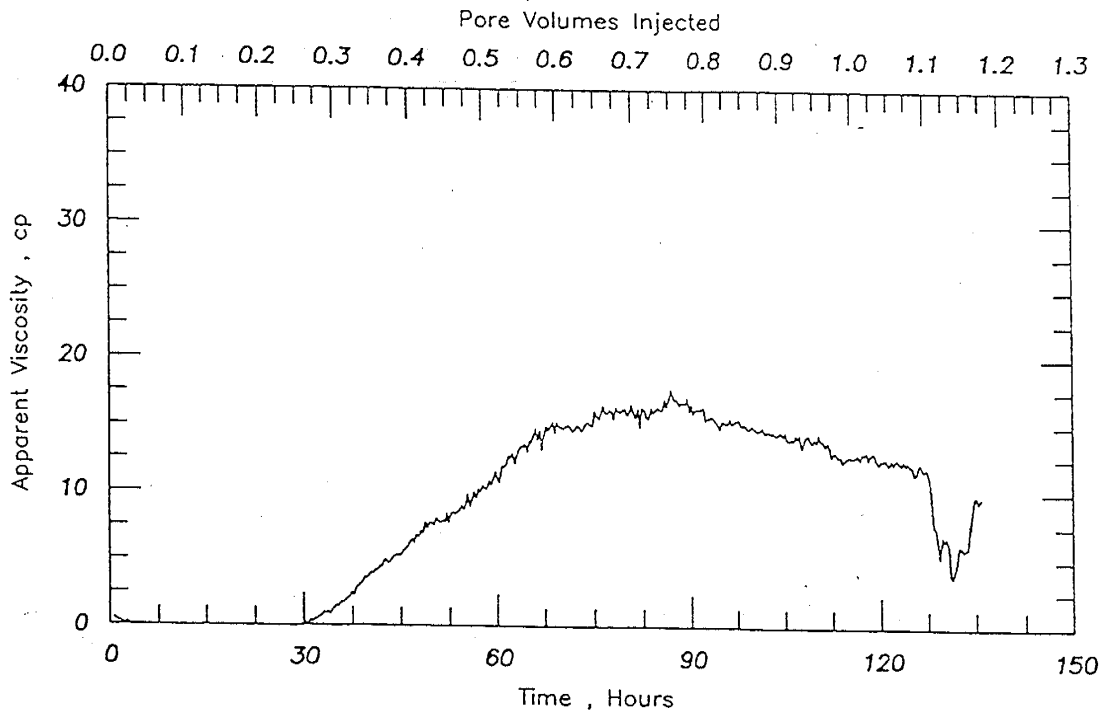


Figure 5.6 Flow Resistance of Section 3 for Gel Displacement SPB

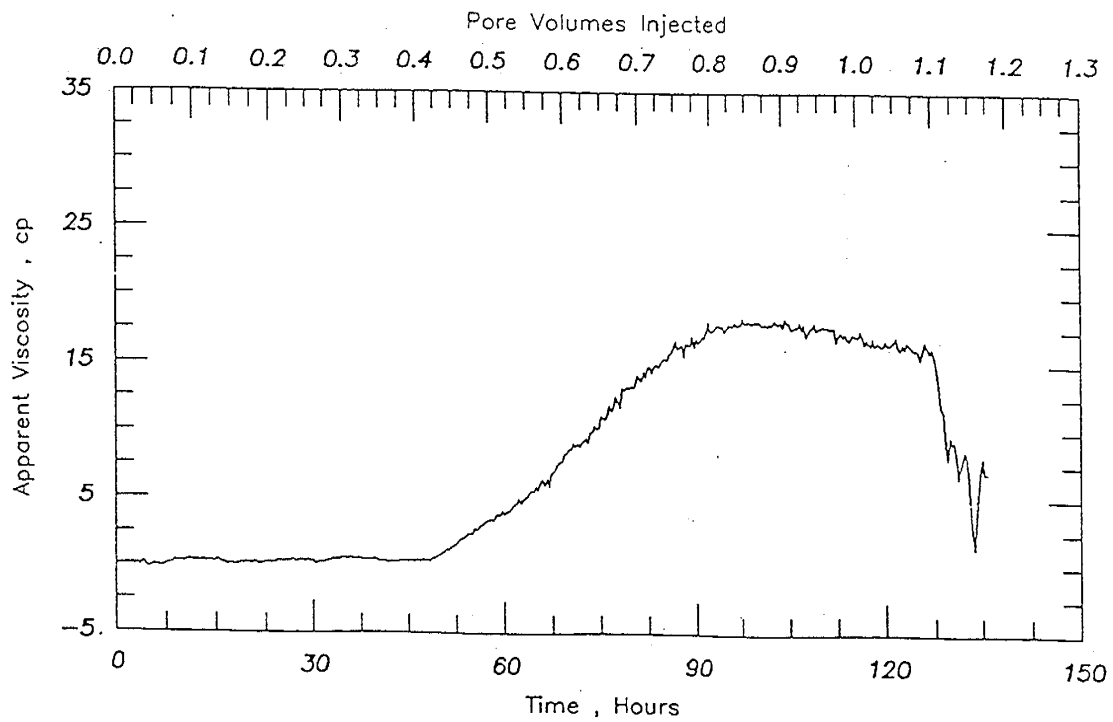


Figure 5.7 Flow Resistance of Section 4 for Gel Displacement SPB

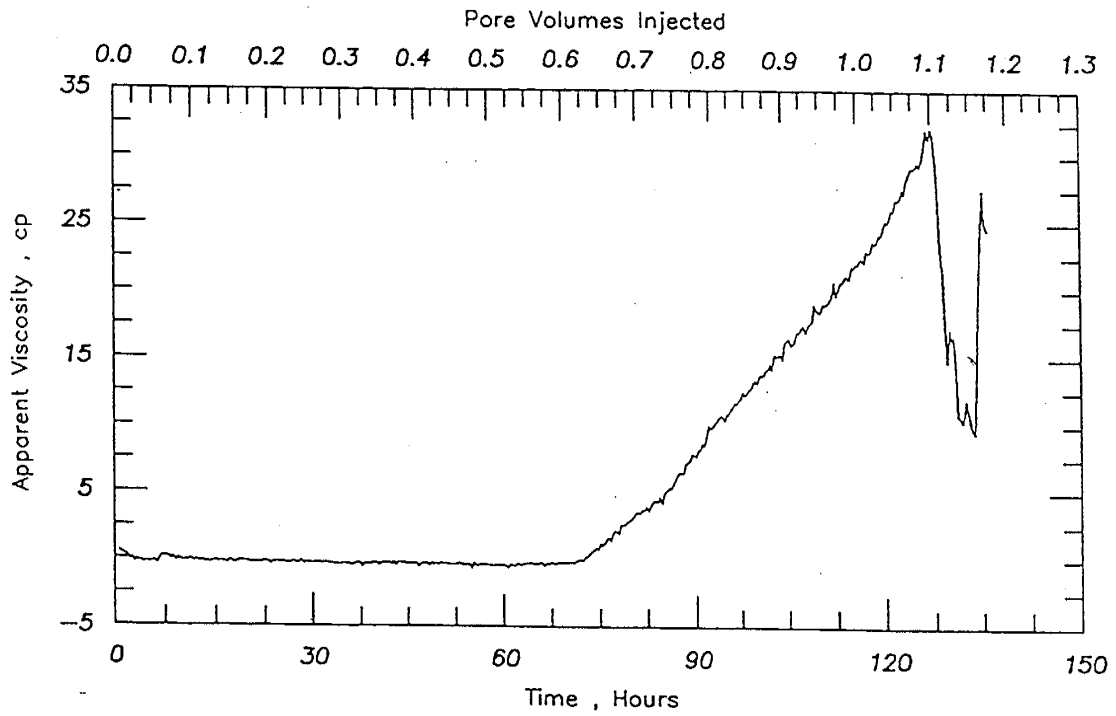


Figure 5.8 Flow Resistance of Section 5 for Gel Displacement SPB

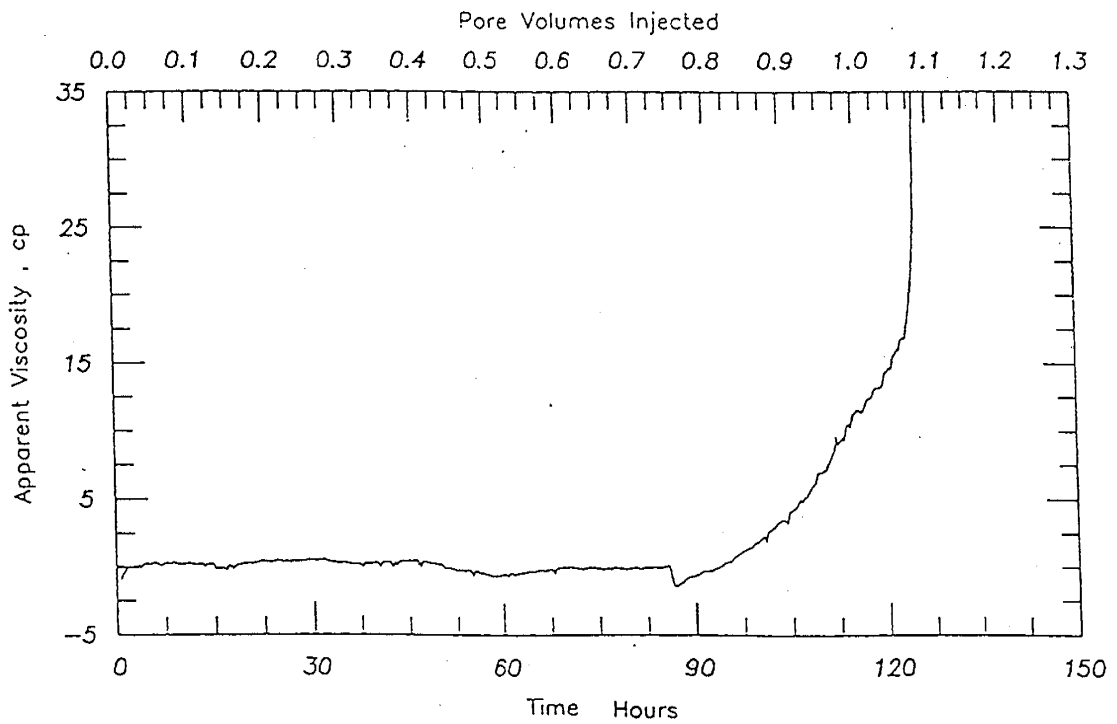


Figure 5.9 Flow Resistance of Section 6 for Gel Displacement SPB

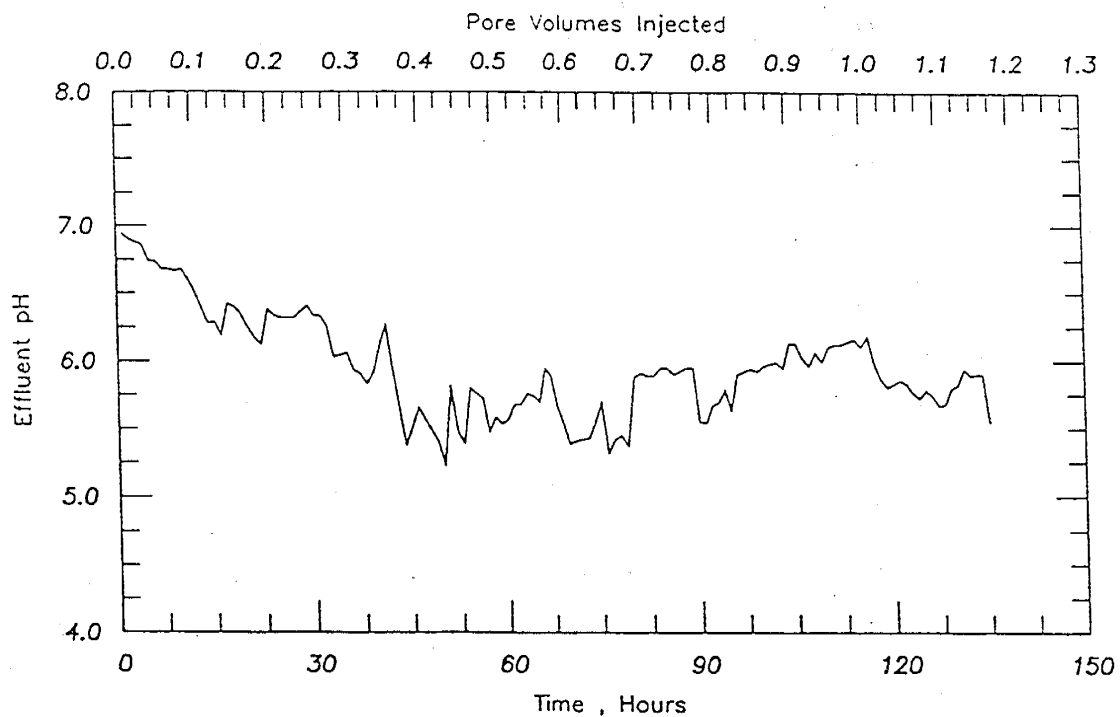


Figure 5.10 Effluent pH for Gel Displacement SPB

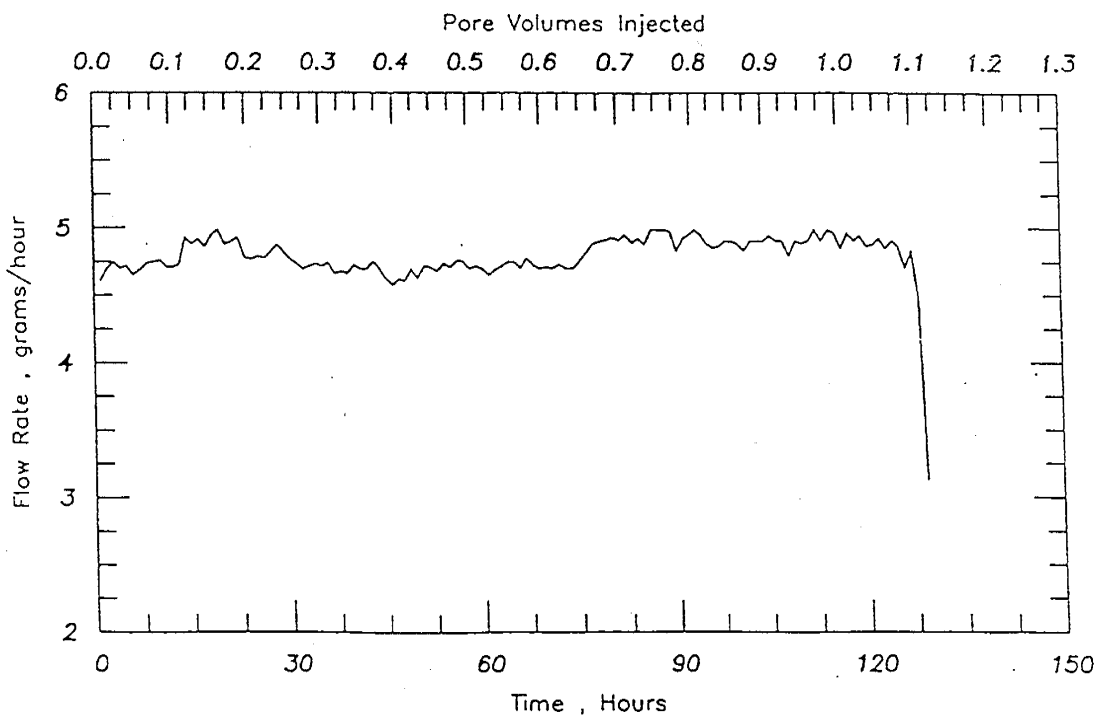


Figure 5.11 Flow Rate for Gel Displacement SPB

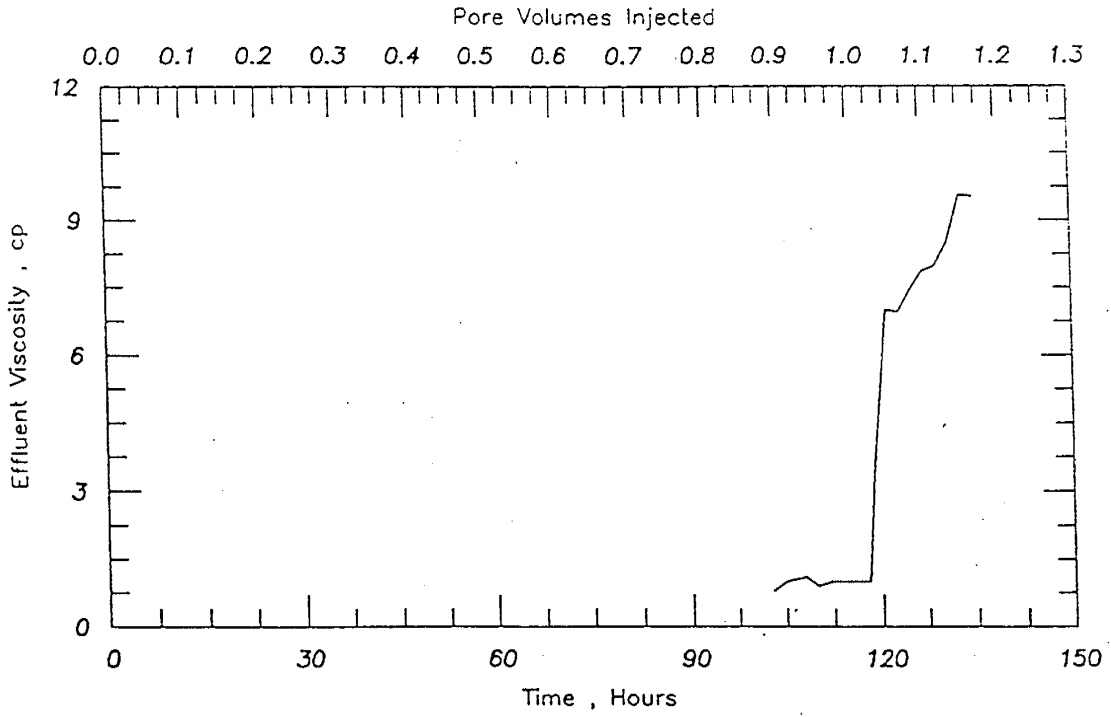


Figure 5.12 Effluent Viscosity for Gel Displacement SPB

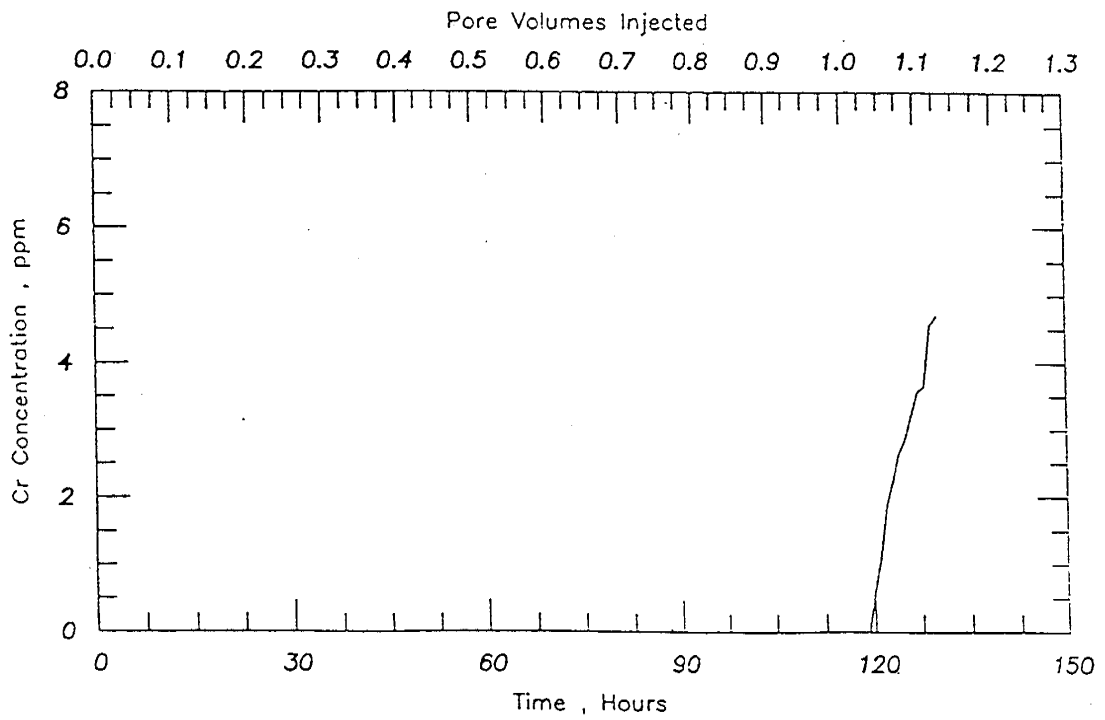


Figure 5.13 Effluent Chromium Concentration for Gel Displacement SPB



## CHAPTER 6

### RHEOLOGY OF POLYSACCHARIDE-CHROMIUM(III) GELLING SOLUTION

Principle Investigators: John L. Thiele, G. Paul Willhite

Graduate Research Assistant: Douglas M. Dolan

#### 6.1 INTRODUCTION

This work was undertaken to obtain a better understanding of the development of structure in a gelling polysaccharide solution. In this and previous work, gel structure and gelation rate were determined by measurement of the storage modulus during gelation. A primary purpose of the study was to provide rheological data under well-defined conditions, to complement in situ experiments with the same gelling solution. Preliminary work, described below, indicated that superimposed shear affects gelation of polysaccharides in a way very different from the way it affects polyacrylamide solutions.

Under zero (net) shear conditions, the effect of initial pH on the initial rate of gelation was determined. Under shearing conditions, both the duration and shear rate were varied; the storage modulus was measured both during and after shearing.

#### 6.2 SUMMARY OF OUR PREVIOUS WORK

An extensive study of the effect of superimposed shear on the gelation rate of polyacrylamide solutions<sup>1,2</sup> showed that superimposed shear had at least two distinguishable effects on these solutions. The imposed shear appears to accelerate gelation through improved mass transfer (improved mixing), and acts to retard gelation, or to degrade the gel through breakage of already formed crosslinks. Either of these effects can be made dominant in some polyacrylamide/chromium(III) solution concentration and shear combinations. Thus, the superposed shear may appear to accelerate or retard the overall gelation rate relative to the gelation rate measured without the superimposed shearing. An initial objective of the current study was to have been to confirm this gelation model for polysaccharides as well.

A previous study of polysaccharide gelation was undertaken<sup>3,4</sup>, in which initial pH was adjusted throughout the study with sodium bicarbonate. It was later determined that the presence of bicarbonate in the solution caused problems with the gelation. Many of these solutions appeared to fracture during gelation, and the course of gelation could not be satisfactorily monitored. The current study improved upon this by using dilute sodium hydroxide to adjust the initial solution pH.

A preliminary study by Bhaskar of the effect of shear on polysaccharide gelation indicated that polysaccharides solutions behave very differently under shear than polyacrylamide solutions<sup>2</sup>. In that study, an imposed shear of  $7.4 \text{ sec}^{-1}$  had the effect of completely inhibiting the formation of structure in the polysaccharide solution, throughout 40 hours of shearing. However, when shearing was stopped after nine hours in a replicate experiment, the storage modulus immediately jumped to a non-zero value, and increased with time thereafter. This indicated that, when shearing stopped, crosslinks which had previously been inhibited (or broken) by shearing could form within a very short time. The current study was intended to explore and clarify this phenomenon.

### 6.3 EXPERIMENTAL APPROACH

#### 6.3.1 Materials

To complement the concurrent in situ studies<sup>5</sup>, a solution was chosen for study consisting of 1500 ppm polysaccharide, 50 ppm chromium(III) (from chromium chloride), 1500 ppm formaldehyde, and variable amounts of sodium hydroxide, to adjust pH.

The polysaccharide used throughout was Flocon 4800MX. Stock solutions of this polymer with a concentration of 1650 ppm were prepared through a carefully standardized filtration and dilution procedure which was intended to remove cell detritus and provide a reproducible starting material<sup>2</sup>. Several such stock solutions were prepared throughout the course of the study, and, to ensure the rheological similarity of the polymer solution, a sample of each stock solution was diluted to 1500 ppm polymer and tested using the Weissenberg rheogoniometer. Figure 6.1 shows the viscosity profile for all eight stock solutions used in the study. This figure also demonstrates the power-law nature of the polymer solution over the shear rate range of interest in our studies.

Chromium stock solutions were prepared at a concentration of 550 ppm Cr(III) in 5000 ppm sodium chloride. These solutions were prepared at least a week in advance, to allow time for chromium hydration.

#### 6.3.2 Experimental Methods

All viscosity and storage modulus measurements were made using the Weissenberg R19 Rheogoniometer equipped with 7.5 cm diameter cone and plate fixtures. This machine is operated in steady-shear mode for measurement of viscosity, oscillatory mode for measurement of storage modulus, or superposition mode for measurement of storage modulus while under shear.

Each gelling sample was prepared by adding the appropriate amount of chromium stock solution by pipette to a stirred jar of polymer solution, then measuring and adjusting pH by adding 0.1 N sodium hydroxide dropwise as

needed. Gelling solutions were prepared just prior to loading them into the cone and plate. Once loaded, the air-exposed edges of the sample were coated with a thin layer of light mineral oil to prevent evaporation. This oil layer was renewed at intervals, as necessary.

In all of the experiments reported here, an oscillation frequency of 0.628 Hz, and an oscillation amplitude of 50 microns was used. The sample was maintained at 25.0°C throughout the gelation. Detailed descriptions of the procedures used are presented elsewhere<sup>6</sup>.

#### 6.4 ZERO NET SHEAR RESULTS

Several replicate gelations were made at pH 6, each with a different filtration batch of polymer stock solution. These data are shown in Figure 6.2. While the storage modulus data diverge somewhat after about 24 hours, the initial slope is seen to be very reproducible in these runs. The storage modulus values are an order of magnitude higher than one would expect with a similar polyacrylamide gelling solution, reflecting the rod-like nature of the polysaccharide, and the correspondingly much stiffer gels produced with this polymer.

Figure 6.3 shows storage modulus data for several runs made at various initial pH. Generally, the higher the initial pH, the higher the initial slope of the storage modulus vs. time curve, up to pH 6. Above pH 6, the trend reverses. At initial pH 6.5 and pH 7 the gels were somewhat cloudy. This indicates precipitation occurred in this system above pH 6. The initial slopes (which are proportional to the rate of crosslinking) of the runs at various pH are plotted against hydrogen ion concentration in Figure 6.4. This relationship is approximately linear in the range of pH 4.7 to 6, and the slope of the line is -1.02, by regression. Thus, the initial gelation rate is inversely dependent on the initial hydrogen ion concentration when not inhibited by precipitation. This is illustrated by plotting against inverse hydrogen ion concentration and observing a straight line, as in Figure 6.5.

#### 6.5 SHEAR RESULTS

Polysaccharide gels exhibit very different behavior while under shear than we expected based on previous superposition work with polyacrylamide gels. With polysaccharides, we found that even at a very low shear rate, the storage modulus is prevented from increasing. In every shear experiment, the initial solution storage modulus typically dropped to zero and remained there for the duration of shearing. Once the shear was removed, the storage modulus usually jumped (i.e., virtually instantly) to some value and, if too much time had not been spent under shear, continued to increase slowly with time, although not at a rate or to a level that was observed in the absence of shear.

Figure 6.6 illustrates some of this behavior. Figure 6.6 is a montage of three separate runs in which the sample was sheared for different periods of time at  $0.592 \text{ sec}^{-1}$  [note that each vertical and horizontal scale is different]. In each case, the storage modulus during shear is near zero, and the storage modulus jumps at the cessation of shearing. One would expect that the duration of shear would affect the subsequent level and rate of change of the storage modulus in some consistent manner. This appears to be the case if only the top and bottom panels are examined. The sample sheared the shortest time (15 hours in the top panel) appears to "recover" and continue building structure after the shearing, while the sample sheared the longest (45 hours in the bottom panel) appears to recover poorly. However, a number of runs turned out like the middle panel, in which the magnitude of the jump on cessation of shear after thirty hours is totally inconsistent with the previous two runs; further, the storage modulus actually decreases slightly thereafter. Thus, the effect of shear on the gel structure based on the observed post-shear storage modulus data was not consistent and requires further study.

#### 6.6 SANDPACK EFFLUENT RESULTS

In related work<sup>5</sup>, the behavior of this gelling system in sandpacks was studied. To assist that study, a few runs were made using the feed solution to the sandpack, and the effluent from the sandpack. The samples were mixed in a sealed, in-line mixing procedure, and were injected into the sandpack at pH 4.7, the "natural" or unadjusted pH of the mixture of the two stock solutions. The feed sample was taken just downstream from the in-line mixer, and placed in the rheogoniometer; this sample was essentially identical to those described previously in this chapter. Effluent samples were taken from the exit port of the sandpack after many pore volumes of the gelling fluid had passed through the sandpack. The residence time of the fluid in the sandpack was about four hours.

Figure 6.7 shows the results of these experiments. Time zero for all curves is the time at which the sample is placed in the rheogoniometer; the effluent samples are thus actually four hours "older" than the apparent time indicated on the axis. The data generally indicate that the effluent samples gel at a slower rate than the corresponding feed samples. It is not possible to tell from the data available whether the lower gelation rate reflects a change in concentration of some reactant (e.g., possible stripping of polymer by the sandpack) or a retardation of the gelation rate due to shear effects in the sandpack.

#### 6.7 CONCLUSIONS

Under zero shear conditions, polysaccharide gels are formed that are significantly stiffer than similar polyacrylamide gels. The initial pH of the solution has the most significant effect on the rate of crosslinking of

the polysaccharide gels, as is the case with polyacrylamide gels. In this study, an inverse relationship was found between hydrogen ion concentration and gelation rate.

While under shear, the formation of permanent crosslinks in the polysaccharide solution appears to be completely inhibited by even very low shear rates. Once shearing is stopped, very rapid crosslink formation may occur. Finally, by studying sandpack feed and effluent, it was shown that the rheological properties of the gel solution were altered by flow through the sandpack.

## REFERENCES

1. Bhaskar, R.K., "Transient Rheological Properties of Chromium/Polyacrylamide Solutions Gelling Under Superposed Steady and Oscillatory Shear Strains", Ph.D. Dissertation, University of Kansas, 1988.
2. Willhite, G.P., Green, D.W., Thiele, J.L., Young, T.-S., and Mertes, K.B., "Investigation of the Application of Gelled Polymer Systems for Permeability Modification in Petroleum Reservoirs - Final Report", DOE/BC/108435-15 (DE90000229), NTIS, U.S. Department of Commerce, Springfield, VA, March, 1990.
3. Willhite, G.P., Green, D.W., Thiele, J.L., Young, T.-S., and Mertes, K.B., "Investigation of the Application of Gelled Polymer Systems for Permeability Modification in Petroleum Reservoirs - Second Annual Report," DOE/BC/108435-10 (DE88001250), NTIS, U.S. Department of Commerce, Springfield, VA, November 1988.
4. Hester, S.K., "Rheological Study of Xanthan Solutions and Xanthan/Chromium(III) Gelling Solutions Using Steady and Small Amplitude Oscillatory Shear," M.S. Thesis, University of Kansas, 1988.
5. Hejri, S., "An Experimental Investigation into the Flow and Rheological Behavior of Xanthan Solutions and Xanthan/Cr(III) Gel Systems in Porous Media," Ph.D. Dissertation, University of Kansas, 1989.
6. Dolan, D.M., "An Experimental Study of the Effects of pH and Shear on the Gelation of a Xanthan-Chromium(III) Solution," M.S. Thesis, University of Kansas, 1989.

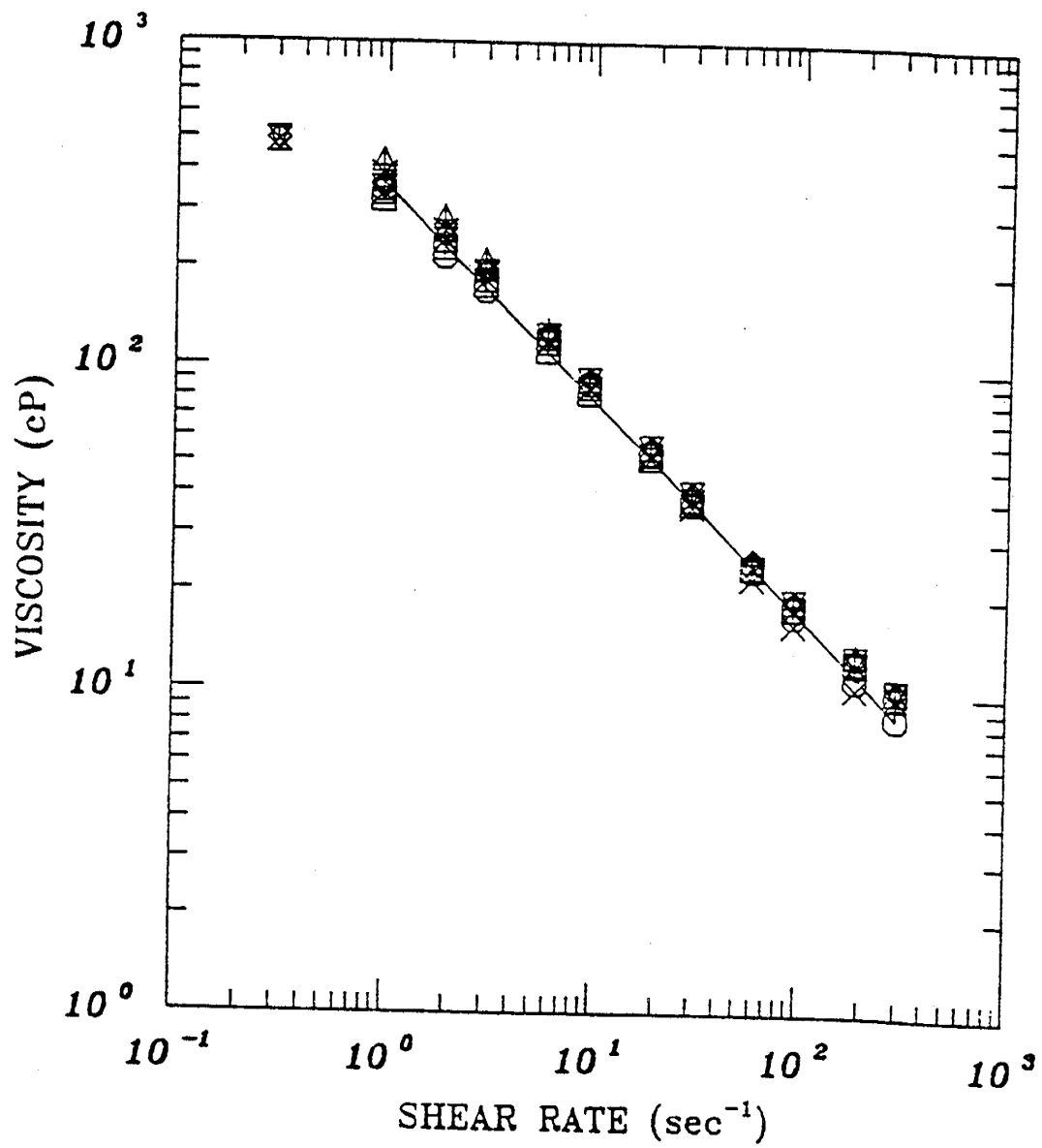


FIGURE 6.1 Rheograms of (1500 ppm filtered) Biopolymer Solutions Used in Gelation Studies

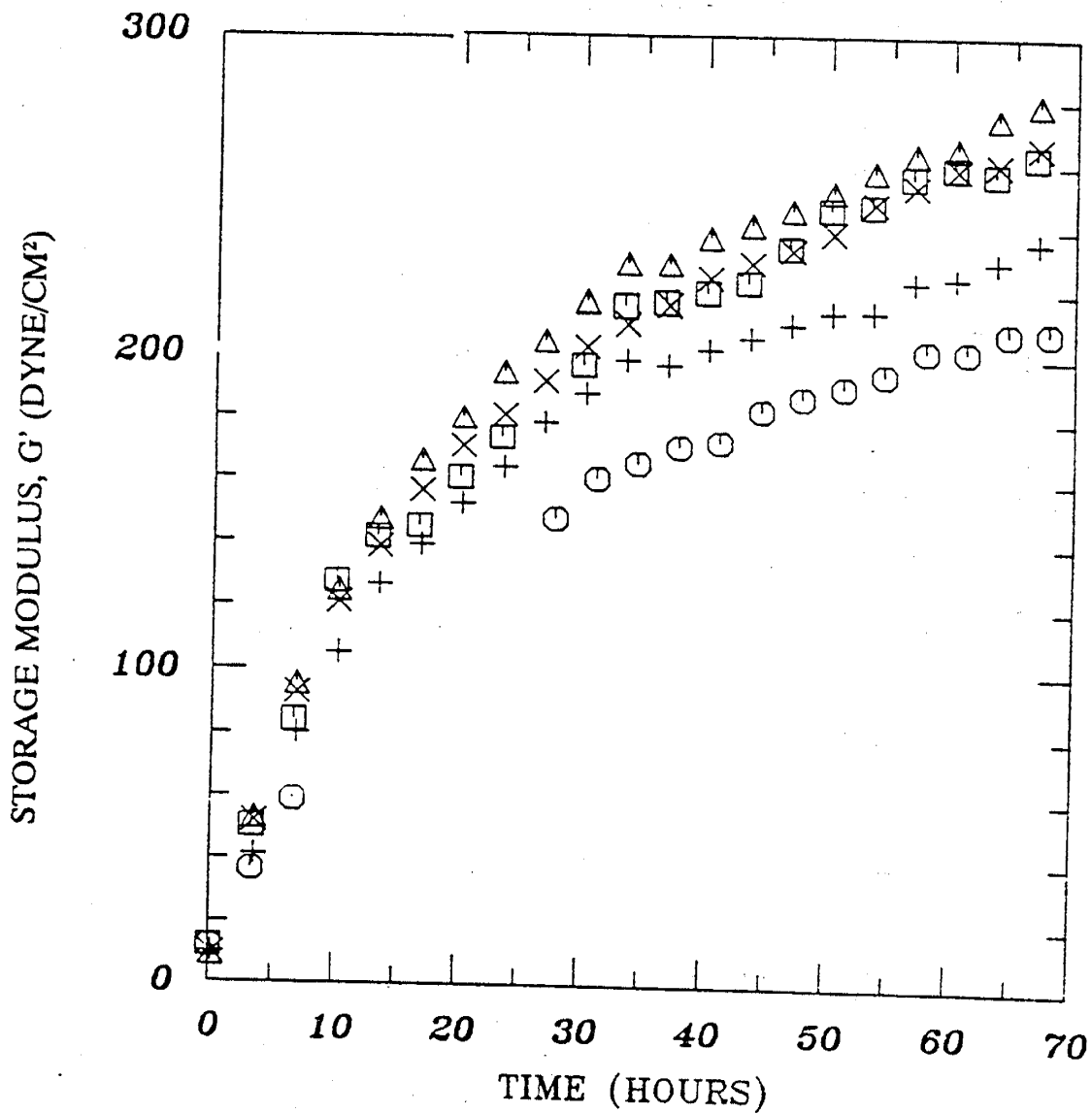


FIGURE 6.2 Development of Storage Modulus at pH 6 for the Xanthan Gel Solution Using Different Polymer Batches

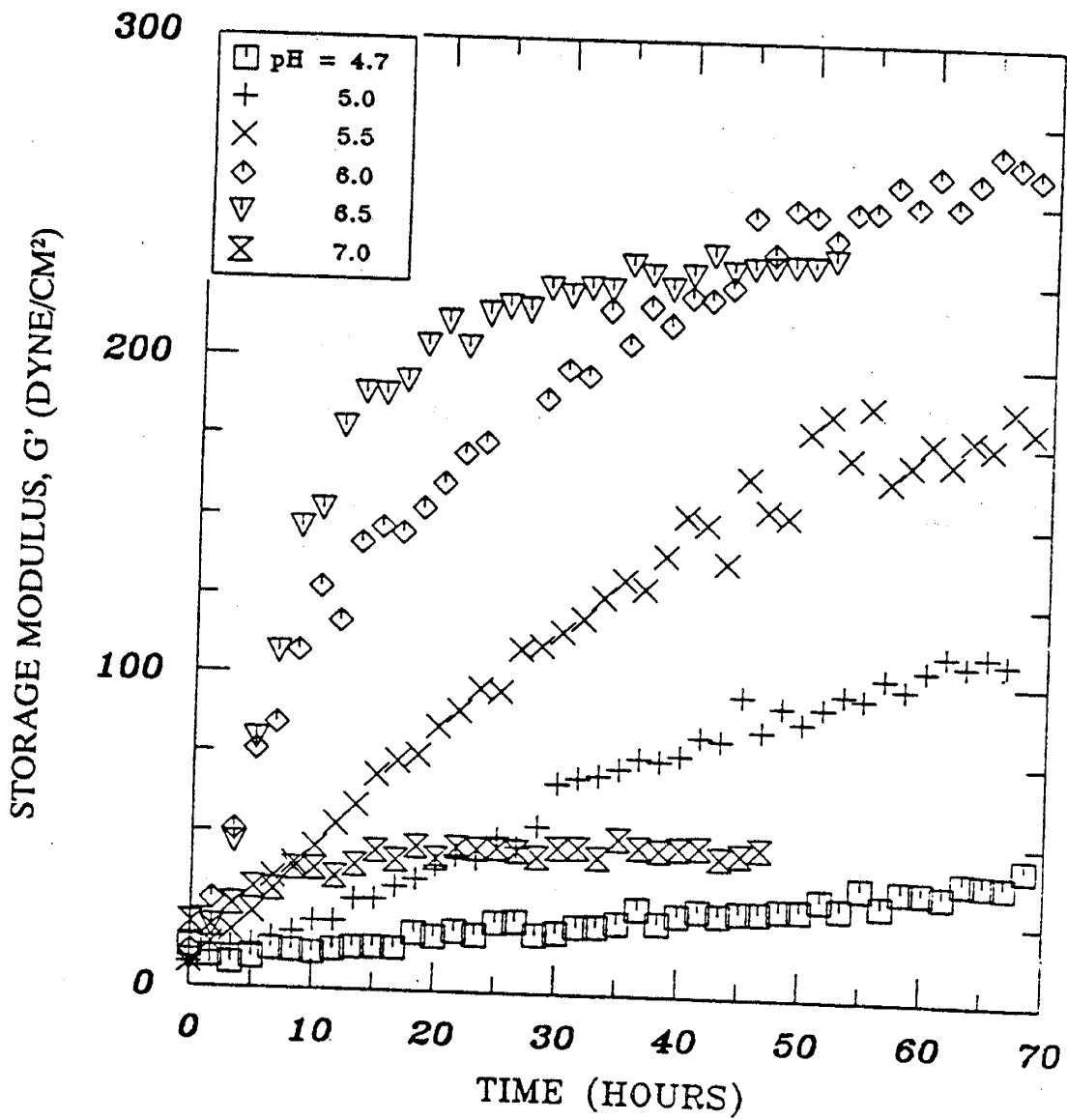


FIGURE 6.3 Effect of Initial pH on the Development of the Storage Modulus of the Gel Solution

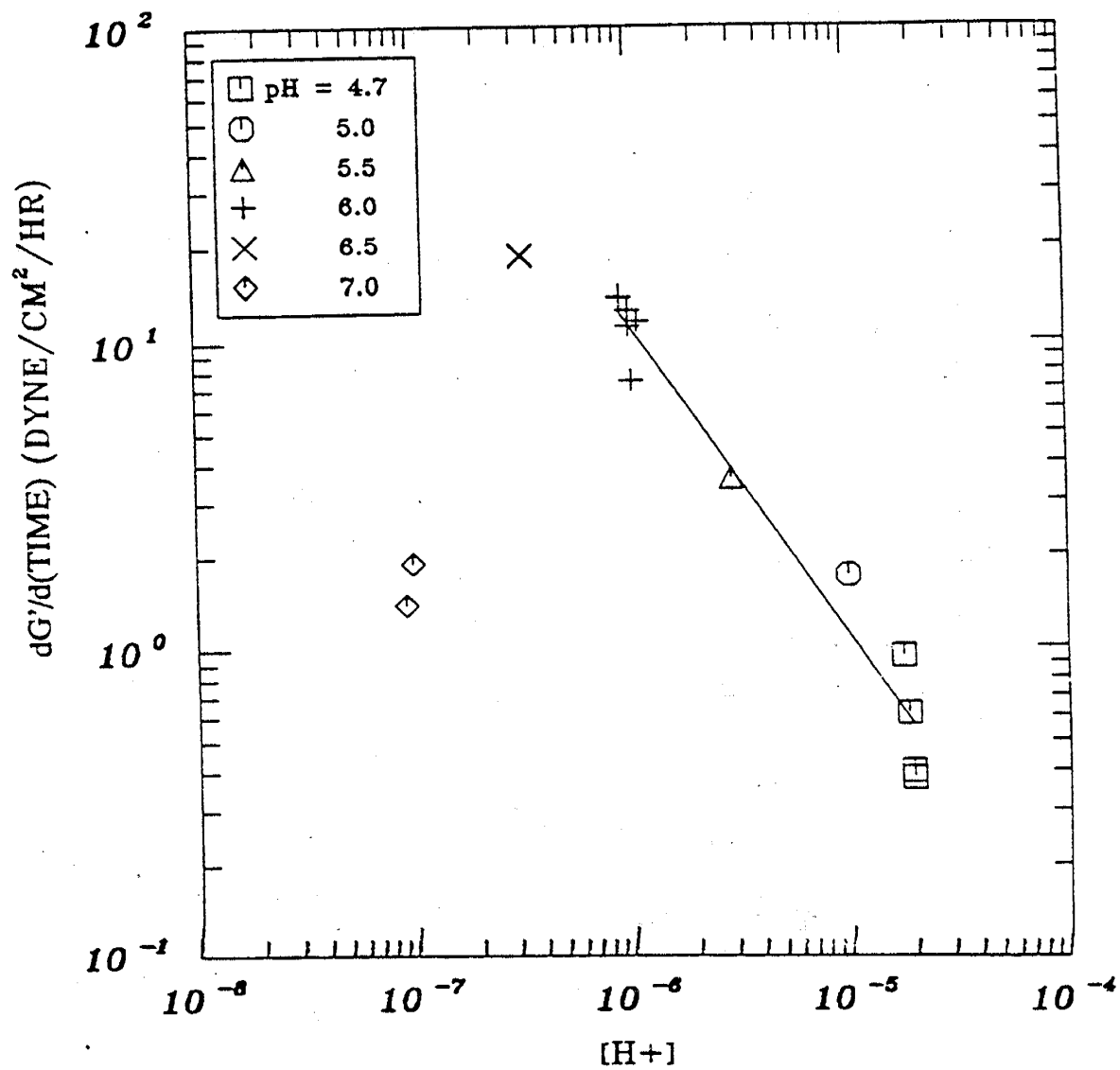


FIGURE 6.4 Correlation of the Initial Rate of Gelation with Hydrogen Ion Concentration

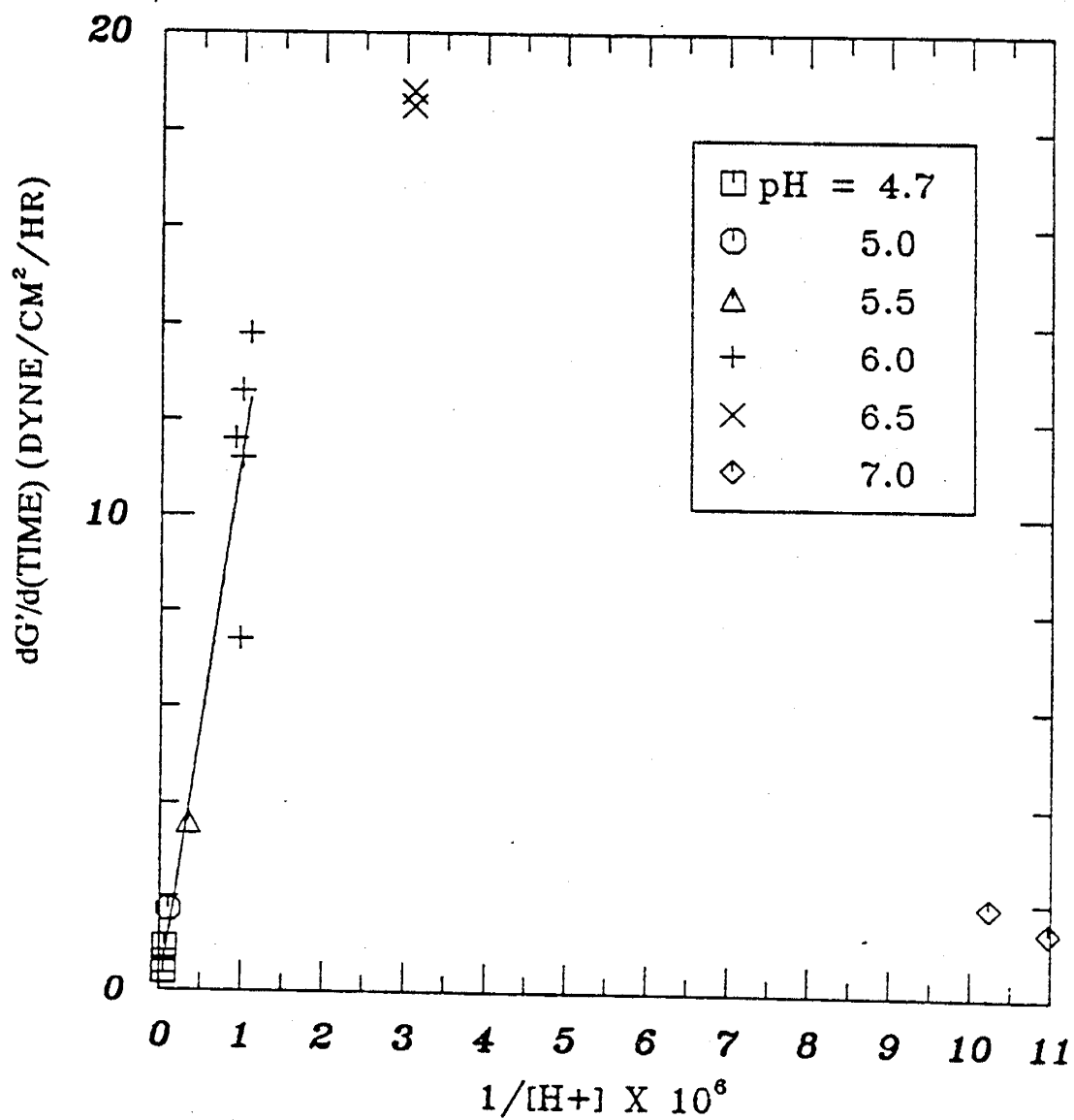


FIGURE 6.5 Correlation of Initial Rate of Gelation with Inverse Hydrogen Ion Concentration

STORAGE MODULUS, G' (DYNE/CM<sup>2</sup>)

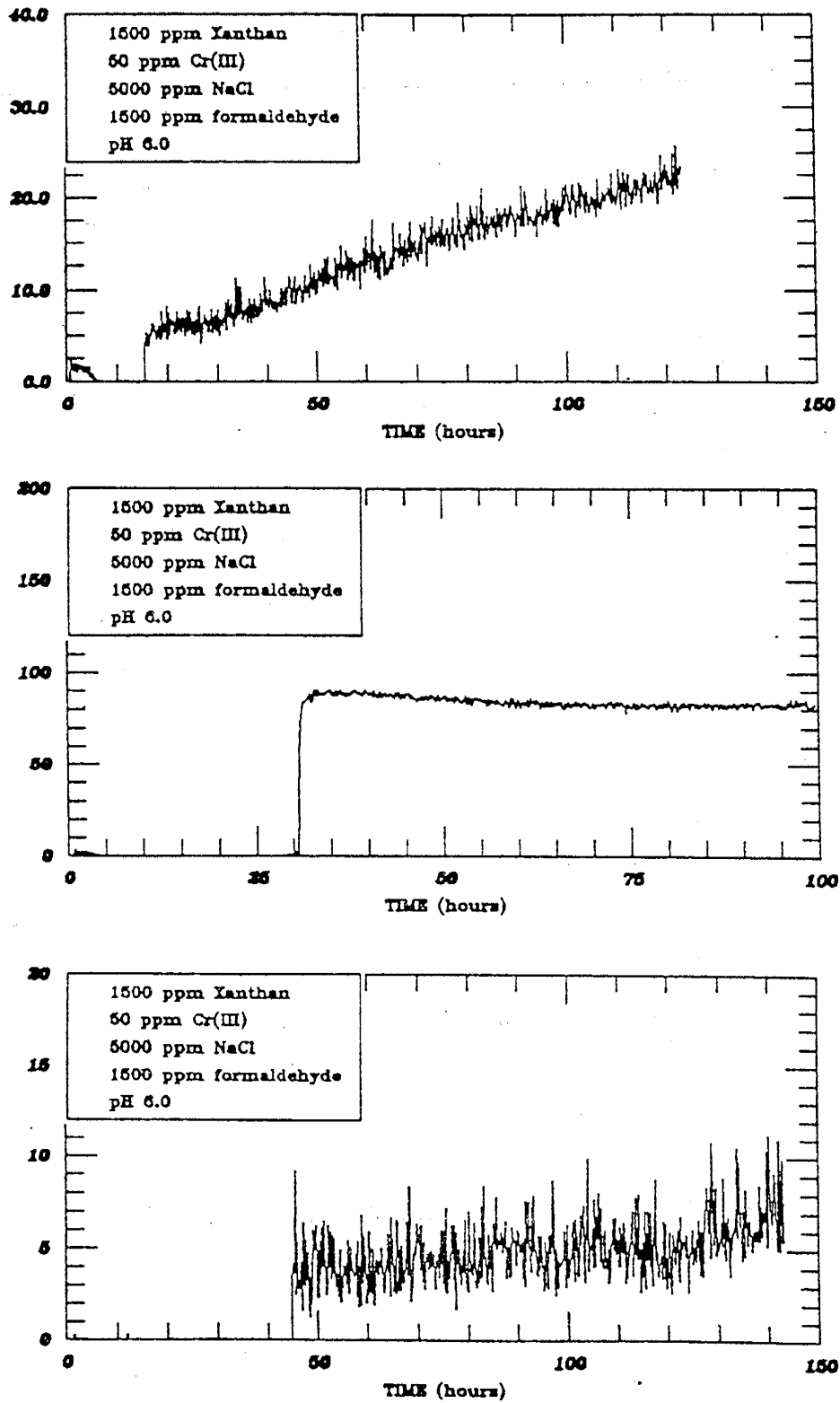


FIGURE 6.6 Effect of Continuous Shear on the Development of the Storage Modulus at pH 6.0

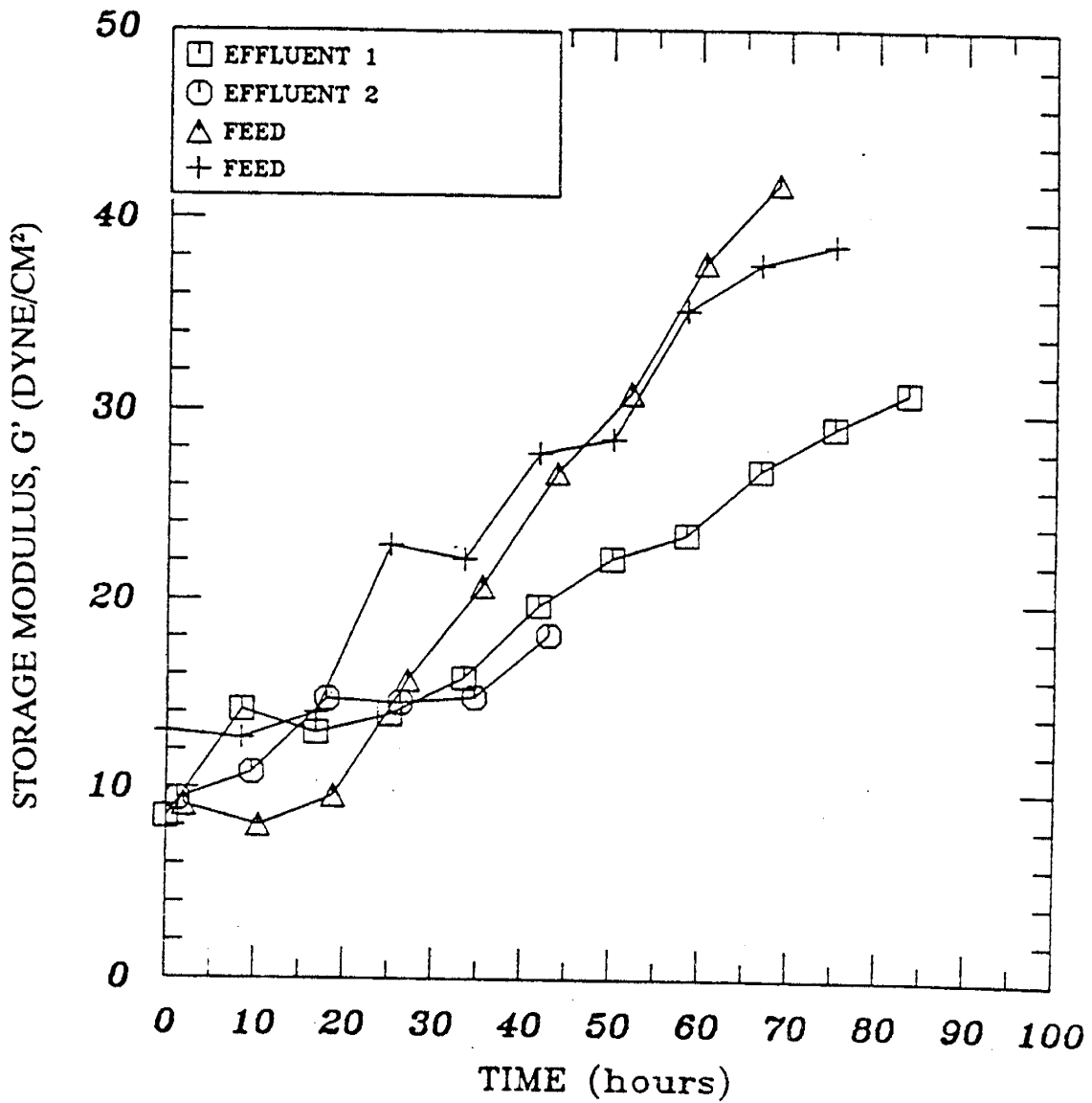


FIGURE 6.7 Development of the Storage Modulus with Time for Feed and Effluent Samples Used in Sandpack Experiments



## CHAPTER 7

### IN SITU GELATION OF A POLYACRYLAMIDE/Cr(III) SYSTEM IN UNCONSOLIDATED POROUS MEDIA

Principal Investigators: D.W. Green, G.P. Willhite

Graduate Research Assistant: Antonio Montes

#### 7.1 INTRODUCTION AND OBJECTIVES

Gelling polymer solutions exhibit complex flow behavior. The rheology of these gelling solutions is not understood fully but is affected by the shear rate that the gel systems experience during gelation. Results have been reported<sup>1</sup> on the effect of shear rate on the gelation of partially hydrolyzed polyacrylamide by Cr(III) using a Weissenberg rheogoniometer. The rate at which the gel structure developed declined with increasing shear rate for several systems studied.

The behavior of polyacrylamide/redox and xanthan/Cr<sup>3+</sup> gelling systems while they are displaced through unconsolidated sandpacks has been reported previously<sup>2</sup>. In situ gelation mechanisms were proposed in which aggregates formed by the reaction of the polymer and Cr(III) were filtered out of the polymer solution by reacting with previously retained molecules. Effects of flow rate (and thus shear rate) were observed in sandpack experiments, reported by Marty<sup>3</sup>, Hejri<sup>4</sup> and Jousset<sup>5</sup>.

This chapter describes studies of the in situ gelation of a polyacrylamide polymer/Cr(III) system in sandpacks. Work is in progress to identify the importance of the various mechanisms contributing to the increase in flow resistance as gel solutions flow through porous media.

The objectives of the research program were: 1) to identify a polyacrylamide polymer-Cr<sup>3+</sup> gelling system composition suitable for sandpack studies; 2) to evaluate the in situ gelation of this system in porous media; and 3) to ascertain the relative importance of the mechanisms involved in the in situ gelation of this system.7.2

#### 7.2 EXPERIMENTAL PROGRAM

The experimental program is based on conducting viscometric experiments in a viscometer and displacement experiments in unconsolidated porous media (sandpacks).

The first series of studies undertaken during the research period was focused on obtaining a Cr(III)-polyacrylamide system that would gel under conditions which can be studied in 4-ft long laboratory sandpacks at

reasonable reservoir flow rates. These results were used either to design in situ gelation experiments or to assist in the explanation of the phenomena observed in the in situ gelation experiments.

The second part of the study involved the displacement of gelling solutions through sandpacks to determine and evaluate the flow mechanisms prevalent in porous media. In situ gelation was studied by measurement and analyses of pressure changes collected during displacement experiments at constant frontal advance rates.

A description of the materials and techniques used in this research follows.

### 7.2.1 Selection of the Chemical System

Polyacrylamide polymer and chromium nitrate were the basic starting constituents of the gelling system, based on previous research carried out in the Tertiary Oil Recovery Project. The gel composition consisted of 5000 ppm polyacrylamide polymer, an amount to be determined of chromium nitrate, and 0.1M potassium nitrate.

The polyacrylamide polymer (PAam) used has a low degree of hydrolysis (below four percent) and a high molecular weight (between one to four million). It was supplied as a dry powder (Aldrich lot TV) and subsequently dispersed in a 0.1M  $\text{KNO}_3$  brine solution. All polymer solutions were stirrer-mixed for a day and then filtered through a 5-micron filter. The polymer solutions were allowed to stand for a few days after filtering for molecular disentanglement. The solutions were used within two weeks from preparation.

The crosslinking agent, Cr(III), was obtained from chromium nitrate salts ( $\text{Cr}(\text{NO}_3)_3 \cdot 9\text{H}_2\text{O}$ ) and was used immediately after dispersion in a 0.1M  $\text{KNO}_3$  solution.

### 7.2.2 Viscometric Studies

In gelling systems, pH is a critical variable. One of the characteristics of polyacrylamide/Cr(III) gelling systems is the reduction of pH upon mixing of the polymer and chromium solutions. All other conditions held constant, initial gel pH determines how fast a solution will gel. Rheological characterization experiments were carried out to evaluate the effect of initial gel pH upon gelation time. These experiments were done using a Brookfield Rheolog viscometer.

Normally, in beaker experiments, the gelling solution pH is either adjusted initially once or kept constant with time by adding a suitable amount of base. If such a batch-mixed system were injected into a sandpack, it would be difficult to control the pH of the injected solu-

tions, since the gel pH changes with time. An alternate way of achieving a constant initial gel pH is by adjusting the pH of the polymer solution before mixing it with the chromium solution. In this manner, the entire gelling solution starts off at the same initial pH and, therefore a constant gel time is obtained.

Viscometric studies were carried out to determine the gel time of the solutions in question under preestablished pH conditions. Figure 1 shows a schematic of the setup. The jacketed beaker was kept at constant temperature by means of a controller.

The polymer solution was weighed and pH-adjusted with potassium hydroxide in the beaker and the chromium solution was added to it. The gelling solution was stirrer-mixed, the spindle and pH electrode were inserted and the mixture was covered with oil to prevent evaporation. The spindle rotation was 12 RPM. As the gel point was approached, the gelling solution started creeping up the spindle. This phenomenon is called the Weissenberg effect and indicates that the solution has gelled. The data acquisition system (chart recorder) recorded the spindle deviation and pH data versus time.

Inconsistent data were obtained while measuring viscosities and gel times of stirrer-mixed gels in beakers in this manner. Stirrer mixing gave irreproducible gel times for the same gelling systems. It was decided to mix the Cr and PAam inline. The gelling solution was mixed with a static inline mixer and then inserted into the viscometer for gel time measurements. This inline mixing procedure more closely approximated mixing of the gelling system components prior to injection into sandpacks. The injection of a gel system through an in-line mixer has previously given satisfactory gels in porous media.

This procedure still gave inconsistent gel time data. It was decided to add sodium azide (a biocide) to the polymer solutions to help stabilize them. This method resulted in very good reproducibility of gel time data, but for reasons other than bacteriological degradation of the polymer solution.

### 7.2.3 Displacement Apparatus

A schematic diagram of the experimental apparatus is shown in Figure 2. The system was enclosed in a constant-temperature air-bath to minimize variations in pumping rates due to thermal variations. Polymer and chromium solutions were displaced by Constametric™ pumps. They were joined at the sandpack inlet by a static inline mixer (Komax). The mixer and sandpack temperatures were held at 25°C by a water bath. An ISCO fraction collector was used to collect effluent fractions for later analysis. Pressure drops were measured across the core length as well as across each sandpack section by Validyne pressure transducers and recorded on a data-acquisition system.

#### 7.2.4 Preparation and Properties of Sandpacks

The coreholder consisted of a 4-ft-long, 1.5"-I.D. plexiglass tube fitted with two endcaps attached with eight screws and sealed with a rubber O-ring. Grooves were cut in the endcaps for uniform flow distribution of entering and exiting fluids. Eleven pressure ports, each 10 cm apart, were drilled along the length of the coreholder and fitted with 1/8-inch pipe, 1/8-inch Swagelok fittings.

An automatic packer built in the Tertiary Oil Recovery Project laboratory was used to pack the tube with acidized Ottawa F-140 sand. The sections at the inlet and outlet of the sandpack contained a coarser grade Ottawa sand to support the finer sand. The permeability in these sections was considerably higher than that of the rest of the sandpack. Thus, these end sections were not included in differential pressure measurements. Also, these sections were omitted from the pressure measurements to eliminate possible end effects.

Teflon screens were placed next to the endcaps to prevent movement of the sand into the inlet and outlet ports and for support. The material placement sequence at the ends of the core was as follows: endcap, coarse screen, fine screen, coarse sand, fine sand. All pressure port fittings were installed with screens as well to prevent port plugging.

The coreholder was checked for leaks before and after packing the sand. The pack was pressurized, saturated with CO<sub>2</sub> and evacuated several times. After evacuation, the sandpack was saturated with 0.1M KNO<sub>3</sub> solution.

Porosity was measured gravimetrically. The cores were weighted before and after saturating them with brine. Permeability was determined by measuring the pressure drop across the core at different flow rates. Permeabilities were compared at three flow rates and averaged over each section. To attain a fairly stable sand pH, ten to twenty pore volumes of brine (at pH = 5.0) were displaced prior to each core flood.

#### 7.2.5 In Situ Gelation Studies

Two Constametric™ pumps (models I and III) were used to displace the polymer and chromium solutions into the inline mixer. During a flow displacement experiment, the sandpack was placed in a water bath. A Fisher Scientific Isotemp Immersion Circulator model 730 temperature controller was used to keep the water temperature constant.

Differential pressure was measured by a series of Validyne pressure transducers. The transducers were calibrated following manufacturer recommendations. Diaphragm sizes ranged from 20 to 100 psi. To determine a pressure drop, the voltage reading under flowing conditions was

subtracted from a baseline reading under no flow conditions. This difference was directly proportional to the pressure drop.

### 7.3 RESULTS AND DISCUSSION

#### 7.3.1 Viscometric Studies

The initial gel pH is an important factor in the behavior of the gels. The initial gel pH can be adjusted in changing the polymer pH before mixing or by adding base to the gelling mixture. In an inline mixing procedure, the first method is preferable. The effect of initial polymer pH is shown in Figure 7-3.

In general, after an induction period of several hours, the solutions began to gel. The point of departure from a baseline in the viscometer readout was considered the gel time. Gels with lower initial pH appeared weaker than higher pH gels. Gel times following this procedure ranged from a few hours to about a day. An example of the viscosity-time behavior for one gelling system is shown in Figure 7-4.

Figure 7-3 shows that gel times in the neighborhood of 15-20 hours may be obtained by suitably modifying the initial polymer pH. A gel time of around 15-16 hours was used in displacement experiments.

The addition of sodium azide to the polymer solutions resulted in consistent gel time behavior. It is believed that the sodium azide is believed to act as a complexing agent in the gelling solution, probably retarding crosslinking of the polymer molecules with  $\text{Cr}^{3+}$  ions.

#### 7.3.2 In situ Gelation

In situ gelation of the polyacrylamide/chromium(III) system in 0.1M  $\text{KNO}_3$  solution was studied in several experiments. Results of three experiments are presented in this report.

Experimental results are presented for two gelation runs at an injection velocity of about 3 ft/day (LSPG3-90, LSPG4-90) and one at a velocity of 8 ft/day (LSPG5-90). Table 7-1 presents the conditions under which these experiments were performed.

Figure 7-5 depicts the behavior of the gelling solution in sandpack LSPG3-90. The figure shows that section A (located near the inlet of the sandpack) plugged after approximately 0.8 to 0.9 pore volumes were injected. In sandpack LSPG4-90 (Figure 7-6), section A plugged almost immediately. In the higher injection velocity experiment (LSPG5-90), almost two pore volumes were injected into the core before it plugged. Figure 7-7 shows the pressure drop behavior along all sections of the sandpack.

Upon examination of the pressure drops in Figure 7-7, a large increase in flow resistance occurred preferentially along the middle sections of the sandpack (sections D, E, F). This behavior is similar to that experienced in sandpacks with other gelling systems, such as the polymer/chromium(IV)/thiourea system.<sup>2</sup>

When the gelling solutions are injected at the lower rates, it is believed that the lower core pH prevents the gel from blocking the porous medium. At a core pH equivalent to that of the incoming gel solution, chromium retention on to the rock may be such that the first core section is immediately plugged up. At the higher injection velocities, we are able to propagate the gelling solution further into the core and chromium deposition on to the rock is not as rapid.

As the gelling solution is propagated through the porous media, gelation is retarded by the lower core pH, even though the injected solution is at the desired pH. After some time, as chromium is retained by the rock, increasing the effective local chromium concentration, the flowing solution finally gels. This gel time behavior with decreasing pH agrees with the gelling solution behavior in viscometric studies.

An increase in flow resistance is observed in the middle sections of the core. At lower flow rates, permeability reduction occurs when incoming polymer is retained by interacting with Cr(III) previously retained on the porous rock.

#### 7.4 CONCLUSIONS

From the experiments previously discussed, it is possible to draw some conclusions about the behavior of the gelling system, both in situ and in beakers.

- A reduction in core pH resulted in an increase in gel time of the injected solution. This is an expected behavior.
- In situ gelation in unconsolidated sandpacks occurred much earlier than gelation in beaker tests where the gel solutions were maintained under conditions of no shear. At higher flow rates, the gelling solution is propagated further into the sandpack.

#### REFERENCES

1. Bhaskar, R.K., Stinson, J.A., Willhite, G.P., and Thiele, J.L., "The Effects of Shear History on the Gelation of Polyacrylamide/Chromium(VI)/Thiourea Solutions," SPE Res. Eng., pp. 1251-1256, (November 1988).

2. McCool, C.S., Green, D.W., and Willhite, G.P., "Permeability Reduction Mechanisms Involved in the In Situ Gelation of a Polyacrylamide/Chromium(VI)/Thiourea System," paper SPE/DOE17333, presented at the SPE/DOE Enhanced Oil Recovery Symposium, Tulsa, OK, April 17-20, 1988.
3. Marty, L., Willhite, G.P. and Green, D.W., "The Effect of Flow Rate on the In Situ Gelation of a Chrome/Redox/Polyacrylamide System," paper SPE 18504, presented at the SPE Symposium on Oilfield Chemistry, Houston, TX, February 8-10, 1989.
4. Hejri, S. Ph.D. Dissertation, University of Kansas, 1989.
5. Jousset, F., Green, D.W. and Willhite, G.P., "Effect of High Shear Rate of the In Situ Gelation of a Xanthan/Cr(III) System," paper SPE/DOE 20213, presented at the SPE/DOE Enhanced Oil Recovery Symposium, Tulsa, OK, April 22-25, 1990.

TABLE 7.1  
Gel Displacement Conditions

LSPG3-90

- Chemical System
  - 5000 ppm PAam, pH adjusted to 5.07
  - 75 ppm chromium nitrate
  - 563 ppm sodium azide
  - 10100 ppm (0.1M) potassium nitrate
  - initial gel pH = 4.88, nominal gel time = 14 hours
- Porous medium
  - porosity = 35.2%, permeability = 3.3 darcy
  - core effluent pH = 4.22
  - average flow rate = 2.3 ft/day

LSPG4-90

- Chemical System
  - 5000 ppm PAam (lot TV) pH adjusted to 5.15
  - 75 ppm chromium nitrate, pH = 3.24
  - 375 ppm sodium azide
  - 10100 ppm (0.1M) potassium nitrate
  - initial gel pH = 4.74, gel time = ~14 hours
- Porous medium
  - porosity = 38.0 %, permeability = 3.6 darcy
  - core effluent pH = 4.90 (at start), 4.77 (at end)
  - average flow rate = 3 ft/day

LSPG5-90

- Chemical System
  - 5000 ppm PAam (lot TV) pH adjusted to 5.14
  - 75 ppm chromium nitrate
  - 563 ppm sodium azide
  - 10100 ppm (0.1M) potassium nitrate
  - initial gel pH = 4.96, rheolog gel time = 36 hours
- Porous medium
  - porosity = 35.1 %, permeability = 4.1 darcy
  - core effluent pH = 5.16 (at start), 5.08 (at end)
  - average flow rate = 7.68 ft/day

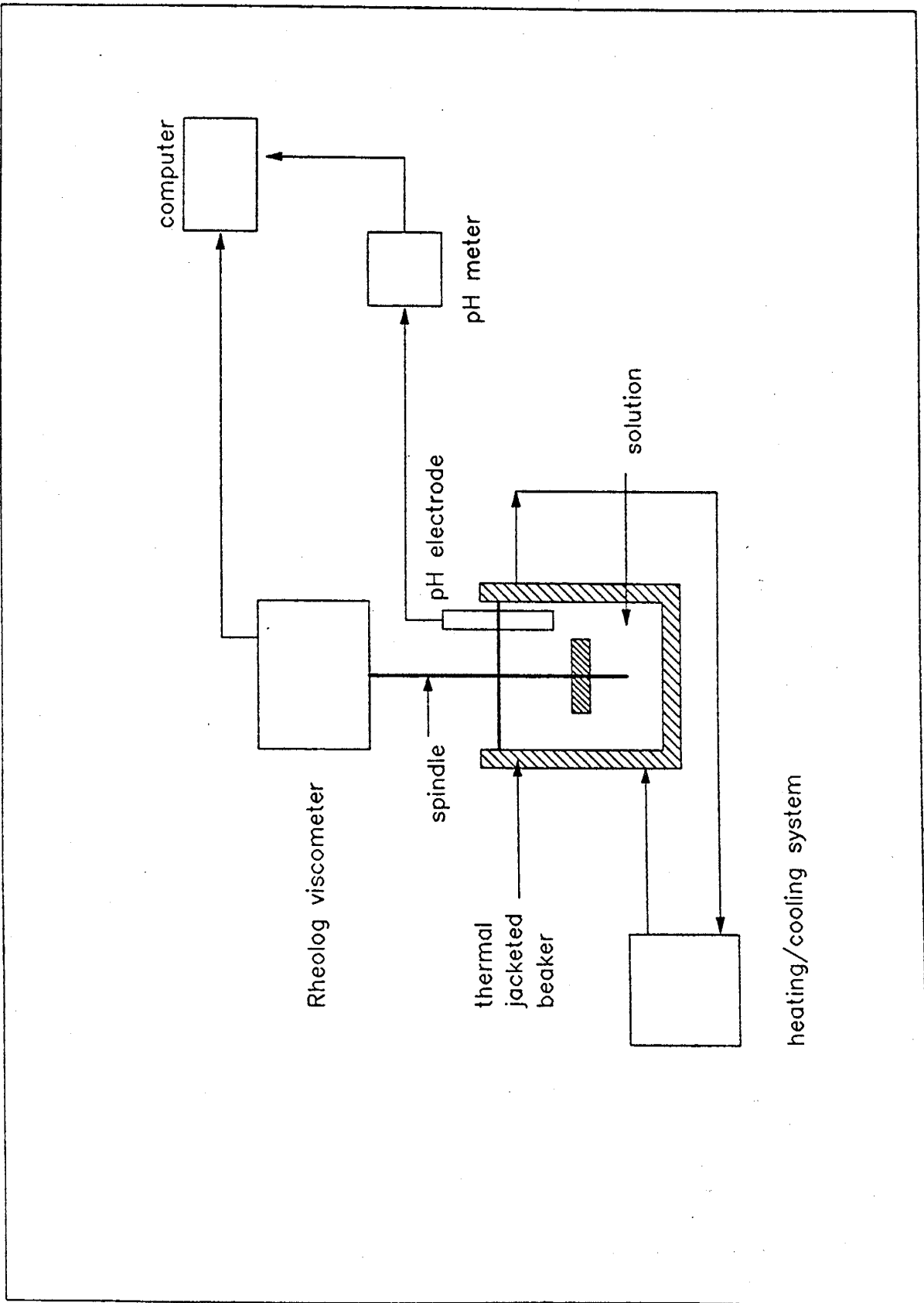


Figure 7-1: Gel Time Experimental Setup

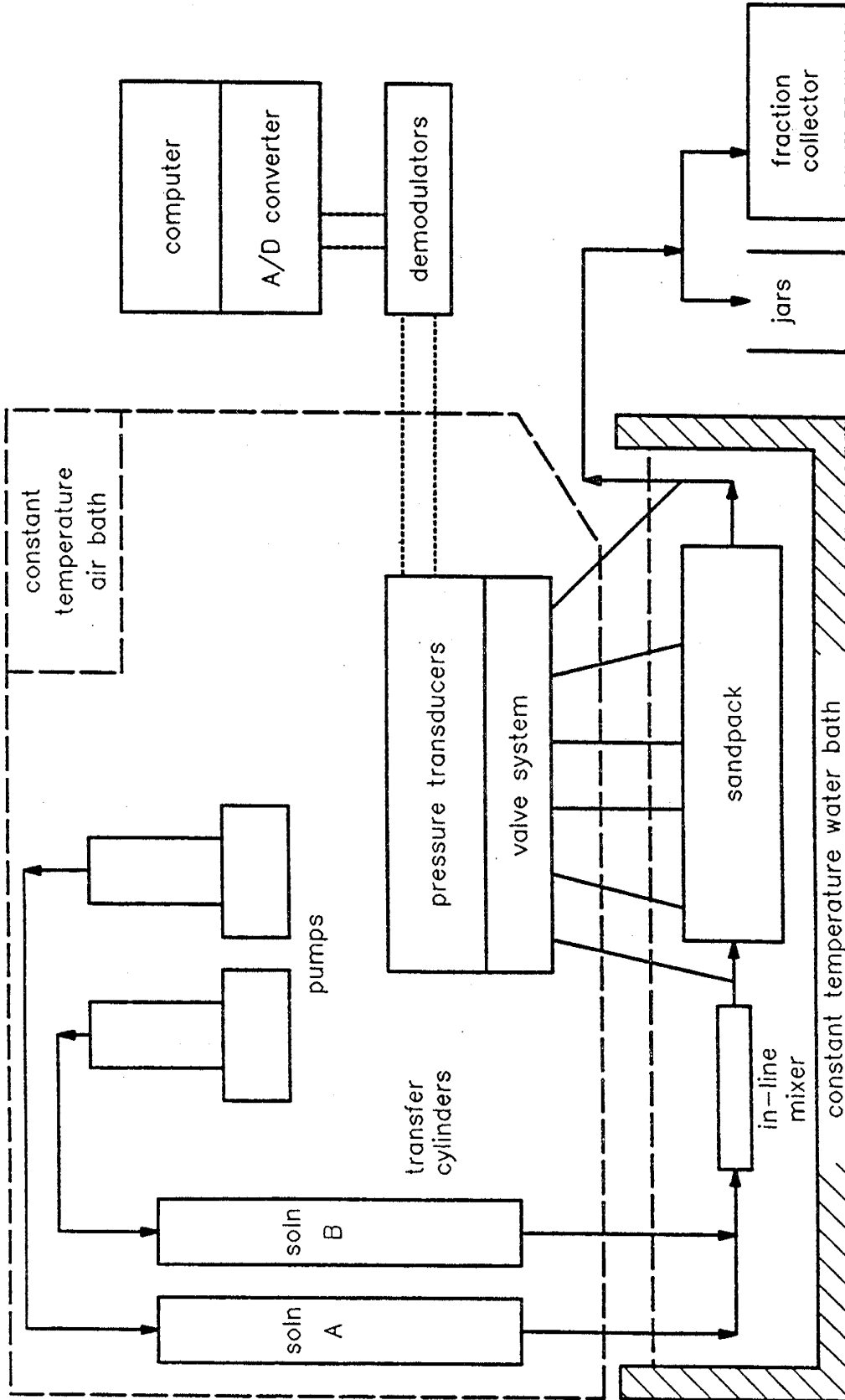


Figure 7-2: Schematic Diagram of the Apparatus for the Gel Displacement Experiments

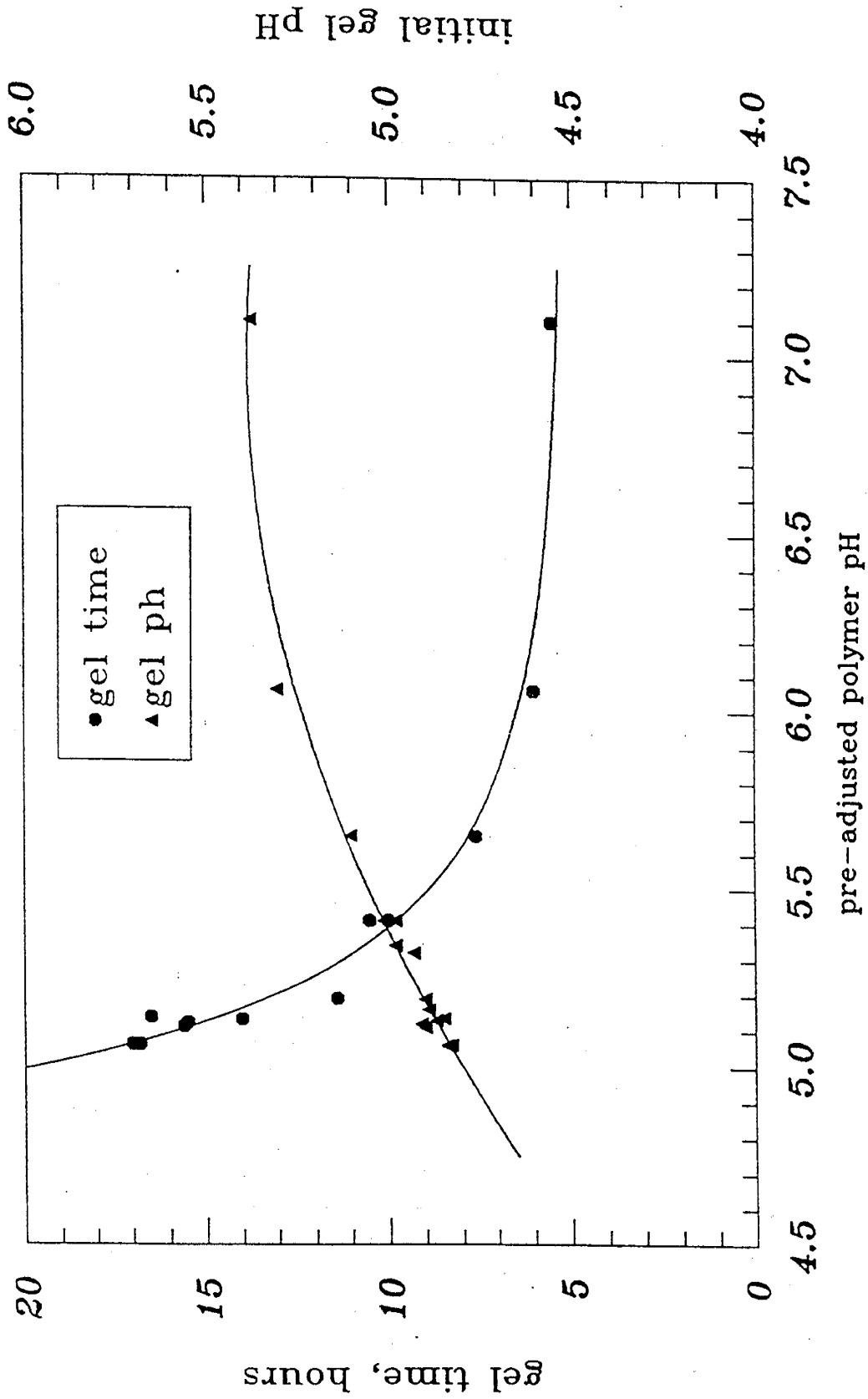


Figure 7-3: Rheolog Viscometer Gel Time and pH  
5000 ppm PAAM (lot TV), 75 ppm Cr<sup>3+</sup> System

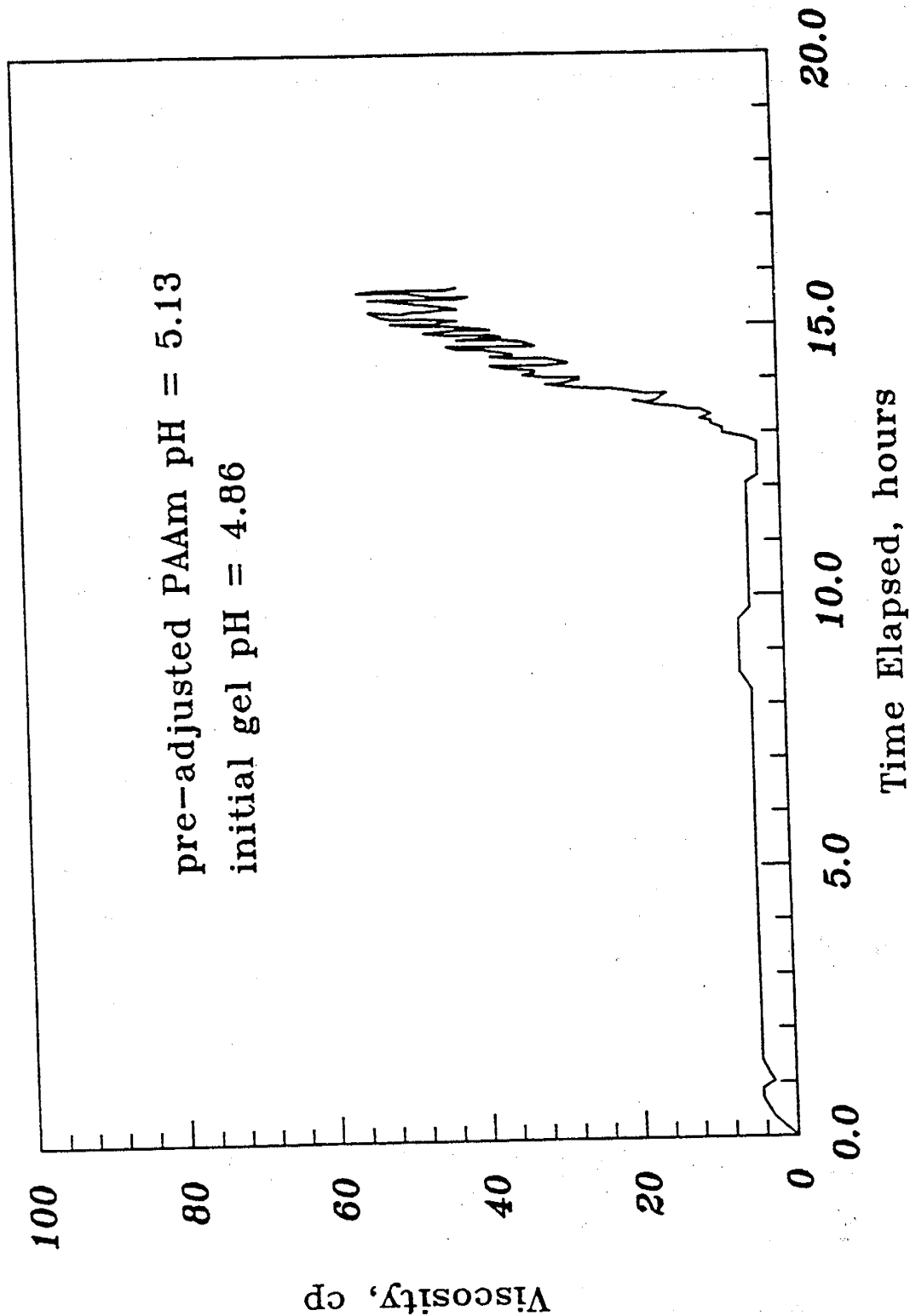


Figure 7-4: Viscosity-Time Behavior for a Typical 5000 ppm PAAM (lot TV), 75 ppm Cr<sup>3+</sup> System

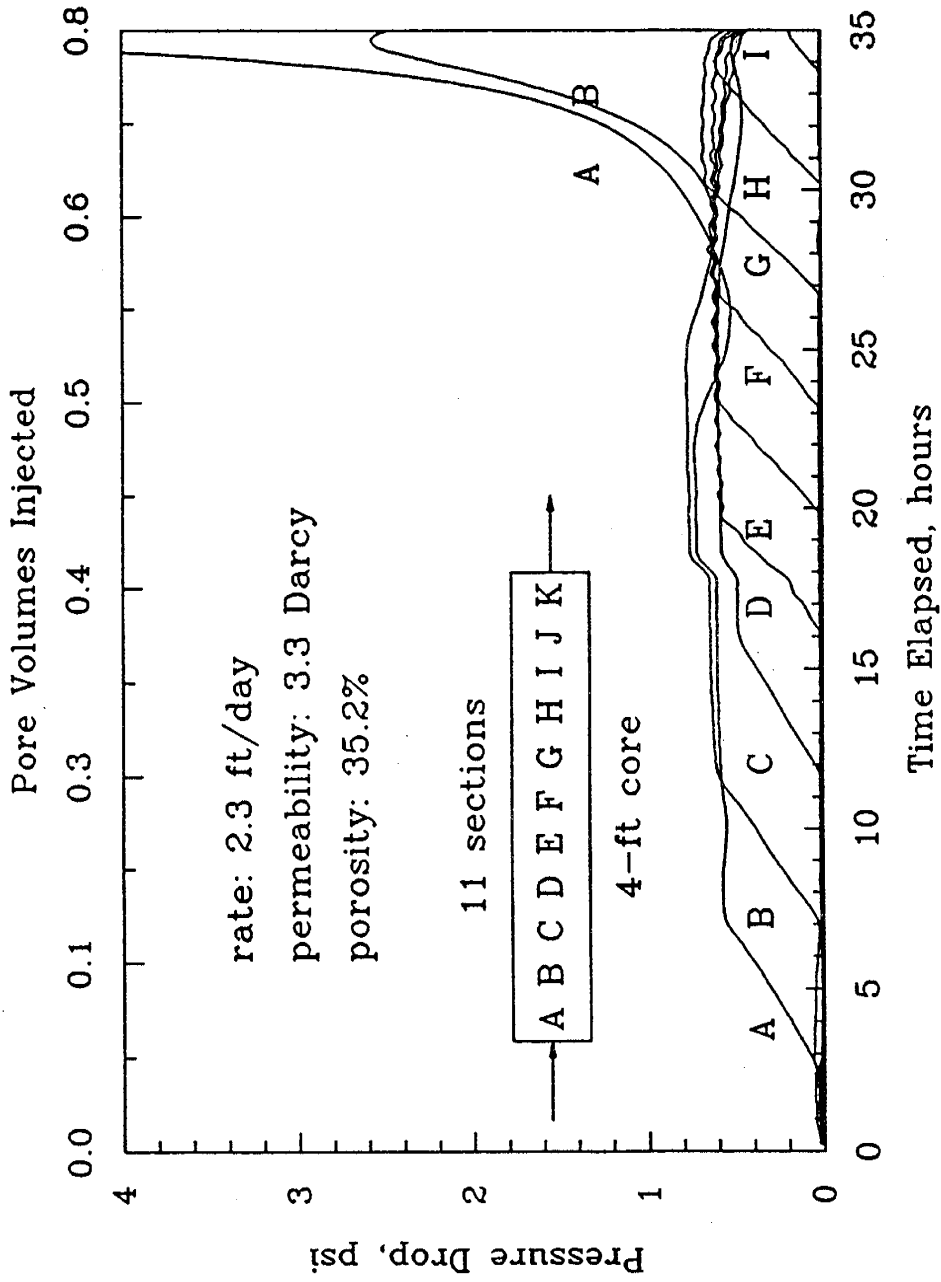


Figure 7-5: Gel Solution Displacement in Sandpack LSPG3-90  
 5000 ppm PAAM (lot TV), 75 ppm Cr<sup>3+</sup> System

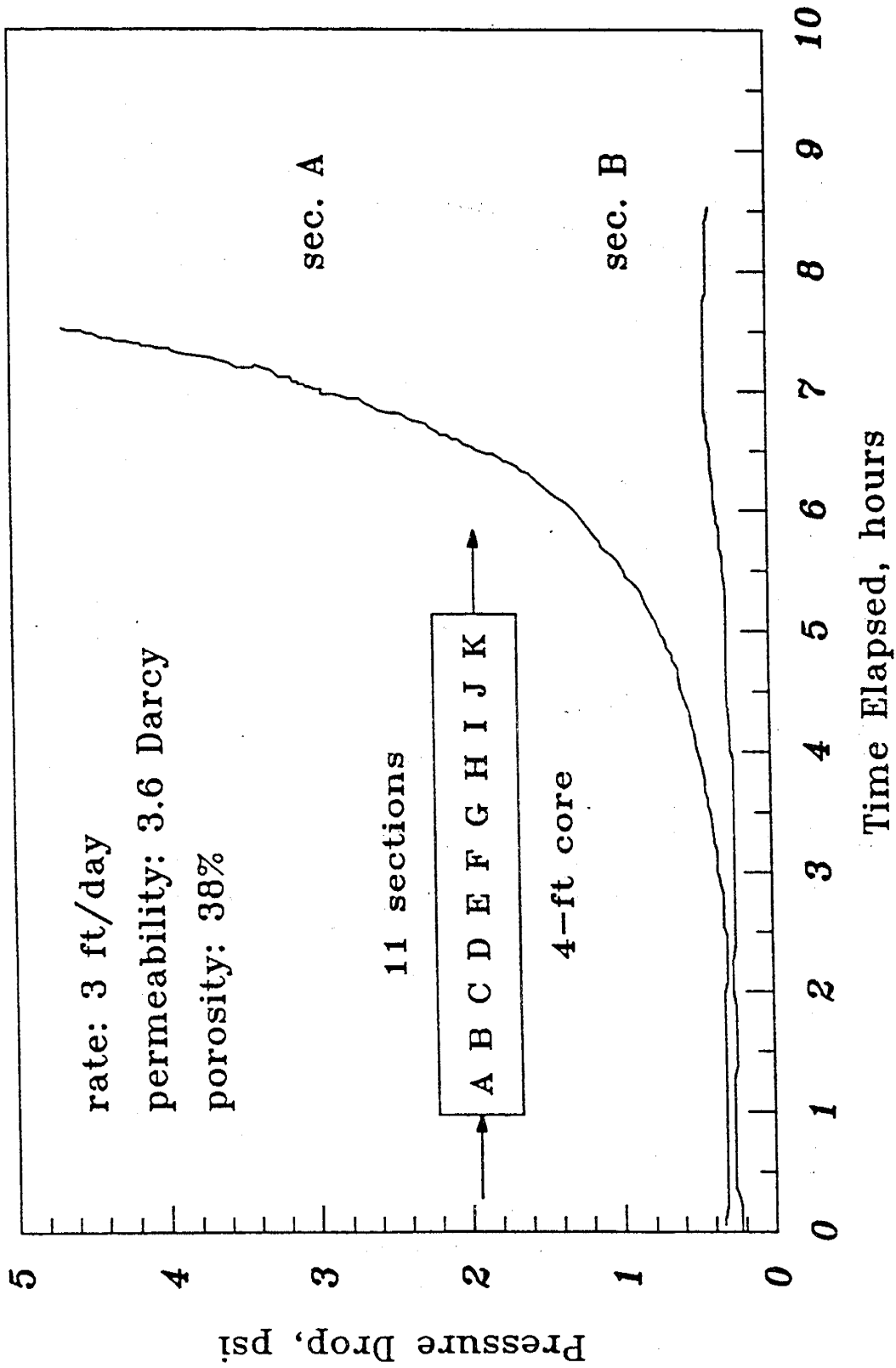


Figure 7-6: Gel Solution Displacement in Sandpack LSPG4-90  
 5000 ppm PAAM (lot TV), 75 ppm Cr<sup>3+</sup> System

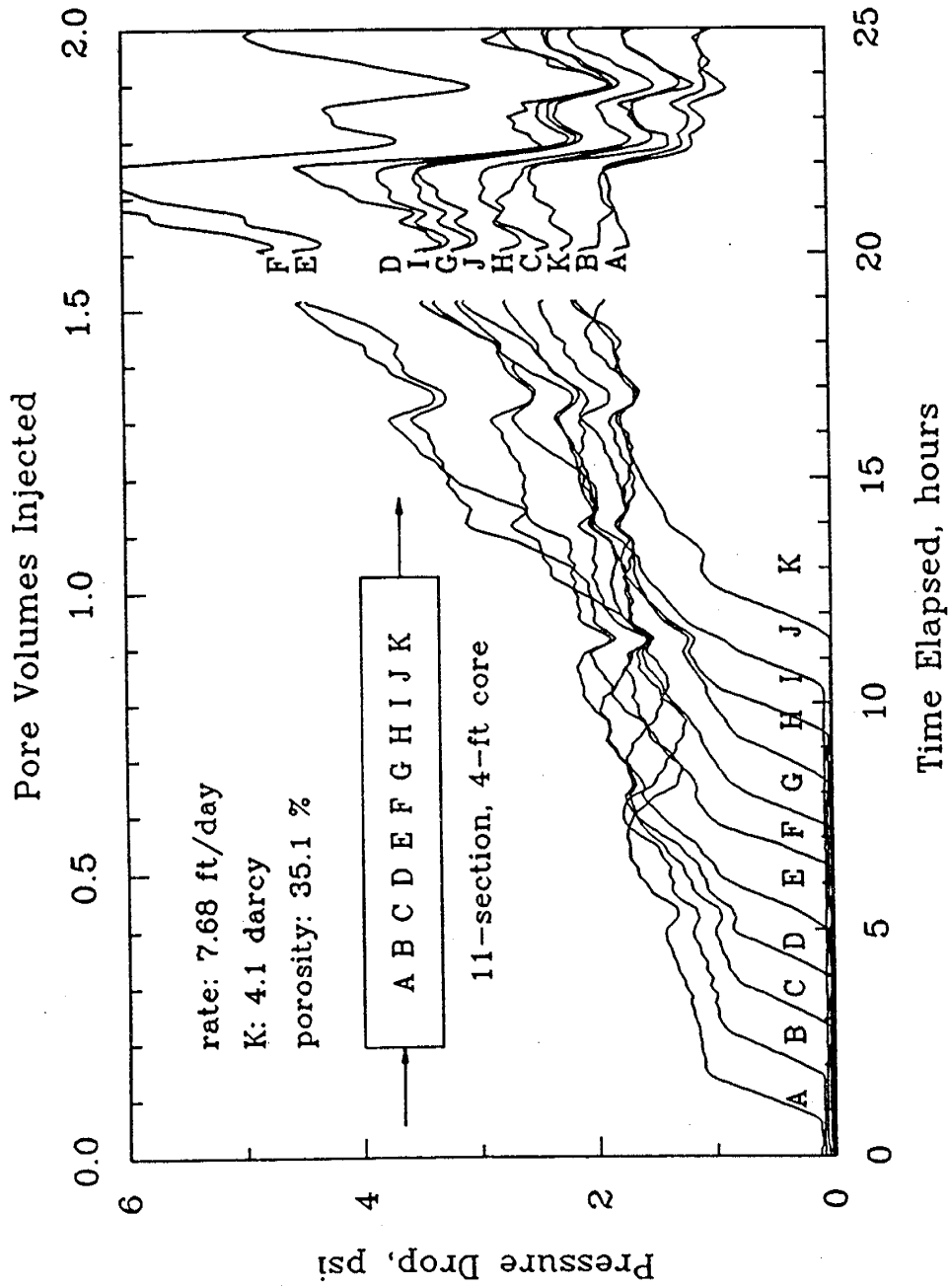


Figure 7-7: Gel Solution Displacement in LSPG5-90  
 5000 ppm PAAM (lot TV), 75 ppm Cr<sup>3+</sup> System



## CHAPTER 8

### MATHEMATICAL MODELING OF IN SITU GELATION IN POROUS MEDIA

Principal Investigators: G.P. Willhite, D.W. Green

Graduate Research Assistant: Burt J. Todd

#### 8.1 INTRODUCTION AND OBJECTIVE

Water injection is usually an efficient, inexpensive secondary recovery method. However, permeability heterogeneities in the reservoir cause channeling of the injected water, lowering sweep efficiency and bypassing oil in lower permeability zones. The in situ gelation process offers a low cost method to redirect injected water from these highly conductive "thief zones" into less permeable zones, which often constitute the bulk of the oil reservoir. The low permeability zones often contain significant reserves of oil not previously swept by injected water. When successful, in situ gelation treatments extend the economic life of waterfloods and generate additional oil reserves.

Experimental results reported by McCool<sup>1</sup>, McCool et al.<sup>2</sup> and Marty et al.<sup>3</sup> show that injecting a mixture of thiourea, dichromate and polyacrylamide into a sandpack gradually plugs the porous medium some distance behind the front of injected chemicals. The buildup of flow resistance occurs in a localized area, and several pore volumes of gelling solution flow through this area before complete plugging occurs (See Figure 8.1). Furthermore, the age of gelling solution moving through the zone of flow resistance is always much younger than the gel time of the solution in a beaker. An in situ gelation mechanism was hypothesized based on filtering large pre-gel clusters out of the gelling solution. The sandpack gradually plugged as additional gelling solution was pumped through the sandpack.

The objective of the research reported in this chapter was to develop a numerical model of the in situ gelation process that is consistent with experimental data and models developed in Tasks I and II. Results from this model were compared to displacement data measured in linear sandpacks by McCool<sup>1,2</sup>, Marty et al.<sup>3</sup>, and Hejri<sup>4</sup>. Because the numerical model correctly simulated those data, the filtration hypothesis was confirmed as a viable explanation of behavior occurring during in situ gelation displacements. The linear model was then converted to radial coordinates and scaled up to reservoir size. The radial model was used to investigate critical process variables and to develop guidelines for the design of field applications.

## 8.2 BACKGROUND

When this project was conceived, there were no mathematical models of in situ gelation available in the literature. During the period of development of the model presented in this report, three models have been described in the literature for simulation of in situ gelation. Sorbie<sup>5,6,7,8</sup> developed a mathematical model of in situ gelation based on bulk gelation of the gel solution as it flowed in porous media. The model did not account for experimental observations that plugging occurred more rapidly in porous media displacements than beaker gel times would indicate. Modifications to the UTCHEM simulation model<sup>9,10</sup> were made to simulate gelation kinetics by adding reaction rate equations based on bulk gelation studies. A similar approach was reported recently<sup>11,12</sup> in which the BOAST reservoir simulator was to be modified to simulate in situ gelation.

## 8.3 MODEL FORMULATION

None of the models described in the previous section correctly simulate the in situ gelation behavior of the gelling systems studied during this research project. The model developed under this contract is based on the filtration of gel aggregates from a gel solution. This section describes a conceptual model of the in situ gelation process and develops mathematical equations to model the process. The model was developed by combining transport equations for the various chemical species in porous media with models of filtration processes. Equations describing chemical reaction kinetics were taken primarily from previous research conducted under this research contract. The numerical model is described in detail in reference 13.

## 8.4 RESULTS: SIMULATION OF MARTY et al.'s SYSTEM

### 8.4.1 Objective

The objective of this task is to develop a numerical model based on physical principles that will predict the location and timing of the large pressure drops that occur during in situ gelation displacements. The model was first verified by matching experimental data by Marty et al.<sup>3</sup>, and later was extended to match displacement data of other experimentalists.

Marty et al.'s system was chosen for the initial match because it is the best-characterized of the gelation systems simulated in this project. The thiourea/dichromate reduction reaction is being studied by Maxcy<sup>14</sup> and was studied by Southard<sup>15,16</sup>, Cr<sup>+3</sup> attachment to polymer

was studied by Hunt et al.<sup>17</sup>, and  $G'$  vs. time data were taken by Bhaskar<sup>18</sup>. Also, Marty et al. performed displacements at five different injection rates, covering a range of shear behavior. This wealth of data allows development of a comprehensive numerical model incorporating the full range of kinetic and rheological mechanisms.

After matching Marty's displacements and establishing base values for the parameters, the model was extended to match the displacements of McCool<sup>1</sup> and McCool et al.<sup>2</sup>. McCool used a gelling system of 4210 ppm of the cationic polyacrylamide Watercut-160, 383 ppm thiourea and 383 ppm sodium dichromate. The cationic polymer is similar to the anionic polyacrylamide used by Marty et al., but exhibits a greater tendency to form large aggregates in membrane dialysis experiments<sup>1,2,3</sup>. The in situ gelation model matched McCool's displacement data with minor adjustments in the parameters. Results of the McCool simulations are presented in Section 8.5.

In situ gelation displacements have also been conducted using solutions of  $Cr^{+3}$  and xanthan biopolymer<sup>4</sup>. Biopolymer molecules are relatively stiff, rod-like structures that behave differently than the more flexible polyacrylamide coils. Alterations made in the model to describe biopolymer systems and the results of the biopolymer simulations are described in Section 8.6.

#### 8.4.2 Multivariate Minimization

The in situ gelation model (named BOB) is based on physically meaningful parameters whenever possible. However, the model contains seven parameters whose numerical value cannot be directly measured. These parameters represent the effect of known physical mechanisms whose behavior is difficult or impossible to isolate and quantify in a laboratory. These seven parameters are

1.  $C_{f(i)}$ ,  $i = 1, 5$  (compaction factors upon deposition for each of the five polymeric size categories).
2. PSR (Pseudo rate constant in the collision efficiency equation).
3. GIP (Gelation Inhibition Parameter - the concentration of any species attached to polymer in a deposited polymer aggregate, divided by the local concentration of that component in solution.)

For each gelling system there are optimal values of these parameters that enable the model to most nearly replicate in situ gelation displacement behavior over a range of flow rates. Finding the parameter optima is then a multi-variate minimization problem.

### 8.4.3 Discussion of Parameters

Because modeling parameters represent the composite effects of several mechanisms, it is useful to describe those mechanisms and their functions in the in situ gelation model. Because the five compaction factors are strongly correlated, the seven total parameters can be condensed into just three groups - compaction factors, the filtration rate constant and the gelation inhibition parameter. This greatly simplifies the multivariate minimization process.

Compaction factors define the amount polymer molecules or clusters compact when they deposit on the porous medium. Polymer molecules in non-gelling polymer solutions are known to occupy less volume when deposited than in solution<sup>19</sup>. Fractal geometry principles imply that large, densely crosslinked polymer aggregates should compact less on deposition than small clusters or single polymer chains. This model includes separate compaction factors for each of the five polymer size categories. Fortunately, the degrees of compaction for each species can be scaled according fractal geometry principles. Using the assumed fractal relationship to scale the compaction factors, the five individual compaction factors are then reduced to a single variable in the minimization process. The compaction factor curve is shifted upwards or downwards to give the correct polymer effluent profile for a given zone of flow resistance.

The filtration rate multiplier (PSR) reflects a standard practice in the filtration literature. When designing a filter to clean a given contaminant suspension, a solution of known contaminant concentration is flowed through a sample section of the filter. The effluent concentration and the pressure drop are measured, and an equation of the form of Equation 8.1 is fit to the data.

$$\frac{d\sigma}{dt} = \Gamma V_i C \quad (8-1)$$

Constants regressed from this fitting procedure are considered universal for the specific filter and contaminant solution, and are used to design industrial scale filters. In this model the scaling parameter PSR is combined with a gelation property ( $[Cr^{+3}]_{upt}$ ) to simulate the onset of rapid filtration and development of the zone of peak flow resistance.

The gelation inhibition parameter (GIP) represents a subtle combination of effects not otherwise accounted for in the model. Figures 8.6B, 8.7B, 8.8B and 8.9B show that large amounts of polymer flow through the zone of peak flow resistance as the permeability slowly decreases (note the advanced polymer fronts downstream of the

zone of peak flow resistance in these figures). The advanced polymer fronts imply that filtration of large polymer aggregates strongly inhibits the depositional ability of polymer remaining in solution.

This phenomena results from a combination of effects not directly included in the model. Polymer aggregates may form a higher percentage of inter-molecular crosslinks after being sheared in the zone of reduced permeability, reducing their ability to form crosslinks with deposited polymer. Also, large polymer aggregates are degraded to some degree by porous media shear rates. Finally, the evolution of storage modulus in gelling solutions near the critical entanglement concentration is poorly understood.

These effects, plus others, are represented in the model by the gelation inhibition parameter (literally [component "i"] in a deposited aggregate divided by [component "i"] in the solution as a whole). The gelation inhibition parameter is applied to all species attached to or associated with polymer, including  $Cr^{+3}_{upt}$ , crosslinks and the rheological property  $G'$ . When polymer is deposited on the porous medium, a proportional amount of these components is also deposited. When GIP is greater than 1.0, relatively more of the components associated with polymer are removed from solution with the deposit than exists in the polymer population at large. This directly inhibits important gelation processes ( $G'$  evolution, the resultant generation of larger polymer aggregates, and the overall filtration rate), thus reducing the gelling solution's ability to produce new crops of filterable clusters.

#### 8.4.4 What Constitutes a Match?

The first difficulty in matching apparent viscosity profiles from in situ gelation experiments lies in determining which of the data to match. The most important properties are these:

1. Location of the zone of large pressure drops (the "Magic Spot").
2. The timing of the flow resistance buildup.
3. The shape of the apparent viscosity profiles.

It is relatively easy to match any one of these properties, but quite difficult to match all of them.

Optimum parameters were determined by an iterative process. Compaction factors represent the amount of porous medium flow resistance generated by a given volume of retained polymer. The amount of retained polymer can be determined by mass balance on the polymer effluent, and the amount of flow resistance correlates to the area under an apparent viscosity versus position plot (see Figures 8.2 and

8.3). Because polymer effluent data were collected for only one of the Marty et al.<sup>3</sup> displacements (Run #6, 2.64 feet/day), compaction factors for Marty's system are based on that single run. Unfortunately, that run is the only Marty displacement not accurately simulated by the in situ gelation model (see discussion in Section 8.4.6).

This difficulty was resolved by first integrating the area under the apparent viscosity plot for Run #6 at a time of 53 hours. Then, Run #6 was simulated and the area under the simulated apparent viscosity profile after 53 hours was integrated. A pseudo-effluent profile was determined by finding the point in the simulated core where the area under the simulated 53-hour viscosity profile (Figure 8.3) matches the area under the displacement data curve (Figure 8.2). Compaction factors were then varied while holding PSR and GIP constant until the simulated polymer effluent concentration matched the actual effluent data (see Figure 8.4). By this process an initial set of compaction factors was determined.

Using these compaction factors, optimum values of PSR and GIP were then determined. A single run was chosen - Marty et al.'s displacement #2 at a frontal velocity of 1.61 ft/day. PSR and GIP were adjusted until the simulated apparent viscosity profiles matched the data as well as possible. Those values of PSR and GIP were then used to simulate the other four displacements. PSR and GIP were again varied to achieve the best matches for all five runs.

Values of PSR and GIP thus determined were used to simulate Run #6, and the compaction factors were varied as before until the simulated and actual polymer effluent concentrations agreed. Better values of PSR and GIP were then determined by re-matching the other four displacements. This process was repeated until the results presented in Section 8.4.6 were obtained.

#### 8.4.5 Match of Marty et al.'s Displacement Data

Results of the Marty et al. displacement simulations are shown in Figures 8.5 through 8.11. Figure 8.5 is a plot of the center of the high resistance zone as a function of flow velocity for each computer simulation and corresponding laboratory displacement. Figures 8.6A through 8.10A are simulated apparent viscosity profiles for flow velocities of 0.88, 1.37, 1.61, 2.25, and 2.64 feet per day, and Figures 8.6B through 8.10B are the corresponding displacement data taken from Marty et al.<sup>3</sup>. Figure 8.11 gives the simulated and actual polymer effluent concentrations for the 2.64 ft/day displacement.

Results in these figures were obtained by the parameter regression scheme discussed above. Optimum parameters are listed in Table 8.1.

#### 8.4.6.1 Location of Zone of Increased Flow Resistance

Figure 8.5 is a plot of the center of Marty et al.'s zone of peak flow resistance as a function of frontal velocity, along with an estimate of the experimental error in the displacements. The error band is based on data by McCool<sup>1,2</sup>, who reported results of three in situ displacements conducted at the same velocity. The center of McCool's region of flow resistance buildup varied by a total of fifteen centimeters from the farthest-downstream to the farthest-upstream peak. Figure 8.5 shows the numerical model correctly places the region of high flow resistance for four of the five displacements.

The simulation of the run performed at a velocity of 2.64 feet/day is the only displacement whose zone of peak flow resistance is not correctly placed by the in situ gelation model. A possible explanation of this poor match is given in Section 8.4.6.3.

#### 8.4.6.2 Timing and Shape of Apparent Viscosity Profiles

Figures 8.6A through 8.10A are simulations of the five Marty et al. runs. The four slowest velocity simulations (Figures 8.6A through 8.9A) correctly place the plugged zone and exhibit the abrupt development of flow resistance. These displacements are conducted largely in the low shear regime and the essential features of the simulations are correct.

Figure 8.10A gives results obtained from simulating the highest velocity run (2.64 feet/day), and the simulated viscosity profiles do not match the data. Although disappointing, there are concrete reasons for suspecting experimental problems in the displacement data. Marty's laboratory notebooks report that the gelling solution of Run #6 had an initial pH of 4.60 and an effluent pH of 5.18<sup>20</sup>, compared to pH values of 4.47 and 5.0 for the other four displacements<sup>3</sup>. This may indicate a mixing error in the injected concentrations of the gelling solution. In addition, Run #6 occurred under relatively high shear rates, and the rheological behavior of gelling solutions under high shear is not well understood. At this time it is not possible to say whether the model or the data most accurately describes the behavior of Marty et al.'s gelling solution at a velocity of 2.64 ft/day.

#### 8.4.6.3 Analysis of Simulation Errors

Figure 8.5 shows that the in situ gelation model places the center on the zone of peak flow resistance for most of Marty et al.'s displacements within the experimental error band defined by the results of McCool. However, even in the best of the simulations there are qualitative and quantitative differences between the displacement data and the simulated results. The major differences between the

simulation and data are summarized for each displacement.

- $V_i = 0.88$  ft/day : The zone of peak flow resistance occurs about eight centimeters farther downstream in the simulation than in the actual data. However, the shape and timing of the apparent viscosity profiles are very similar.
- $V_i = 1.37$  ft/day : The same comments apply as for the slowest velocity displacement, except the simulated zone of flow resistance is only about five centimeters downstream of the actual data.
- $V_i = 1.61$  ft/day : This is the best of the Marty et al. displacement simulations. The peak flow resistance zone is correctly located, and the timing of the simulated apparent viscosity peaks is only slightly accelerated (about six hours).
- $V_i = 2.25$  ft/day : The zone of peak flow resistance is correctly located, but the timing is off. In the actual displacement the core plugged after 50.5 hours, while the simulated displacement did not plug until 60 hours.
- $V_i = 2.64$  ft/day : The zone of peak flow resistance develops more slowly and far upstream of the actual zone of peak flow resistance.

What do these differences mean? There appears to be a bias in the shear-dependent properties. The two slowest displacements (0.88 and 1.37 ft/day) plugged the core upstream of the corresponding simulation, while the two intermediate rate displacements correctly located the zone of peak flow resistance. Possibly this means the parameters describing  $G'$  evolution underpredict the rate of gelation at low shear rates. This is not surprising since the redox gelation model is based on rather large extrapolations of Bhaskar's gelation data. The shear-dependent parameters are insensitive to shear rate changes below  $3.2 \text{ sec}^{-1}$ , which would explain the delayed plugging of the core at low shear rates.

The other major difference between the simulated and actual data is the early gelation of the higher shear rate displacements. The displacement at 2.25 ft/day plugged the sandpack after 50.5 hours, and

the displacement at 2.64 ft/day plugged the sandpack after 53.0 hours. Although the gelling solution going through the magic spot is of similar age in all the Marty et al. displacements, the two intermediate shear runs plugged the sandpack ten to fifteen hours earlier than in the two lowest shear displacements. This difference also reflects our incomplete understanding of gelation under shear.

How significant are these differences? A partial answer to this question lies in the gelation displacements performed by McCool<sup>1,2</sup>. McCool performed three replicate displacements at frontal velocities of approximately 0.65 feet/day. In each displacement a short section of the sandpack (20-30 centimeters) gradually plugged as several pore volumes of gelling solution were injected through the plugging zone. However, the location and timing of the plugging zone varied significantly between the three displacements. Significant results of each displacement are summarized in Table 8.2. Although these runs were intended to be replicates, the center of the zone of flow resistance varied by fifteen centimeters (19% of the average). The time of final plugging varied by 52 hours (23% of the average), and even the flow rate varied by 8% of the average. Analysis of McCool's data indicates these differences in flow rates, plugging times and flow resistance locations represent a normal range of experimental error for typical in situ gelation displacements<sup>1</sup>.

Using the data in Table 8.2 as a reference, it is clear that the differences between Marty et al.'s data and the computer simulations are smaller than the range of experimental variation reported by McCool. Without further displacement data to simulate it is not possible to determine whether the in situ gelation model or the displacement data is more correct.

#### 8.5 RESULTS: SIMULATION OF McCool'S POLYACRYLAMIDE/REDOX SYSTEM

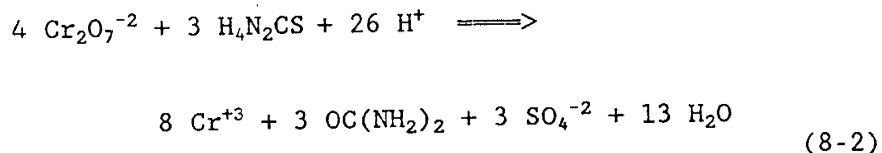
Prior to the work by Marty et al.<sup>3</sup>, McCool<sup>1,2</sup> performed in situ gelation displacements using a system of 383 ppm sodium dichromate, 383 ppm thiourea and 4210 ppm of the cationic polyacrylamide CatAn-160. These low concentrations of thiourea and dichromate result in a slow gelling system with a nominal beaker gel time of 250 hours. McCool performed three replicate displacements at an average frontal velocity of 0.67 feet/day, giving the gelling solution a residence time of 150 hours in the sandpack. During each gelling solution displacement a region of high flow resistance developed in the interior portions of the sandpack. Simulation of McCool's system is described in this chapter.

### 8.5.1 Modifications to Gelation Kinetics

CatAn-160 is a cationic polyacrylamide copolymer obtained from TIORCO Inc., and has approximately twenty percent positively charged functional groups<sup>1</sup>. In contrast, Marty et al.<sup>3</sup> used an anionic polyacrylamide sold by Aldrich Inc. having approximately five percent negatively charged functional groups<sup>21</sup>. The positively charged functional groups on the cationic polymer imply a different crosslinking mechanism than used by Marty's anionic polymer. Also, membrane dialysis data reported by McCool<sup>1</sup> and Marty et al.<sup>3</sup> indicate the cationic polymer forms larger aggregates than the anionic polymer. These differences require modifications in the kinetic and rheological models used to simulate Marty's displacements. However, the filtration and mass transport components of the in situ gelation model remain the same. Changes in gelation kinetics describing McCool's system are given below.

#### 8.5.1.1 Reduction Reaction Kinetics

The rate controlling step in gelation kinetics is the rate of Cr<sup>+3</sup> generation by the reduction reaction.



$$\frac{d[\text{Cr}_2\text{O}_7^{-2}]}{dt} = -\frac{1}{2} \left[ k_1 [\text{HCrO}_4^-][\text{H}_4\text{N}_2\text{CS}][\text{H}^+] + k_2 [\text{HCrO}_4^-][\text{H}_4\text{N}_2\text{CS}][\text{H}^+]F[\text{PAam}] \right] \quad (8-3)$$

The redox rate equation developed by Maxcy<sup>14</sup> should apply equally well to the Marty and McCool gelling systems. The differences in the two systems would be felt in the second term of Equation 8.3, which includes the concentration of chemically active polymer functional groups. Because  $k_2$  is an order of magnitude smaller than  $k_1$ , the dichromate reduction rate is not strongly affected by the differences in polymer systems. So, McCool's system was modeled using the same reduction reaction kinetics and rate constants as were used to simulate Marty et al.'s system.

### 8.5.1.2 Cr<sup>+3</sup> Attachment to Polyacrylamide

Our knowledge of the Cr<sup>+3</sup> interactions with CatAn-160 polymer is limited. Hunt<sup>17</sup> measured the rate of Cr<sup>+3</sup> attachment to the anionic Aldrich polyacrylamide, but did not measure Cr<sup>+3</sup> attachment rates to cationic polymers. Although it does not directly apply to McCool's system, Hunt's Equation 8.4 giving the rate of Cr<sup>+3</sup> attachment to polymer was used in these simulations.

$$\frac{d[CR^{+3}]_{upt}}{dt} = k_{upt} \frac{[CR^{+3}]^{1.32}}{F^{0.8} [H^+]} [F[PAam] - [CR^{+3}]_{upt}]^{0.8} \quad (8-4)$$

A rate constant  $k_{upt}$  for McCool's gelling system of 0.00025 (liter/mole)<sup>1.12</sup>/hour was back-calculated by the procedure described in Section 8.5.1.3. Hunt's<sup>17</sup> value of 0.05 for the parameter F was used in simulations of McCool's displacements.

Crosslinking the CatAn-160 polymer requires more than just chromium oligomers interacting with polymer to form interchain bonds. McCool<sup>1</sup> reported the CatAn-160 polymer gelled in a beaker when mixed with thiourea and sodium dichromate, but did not gel when mixed with only sodium dichromate or only ionic Cr<sup>+3</sup>. In contrast, the Aldrich polyacrylamide is known to gel in both redox and ionic Cr<sup>+3</sup> solutions<sup>7</sup>. Although the exact physical nature of the crosslinking process is unknown, correlating the attached Cr<sup>+3</sup> concentration to the rate of crosslinking does provide an acceptable fit to rheological data (see Section 8.5.1.3). For this reason Equation 8.4 was used as the basis for crosslinking kinetics in simulations of McCool's gelling system.

### 8.5.1.3 Rheological Behavior

Bhaskar<sup>18</sup> measured the storage modulus and viscosity of a gelling solution of 2341 ppm CatAn-160 polymer, 3916 ppm thiourea and 3988 ppm sodium dichromate. The solution had an initial pH of 4.0 and a shear rate of 0.236 sec<sup>-1</sup>, and experienced a rapid increase in storage modulus beginning after ten hours. These data were modeled by coupling the redox and Cr<sup>+3</sup> uptake equations with Bhaskar's equation for storage modulus evolution.

$$\frac{dG'}{dt} = R_k [CR^{+3}]_{upt} G' \left[ 1 - \frac{G'}{G_{max}} \right] \quad (8-5)$$

Because no endpoint pH was reported, a pH of 4.5 after ten hours was assumed.

The kinetic model combining Equations 8.2, 8.3, 8.4, and 8.5 contains three parameters that were never measured for McCool's gelling system -  $K_{upt}$ ,  $R_k$  and  $G'_{max}$ . However, by making discreet assumptions and using Bhaskar's rheological data, an internally consistent set of these parameters was developed. Values of  $R_k$  and  $G'_{max}$  were calculated at  $0.236 \text{ sec}^{-1}$  using the same shear dependent parameters as were used for the redox/Aldrich polymer solutions. Then, the rate constant for the  $\text{Cr}^{+3}$  uptake equation was varied until the predicted  $G'$  curve fit rheological data taken by Bhaskar<sup>18</sup> (see Figure 8.12). The best fit was obtained using a  $\text{Cr}^{+3}$  uptake rate constant of  $0.00025 \text{ (liter/mole)}^{1.12}/\text{hour}$  and the rheological parameters of  $R_k$  equal to 853.25 and  $G'_{max}$  equal to 57.25 (at a shear rate of  $0.236 \text{ sec}^{-1}$ ).

Viscosity is correlated to the crosslink density of the gelling solution using the empirical correlation

$$\mu_p = \mu_o \left[ \frac{n}{n_{en}} \right]^{2.05}$$

(8-6)

Figure 8.13 gives the viscosity curve associated with the  $G'$  data presented in Figure 8.12. Equation 8.6 matches the data well up to about fourteen hours, at which point the gel fractures and the viscosity decreases.

The data in Figures 8.12 and 8.13 were measured on a system with high concentrations of thiourea and dichromate, resulting in a nominal gel time of about fifteen hours<sup>18</sup>. In contrast, McCool's system had a beaker gel time of 250 hours<sup>1,2</sup>. Thus, the viscosity decrease in Figure 8.13 after fifteen hours corresponds to behavior that would be exhibited by McCool's gelling solution after it had exited the sandpack. It was decided to ignore the later data and model only the first fifteen hours of the data, because we are most interested in viscosity behavior prior to the point of beaker gelation.

#### 8.5.1.4 pH Behavior

As with Marty's gelling system, no theoretical model of pH behavior exists for the McCool gelling system. However, beaker pH data reported by McCool are described by Equation 8.7 and are plotted in Figure 8.14.

$$[H^+] = \frac{1}{A + B \cdot t^C}$$

(8-7)

These data start with an initial pH of 4.8 and rise to 5.15 after 250 hours.

The pH behavior of McCool's gelling system in a porous medium differs slightly from the beaker pH data. Gelling solutions used by McCool<sup>1,2</sup> in his sandpack displacements had an initial pH of 4.72 and effluent pH's ranging from 5.15 to 5.24. These values are plotted with the beaker pH data in Figure 8.15. The initial pH lies above the beaker pH data, and the effluent pH's fall below the beaker pH data, indicating porous medium interactions accelerate pH increase. Gelling solution pH in a porous medium was modeled using the measured initial and effluent pH's as the endpoints of the pH curve, and taking the curvature exponent "C" of 0.80 from the beaker pH data (Figure 8.14). The resulting curve is plotted in Figure 8.15 and defines the pH behavior used to simulate McCool's displacements.

#### 8.5.2 Match of McCool's Displacement Data

McCool performed three gelation displacements at frontal velocities of approximately 0.67 feet/day. In each displacement the characteristic "magic spot" developed - i.e. a short section of the sandpack (20-40 centimeters) gradually plugged as several pore volumes of gelling solution passed through the plugging zone. Because the three McCool displacements are essentially replicates, it was decided to average the flow rates and conduct a composite simulation of the three runs. Gelling solution concentrations and sandpack properties were taken from McCool<sup>1</sup>, and the kinetic modifications given above were installed in the in situ gelation model. Locations of the zone of flow resistance and the time of final sandpack plugging for the simulation and each displacement are summarized in Table 8.3.

##### 8.5.2.1 Location and Character of McCool's Magic Spots

Figure 8.16 presents the simulated apparent viscosity profiles, which feature a zone a flow resistance centered 76.4 centimeters from the sandpack inlet. Figures 8.17a through 8.17c show that McCool's displacements also plugged this portion of the sandpack. Figure 8.18 shows good agreement between the simulated and actual polymer effluent concentrations. Because the location of the zone of flow resistance is the critical variable in an in situ gelation treatment, these results mean the model describes the system well enough to be used as a basis

for treatment design.

However, the shape of the apparent viscosity profiles generated by the computer model differs qualitatively from the actual data. Whereas the modeled results show a steady increase in flow resistance progressing down the sandpack, the actual data show little development of flow resistance in the first sixty centimeters, followed by an abrupt increase in flow resistance over the next twenty to forty centimeters. This difference in the shape of the apparent viscosity profiles probably results from the incomplete description of the gelation kinetics involving cationic polyacrylamide.

#### 8.5.2.2 Discussion of Model Parameters

Kinetic differences between the McCool and Marty gelling systems means the matching parameters regressed for Marty's system will not match McCool's displacement data. However, Marty's parameters were used as first approximations when regressing parameters specific to McCool's system. First, PSR and GIP were held constant while adjusting the compaction factors until the simulated polymer effluent concentrations matched those of McCool. Then, the compaction factors were held constant and PSR and GIP were varied until the apparent viscosity profiles matched data from McCool's three displacements. The compaction factors were then adjusted to improve the match of effluent concentrations. This process was repeated until the most representative match was achieved using the parameters in Table 8.4.

Comparing the two sets of parameters shows good agreement between the two systems. The compaction factors and gelation inhibition parameters are nearly the same for the two systems. The filtration matching parameter (PSR) of 0.00135 for McCool's system is much lower than Marty's value (0.00290), reflecting the overall slower kinetics of McCool's system. In general, the differences in the parameters regressed for the two systems are of the same magnitude as the differences in the systems themselves.

#### 8.5.2.3 Summary of McCool's Simulations

Manipulation of the matching parameters allowed the in situ gelation model to correctly place the zone of flow resistance. Because this is the critical variable in treatment design, simulation of McCool's system was a success. This match indicates the in situ gelation model may apply to a range of polyacrylamide-based gelling systems. Also, the similarity of the two sets of matching parameters reported in Table 8.4 indicates the compaction factors and the gelation inhibition factor vary over narrow ranges for different polyacrylamide systems. Matching McCool's displacement data extends the in situ gelation model's applicability to a wide range of polyacrylamide/redox

gelling systems.

However, shortcomings in the description of gelation kinetics prevented an exact qualitative match of McCool's gelation displacements. Although the simulated zone of flow resistance is located correctly, the simulated apparent viscosity profiles do not reflect the abrupt nature of the actual displacement data. This discrepancy could be corrected with a rheological and kinetic investigation of CatAn-160's crosslinking kinetics.

## 8.6 RESULTS: SIMULATION OF HEJRI'S BIOPOLYMER/Cr<sup>+3</sup> SYSTEM

The in situ gelation model was written to explain the displacement results of McCool<sup>1,2</sup> and Marty<sup>3</sup> - both of whom used polyacrylamide gelling systems crosslinked with a metal cation generated by a reduction reaction. Reaction kinetics and particle evolution as described in Chapter IV, Reference 22 apply to both polyacrylamide/redox systems.

Hejri<sup>4</sup> performed displacements using a gelling system of 1500 ppm FLOCON 4800 biopolymer mixed with 50 ppm of ionic Cr<sup>+3</sup>, a system which plugged the sandpack after several pore volumes of polymer injection. Because biopolymer displacements are similar in some respects to polyacrylamide displacements, an attempt was made to model Hejri's displacement data. Changes made in the numerical model to describe biopolymer/Cr<sup>+3</sup> gelation and the results of the simulation work are reported in this chapter.

### 8.6.1 Biopolymer Model Changes

Biopolymer/Cr<sup>+3</sup> solutions have more complex rheological behavior, significantly different reaction and crosslinking kinetics, and different filtration and depositional behavior. The following sections describe modifications made in the in situ gelation model to describe biopolymer gelling systems. FORTRAN code in the numerical model is constructed such that either biopolymer or polyacrylamide subroutines can be selected as options from the main in situ gelation model.

#### 8.6.1.1 pH Behavior

As with redox/polyacrylamide systems, pH behavior of the Cr<sup>+3</sup>/biopolymer system is poorly understood. Formation of chromium oligomers releases protons, thus decreasing pH. Cr<sup>+3</sup> attachment to biopolymer may or may not affect pH, depending on which functional group provides the attachment site. In addition, different chromium species maintain equilibria that provide a buffering effect on the solution. The actual kinetics of pH behavior for this gelling system

are beyond the scope of this model.

Hejri<sup>4</sup> fit beaker pH data from his gelling system to the expression

$$\text{pH} = 4.097 e^{[(0.131)(0.962)^t]} \quad (8-8)$$

where t is the time in hours. The pH predicted by this equation matches sandpack effluent pH's within experimental accuracy, indicating fluid/porous media interactions do not strongly influence pH in Hejri's system.

#### 8.6.1.2 Cr<sup>+3</sup> Attachment to Polymer

As with polyacrylamide gelling systems, crosslinking in biopolymer systems involves Cr<sup>+3</sup> ions or oligomers forming bridges between biopolymer chains. An early step in this process is the attachment of Cr<sup>+3</sup> aggregates to functional groups on biopolymer molecules. The rate of Cr<sup>+3</sup> uptake onto polyacrylamide molecules is given by Hunt<sup>17</sup>.

$$\frac{d[\text{Cr}^{+3}]_{\text{upt}}}{dt} = k_{\text{upt}} \frac{[\text{Cr}^{+3}]^{1.32}}{F^{0.8} [\text{H}^+]} [F[\text{PAam}] - [\text{Cr}^{+3}]_{\text{upt}}]^{0.8} \quad (8-9)$$

where F is approximately the fraction of polymer repeat units capable of accepting a Cr<sup>+3</sup> ion (0.05 in Hunt's system) and k<sub>upt</sub> is a rate constant of 0.00017 (liter/mole)<sup>1.12</sup>/hour.

This equation was modified to fit membrane dialysis data taken on a biopolymer/Cr<sup>+3</sup> solution by McCallister<sup>23</sup>. These data show an appreciable attached chromium concentration at zero time, which was treated as an initial attached Cr<sup>+3</sup> concentration. The total attached chromium concentration is then given by

$$[\text{Cr}^{+3}]_{\text{upt}} = k_{\text{upt}} \int_{t=0}^t \frac{[\text{Cr}^{+3}]^{1.32}}{F^{0.8} [\text{H}^+]} [F[\text{BIOP}] - [\text{Cr}^{+3}]_{\text{upt}}]^{0.8} dt + [\text{Cr}^{+3}]_{\text{upt}}(\text{initial}) \quad (8-10)$$

where [BIOP] is the concentration of biopolymer repeat units in solution. Best fits were obtained using a  $k_{upt}$  of 0.0035 (liter/mole)<sup>1.12</sup>/hour and a fractional degree of hydrolysis (F) of 0.1975. A comparison of Equation 8.10 and the McCallister dialysis data over a pH range of 4.93 to 4.74 is given in Figure 8.19.

Fitting the McCallister data required large values of  $k_{upt}$  and F, reflecting the increased reactivity of biopolymer molecules. Structural information on the FLOCON 4800 biopolymer<sup>24</sup> shows xanthan molecules have a high percentage of repeat units with functional groups attached. These groups provide attachment sites for Cr<sup>+3</sup> ions, and their abundance on xanthan molecules explains biopolymer's reactivity and rapid chromium attachment.

### 8.6.1.3 Effect of Chromium Oligomerization On Biopolymer Gelation

Comparing rheological and kinetic data shows that biopolymer gelation kinetics involve more than simply Cr<sup>+3</sup> molecules attaching to polymer. Figure 8.19 shows that nearly three fourths of all Cr<sup>+3</sup> attachment occurs during the first two hours of contact with biopolymer. However, G' data under zero shear show that gelation is a gradual process extending over many hours (see Figure 8.20). Likewise, zero shear viscosity data by Hejri<sup>4</sup> indicate enhanced gelation ability beginning after fifteen hours (see Figure 8.21). Clearly, there must be intermediate steps between Cr<sup>+3</sup> attachment to biopolymer and actual crosslinking.

Fei<sup>25</sup> noted widely differing gelation rates in biopolymer solutions containing distilled fractions of pure monomer, pure dimer and pure trimer. At pH 5.0 monomer solutions gelled after eight days, dimer solutions gelled after twenty hours, and trimer solutions gelled almost immediately. These data imply the intermediate step in biopolymer gelation involves the formation of larger chromium species. When attached to polymer molecules, these large chromium oligomers provide greatly enhanced crosslinking ability.

A numerical model for the evolution of higher chromium species was written based on papers by Rotzinger et al.<sup>26</sup> and Stünzi et al.<sup>27</sup>. These papers give reaction rates for chromium monomer conversion to larger species, and postulate that monomer conversion to larger species is second order in monomer concentration.

$$\frac{d[\text{monomer}]}{dt} = - 2.0 K_{\text{obs}} [\text{monomer}]^2$$

(8-11)

Rotzinger et al. measured  $K_{obs}$  as a function of pH and found reasonable agreement over a range of initial chromium concentrations<sup>26</sup>. These rate constants are plotted versus hydrogen ion concentration in Figure 8.22.

#### 8.6.1.3.1 Chromium Species Model

A model of chromium oligomerization based on Rotzinger et al.'s second order kinetics and reaction rate data was written. The model predicts the concentration of five chromium oligomers: monomers, dimers, trimers, tetramers and all aggregates larger than tetramers ("large-mers"). The four smaller species react with each other to form larger species. The fifth and largest category is a catch-all group including pentamers, hexamers, heptamers and octomers. In real kinetic systems these large molecules actively combine with smaller species to form more large species, and decompose into smaller species, primarily trimers<sup>27</sup>. In this model a simplifying assumption was made, i.e. the rate of large aggregate formation by large species combining with other species equals the rate of large aggregate decomposition into smaller species. Thus, only the four smallest species actively participate in reaction kinetics.

Assuming second order kinetics, the rate of monomer conversion to all larger species is given by

$$\begin{aligned} \frac{d[\text{monomer}]}{dt} &= - 2.0 K_{11} [\text{monomer}]^2 \\ &\quad - K_{12} [\text{monomer}][\text{dimer}] - K_{13} [\text{monomer}][\text{trimer}] \\ &\quad - K_{14} [\text{monomer}][\text{tetramer}] \end{aligned} \tag{8-12}$$

A similar set of equations can be written for the rate changes of dimer, trimer, tetramer and larger species.

$$\begin{aligned} \frac{d[\text{dimer}]}{dt} &= K_{11} [\text{monomer}]^2 \\ &\quad - K_{21} [\text{dimer}][\text{monomer}] - 2.0 K_{22} [\text{dimer}][\text{dimer}] \\ &\quad - K_{23} [\text{dimer}][\text{trimer}] - K_{24} [\text{dimer}][\text{tetramer}] \end{aligned} \tag{8-13}$$

$$\begin{aligned}
\frac{d[\text{trimer}]}{dt} &= K_{12} [\text{monomer}][\text{dimer}] \\
&- K_{31} [\text{trimer}][\text{monomer}] - K_{32} [\text{trimer}][\text{dimer}] \\
&- 2.0 K_{33} [\text{trimer}]^2 - K_{34} [\text{trimer}][\text{tetramer}]
\end{aligned}
\tag{8-14}$$

$$\begin{aligned}
\frac{d[\text{tetramer}]}{dt} &= K_{22} [\text{dimer}]^2 \\
&+ K_{13} [\text{monomer}][\text{trimer}] - K_{41} [\text{tetramer}][\text{monomer}] \\
&- K_{42} [\text{tetramer}][\text{dimer}] - K_{43} [\text{tetramer}][\text{trimer}] \\
&- 2.0 K_{44} [\text{tetramer}]^2
\end{aligned}
\tag{8-15}$$

$$\begin{aligned}
\frac{d[\text{large-mer}]}{dt} &= K_{14} [\text{monomer}][\text{tetramer}] \\
&+ K_{23} [\text{dimer}][\text{trimer}] + K_{24} [\text{dimer}][\text{tetramer}] \\
&+ K_{33} [\text{trimer}][\text{trimer}] + K_{34} [\text{trimer}][\text{tetramer}] \\
&+ K_{44} [\text{tetramer}]^2
\end{aligned}
\tag{8-16}$$

Note that every negative term in one rate equation is offset by a positive term in another rate equation. The equation for the rate change of large-mers has only positive terms, meaning that once formed the largest species neither increases nor decreases in size.

Solving Equations 8.12 through 8.16 requires knowledge of the rate constants  $K_{ij}$ . Rotzinger et al.<sup>26</sup> published values of  $K_{obs}$  (overall monomer conversion rate) over a pH range of 3.5 to 5.0. Their measured values of  $K_{obs}$  include the combined contributions of  $K_{11}$ ,  $K_{12}$ ,  $K_{13}$ , and  $K_{14}$ . Also, Rotzinger et al.<sup>26</sup> and Stünzi et al.<sup>27</sup> published chromium oligomer concentrations as a function of time over the same range of pH's. Finally, Besso<sup>28</sup> published observed rate constants for tetramer formation from the dimer-dimer reaction over the pH range of 4.0 to 5.0. Besso's rate constants appear to predict lower concentrations of tetramer than were observed by Rotzinger et al. and Stünzi et al.

#### 8.6.1.3.2 Matching Literature Data

Development of a kinetic model of chromium oligomerization was achieved by solving Equations 8.12 through 8.16, holding the monomer-monomer rate constant equal to Rotzinger et al.'s value of  $K_{obs}$  and varying the other rate constants to match published chromium speciation data.

Rate constants for all reactions other than the monomer-monomer reaction were estimated as follows. First, all rate constants except  $K_{11}$  were scaled to  $K_{22}$  by the relationships given in Table 8.5. These scaling relationships are based strictly on the size of the reactive molecules. (For instance, the rate constant for the combination of monomer with dimer is one half the rate constant for the combination of dimer with dimer.) The ratio  $K_{22}/K_{11}$  then defines all rate constants of higher order than  $K_{22}$ . Next, the ratio  $K_{22}/K_{11}$  was varied until the model matched oligomer concentration data taken from Rotzinger et al.<sup>26</sup> and Stünzi et al.<sup>27</sup>. Excellent matches were obtained for two data sets in which the pH was held constant by adding base, and a reasonably good match was obtained for a data set where the pH was allowed to float.

Rotzinger et al. present oligomerization data for a 0.04 Molar Cr(III) solution at pH 4.51 and a 0.02 Molar Cr(III) solution at pH 4.81 (Tables Ia and Ib, reference 26). In both data sets solution pH was held constant by adding base. Simulations of these data are given in Figures 8.23 and 8.24. Excellent agreement was obtained with  $K_{22}/K_{11}$  ratios of 6.0 and 5.5, as the model predicted monomer and dimer concentrations well within experimental accuracy.

Stünzi et al. present data for a 0.036 M solution of Cr(III) whose pH floats from 4.74 to 3.82 (Table II, reference 27). Because oligomerization rates vary with pH, values of the monomer conversion rate were interpolated from Figure 8.22 as a function of pH during the simulation. The simulation of that data set is given in Figure 8.25, and was achieved by scaling  $K_{22}$  12.5 times larger than  $K_{11}$ . The match is fairly good, but exposes the critical limitations of the model. In the early time period there is excessive conversion of monomer into

dimer, and the trimer and tetramer matches are mediocre as well. Difficulties simulating this data set probably result because the ratio  $K_{22}/K_{11}$  is not constant under variable pH<sup>26,28</sup>. However, the model matches the data well in the later time intervals and gives good final matches of the major species concentrations.

Besso<sup>28</sup>, an associate of Rotzinger and Stünzi, published reaction rate constants for the dimer-dimer reaction. These rate constants are only 2.0 to 2.5 times larger than the monomer conversion rate constants reported by Rotzinger et al.<sup>26</sup>, and are too low to match the concentrations of tetramer reported by Rotzinger et al.<sup>26</sup> and Stünzi et al.<sup>27</sup>. The apparent conflict between these publications from the same research group emphasizes the difficulty in characterizing chromium oligomerization reactions.

The concentrations of larger species calculated by this model are less accurate than the calculated monomer concentration for two reasons. First, no measured rate constants exist for the higher order oligomerization reactions. Also, in this model no dimers, trimers or tetramers are allowed to form by decomposition of the largest species, causing excessively high populations of large species in the late stages of a simulation. Simulation of larger species in solutions held at constant pH is further complicated by the formation of large chromium oligomers near the pH titrator, causing an early bias in the data towards larger species<sup>26</sup>. However, in most cases the agreement between the model and data is safely within experimental accuracy.

#### 8.6.1.3.3 Extrapolation to Hejri's Gelling System

After matching literature data, the oligomerization model was used to simulate chromium kinetics occurring in Hejri's<sup>4</sup> biopolymer/ $\text{Cr}^{+3}$  system. Ionic  $\text{Cr}^{+3}$  in Hejri's system passes through three distinct phases during an experiment.  $\text{Cr}^{+3}$  is originally mixed in a stock solution at 1165 ppm and allowed to stabilize for one to five days. Then, the solution is diluted to 300 ppm, held in a reservoir, in-line mixed and finally injected into the porous medium at a concentration of 50 ppm<sup>4</sup>. Each step in the process affects chromium oligomerization kinetics. The model was used to simulate the species reactions and monitor the formation of larger chromium species as the gelling solution progresses through the porous medium.

Rotzinger et al.<sup>26</sup> measured monomer conversion rates over a range of chromium concentrations and pH's. Reaction rate constants at different pH's from that paper are plotted in Figure 8.26, which shows the first two dilutions performed by Hejri are within the range over which Rotzinger et al. measured  $K_{\text{obs}}$ . Although the final dilution (to 50 ppm) is outside the range of data reported, the reaction rate constant does not appear to vary with concentration.

To simulate the Hejri system,  $K_{obs}$  was taken from Rotzinger et al.<sup>26</sup> and other values of  $K_{ij}$  were based on the simulations of Rotzinger et al.'s Tables Ia and Ib. These data sets were chosen because the matches were good and the data cover a pH range similar to that of Hejri's gelling system during the displacement period. Starting with an initial concentration of 100.0% monomer, the concentrations of monomer, dimer, trimer, tetramer and larger species are followed through the dilutions performed by Hejri. pH behavior for the three phases of the simulation is given in Table 8.6.

The chromium species model simulates the progress of the chromium reactions, and records the weight fraction of each species beginning at the dilution to 50 ppm. Results from this simulation are given in Figure 8.27. The weight fractions of large chromium species are then incorporated into the kinetic filtration efficiency term (see Section 8.6.1.7).

#### 8.6.1.4 Evolution of Storage Modulus

Bhaskar<sup>18</sup> showed that gelling solutions of  $Cr^{+3}$  and polyacrylamide develop large increases in storage modulus ( $G'$ ) over a range of shear rates. However, Dolan<sup>29</sup> showed solutions of FLOCON 4800 biopolymer and  $Cr^{+3}$  exhibit no increase in  $G'$  as long as the gelling solution remains in a shear field. If the shearing motion is stopped, sometimes a rapid increase in  $G'$  is observed (see Figure 8.28). The magnitude of the jump is not reproducible. However, the suppression of  $G'$  under steady shear holds for any shear rate exceeding  $0.592 \text{ sec}^{-1}$  over a range of polymer and chromium concentrations.

These data imply that pre-gel cluster growth is severely inhibited in the shear field created during biopolymer porous media displacements. In this model all biopolymer molecules are assumed to be aggregates smaller than one micron in diameter. The small size of biopolymer aggregates means straining interception is relatively unimportant during biopolymer displacements.

#### 8.6.1.5 Non-Newtonian Fluid Rheology

Hejri et al.<sup>73</sup> measured rheological properties of FLOCON 4800 biopolymer over the range of zero to 2000 ppm. They found biopolymer solutions act as power law fluids at Darcy flow velocities over 1 ft/day. Power law fluid viscosity is given by

$$\mu = K' (\text{S.R.})^{n'-1} \quad (8-17)$$

where S.R. is the shear rate in reciprocal seconds. The power law parameters  $n'$  and  $K'$  for FLOCON 4800 were measured on a Weissenberg rheogoniometer, and are correlated by the expressions

$$n' = \frac{1}{1 + 0.002 C_p^{0.943}} \quad (8-18)$$

- and -

$$K' = 5.435 + 0.00002362 C_p^{2.286} \quad (8-19)$$

where  $C_p$  is the biopolymer concentration in ppm.

The expressions given above were measured on non-gelling biopolymer solutions with no crosslinking agent added, and do not directly apply to Hejri's gelling solutions. However, shear evolution data by Dolan<sup>29</sup> (see Figure 8.28) imply gelation kinetics do not strongly affect rheological properties of biopolymer/Cr<sup>+3</sup> solutions placed in shear fields. In this work gelation kinetics are assumed to have no effect on fluid viscosity while the fluid is under shear. Under this assumption Equations 8.17, 8.18, and 8.19 are applied to Hejri's gelling systems without modification.

#### 8.6.1.6 Porous Media Shear Rate

Power law fluid viscosity varies with shear rate. Hejri<sup>4</sup> measured the apparent porous media shear rate of non-gelling solutions of 1500 ppm biopolymer and developed the expression for porous media shear rate

$$S.R. = \left[ \frac{K' \lambda_p^*}{k_{wp}} \right] V_D \left[ \frac{1}{1-n'} \right] \left[ \frac{1-n_c}{1-n'} \right] \quad (8-20)$$

$V_D$  is the Darcy fluid velocity and  $k_{wp}$  is the sandpack permeability to brine after the sandpack has been flooded with a non-gelling polymer solution.  $k_{wp}$  is correlated with initial porous media permeability by the expression

$$k_{wp} = 0.377 k_{wi}^{1.088} \quad (8-21)$$

where  $k_{wi}$  is the brine permeability of the sandpack before contact with polymer.  $n_c$  is the power law constant for polymer flow in a porous medium, and is given by

$$n_c = 0.870 n' + 0.132 \quad (8-22)$$

$\lambda_p^*$  is the polymer mobility constant, and is given by Equation 8.23. This expression is accurate for biopolymer concentrations between 0 and 2000 ppm.

$$\lambda_p^* = 2.685 \lambda_{pBk}^{*0.884} \quad (8-23)$$

$\lambda_{pBk}^*$  is the polymer mobility constant for the Blake-Kozeny model and is given by

$$\lambda_{pBk}^* = \frac{12 (0.0089)^{n'-1} \left[ \frac{9n'+3}{n'} \right]^{-n'} (150 \phi)^{\left[ \frac{n'-1}{2} \right]} k_{wp}^{\left[ \frac{n'+1}{2} \right]}}{K'} \quad (8-24)$$

Taken together, Equations 8.17 through 8.24 provide a rather complete picture of the rheological and porous media shear behavior of gelling solutions of FLOCON 4800 biopolymer and  $Cr^{+3}$ .

#### 8.6.1.7 Filtration of Biopolymer

Physical forces causing filtration are the same for biopolymer and polyacrylamide systems. However, the relatively rigid, rod-like biopolymer molecules respond differently to those forces than do the larger, more globular polyacrylamide aggregates. This section

describes assumptions made in the filtration model to simulate biopolymer displacements.

Uncrosslinked FLOCON 4800 biopolymer is a helical coil 0.6 to 1.5 microns in length, and has a diameter of about 2.0 nanometers<sup>4</sup>. Although the increase in  $G'$  is small for gelling biopolymer solutions under shear, Dolan's rheological data may indicate the formation of small biopolymer-chrome aggregates<sup>29</sup>. These small aggregates are approximated by rough spheres of diameter equal to the length of the coil (see Figure 8.29). The average aggregate diameter was assumed to be 1.0 micron.

Biopolymer deposits have a more compact morphology than polyacrylamide deposits. Analysis of polymer effluent concentrations indicates much biopolymer is retained in the sandpack. Deposit compaction factors of 7.0 or higher were needed to simulate biopolymer effluent concentrations, compared to a factors of 1.0 to 1.43 for polyacrylamide simulations (refer to Sections 8.4 and 8.5).

The last elements needed to model biopolymer filtration are the expressions for interception filtration efficiency. Biopolymer filtration efficiency is affected by two mechanisms - a kinetic term correlated with the  $Cr^{+3}$  oligomer concentration in the solution, and a shear-dependent term that terminates filtration above some threshold shear rate.

The kinetic efficiency term is intended to reflect the kinetic maturity of the gelling solution - the "stickiness" of the polymer molecules as they collide with previously deposited polymer. Interception efficiency for polyacrylamide filtration is given by<sup>13,27</sup>

$$\epsilon_1 = \left[ \text{PSR} \frac{MW_p}{MW_{ru}} \frac{[Cr^{+3}]_{\text{upt(soln)}}}{[PAam]_{\text{soln}}} \right]$$

(8-25)

This expression is literally the squared fraction of polymer repeat units carrying a  $Cr^{+3}$ . This expression erroneously implies that all chromium species are monomers, but appears to adequately describe redox gelling solutions (Sections 8.4 and 8.5).

Equation 8.25 was modified to give the kinetic interception efficiency for biopolymer filtration. The first quotient remains the same. The second quotient, intended to reflect kinetic maturity, was modified to give the fraction of repeat units with a chromium trimer,

tetramer or larger species attached.

$$\epsilon_k = \left[ \frac{MW_p}{PSR \cdot MW_{ru}} \left[ \frac{W_f(\text{tri})}{3} + \frac{W_f(\text{tet})}{4} + \frac{W_f(\text{big})}{B_n} \right] \left[ \frac{[Cr^{+3}]_{upt}}{[BIOP]} \right] \right]^2 \quad (8-26)$$

[BIOP] gives the concentration of biopolymer repeat units and PSR is a scaling multiplier determining the overall rate of filtration.  $B_n$  is the average number of chromium molecules in a large chromium aggregate.

The shear efficiency term reflects trends observed in gelation displacements performed by Hejri<sup>4</sup>. Comparison of displacements conducted at initial shear rates of 6.4 and 12.8 sec<sup>-1</sup> show the lower shear displacements generate higher final flow resistances than do the higher shear displacements. This observation was interpreted to mean the higher shear rates inhibit the deposition of biopolymer on the porous medium. This effect was incorporated into the filtration model by the expression

$$\epsilon_{shr} = \frac{(S.R._{max} - S.R.)}{(S.R._{max})} \quad (8-27)$$

The best match for Hejri's displacements was found using a maximum shear rate of 16.0 sec<sup>-1</sup>. Equations 8.26 and 8.27 were then incorporated into the interception efficiency expression.

$$\epsilon_i = \epsilon_k \epsilon_{shr} \quad (8-28)$$

#### 8.6.1.8 Permeability Reduction by Filtration

The permeability reduction model used in the redox/polyacrylamide simulations was modified slightly to simulate the displacement behavior exhibited by Hejri's biopolymer/Cr<sup>+3</sup> system. Permeability reduction due to the adsorption layer is approximated by Equation 8.21. Permeability reduction due to subsequent biopolymer deposition is given by a modified version of the polyacrylamide permeability reduction model.

$$k_x = k_{wp} \left[ \frac{(1.0 - \sigma_{ads} - \sigma_i - \sigma_s)}{(1.0 - \sigma_{ads})} \right]^m$$

(8-29)

This completes the modifications necessary to model biopolymer systems. All changes were installed in the form of separate subroutines which can be called by selecting the biopolymer option.

#### 8.6.2 Simulation of Biopolymer Displacements

Hejri<sup>4</sup> used a system of 1500 ppm FLOCON 4800 biopolymer crosslinked with 50 ppm ionic Cr<sup>+3</sup> to investigate the effect of shear rate variation on the gelation of biopolymer/Cr<sup>+3</sup> systems. Although Hejri performed numerous gelation displacements, the essential features of his work were summarized in the runs conducted in sandpacks numbers 4, 6, and 7. Conditions of those displacements are summarized in Table 8.7.

Using the numerical model described in the preceding sections, the displacements listed in Table 8.7 were simulated. Results of these simulations are given in the following sections.

##### 8.6.2.1 Results of Biopolymer Simulations

Hejri conducted his displacements in sandpacks separated into five sections approximately twenty-five centimeters long, and measured the resistance factor across each section. The resistance factor is defined as the pressure drop across a sandpack section during a gelation displacement, divided by the pressure drop across the same section experienced during a water displacement. The resistance factor then represents the combined effects of the high viscosity of the gelling solution and any permeability reduction resulting from biopolymer deposition on the porous medium. Section-by-section plots of resistance factor versus time for Hejri's sandpacks 4, 6 and 7 are presented as Figures 8.30, 8.33, and 8.36.

Simulation of the displacement conducted in sandpack 4 is presented in Figure 8.31. The primary flow resistance develops in section C and a lesser flow resistance in section B, which is the same in both the simulation and the data. However, the simulated section C flow resistance develops about twenty hours later than in the displacement data. Also, much less flow resistance develops in the section D and E displacement data than in the simulation.

Figure 8.32 compares simulated and actual effluent viscosities for sandpack 4. Although the viscosity values are similar, significant qualitative differences exist between the data and the simulated values. The data show a high viscosity on initial breakthrough, followed by a viscosity dropoff and subsequent rise in the later time periods. This viscosity trend agrees with the relatively high resistance factors measured in sections D and E between 30 and 40 hours, followed by a decrease in flow resistance in those sections between 40 and 100 hours and a subsequent rise after 100 hours (Figure 8.30). These differences suggest the model does not correctly describe some essential filtration mechanism occurring in biopolymer/Cr<sup>+3</sup> displacements.

The trends observed in Figures 8.30 through 8.32 are repeated in the simulations of sandpacks 6 and 7. Figures 8.33 and 8.34 are the real and simulated flow resistance plots for sandpack 6. As before, the flow resistance develops in the correct sections and increases to approximately the same final values. However, the effluent viscosity comparison (Figure 8.35) reveals opposing trends showing the model does not correctly simulate the biopolymer retention mechanism.

Similarly, Figures 8.36 and 8.37 are the actual and simulated flow resistance plots of the displacement conducted in sandpack 7. Again, the flow resistance develops in the correct sections. Possible pressure port plugging during the displacement obscures the correct values of flow resistance, but the actual flow resistance values do exceed the simulated flow resistances. Again, the effluent viscosity comparison (Figure 8.38) reveals fundamentally different trends between the simulated and actual data.

#### 8.6.2.2 Discussion of Matching Parameters

Table 8.8 compares matching parameters used to simulate Marty's<sup>1</sup> polyacrylamide/redox displacements and Hejri's biopolymer/Cr<sup>+3</sup> data. This comparison shows large parameter differences that reflect the kinetic and structural differences in the two systems. The large biopolymer pseudo rate constant reflects the rapid kinetics of the ionic Cr<sup>+3</sup> crosslinking system compared to the redox system. The lower value of the gelation inhibition parameter corresponds to the lesser degree of solution degradation observed in biopolymer displacements. The extremely large compaction factor needed to approximate biopolymer viscosity effluents indicates the dense, high polymer concentration of biopolymer porous media deposits.

#### 8.6.2.3 Discussion of Simulation Errors

Although the simulated plots of flow resistance exhibit some agreement with the displacement data, qualitative differences in

effluent viscosity plots reveal the model does not accurately describe the physical processes occurring during biopolymer/Cr<sup>+3</sup> displacements. There are several reasons why this should be so.

The kinetic oligomerization model described in Section 8.6.1.3. probably is inadequate to describe gelation kinetics in Hejri's system. Although the basic structure of the model is correct, the rate constants  $K_{i,j}$  are based on large extrapolations of Stünzi et al.'s<sup>27</sup> and Rotzinger et al.'s<sup>26</sup> data. Also, the rate constant scaling for the higher oligomerization reactions is not correct under variable pH. A kinetic study of the oligomerization process is needed to accurately define these rate constants.

Another area of concern is the rheological model described in Sections 8.6.1.4 through 8.6.1.6. This rheological model assumes the viscosity of gelling solutions under shear is the same as the viscosity of non-gelling solutions. Although the biopolymer/Cr<sup>+3</sup> rheological study conducted by Dolan<sup>29</sup> does not provide a basis for a comprehensive biopolymer viscosity model, that rheological study does raise concerns about the interpretation of effluent viscosity and resistance factor data.

The characteristic behavior of the effluent viscosity profiles indicates a retention mechanism not represented in the filtration model. A relatively high concentration of polymer breaks through initially, followed by a steep dip in concentration during the period of rapid filtration. If the displacement continues long enough, a rise in effluent viscosity follows the period of rapid filtration (see Figure 8.32).

A possible scenario describing this mechanism is as follows:

1. The adsorption layer of biopolymer kinetically reacts with chromium ions and oligomers in solution, "conditioning" the adsorbed polymer to allow rapid crosslinking with colliding biopolymer aggregates. During this initial phase filtration rates are slow.
2. Once the deposited biopolymer layer is saturated with chromium oligomers, a period of rapid filtration ensues. This corresponds to the periods of viscosity decrease in the Figures 8.32, 8.35, and 8.38.
3. If filtration continues long enough, the retention capacity of the porous medium is satisfied and the filtration rate declines. This phase was apparent only in the viscosity effluents shown in Figure 8.32.

Variations of this filtration sequence were tried in the in situ gelation model. However, uncertainties in the kinetic model of gelation made these simulation results inconclusive.

## 8.7 RADIAL MODELING OF IN SITU GELATION

Matching the Marty and McCool displacement data in linear sandpacks shows the in situ gelation model accurately represents the physical mechanisms causing filtration of aggregates from gelling polyacrylamide solutions. Based on the successful sandpack simulations, the linear model was converted to a one-dimensional radial model. Radial coordinates more nearly represent the geometry of the near-wellbore area and allow the model to simulate cases of practical importance to the oil industry.

Conversion to radial coordinates affects the mass transport and pressure equations because the interstitial fluid velocity now varies with position. Pressure behavior in radial coordinates for fluids of small and constant compressibility is given by<sup>31</sup>

$$\frac{1}{r} \frac{\partial}{\partial r} \left[ r \frac{\partial p}{\partial r} \right] = \frac{\phi \mu C_t}{k} \frac{\partial p}{\partial t},$$

(8-30)

where  $r$  is the radial distance from the center of the wellbore. The mass transport equation in radial coordinates for the ten chemical species can be expressed as

$$\frac{\partial(\phi C_i)}{\partial t} = -V_D \frac{\partial C_i}{\partial r} + \frac{K_r}{r} \frac{\partial}{\partial r} \left[ r \frac{\partial C_i}{\partial r} \right] - \phi_o C_{i(d)} \frac{\partial \sigma}{\partial t} + R_i \phi$$

(8-31)

However, the remaining equations in the radial model are not affected by the change in system coordinates. Nonlinear kinetic terms ( $R_i \phi$ ) are calculated the same as in the linear model, except the shear rate now varies with position. This affects shear dependent parameters in the fluid rheology equations. Filtration equations are different only in

that the interstitial fluid velocity varies with position. Matching parameters determined from the linear simulations of Marty's displacement data (see Section 8.4) were used in the radial model with no changes.

Because fluid velocity and pressure gradients are large near the wellbore, most single-well radial models use a logarithmically distributed grid system. This grid system spaces the grid nodes tightly near the wellbore and more coarsely progressing away from the wellbore (see Figure 8.39). Distances to the centers of the radial rings are calculated by the recursion relationships

$$r_{i+1} = r_i \alpha \quad (8-32a)$$

$$r_i = r_w \frac{\ln(\alpha)}{\alpha - 1} \quad (8-32b)$$

$$\alpha = \left[ \frac{r_e}{r_w} \right]^{1/N_r} \quad (8-32c)$$

In a logarithmic grid system the radial rings are separated by equal increments of  $\ln(r)$ . So, the mass transport equation (Equation 8.31) can be transposed using equal increments of  $\ln(r)$ , giving the expression

$$\frac{\partial(\phi C_i)}{\partial t} = - \frac{V_D}{r} \frac{\partial C_i}{\partial S} + \frac{K_r}{r^2} \frac{\partial^2 C_i}{\partial S^2} - \phi_o C_{i(d)} \frac{\partial \sigma}{\partial t} + R_i \phi \quad (8-33)$$

where  $S = \ln(r)$ . A logarithmically distributed grid allows the most accurate representation of flow behavior near the wellbore.

However, the primary dynamics of an in situ gelation displacement occur some distance from the wellbore. The zones of peak flow resistance develop deep in the reservoir, and constitute the most critical feature of the process being modeled. Radial distribution of grid nodes hinders this objective, because the grid spacing is most coarse where the interesting features of the process occur. For this reason, mass transport of chemical species was modeled using Equation

8.31, which was discretized using equal increments of "r" as shown in Figure 8.40. Equal radial increments allow adequate grid refinement in the zones of rapid kinetic and filtration changes. Pressure behavior near the wellbore was compared using the two grid schemes with acceptable agreement (See Figure 8.41).

The equally-spaced radial grid described above makes it difficult to place the external reservoir radius far enough from the wellbore so that the wellbore pressure is unaffected by the reservoir boundary. This problem was addressed by generating a grid with equally-spaced grid blocks through the first fifteen feet of the reservoir, followed by a radially distributed grid out to an external reservoir radius of fifty feet. This combination allows adequate grid refinement in the region of rapid gelation kinetics, while still placing the external reservoir radius a reasonable distance from the wellbore.

The radial model described above is not a true simulator of actual wells. Because the model contains only one dimension, no vertical flow effects occur. Likewise, effects of man-made or natural fractures are not included. Fluid interactions with the porous medium are not explicitly modeled, which is a significant limitation when simulating natural porous media displacements. However, the model's radial geometry does approximate radial reservoir flow and shear behavior and provides a tool to investigate cases of practical interest. In the following sections several cases are discussed.

#### 8.7.1 Effect of Reservoir pH

The reduction of dichromate by thiourea releases ionic  $\text{Cr}^{+3}$  necessary for crosslinking, and is strongly affected by the pH of the gelling solution. Both terms in the redox rate equation (Equation 8.35) vary linearly with hydrogen ion concentration. The pH of Marty's gelling system varied from 4.5 at the sandpack inlet to about 5.0 at the outlet, a pH range over which the gelling solution plugs the porous medium within sixty-five hours. In contrast, reservoir pH's are typically on the order of 7.0 or higher. This raises the question of whether satisfactory gels can be developed at reservoir pH's.

To answer this question a set of test conditions was composed. Marty et al.'s gelling solution of 1500 ppm thiourea, 400 ppm of sodium dichromate and 5000 ppm Aldrich polyacrylamide was injected into a radial reservoir with properties similar to the sandpacks used by Marty et al.<sup>3</sup> and McCool<sup>1,2</sup>. The gelling solution was injected at a rate of ten barrels per day per vertical foot for three days, followed by a shutin period of seven days<sup>32</sup>. Gelation kinetics during the shutin period are characterized by the evolution of storage modulus ( $G'$ ) with time. If the storage modulus at the end of the shutin period exceeds

thirty dynes per square centimeter, the treatment was judged to be a success.

The hydrogen ion concentration of solutions injected into natural porous media is strongly affected by fluid-rock interactions, which are not explicitly included in this model. The pH of the injected solution can be controlled easily, but once in the reservoir the solution pH eventually rises to the reservoir pH. So, three different pH trends were used to simulate fluid-porous medium interactions - an initial pH of 4.5 rising to 5.0 after forty hours, an initial pH of 4.5 trending to 6.0 after forty hours, and an initial pH of 4.5 increasing to 7.0 after forty hours (see Figure 8.42). These pH trends were chosen to cover a range of reservoir pH behavior, and provide insight into conditions necessary for successful field applications of the in situ gelation process.

#### 8.7.1.1 Results of pH Simulations

The first case is a duplicate of Marty et al.'s<sup>3</sup> conditions - the pH rises from 4.5 initially to 5.0 after forty hours and ends at 5.6 after 240 hours. As expected, this system plugged the porous medium during the displacement phase of the treatment. Figure 8.43 is a plot of flow resistance versus position, and shows a zone of high flow resistance located between six and ten feet from the wellbore. This caused the wellbore pressure to rise 63.7 psi above the external well pressure, and might eventually have become sufficiently high to terminate injection. Figure 8.44 is a plot of storage modulus development during the shutin period, and shows the liquid polymer gelled over most of the covered interval during the first 132 hours of the shutin period.

Figure 8.43 exhibits a significant characteristic of the radial model. Note the abrupt rise of the apparent viscosity profiles, followed by a rapid decrease in apparent viscosity near the gelling solution front. This contrasts sharply with displacement behavior in linear sandpacks, where a long polymer concentration tail develops downstream of the zone of peak flow resistance. The difference is strictly due to the effect of radial geometry. Because the volume of the radial rings increases going away from the wellbore, the leading edge of the gelling solution is confined in a relatively short radial distance.

The plot of storage modulus versus radial position (Figure 8.44) also exhibits a characteristic model behavior. The curve for 72 hours represents the storage modulus at the start of the shutin period, and shows that  $G'$  steadily decreases during the period of fluid injection. At an injection rate of ten barrels per day per foot, the porous media shear rate exceeds  $6.0 \text{ sec}^{-1}$  until the fluid is over six feet from the

wellbore, which inhibits  $G'$  development during the displacement phase of the treatment. The deleterious effects of aggregate filtration gradually reduce the storage modulus, especially in the region downstream of the zone of high flow resistance.

The  $G'$  curve has an abrupt discontinuity 8.8 feet from the center of the wellbore. This discontinuity represents the effect of a critical model assumption. When the gelation inhibition parameter (GIP) exceeds 1.0, more attached  $Cr^{+3}$ , crosslinks and the rheological parameter  $G'$  are concentrated in the deposited increment of fluid than remain in the gelling solution. Downstream of the zone of peak flow resistance these parameters are depleted, and characteristic oscillations in the explicit solution method may cause negative values in these quantities. For these reasons a floor value of  $G'$  was set for the gelling solution at the start of the shutin period, namely,

$$G' > \frac{1}{2} G'_{en} \left[ \frac{[PAam]}{[PAam]_{injected}} \right]$$

(8-34)

Establishing this floor value of  $G'$  reflects the degraded nature of the gelling solution downstream of the zone of flow resistance, but still provides enough entanglement "crosslinkages" to eventually gel under zero shear conditions.

The gelling solution used in Case 2, where the solution pH rose from 4.5 initially to 6.0 after forty hours and to 6.7 after 240 hours, also successfully plugged the porous medium (see Figures 8.45 and 8.46). However, the reaction kinetics of the gelling solution are much slower than in Case 1, and very little flow resistance developed during the three-day injection period. A zone of flow resistance began forming between six and ten feet from the wellbore, but developed more slowly than in Case 1 and caused only a 19.7 psi pressure increase at the wellbore. During the shutin period the storage modulus grew steadily and formed a stiff gel before the seven-day shutin period ended.

Figures 8.45 and 8.46 represent optimum displacement behavior for in situ gelation displacements. Because gelation kinetics progress more slowly than in Case 1, flow resistance built up slowly and did not hamper fluid injection. Simulated injection into this reservoir could have continued long past three days before wellbore injection pressure would become excessive. However, enough  $Cr^{+3}$  is liberated early in the displacement for the solution to gel during the seven-day shutin

period. For Marty et al.'s<sup>3</sup> system the pH range of 4.5 to 6.7 provides an optimum combination of deep gel penetration followed by satisfactory gelation capabilities during the shutin period.

Case 3 simulates injection of Marty et al.'s gelling system into a reservoir with excessively high pH. In this test case the initial pH of 4.5 increased to 7.0 after 40 hours and to 7.7 after 240 hours. The apparent viscosity profiles (Figure 8.47) show no flow resistance buildup during the injection period, and the storage modulus grew slowly during the shutin period (Figure 8.48). If the shutin period was extended for an additional three weeks, the model predicts an acceptable final level of storage modulus (dashed lines, Figure 8.48). However, a traditional injection sequence into this pH environment would result in a treatment failure.

#### 8.7.1.2 Increased Thiourea Concentration Cases

The results of Case 3 are disturbing because that the pH trend approximates the pH trends found in petroleum reservoirs. A fourth case was run to determine whether the deleterious pH effects in Case 3 could be overcome by using higher concentrations of the redox ingredients. Lange's Handbook of Chemistry<sup>33</sup> reports the solubility limit for thiourea is 9 grams per 100 grams of solvent, and the solubility limit of sodium dichromate-dihydrate is 208 grams per 100 grams of solvent. These concentrations are 59 and 6300 times higher than the concentrations used in Marty's gelling system. There is clearly some room to manipulate reaction kinetics through the concentrations of the redox ingredients.

##### 8.7.1.2.1 High pH Displacement : Case 4

Case 4 represents the first attempt to model an in situ gelation displacement into a high pH environment and still plug the reservoir. The conditions of this case are identical to those of Case 3, except the injected thiourea concentration is 15,000 ppm (ten times higher than Case 3's thiourea concentration). It was originally thought the tenfold increase in thiourea concentration would offset the tenfold decrease in hydrogen ion concentration, and give gelation behavior similar to that of Case 2. However, the kinetic conditions of Case 4 result in much different gelation behavior than Case 2.

Figure 8.49 plots apparent viscosity profiles for Case 4, and exhibits a well-developed zone of peak flow resistance between three and seven feet from the wellbore. The flow resistance is much higher than in Case 2, and three feet upstream of the zones of peak flow resistance developed in Cases 1 and 2. This behavior is surprising, but correct for this system's gelation kinetics.

The tenfold increase in thiourea concentration makes Case 4 comparable to Case 2 over most of the simulation. However, in the very early time period the hydrogen ion concentrations of the two systems are less than a factor of ten different, and Case 4 actually runs faster than both Case 2 and (for a short period of time) Case 1. This kinetic scenario liberates a large amount of  $\text{Cr}^{+3}$  during the early time period, which rapidly attaches to the polymer as the pH rises. (Compare Figures 8.50 and 8.51). This combination of effects plugs the reservoir very close to the wellbore.

During the shutin period the storage modulus evolves through time to develop a stiff gel over most of the interval covered by injection (see Figure 8.52). However, the high pH retards gelation kinetics sufficiently so that the full seven days of shutin time are needed to gel the injected solution at the leading edge of the front.

#### 8.7.1.2.2 High pH Displacement : Case 5

As Figure 8.52 shows, the kinetic system employed in Case 4 successfully plugged the porous medium. However, the high flow resistance that developed near the wellbore is undesirable because it limits the time in which fluid can be injected without undue wellbore pressure buildup.

A second simulation was performed to determine whether Marty et al.'s gelling solution can be injected into a high pH environment without early development of high flow resistance. Case 5 is identical to Case 4, except the initial pH is 5.5, which rises to 7.0 after 40 hours and terminates at 7.9 after 240 hours. As with Case 4, the injected thiourea concentration is 15,000 ppm.

Figures 8.53 and 8.54 show this combination of gelation kinetics provides better displacement behavior than Case 4. A zone of peak flow resistance begins forming between five and eight feet from the wellbore, which is two feet downstream of Case 4's zone of flow resistance. Also, much less flow resistance develops in this displacement, which would allow fluid injection for a longer period of time before rising wellbore pressures halt fluid injection. Finally, the storage modulus developed more evenly during the shutin period over the area covered by injection (compare Figures 8.52 and 8.54). This favorable development occurs because the gelling solution downstream of the zone of flow resistance was not severely degraded by the effects of rapid filtration.

#### 8.7.1.2.3 Conclusions Regarding pH Cases

Analysis of the five pH cases studied leads to several conclusions and identifies optimal conditions for gelling solutions

composed of polyacrylamide, thiourea and dichromate. It is hoped these findings will aid in the design of field injection treatments.

The pH range of 4.5 to 6.7 (Case 2) offers the optimal combination of low flow resistance during displacement followed by acceptable storage modulus growth during the shutin period. Over this pH range the gelling solution could be injected beyond three days before well injection pressure becomes excessive. Lower pH's cause sufficient wellbore injection pressure to halt fluid injection, and higher pH's limit  $\text{Cr}^{+3}$  generation by reduction kinetics and prevent a plugging gel from forming during the shutin period.

When injecting into high pH reservoirs the gelling ability of the polyacrylamide/redox solution is greatly inhibited. This can be compensated by increasing the concentration of ingredients for the reduction reaction. However, if the initial gelling solution pH is not raised above 4.5, this practice results in a very rapid redox reaction during the early time interval and plugs the porous medium very near the wellbore. The most favorable displacement behavior into a high pH environment was achieved using an initial pH of 5.5 and a thiourea concentration of 15,000 ppm.

Another approach to controlling gelling solution kinetics would be to preflush clean sandstone reservoirs with an acidic solution to reduce the reservoir pH. This could be achieved with minimal effort and cost by adding the acidic solution to the well's injection water for several days prior to the gelling displacement. The degree of reservoir pH modification possible would vary for each reservoir fluid/rock system, and would require a laboratory investigation to generate effluent pH versus pore volumes of preflush data for each reservoir studied.

Knowing the amount of preflush necessary to produce a range of reservoir pH's, the design engineer could optimize the volume of preflush and the concentrations of injected chemicals needed for a successful treatment. This could be achieved by running the model with a range of preflush volumes and gelling solution concentrations, and selecting the least expensive combination of preflush and gelling system that produces a good gel in the reservoir.

#### 8.7.2 Effect of Multi-Layered Reservoirs

In petroleum reservoirs permeability heterogeneities take many forms. Permeability may vary laterally due to local depositional environments or fractures, either natural or induced. Also, rock permeability may vary vertically among different layers in a laminated reservoir. The effect of layered vertical permeability variation on in situ gelation treatments is investigated in this section.

An in situ gelation treatment into a multi-layered reservoir such as the one shown in Figure 8.55 was simulated using the radial in situ gelation model. The model reservoir consists of three isolated layers with permeabilities varying over two orders of magnitude. During water injection the upper, high permeability zone takes most of the injected water and is depleted first. Conversely, the two lower permeability zones take less water and retain considerable reserves of oil. After water breaks through the high permeability zone into the offset producing wells, an in situ gelation treatment is desired to restrict injection into that zone and divert injected water into the two lower permeability zones. The question evaluated is whether the lower permeability zones will also be plugged by the in situ gelation treatment.

The single-layer gelation model was applied to this situation by holding the fluid injection pressure constant at 10.0 psi above the reservoir pressure and allowing the injection rate to vary. Three separate single-layer simulations using each zone's porous media properties were then run to determine the degree of gelling solution penetration into each layer. The pH trend and kinetic conditions used in these simulations are identical to those of Case 2 in section 8.7.1. Porous media properties for each layer are presented in Table 8.9.

#### 8.7.2.1 Results of Multi-Layer Simulations

Conducting three simulations with a constant wellbore injection pressure gives the effect of injecting into three separate layers simultaneously. This section describes the degree of gel penetration into each of the three formations, and discusses the effectiveness of injecting into three layers simultaneously. The results of Case 2 indicate this pH trend allows satisfactory gelation during the shutin period, so no shutin time was included in these simulations.

Figure 8.56 shows the apparent viscosity profiles resulting from the displacement into the high permeability (3.5 Darcy) zone. The gelling solution penetrated to a radial depth of ten feet, and produced a small zone of flow resistance between five and eight from the wellbore. The resulting permeability reduction did not substantially reduce the injection rate into the reservoir; note the advancing injection front after each twelve-hour interval. Continued injection with a ten psi differential pressure into the formation would continue to displace gelling solution into the reservoir.

Figure 8.57 gives the apparent viscosity profiles for the displacement into the intermediate permeability (0.35 Darcy) zone. The radial injection front extended 5.4 feet into the reservoir and formed a zone of flow resistance between two and four feet into the reservoir. Because this zone has lower porosity, fillup due to filtration was more

rapid and the apparent viscosity profiles rose to higher levels than in the high permeability zone. However, the zone did not completely plug and the injection front was still advancing after 72 hours of injection.

Figure 8.58 shows that the gelling solution injected into the 0.035 Darcy zone only penetrated 2.7 feet into the reservoir. Filtration rates in the low permeability zone are rapid because of the small pore dimensions and the low initial porosity. The combination of low initial permeability, followed by rapid porosity fillup due to filtration essentially plugged this zone during the 72 hour displacement. (Note that the injection front barely advances during the last twelve hour time increment.) Although gelling solution did not penetrate deeply into this zone, enough gelling solution was placed in the reservoir to effectively plug the porous interval.

The displacement into the low permeability zone points out an important feature of this model. Although the porous media shear rates exceed  $1000 \text{ sec}^{-1}$  in the region surrounding the wellbore, the gelling solution still plugged the formation. Filtration in this model is a much stronger function of attached  $\text{Cr}^{+3}$  concentration than gel aggregate size or any other shear dependent property.

#### 8.7.2.2 Conclusions About Multiple-Zone Displacements

Ideally, gelation displacements into laminated reservoirs would preferentially enter the highest permeability stringer, leaving the lower permeability formations unplugged. However, analysis of Figures 8.56 through 8.58 indicates that under constant pressure injection each zone will take fluid at a rate directly proportional to the rock permeability. Although the low permeability zones take little fluid, enough gelling solution enters the formation to plug those zones. Indeed, the low permeability zones actually plug before the high permeability zones due to their low initial porosity.

Wherever possible, each layer in a multiple-zone formation should be mechanically isolated with a bridge plug and stimulation packer before performing an in situ gelation treatment. This will insure that permeability reduction occurs only in the highest permeability "thief zones", while the unswept, low permeability zones remain unplugged.

In layered reservoirs where the zones are tightly spaced it may not be practical to mechanically isolate each zone. However, the in situ gelation process may still be applicable to such formations if the primary permeability heterogeneities are induced or natural fractures. Plugging the fracture network should re-distribute the injected water regardless of the permeability of the rock matrix.

## 8.8 CONCLUSIONS AND RECOMMENDATIONS

1. A numerical model of the in situ gelation process based on the filtration of gel aggregates from a gelling solution was developed for chromium/polyacrylamide systems.
2. The filtration hypothesis provides a viable explanation for the zones of high flow resistance developing during in situ gelation displacements performed by McCool<sup>1,2</sup> and Marty<sup>3</sup>. The location of the zone of rapid filtration is determined by gelation kinetics.
3. For the Aldrich polyacrylamide/redox system used by Marty et al.<sup>3</sup>, the buildup of flow resistance is a linear function of flow velocity over the range investigated. No evidence of shear effects exists over the range of shear present in the runs simulated.
4. The numerical model correctly located the zone of flow resistance developed in three gelling displacements performed by McCool<sup>1</sup> and McCool et al.<sup>2</sup>. Qualitative differences between the simulated and measured apparent viscosity profiles result from our incomplete description of gelation kinetics for that system.
5. The in situ gelation model was unable to simulate all aspects of the gelation behavior of a biopolymer/Cr<sup>+3</sup> gelling system used by Hejri<sup>4</sup>. The lack of a satisfactory match results from an inadequate description of biopolymer gelation kinetics, particularly the oligomerization of chromium ions.
6. The effectiveness of in situ gelation treatments using the thiourea/dichromate reduction reaction to generate the crosslinking agent is strongly affected by the pH of the porous media. For the gelling system used by Marty et al.<sup>3</sup>, reservoir pH's below 7.0 provide optimal displacement behavior while reservoir pH's approaching 8.0 destroy the effectiveness of the gelling system.
7. The deleterious effects of high reservoir pH can be partially controlled by increasing the concentrations of the reduction reaction ingredients. When manipulating gelation kinetics through the reduction reaction, the solution pH must be raised above 4.5 to prevent an initially rapid reduction reaction and premature plugging of the reservoir.
8. When performing in situ gelation displacements in formations with multiple stringers of widely varying permeability, each zone allows entry of the gelling solution at rates proportional to the permeability of the zone. Even the lowest permeability zone

simulated (0.035 Darcies) was plugged by the gelling solution. The lowest porosity zones plugged most rapidly.

9. The pH model based on pH measurements from beaker gelation data is inadequate to describe pH behavior in porous media displacements. This model neglects the effects of fluid/porous media interactions.
10. Retention of  $\text{Cr}^{+3}$  on the porous medium should be considered for all rocks other than clean sandstones.
11. A three-dimensional radial model capable of simulating fractures and vertical permeability variation is needed to design in situ gelation treatments into real petroleum reservoirs.

#### 8.8.1 Recommendations and Future Objectives

1. A three-dimensional radial simulator should be written to model in situ gelation displacements into water injection wells. The model should include a propped vertical fracture leading away from the wellbore, a description of the interactions between porous medium clays and cations in the gelling solution, and a pH model including fluid/porous medium interactions and equilibria between different chromium species.
2. A model of pH behavior for redox/polyacrylamide gelation kinetics should be developed. This model should be based on the consumption of hydrogen ions by the reduction reaction, the generation of hydrogen ions by chromium attachment to polyacrylamide, and the equilibria existing between different chromium species. Provision should be made to include porous media/fluid interactions.
3. Laboratory displacements using the Aldrich polyacrylamide/redox system developed by Marty et al.<sup>3</sup> should be conducted at higher flow velocities (> 3.0 feet/day) and simulated with the in situ gelation model. The objective of this work would be to determine whether higher porous media shear rates affect polyacrylamide/redox in situ gelation systems.
4. A kinetic study of chromium oligomerization and its relationship to gelation of polymer solutions should be conducted. Oligomerization rate constants resulting from this study should be installed in the biopolymer gelation model to see if the Hejri<sup>4</sup> displacement data can be simulated.

5. In future field in situ gelation displacements the effect of reservoir pH should be considered. Based on known or assumed reservoir pH behavior, gelling solutions can be tailored to a specific well and formation environment by varying the concentrations of reduction reaction ingredients and the injected solution pH.
6. When injecting into a formation with multiple zones of widely varying permeability, the highest permeability zones should be mechanically isolated with stimulation tools to force the injected solution into those zones. If this is not possible all open zones will be plugged by the in situ gelation treatment, requiring remedial treatments to reopen lower permeability, potentially oilbearing zones.

## Definition of Variables

### Arabic Characters:

A,B,C	: curve fitting parameters, $[H^+]$ equation
C	: concentration of particles to be filtered on a volume per volume basis
$C_i$	: concentration of component i on a mass per volume basis
$C_{fi}$	: the factor by which polymer species "i" compacts when deposited
$C_{i(d)}$	: concentration of component "i" in a deposit
$C_p$	: local polymer concentration, moles/liter
$C_t$	: total fluid compressibility, 1/psi
F	: curve fitting parameter, $Cr^{+3}$ uptake equation
$G'$	: storage modulus of a gelling fluid, force/area
$G'_{en}$	: initial storage modulus of a gelling fluid, caused by polymer entanglements, force/area
$G'_{max}$	: maximum storage modulus of a gelling fluid, force/area
GIP	: gelation inhibition parameter
$K_{obs}$	: observed rate constant for the chromium monomer-monomer reaction, liter/mole
$K_{i,j}$	: rate constant for higher oligomerization reactions, liter/mole
$K_r$	: longitudinal dispersion constant in radial coordinates, length <sup>2</sup> /time
$K'$	: fluid consistency index of a polymer solution
$k_1, k_2$	: reaction rate constants for Maxcy's <sup>5</sup> reduction reaction equation
$k_{upt}$	: reaction rate constant for the $Cr^{+3}$ uptake reaction
$k_{wp}$	: permeability of a sandpack to brine after contact with polymer
$k_{wi}$	: initial permeability of a sandpack to brine before contact with polymer
$k_x$	: permeability in the x direction, adjusted for deposition, length <sup>2</sup>
$MW_{ru}$	: molecular weight of a polymer repeat unit, gm/mole
$MW_p$	: molecular weight of a polymer chain, gm/mole
n	: crosslink density, crosslinks per unit volume.
$n_c$	: flow behavior index of a polymer solution in a core
$n_{en}$	: entanglement crosslink density due to $G'_{en}$ in crosslinks per unit volume of fluid
$n'$	: flow behavior index of a polymer solution

$N_r$  : dimensionless particle diameter. Also, the number of radial grid nodes in a radial well model  
 $p$  : pressure in the liquid phase, force/area  
 $PSR$  : psuedo rate constant in the filtration equation  
 $R_i$  : non-linear kinetic reaction term, volume/volume/time  
 $R_k$  : curve matching parameter, G' equation  
 $r$  : reservoir radius, length  
 $r_w$  : wellbore radius, length  
 $r_e$  : external reservoir radius, length  
 $S.R.$  : shear rate in the porous media, 1/time  
 $t$  : time  
 $V_D$  : Darcy fluid velocity, length/time  
 $V_i$  : interstitial fluid velocity, length/time  
 $W_f$  : weight fraction of chromium oligomer species

Greek Characters:

$\alpha$  : parameter for radial grid generation  
 $\epsilon_i$  : the fraction of interception collisions that result in deposition of the colliding particle  
 $\epsilon_k$  : interception efficiency resulting from kinetic interactions of the floating particle with previously deposited polymer  
 $\epsilon_{shr}$  : interception efficiency resulting from shearing forces at the porous media interface  
 $\Gamma$  : the filtration rate coefficient, 1/length  
 $\phi$  : current porosity adjusted for deposition  
 $\lambda^*_p$  : polymer mobility constant  
 $\lambda^*_{PEK}$  : polymer mobility constant for the modified Blake-Kozeny model  
 $\mu$  : fluid viscosity, cp  
 $\mu_p$  : viscosity of polymer solution at 100% of injected polymer concentration, cp  
 $\mu_o$  : viscosity of polymer solution having only entanglement crosslinks, cp  
 $\sigma$  : total fraction of porosity occupied by deposits in all of the pores  
 $\sigma_{ads}$  : the fraction of porosity occupied by the adsorbed polymer layer  
 $\sigma_i$  : the fraction of porosity occupied by interception deposits  
 $\sigma_s$  : the fraction of porosity occupied by straining deposits

## REFERENCES

1. McCool, C.S., "An Experimental Study of the In Situ Gelation Polyacrylamide/Chromium(III)/Thiourea System in a Porous Medium", Doctoral Dissertation, University of Kansas, 1988.
2. McCool, C.S., Willhite, G.P. and Green, D.W., "Permeability Reduction Mechanisms Involved in In Situ Gelation of a Polyacrylamide/Chromium(VI)/Thiourea System", SPE/DOE 17333, presented at the SPE/DOE Enhanced Oil Recovery Symposium, Tulsa, Oklahoma, April 17-20, 1988.
3. Marty, L., Green, D.W. and Willhite, G.P., "The Effect of Flowrate on the In Situ Gelation of a Chrome/Redox/Polyacrylamide System", SPE 18504, Presented at Society of Petroleum Engineers International Symposium on Oilfield Chemistry, February 8-10, 1989, Houston, Texas.
4. Hejri, S., "An Experimental Investigation into the Flow and Rheological Behavior of Xanthan Solutions and a Xanthan/Cr(III) Gel System in Porous Media", Doctoral Dissertation, University of Kansas, 1989.
5. Sorbie, K.S., Roberts, L.J. and Clifford, P.J., "Calculations on the Behavior of Timesetting Polymer Gels in Porous Media", presented at the AIChE National Spring Meeting, Houston, Texas, 1985.
6. Sorbie, K.S., Roberts, L.J. and Clifford, P.J., "Experimental and Theoretical Study of Polymer Flow in Porous Media", SPE #14231, presented at the Annual Technical Conference at Las Vegas, Nevada, September 22-25, 1985.
7. Scott, T., Roberts, L.J. and Short, S.R., "In Situ Gel Calculations in Complex Reservoir Systems Using a New Chemical Flood Simulator", SPE #14234, presented at the Annual Technical Conference at Las Vegas, Nevada, September 22-25, 1985.
8. Hubbard, S., Roberts, L.J. and Sorbie, K.S., "Experimental and Theoretical Investigation of Timesetting Polymer Gels in Porous Media", SPE #14959, presented at the Fifth Symposium on Enhanced Oil Recovery, Tulsa, Oklahoma, April 20-22, 1986.
9. Hortes, E., "Development of a Reservoir Model for Polymer/Gel Treatments", Report 87-3, University of Texas at Austin, 1986.
10. Pope, G.A., Lake, L.W. and Sepehrnoori, K., "Modeling and Scale-up of Chemical Flooding - Final Report", work performed under DOE Contract No. AC19-85BC10846, March, 1987.

11. French, T.R., "Development of Improved Mobility Control Methods", work performed under DOE Cooperative Agreement No. DE-FC22-83FE60149, Project BE4C, published in Quarterly Progress Review, US Department of Energy, December 31, 1987.
12. French, T.R. and Gao, H.W., "Development of Improved Mobility Control Methods", work performed under DOE Cooperative Agreement No. DE-FC22-83FE60149, Project BE4C, published in Quarterly Progress Review, US Department of Energy, June 30, 1988.
13. Todd, B.J., "Numerical Modeling of In Situ Gelation in Porous Media", Doctoral Dissertation, University of Kansas, 1990.
14. Maxcy, T.A., Ph.D Dissertation in Progress, University of Kansas, 1990.
15. Southard, M.Z., "A Kinetic Study of the Reaction Between Chromium(VI) and Thiourea at 80 Degrees in the Presence of Polyacrylamide", M.S. Thesis, University of Kansas, 1983.
16. Southard, M.Z., Green, D.W. and Willhite, G.P., "Kinetics of the Chromium(VI)/Thiourea Reaction in the Presence of Polyacrylamide", SPE #12715, presented at the Fourth Symposium on Enhanced Oil Recovery, Tulsa, Oklahoma, April 15-18, 1984.
17. Hunt, J.A., "An Experimental Study of the Kinetics of the Cross-Linking Reaction Between Chromium(III) and Polyacrylamide", Doctoral Dissertation, University of Kansas, 1987.
18. Bhaskar, R.K., "Transient Rheological Properties of Chromium/Polyacrylamide Solutions under Superposed Steady and Oscillatory Shear Strains", Doctoral Dissertation, University of Kansas, 1988.
19. Willhite, G.P. and Dominguez, J.G., "Mechanisms of Polymer Retention in Porous Media", Improved Oil Recovery by Surfactant and Polymer Flooding, Academic Press, New York, 1977.
20. Marty, L., Laboratory Notebooks, University of Kansas, 1988.
21. Hunt, J.A., Young, T-S., Green, D.W. and Willhite, G.P., "Application of Size Exclusion Chromatography in the Measurements of Concentration and Molecular Weight of Some EOR Polymers", SPE #14949, presented at the Fifth Symposium on Enhanced Oil Recovery, Tulsa, Oklahoma, April 20-23, 1986.
22. Willhite, G.P., Green, D. W. Thiele, J.L., Young, T-S and Mertes, K.B., "Investigation of the Application of Gelled Polymer Systems for Permeability Modification in Petroleum Reservoirs -- Final Report" Work Performed under DOE Contract No. DOE/BC/10843-15, March, 1990.

23. McCallister, P., Internally generated report, Tertiary Oil Recovery Project, University of Kansas, 1987.
24. FLOCON Biopolymer 4800, "Mobility Control for Enhanced Oil Recovery", Pfizer Inc., Chemical Division, 1986.
25. Fei, R-J., "Personal Communication", University of Kansas, 1990.
26. Rotzinger, F.P., Stünzi, H. and Marty, W., "Early Stages of the Hydrolysis of Chromium(III) in Aqueous Solution 3. Kinetics of Dimerization of the Deprotonated Aqua Ion", Inorganic Chemistry, 1986, Volume 25, pages 489-495.
27. Stünzi, H. and Marty, W., "Early Stages of the Hydrolysis of Chromium(III) in Aqueous Solution 1. Characterization of a Tetrameric Species", Inorganic Chemistry, 1982, Volume 22, pages 2145-2150.
28. Besso, C., "Etude Cinetique et Mecanistique de la Dimerisation du Dimer du Cr(III)", Doctoral Dissertation, University of Neuchatel, 1983.
29. Dolan, D.M., "An Experimental Study of the Effects of pH and Shear on the Gelation of a Xanthan-Chromium(III) Solution", M.S. Thesis, University of Kansas, 1989.
30. Hejri, S., Willhite, G.P., and Green, D.W., "Development of Correlations to Predict Flocon 4800 Biopolymer Mobility in Porous Media", SPE/DOE 17396, presented at the SPE/DOE Enhanced Oil Recovery Symposium, Tulsa, Oklahoma, April 17-20, 1988.
31. Dake, L.P., Fundamentals of Reservoir Engineering, Elsevier Press, New York, 1978.
32. Schoeling, L.J., "Personal Communication", University of Kansas, 1990.
33. Lange, N.A., "Lange's Handbook of Chemistry", Handbook Publishers, Inc., Sandusky, Ohio, 1985.

TABLE 8.1

Parameters used in Marty et al. Gelation Simulations

PSR	:	0.00290
GIP	:	3.00
Compaction factor (small-mer)	:	1.43
Compaction factor (medium-mer)	:	1.35
Compaction factor (big-mer)	:	1.30
Compaction factor (huge-mer)	:	1.22
Compaction factor (gel-mer)	:	1.10

TABLE 8.2

Location and Extent of McCool's Zones of Flow Resistance

Displacement Number	Flow Rate (cc/hour)	Time of Final Plugging (hours)	Position of Magic Spot (cm)
SP7	3.4	198	67-77
SP8	3.7	250	67-87
SP10	3.5	240	77-97

TABLE 8.3

Comparison of Simulated and Actual Zones of Flow Resistance for McCool's System

Displacement Number	Time of Final Plugging (hours)	Center of Magic Spot (cm from inlet)
SP7	198	72
SP8	250	77
SP10	240	87
Simulation	240	76.4

TABLE 8.4

## Parameters used in Gelation Simulations

Parameter	McCool	Marty
Pseudo Rate Constant	0.00135	0.0029
Gelation Inhibition Parameter	2.75	3.00
Compaction factor (small-mer)	1.24	1.43
Compaction factor (medium-mer)	1.21	1.35
Compaction factor (big-mer)	1.18	1.30
Compaction factor (huge-mer)	1.15	1.22
Compaction factor (gel-mer)	1.10	1.10

TABLE 8.5

## Scaling Relationships for Chromium Species Rate Constants

	monomer	dimer	trimer	tetramer
monomer	$K_{11}$	$K_{22}/2$	$3K_{22}/4$	$K_{22}$
dimer	$K_{22}/2$	$K_{22}$	$3K_{22}/2$	$2K_{22}$
trimer	$3K_{22}/4$	$3K_{22}/2$	$9K_{22}/4$	$3K_{22}$
tetramer	$K_{22}$	$2K_{22}$	$3K_{22}$	$4K_{22}$

TABLE 8.6

## pH Trends for Chromium Oligomerization Simulations

Time Interval (hours)	Concentration (ppm)	pH History (initial - final)
0.0 - 48.0	1165.0	3.4 - 3.0
48.0 - 53.0	300.0	3.3 - 3.3
53.0 - 103.0	50.0	4.76 - 4.3

TABLE 8.7

## Essential Features of Hejri's Biopolymer Displacements

Sandpack	Darcy velocity (ft/day)	Shear rate (sec <sup>-1</sup> )	Permeability (Darcy)
4	1.10	6.4	5.47
6	2.26	12.8	4.91
7	1.38	12.8	2.61

TABLE 8.8

Comparison of Parameters used in Polyacrylamide/Redox  
and Biopolymer/Cr<sup>+3</sup> Simulations

Parameter	Marty et al.	Hejri
Pseudo Rate Constant	0.0029	0.330
Gelation Inhibition Parameter	3.00	2.25
Compaction Factors	1.10 - 1.43	7.0

TABLE 8.9

Porous Media Properties for the  
Multiple-Layer Reservoir Simulation

	Upper Layer	Middle Layer	Lower Layer
Permeability (Darcies)	3.50	0.350	0.035
Porosity (fraction)	0.350	0.162	0.080
Grain Diameter (microns)	91.4	66.5	60.0
Pore length (microns)	85.0	56.9	49.7
Pore Throat Diameter (microns)	11.4	8.3	7.5

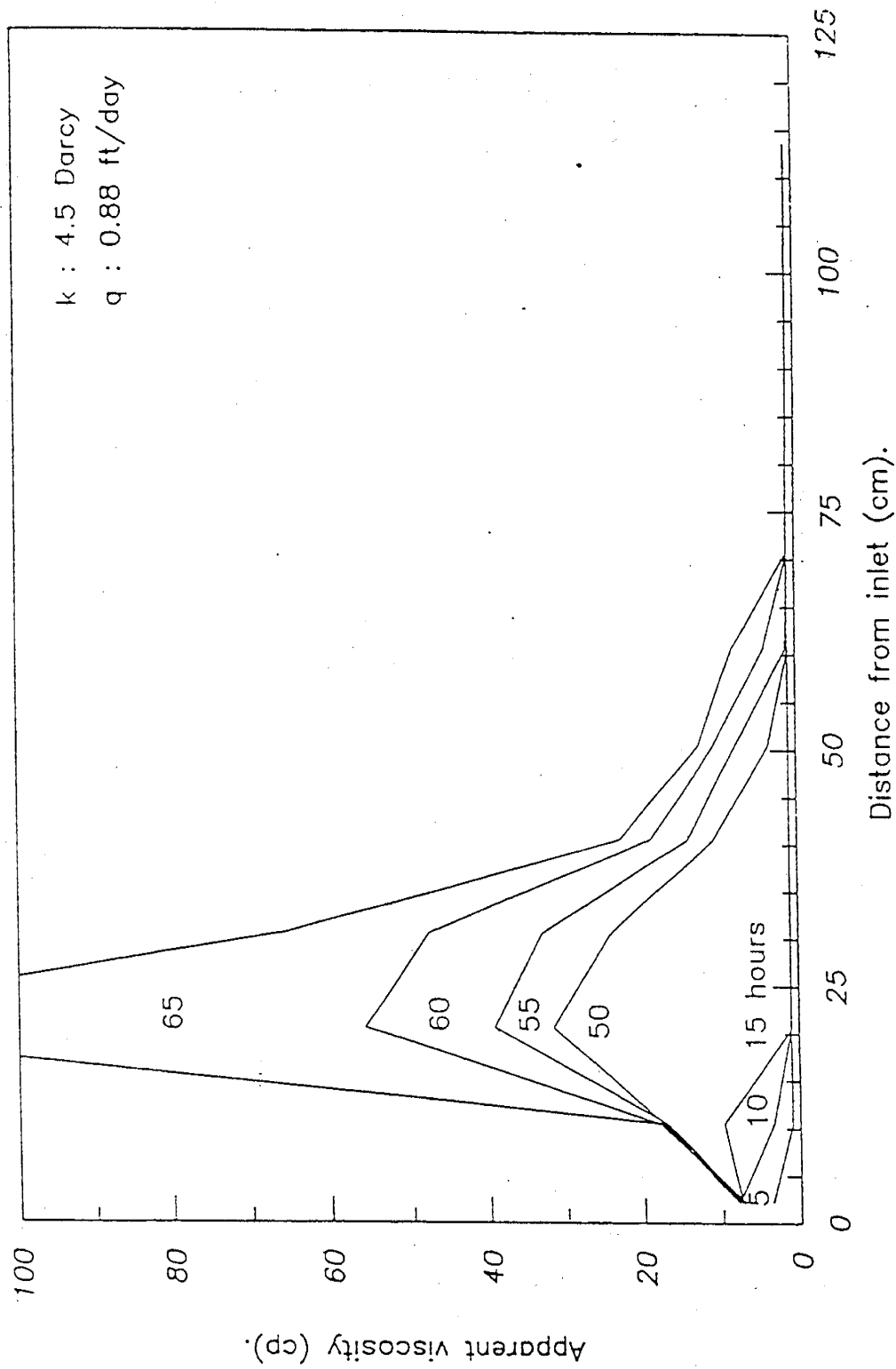


Figure 8.1 Representative Displacement Data by Marty [see Reference 3]

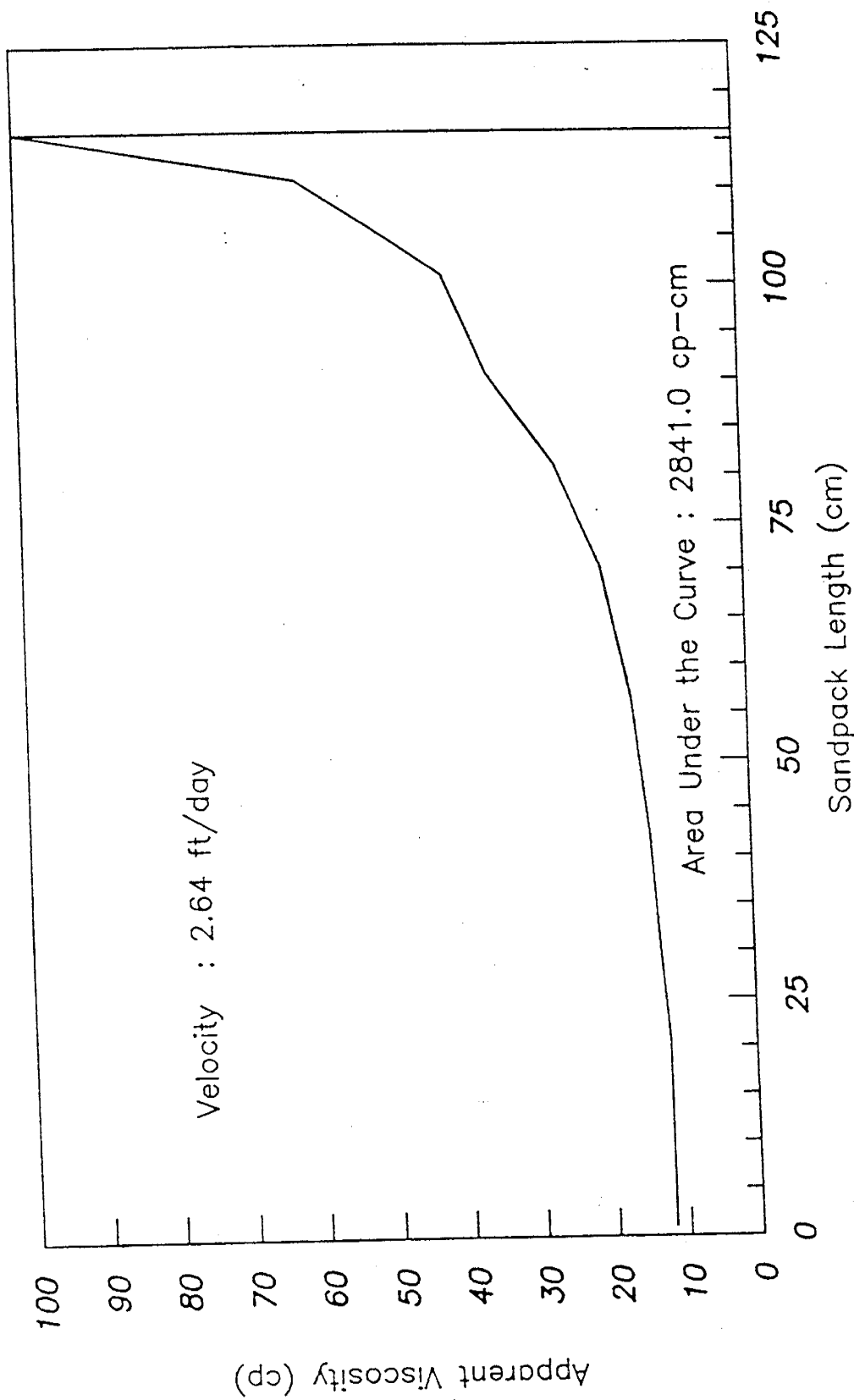


Figure 8.2 Area Under the Apparent Viscosity Profile of Marty Run #6 after 53 hours [see Reference 3]

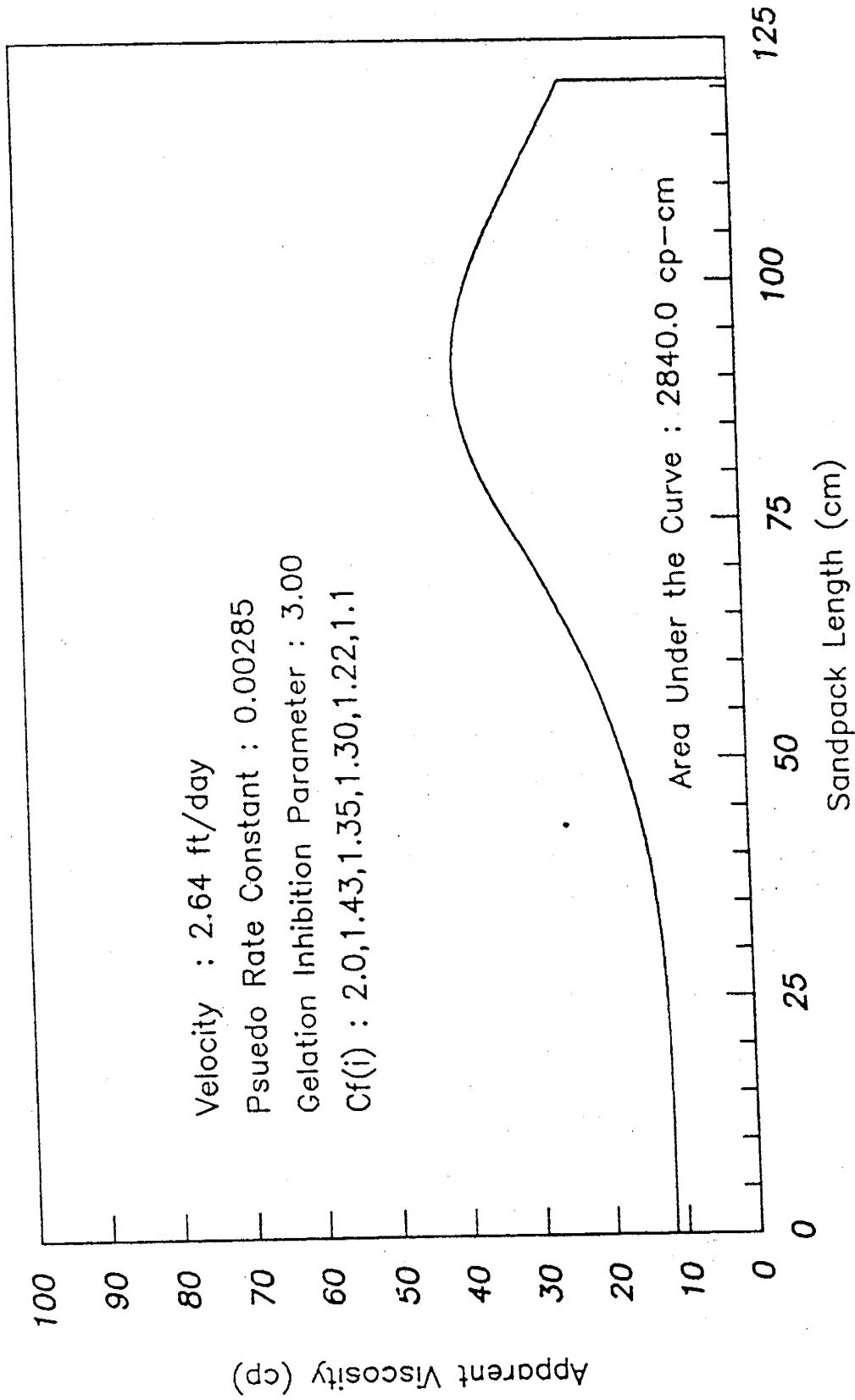


Figure 8.3 Area Under the Simulated Apparent Viscosity Profile of Marty Run #6 after 53 hours [see Reference 3]

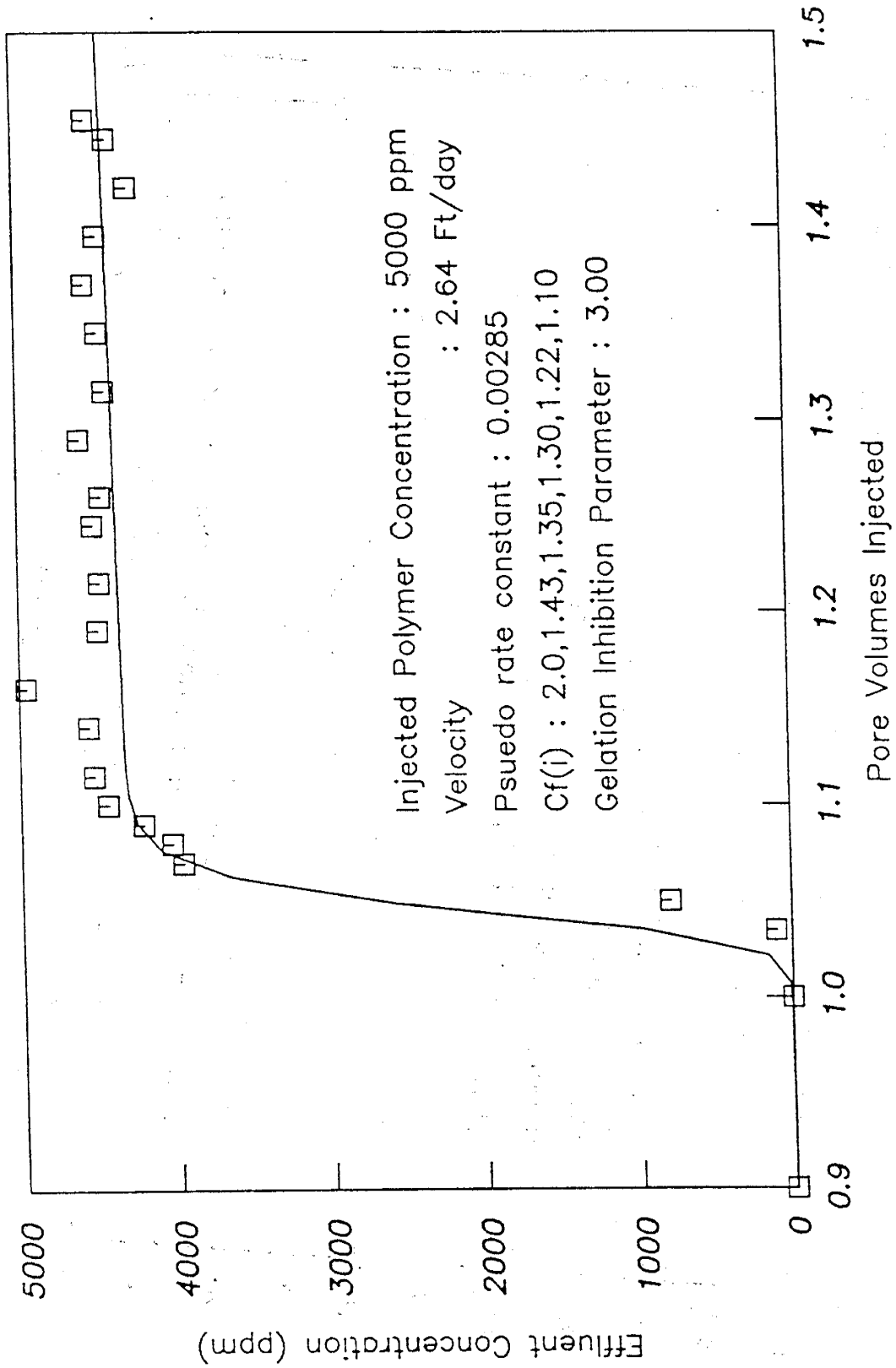


Figure 8.4 Effluent Plots from Figures 8.2 and 8.3

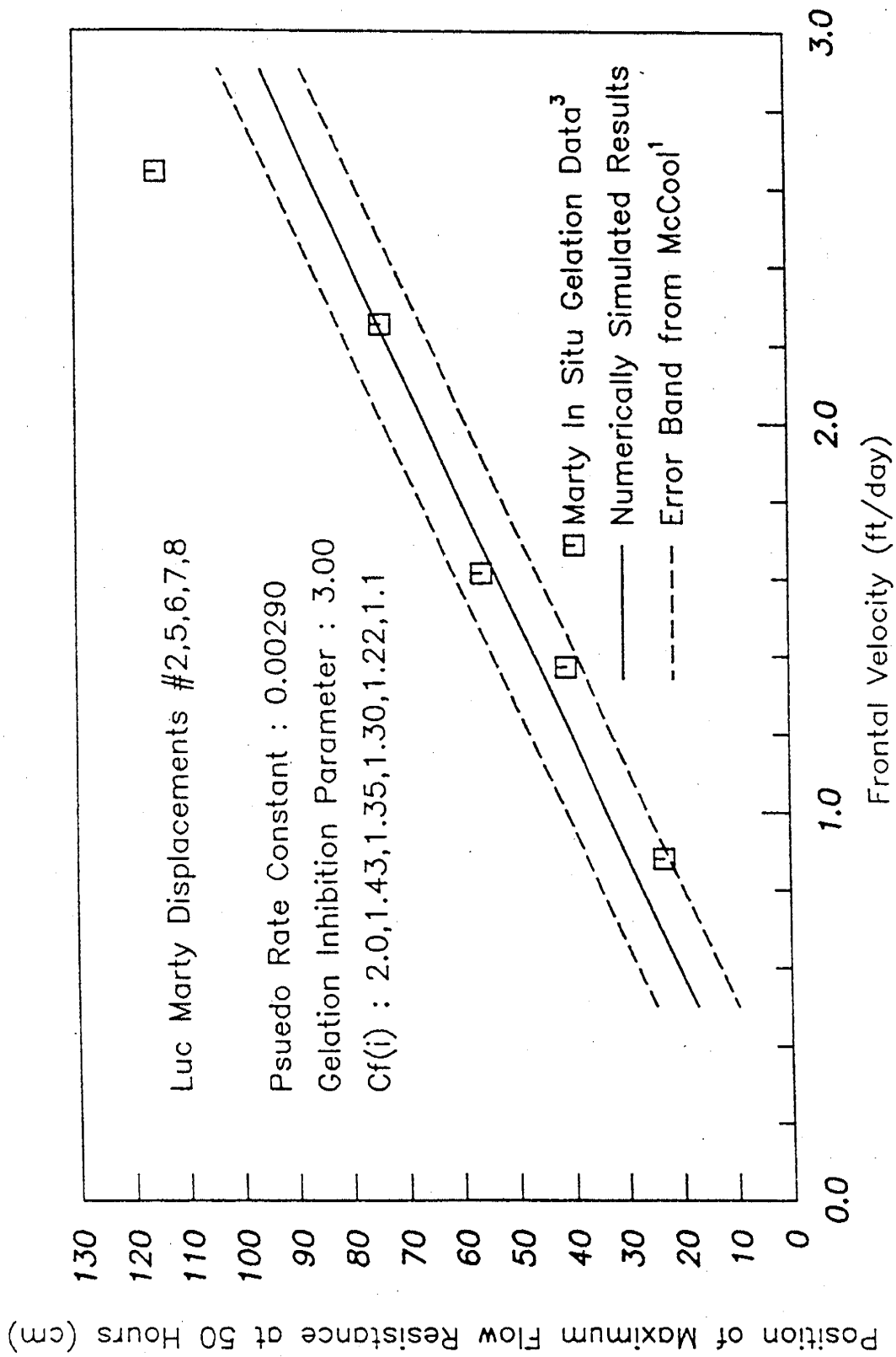


Figure 8.5 Comparison of Marty Displacement Data with Numerically Simulated In Situ Gelation Runs [see Reference 3]

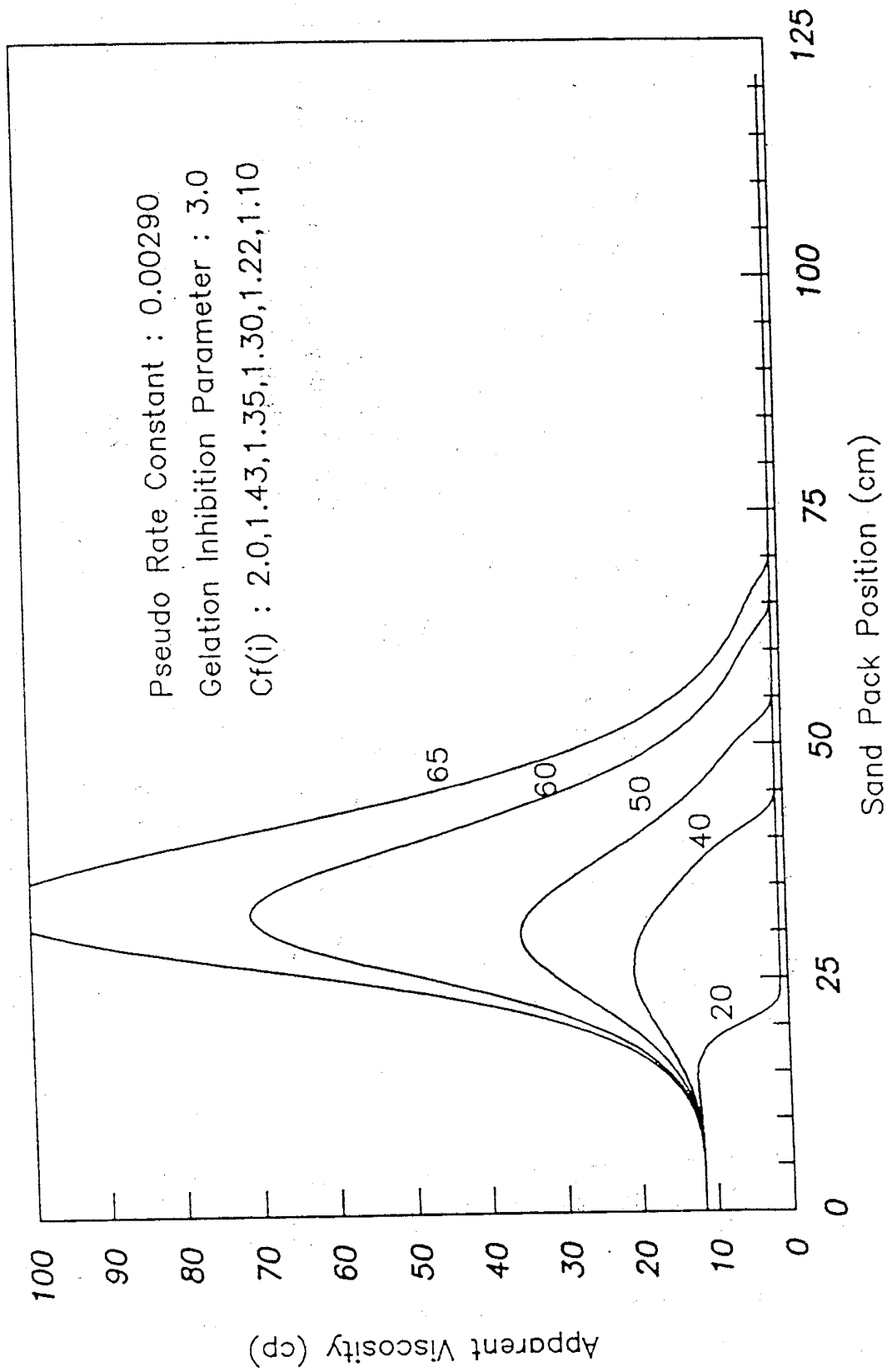


Figure 8.6A Simulated Gelation Run (0.88 ft/day)

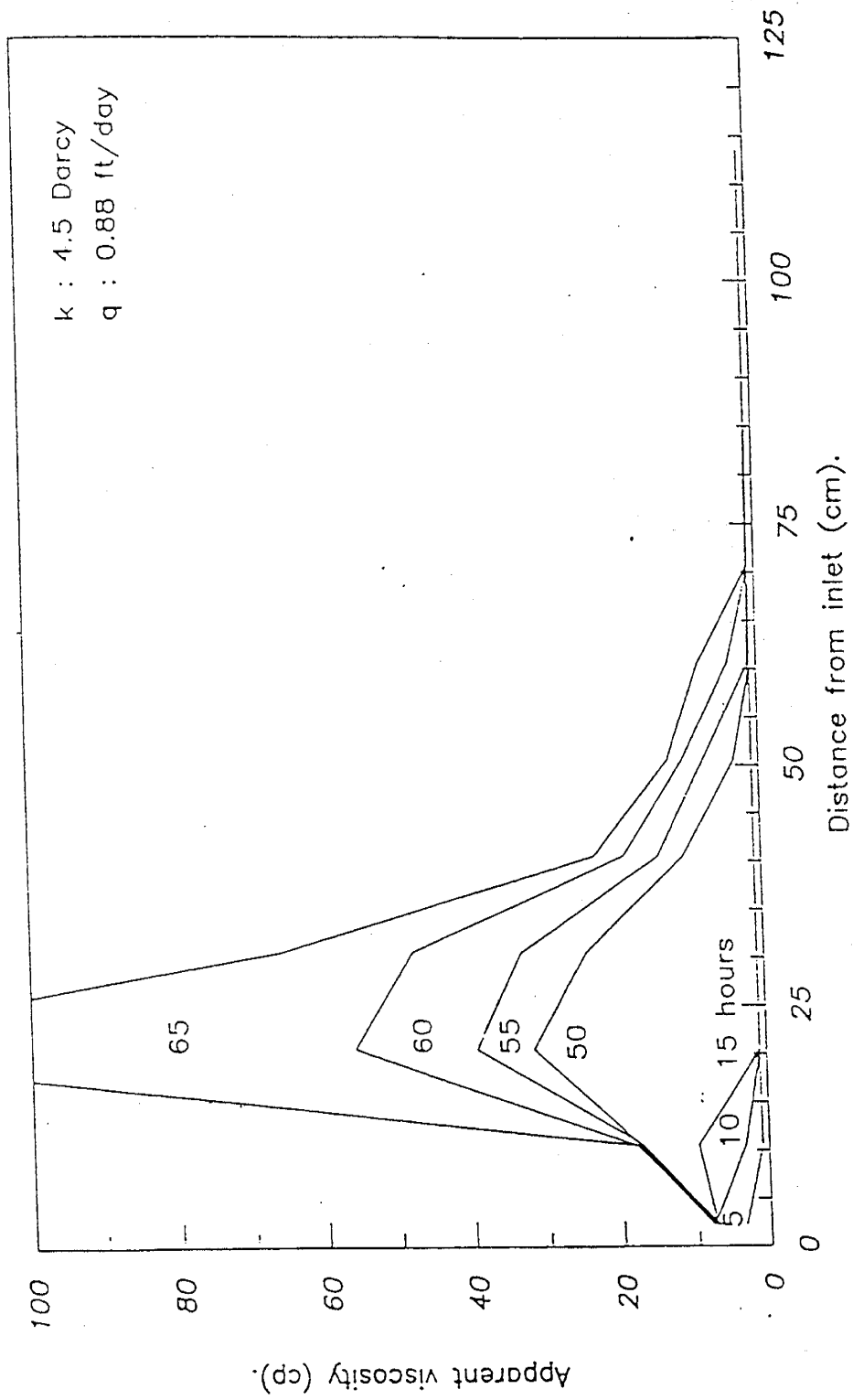


Figure 8.6B Marty Gelation Data (0.88 ft/day) [see Reference 3]

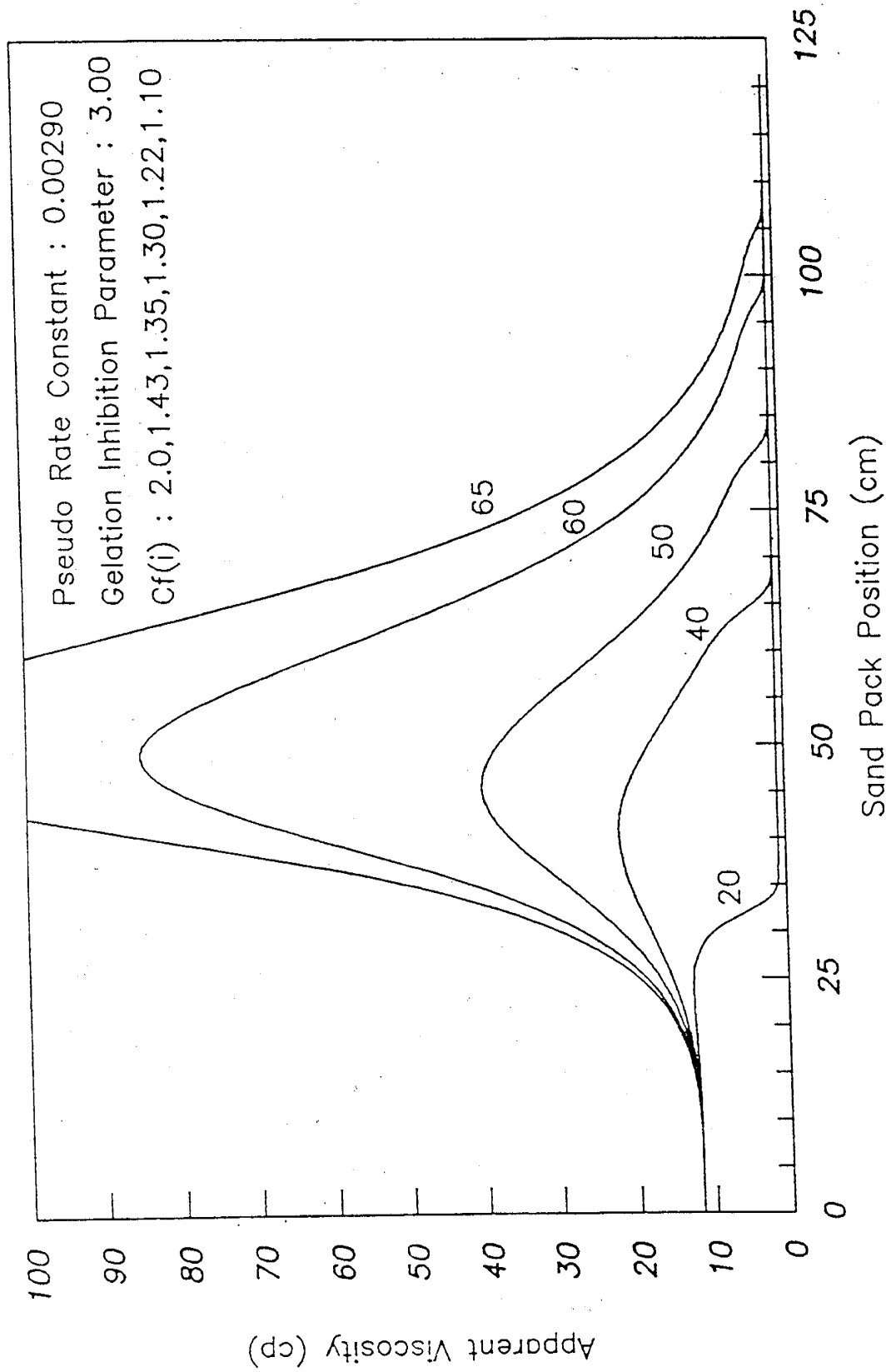


Figure 8.7A Simulated Gelation Run (1.37 ft/day)

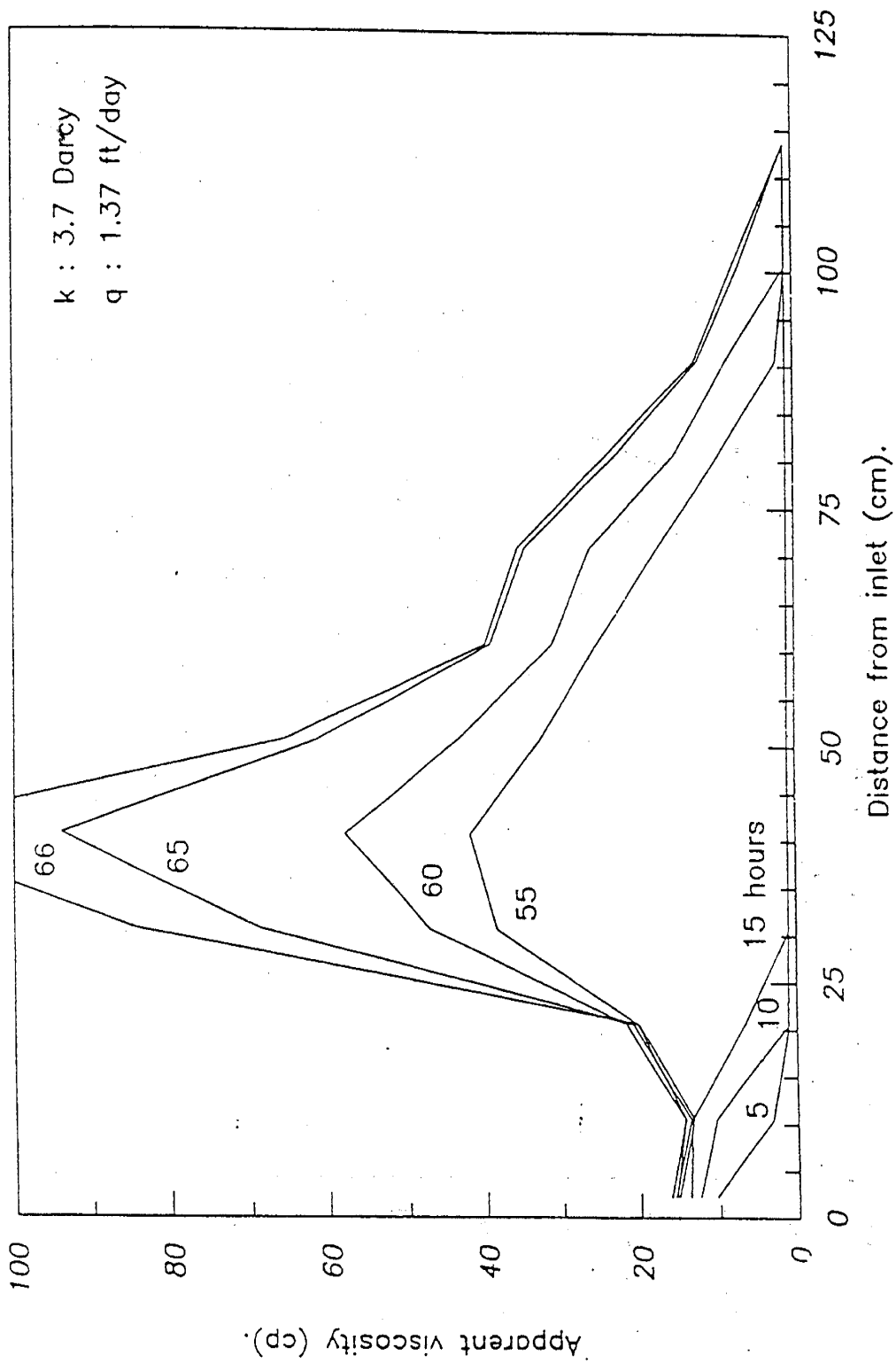


Figure 8.7B Marty Gelation Data (1.37 ft/day) [see Reference 3]

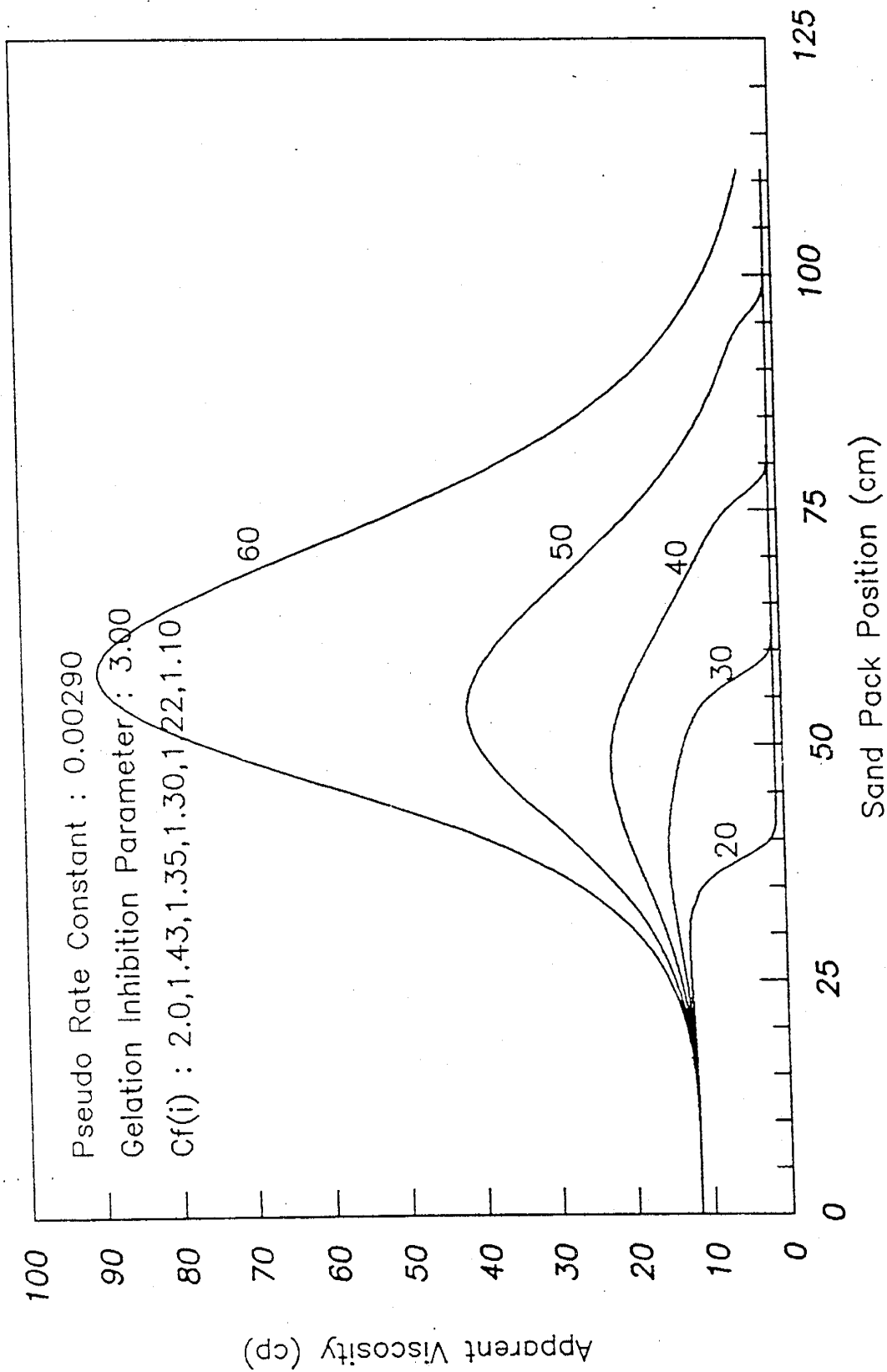


Figure 8.8A Simulated Gelation Run (1.61 ft/day)

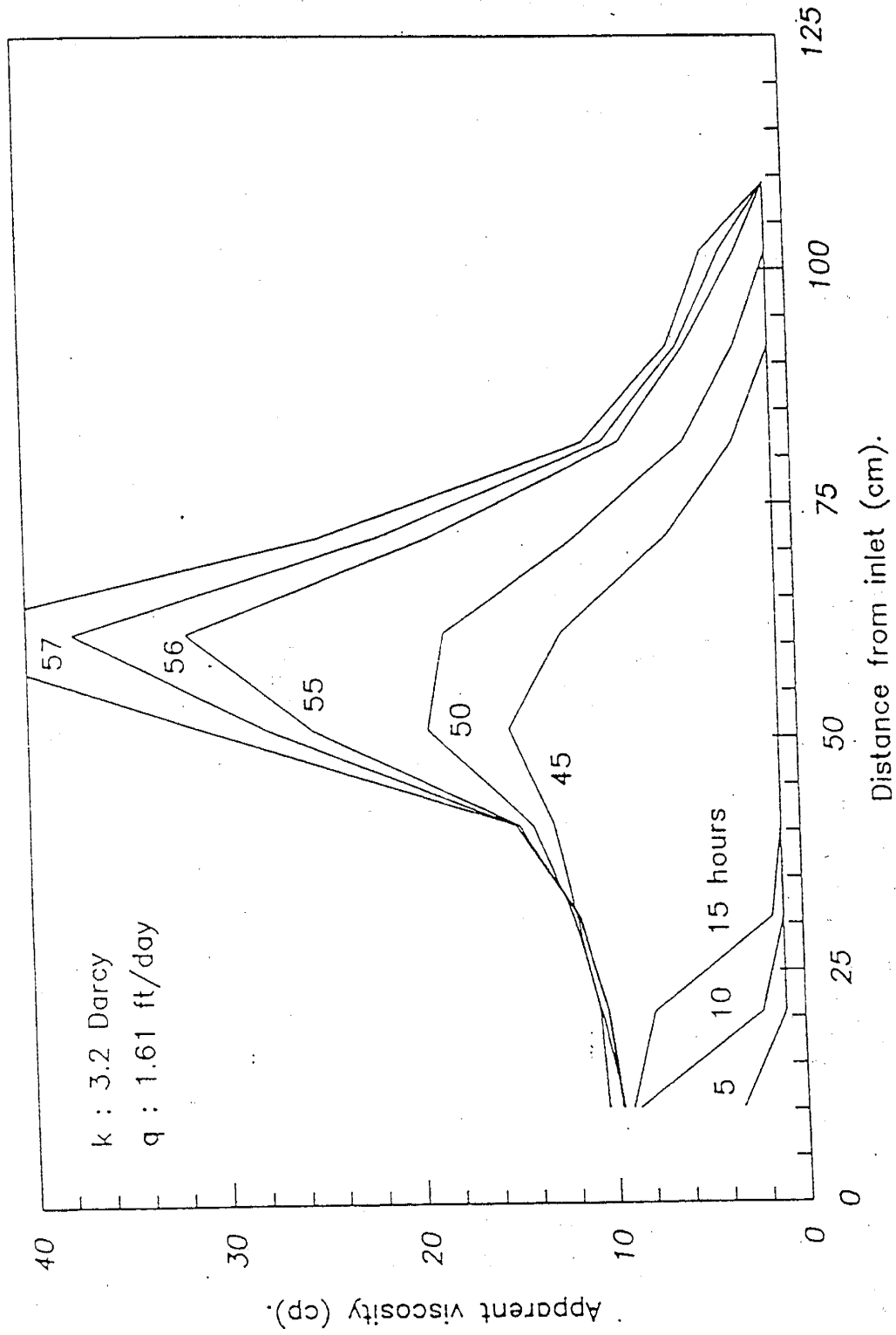


Figure 8.8B Marty Gelation Data (1.61 ft/day) [see Reference 3]

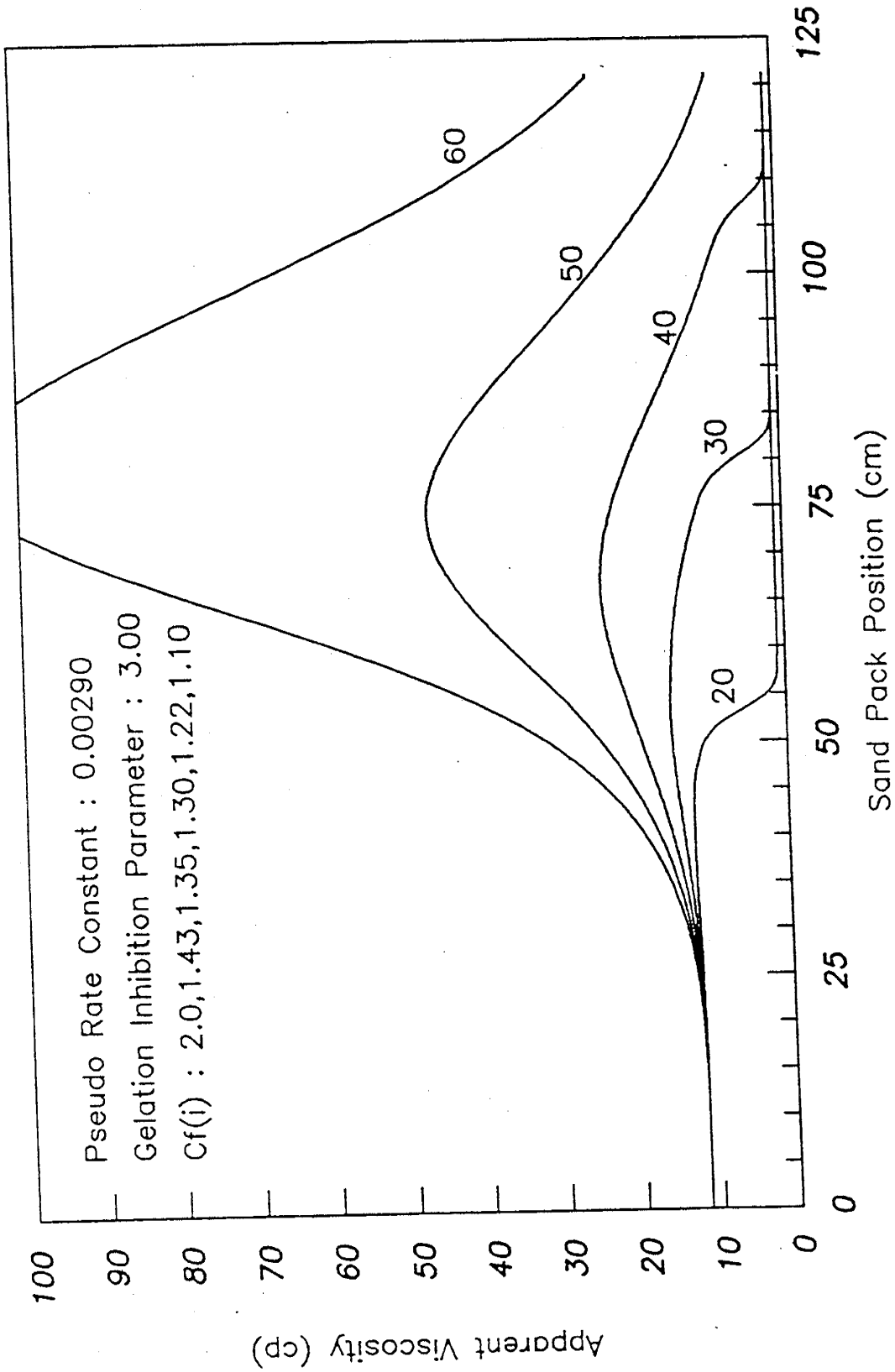


Figure 8.9A Simulated Gelation Run (2.25 ft/day)

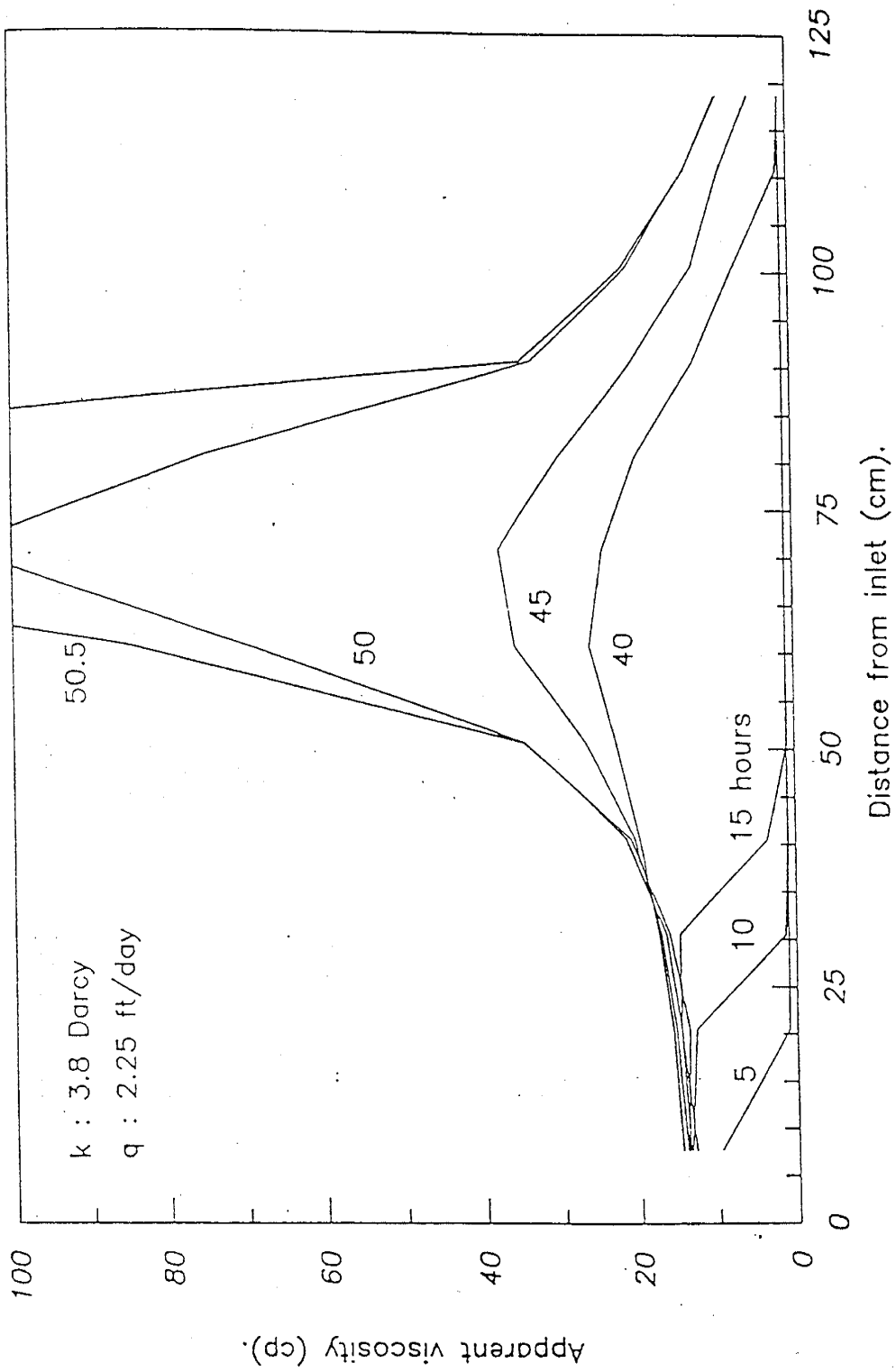


Figure 8.9B Marty Gelation Data (2.25 ft/day) [see Reference 3]

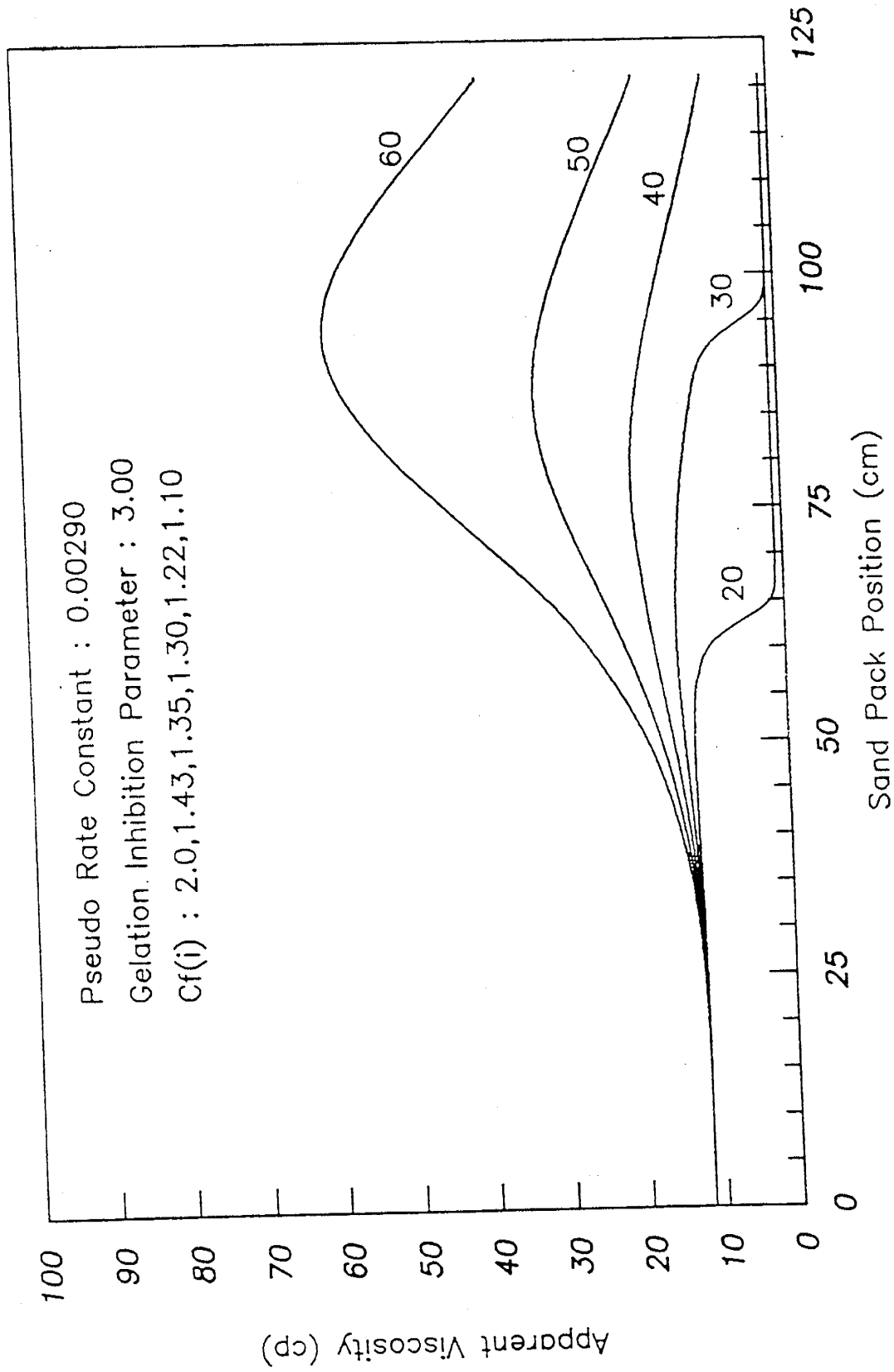


Figure 8.10A Simulated Gelation Run (2.64 ft/day)

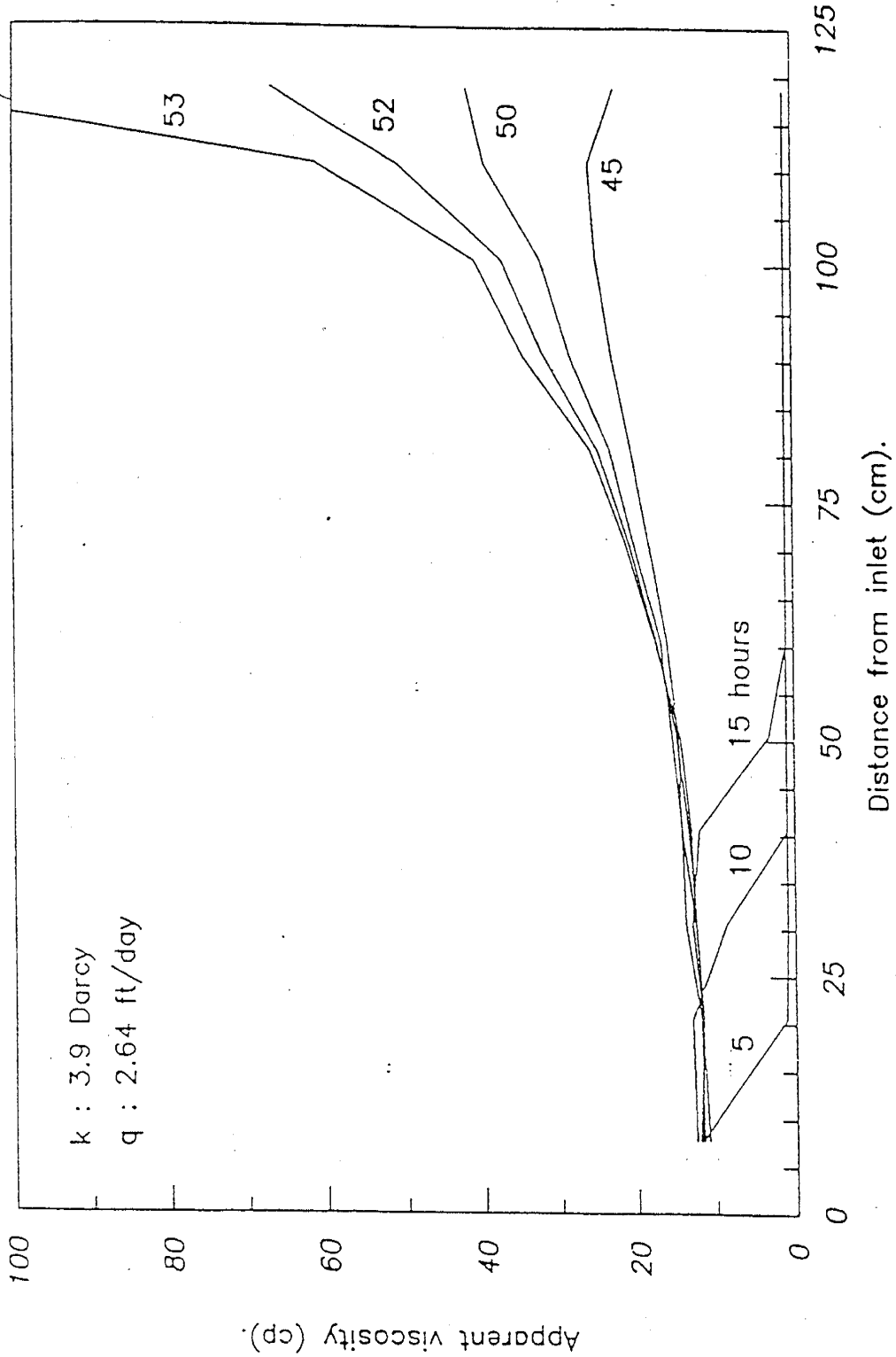


Figure 8.10B Marty Gelation Data (2.64 ft/day) [see Reference 3]

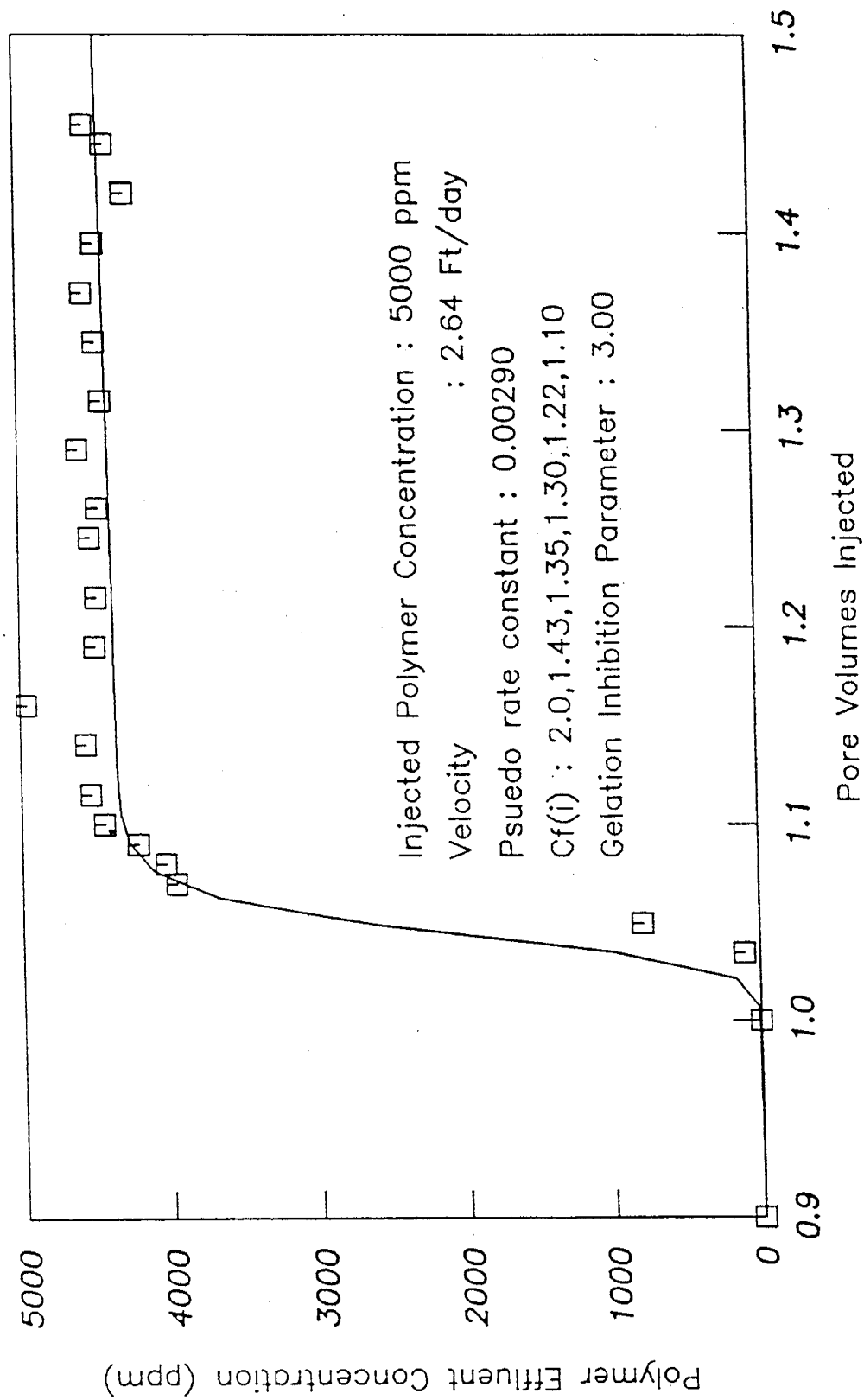


Figure 8.11 Comparison of Simulated and Actual Polymer Effluent Data (2.64 ft/day)

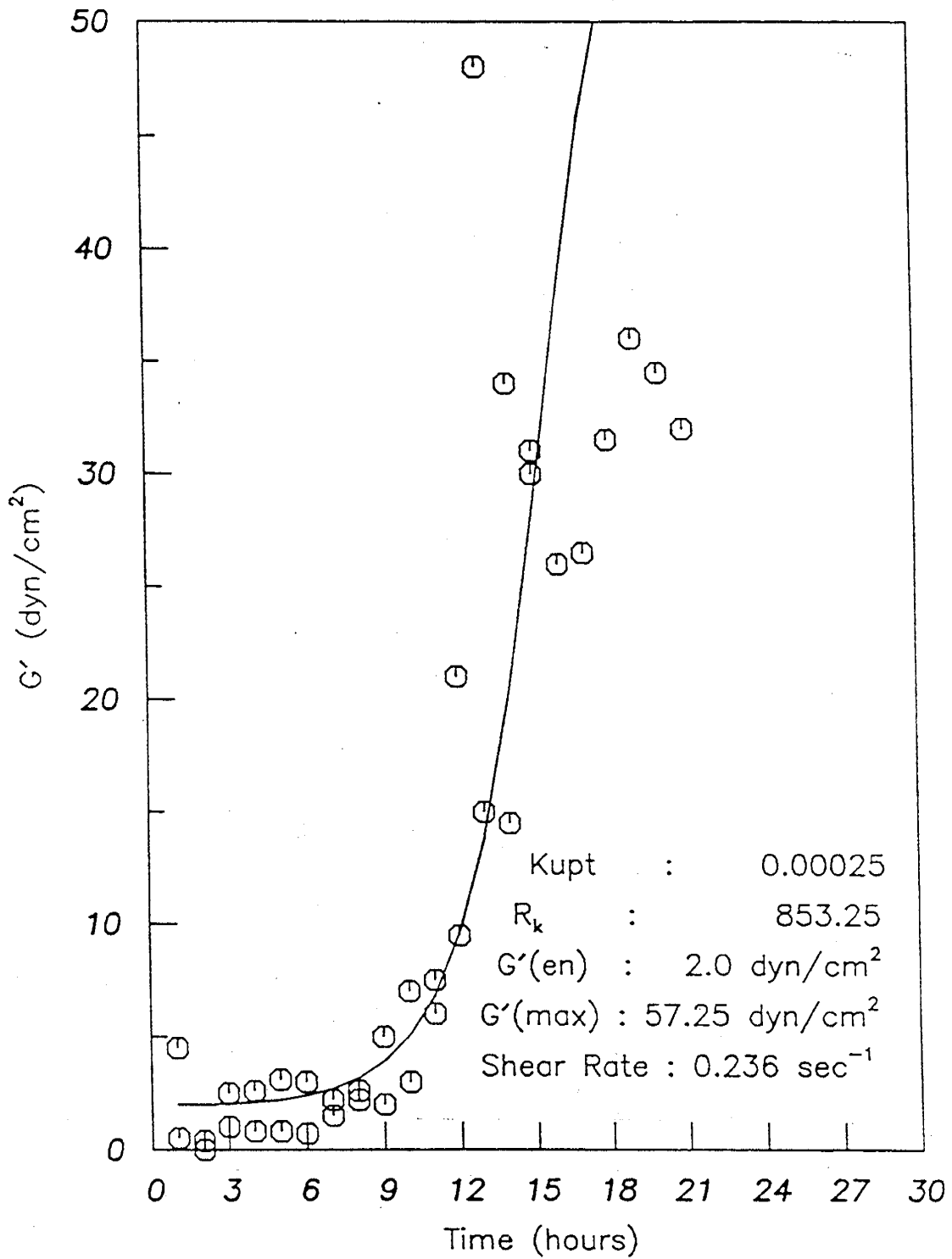


Figure 8.12 Storage Modulus Growth for Fast-Gelling Solutions Containing CatAn-160 Polyacrylamide

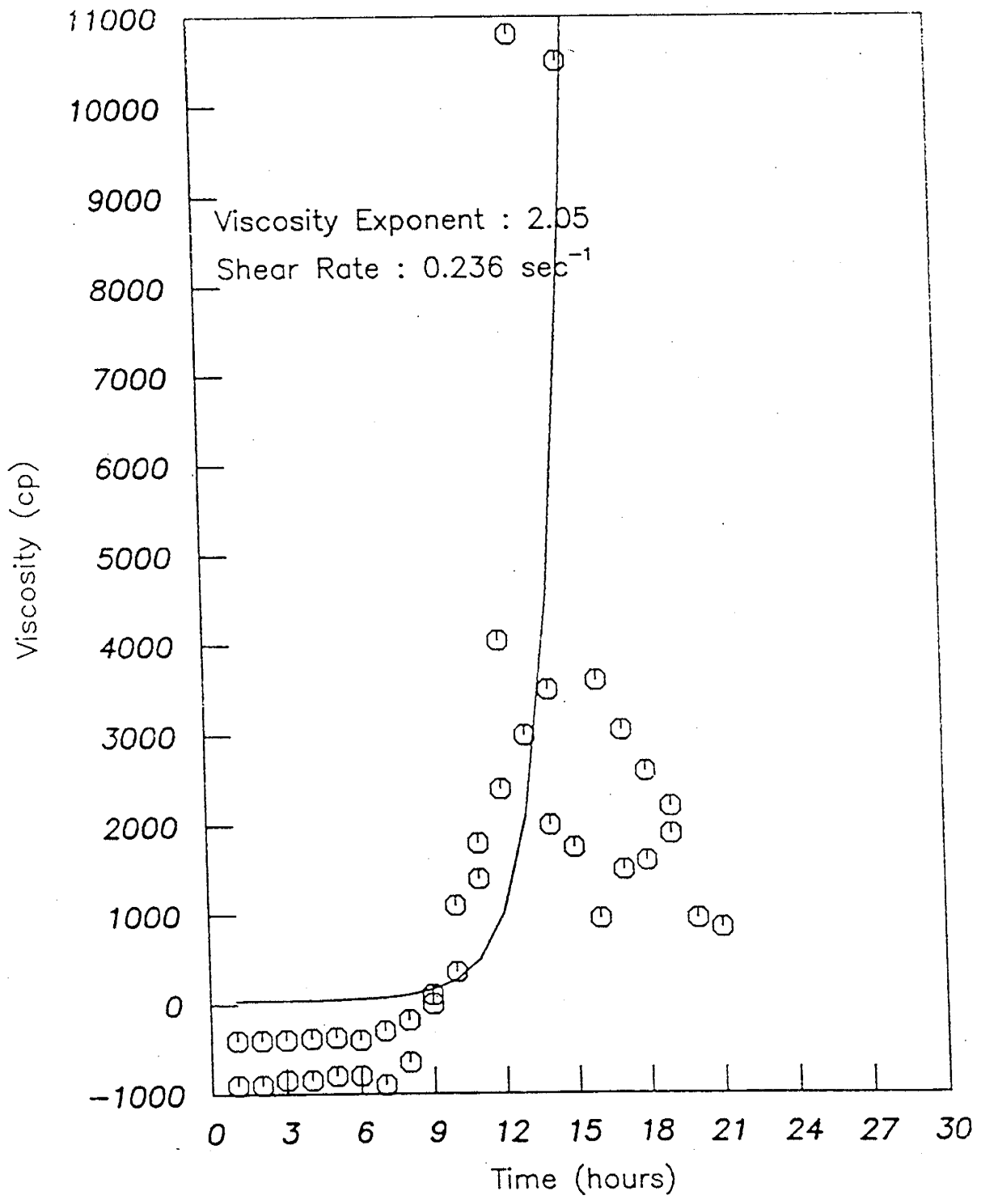


Figure 8.13 Viscosity Growth for Fast-Gelling Solutions Containing CatAn-160 Polyacrylamide

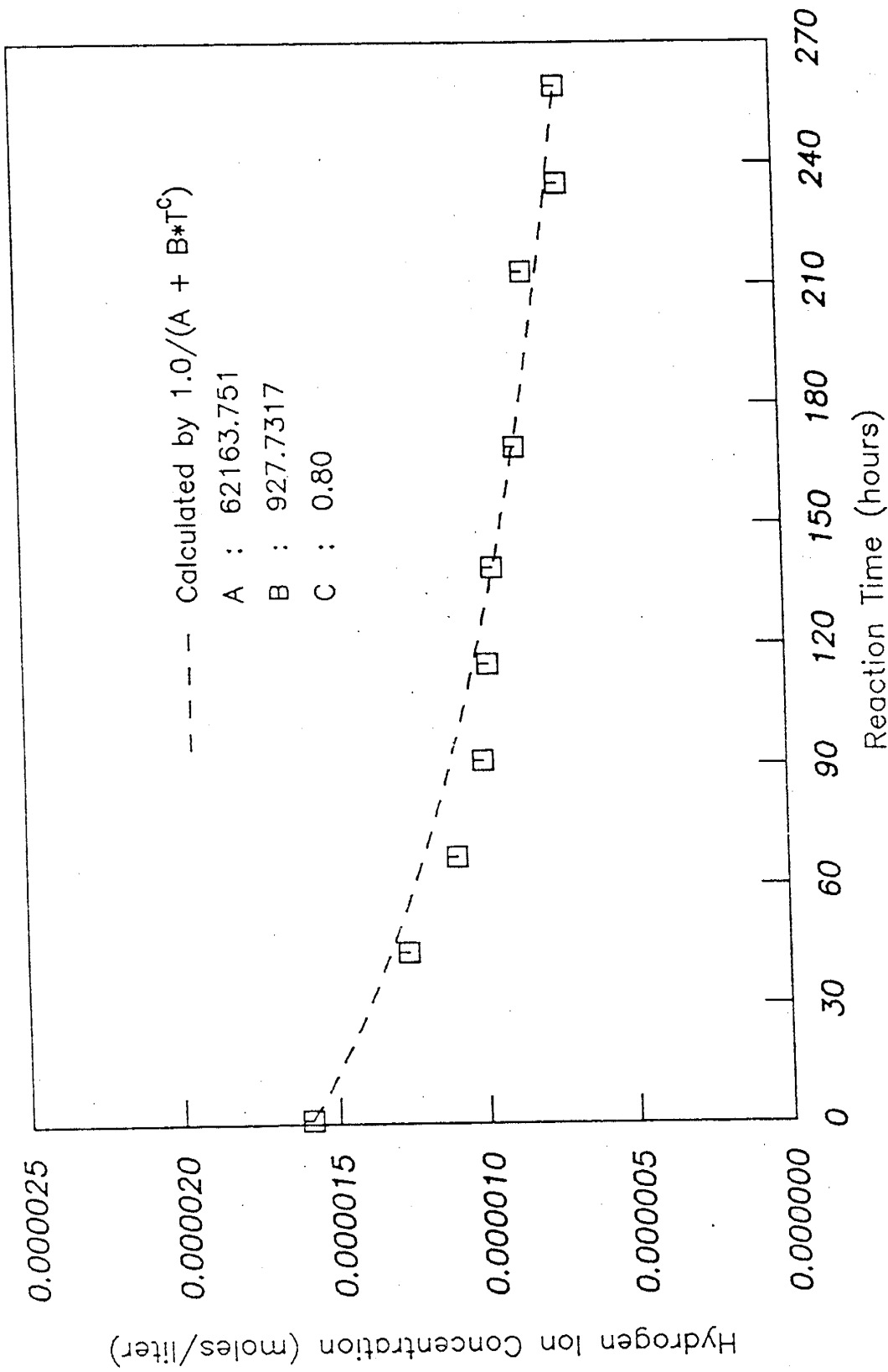


Figure 8.14 Representative Hydrogen Ion Concentration Data

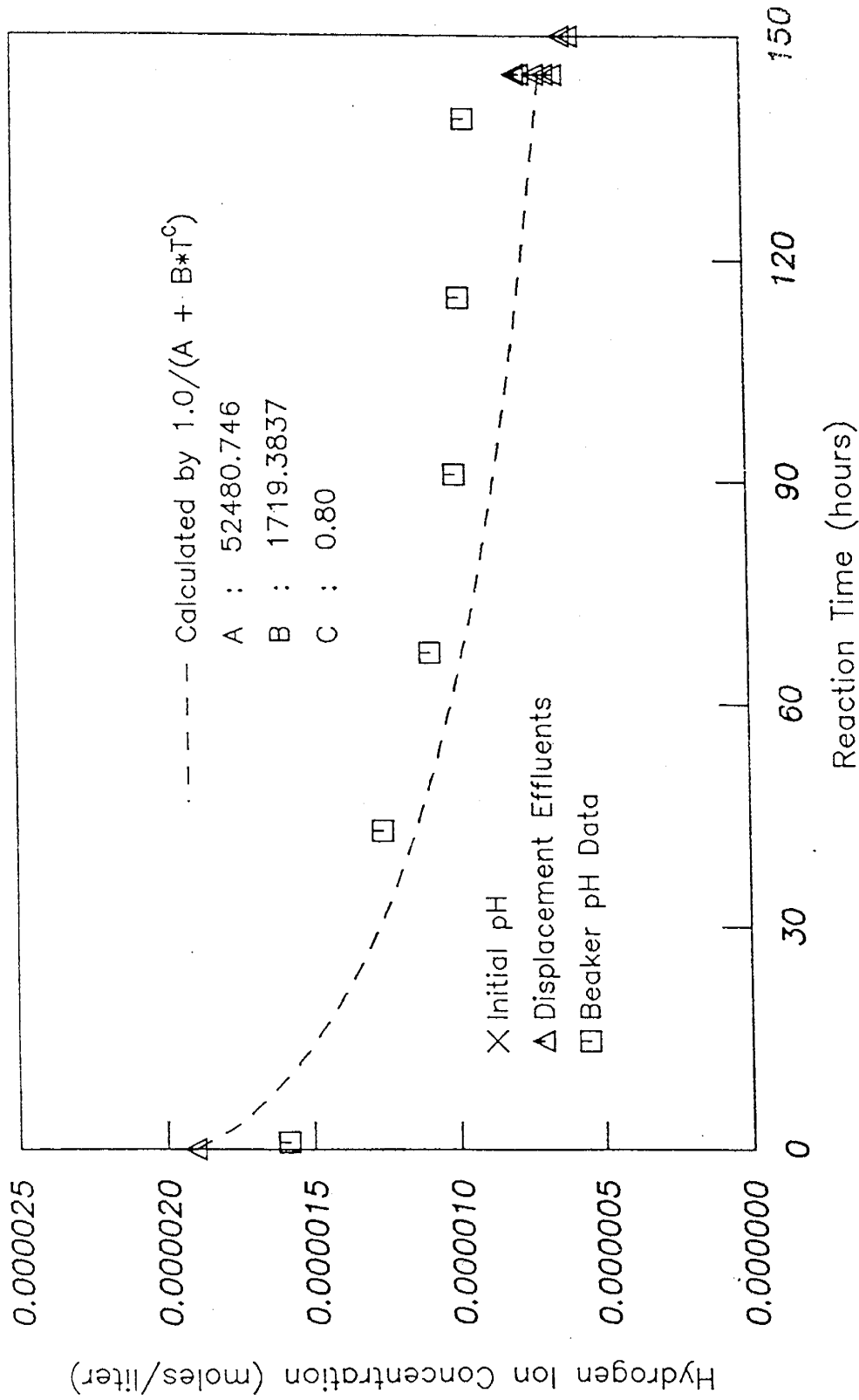


Figure 8.15 Hydrogen Ion Concentration Model for McCool Gelation Displacements [see Reference 1]

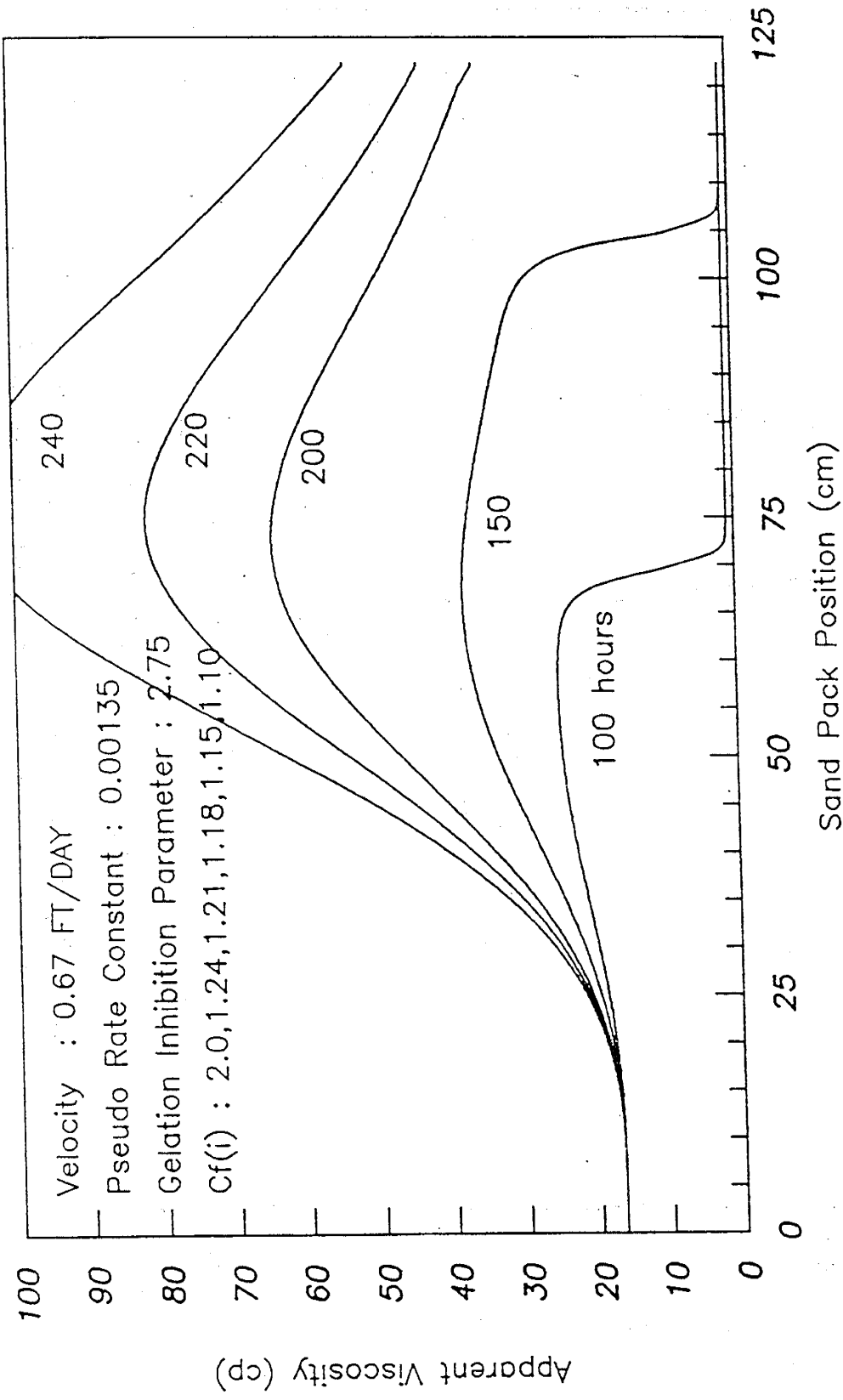


Figure 8.16 Simulation of McCool Gelation Displacements SP7, SP8, SP10 [see Reference 1]

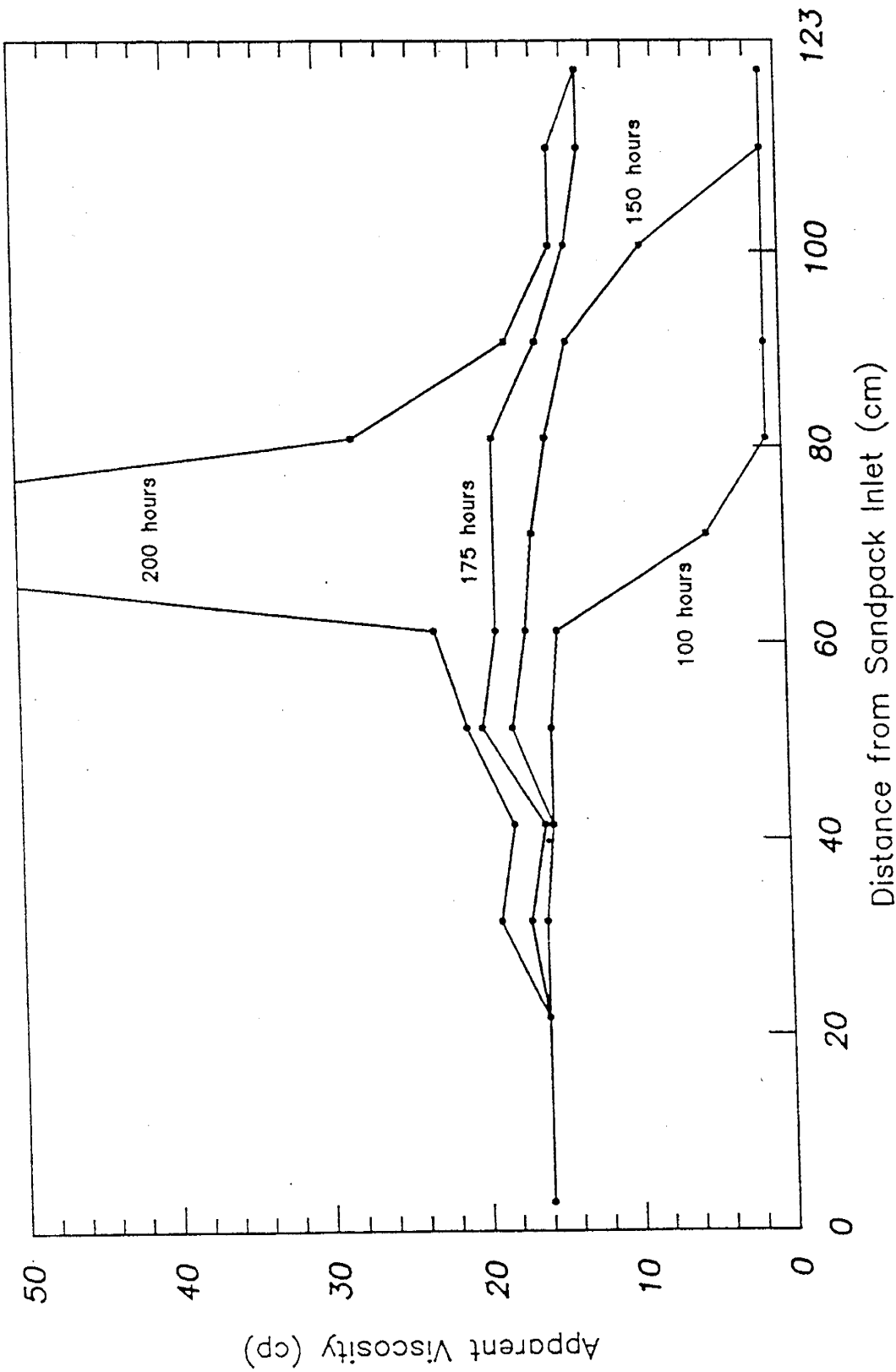


Figure 8.17a Apparent Viscosity Profiles for McCool Gel Solution Displacement SP7 [see Reference 1]

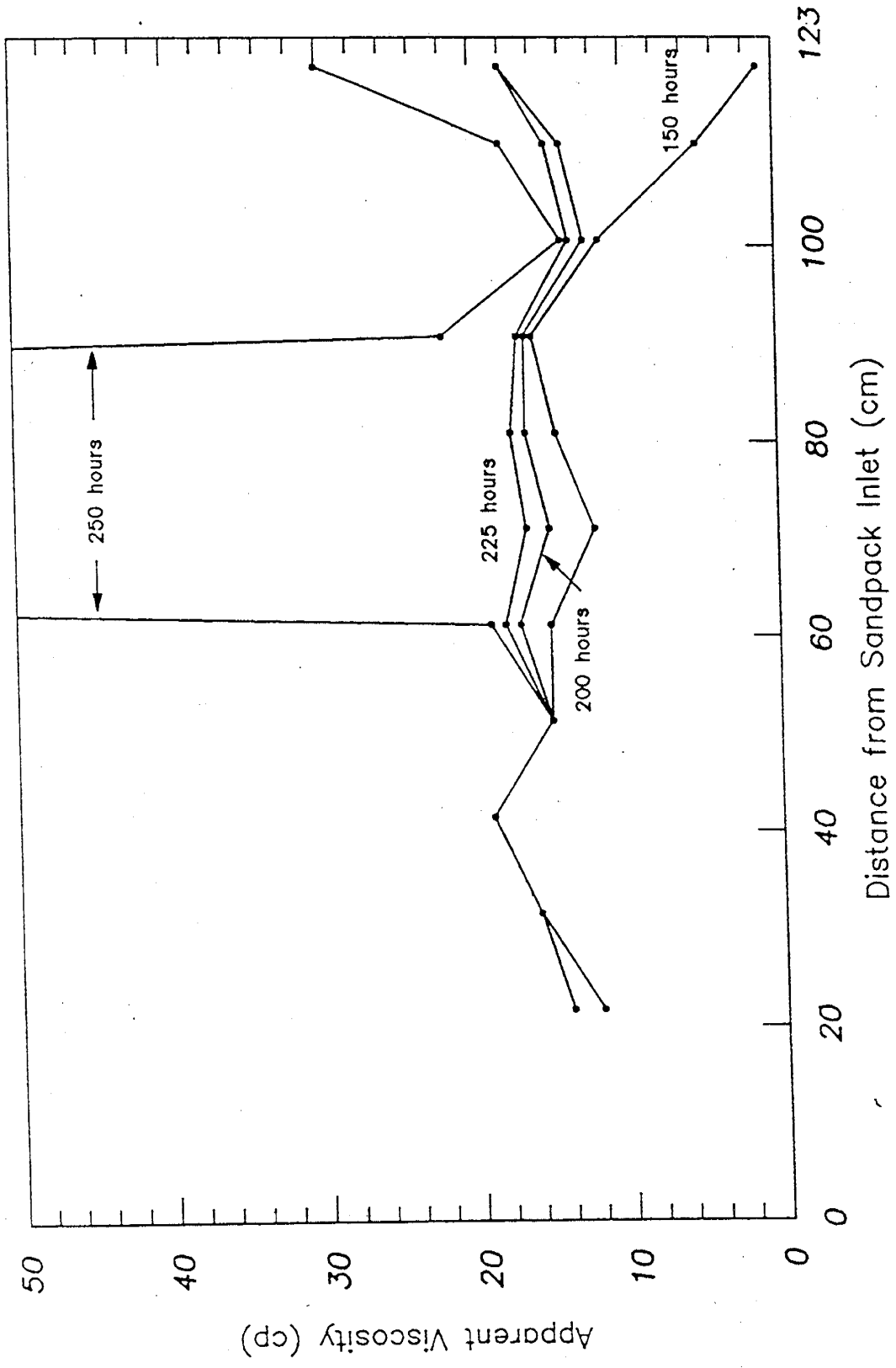


Figure 8.17b Apparent Viscosity Profiles for McCool Gel Solution Displacement SP8 [see Reference 1]

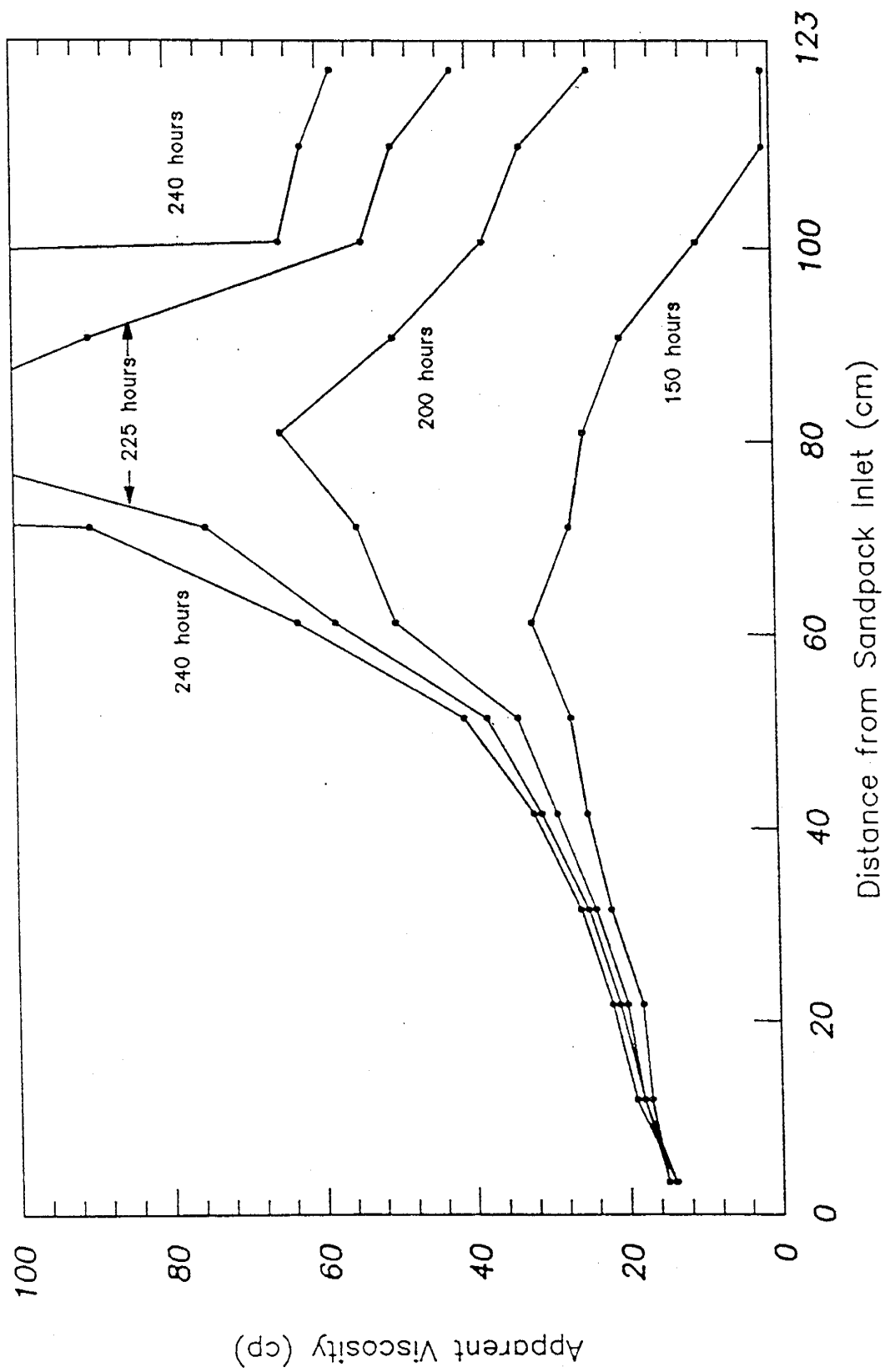


Figure 8.17c Apparent Viscosity Profiles for McCool Gel Solution Displacement SP10 [see Reference 1]

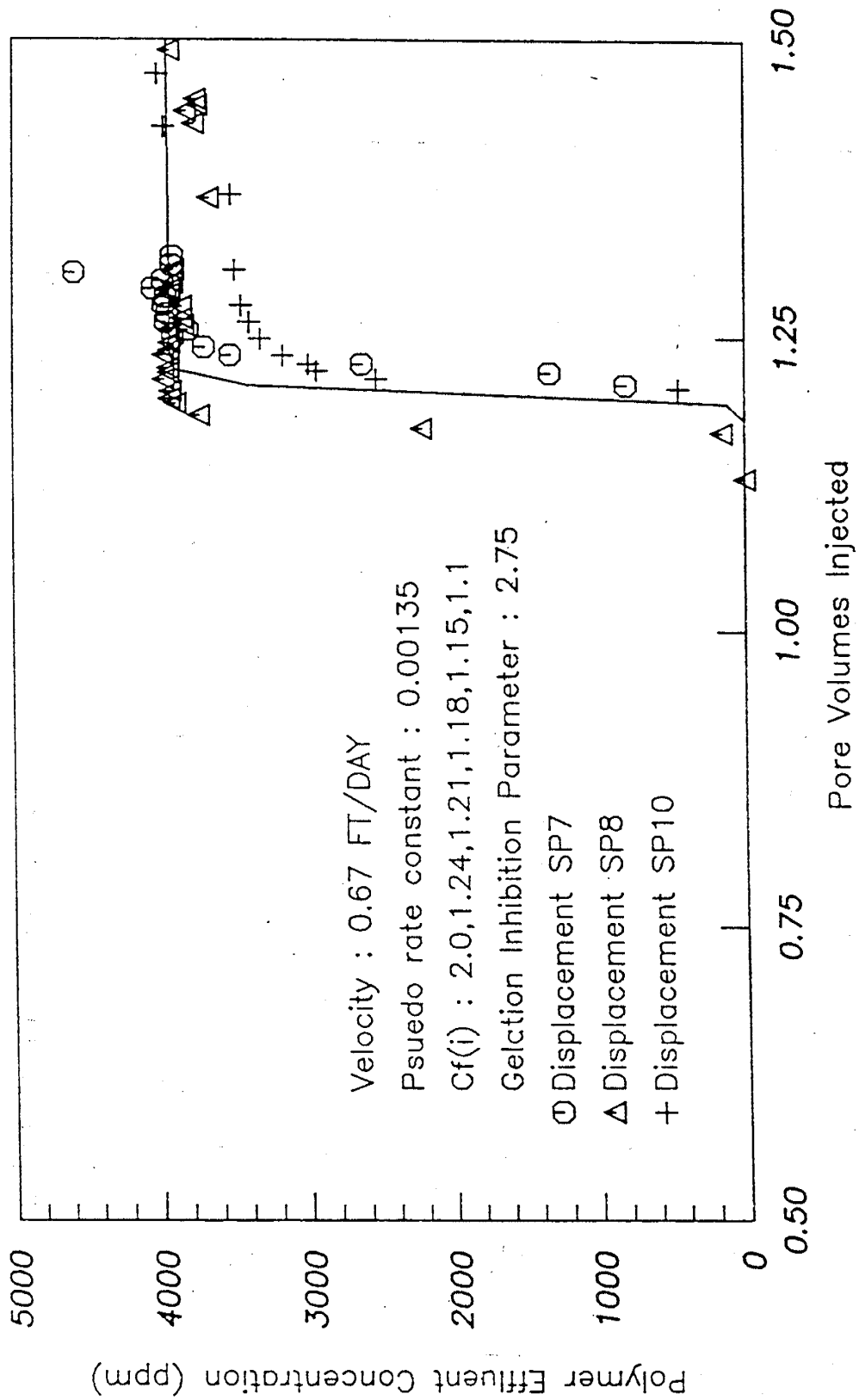


Figure 8.18 Simulated Polymer Effluent Profiles for McCool  
 Gelation Displacements SP7, SP8 and SP10  
 [see Reference 1]

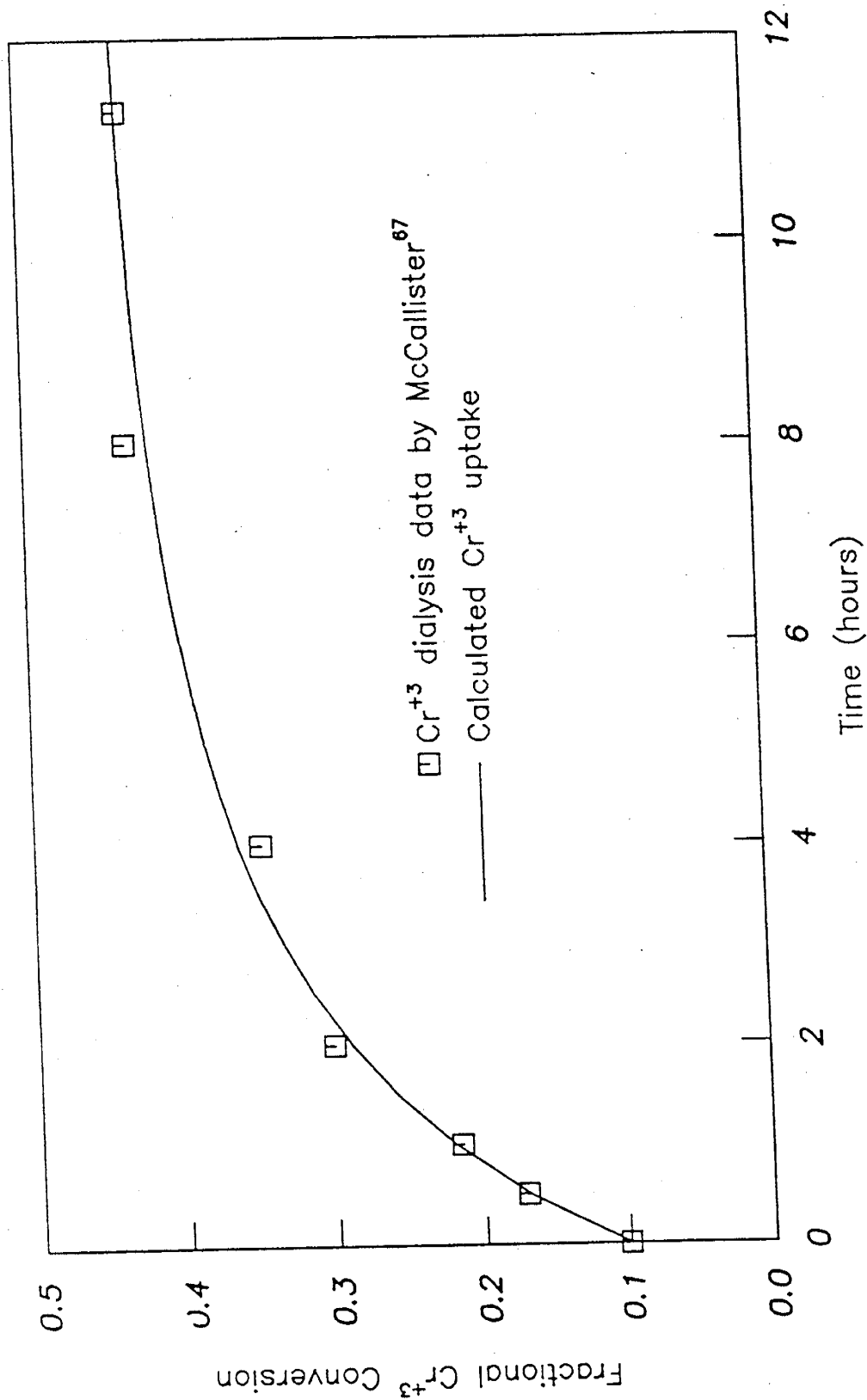


Figure 8.19  $\text{Cr}^{+3}$  Uptake Versus Time for Solutions of Biopolymer and  $\text{Cr}^{+3}$

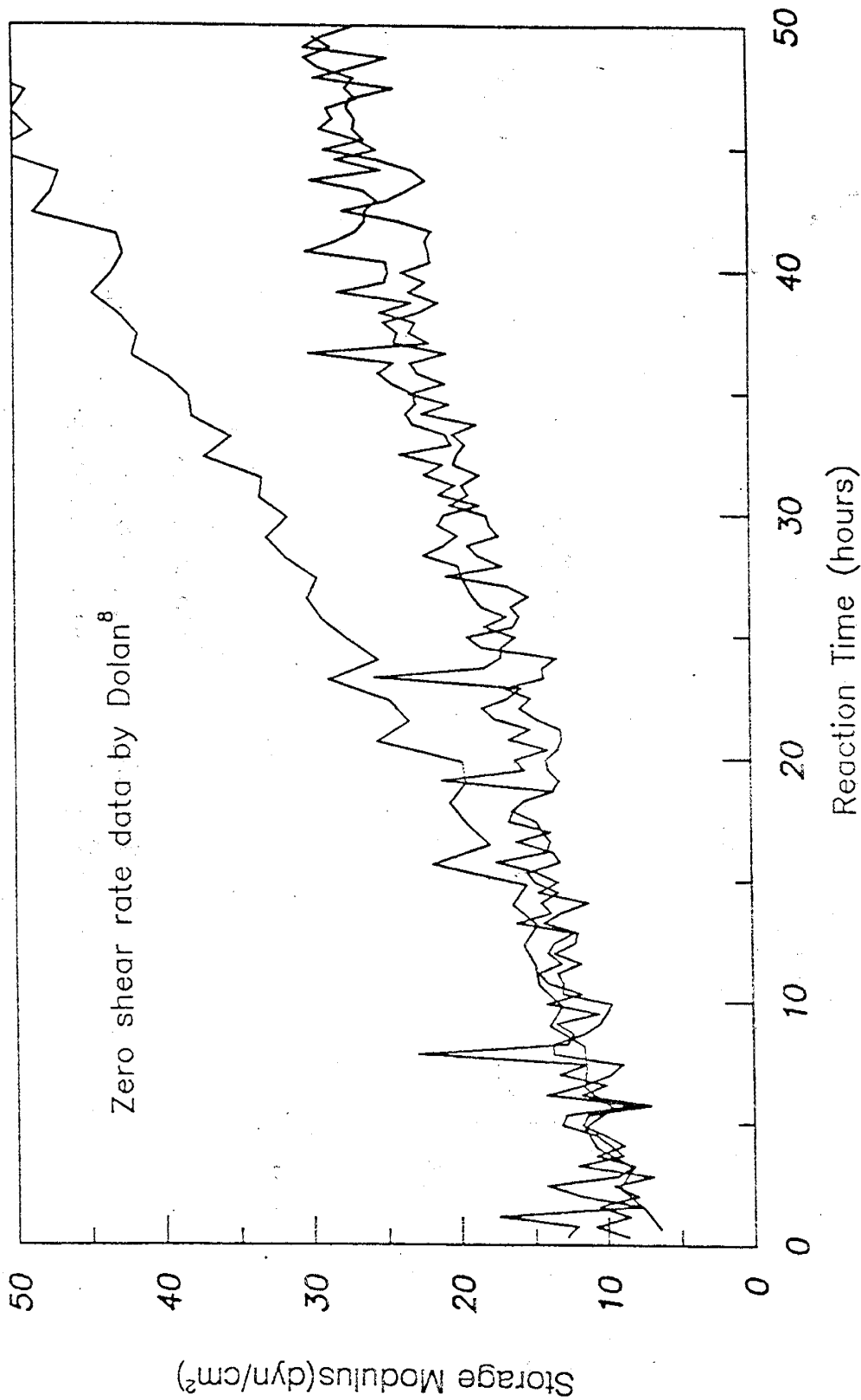


Figure 8.20 Storage Modulus Evolution for 1500 ppm FLOCON  
4800 and 50 ppm Cr<sup>3+</sup>

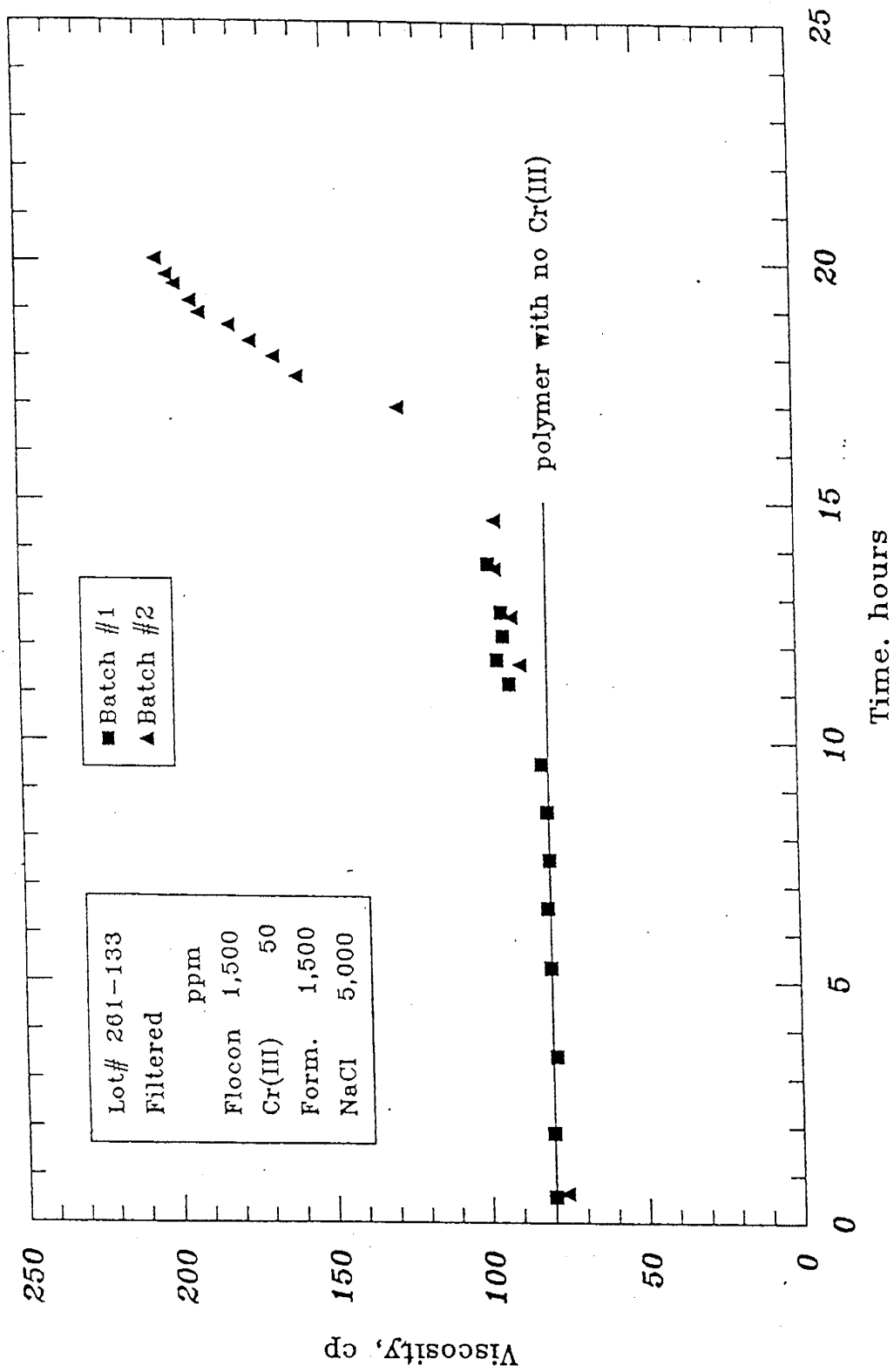


Figure 8.21 Viscosity versus Time for 1500 ppm Biopolymer and 50 ppm Cr<sup>+3</sup> Under Zero Shear

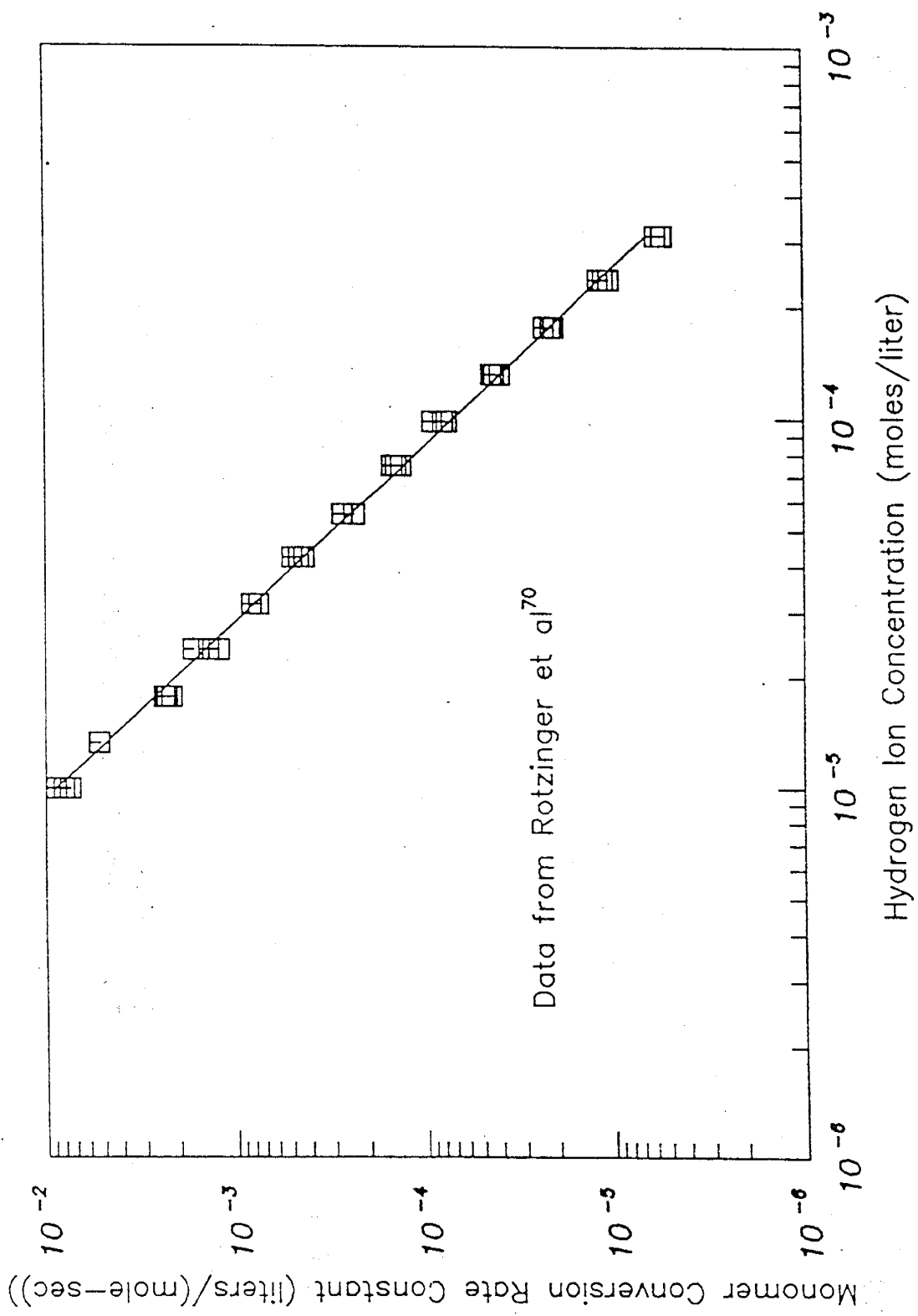


Figure 8.22 Rate of Conversion of Monomer as a Function of pH

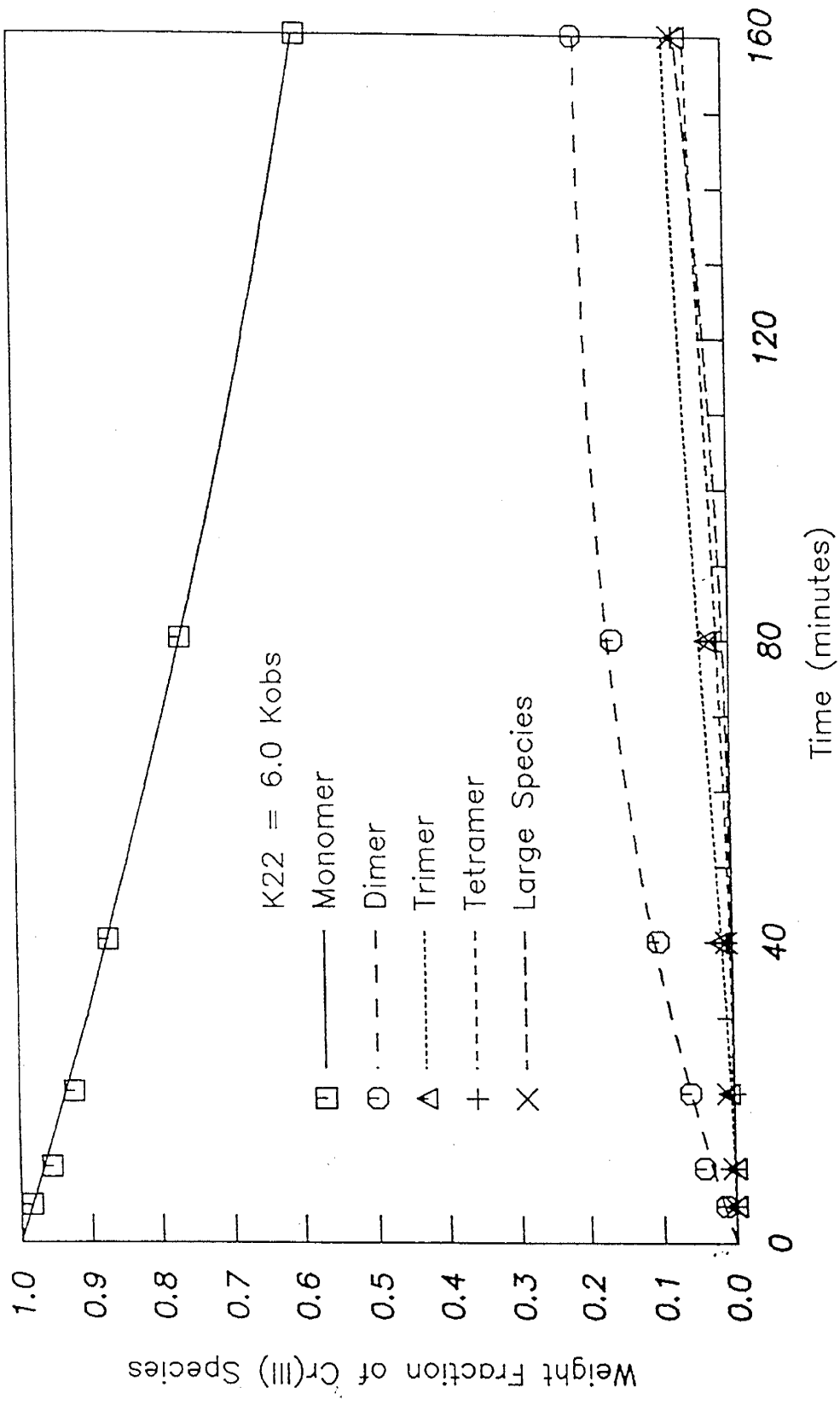


Figure 8.23 Comparison of Rotzinger et al. Table Ia with Dimerization Model Results [see Reference 26]

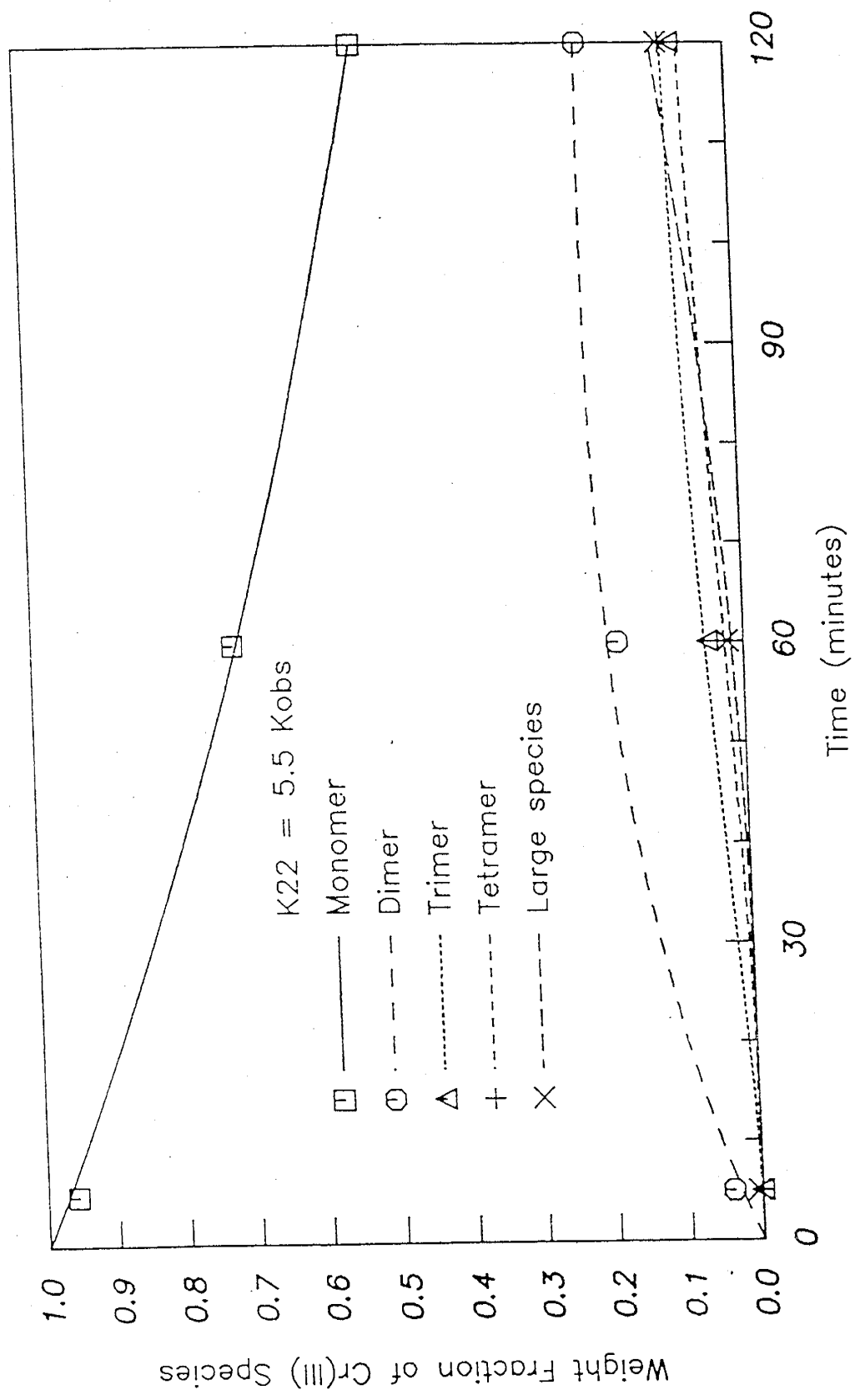


Figure 8.24 Comparison of Rotzinger et al. Table Ib with Dimerization Model Results [see Reference 27]

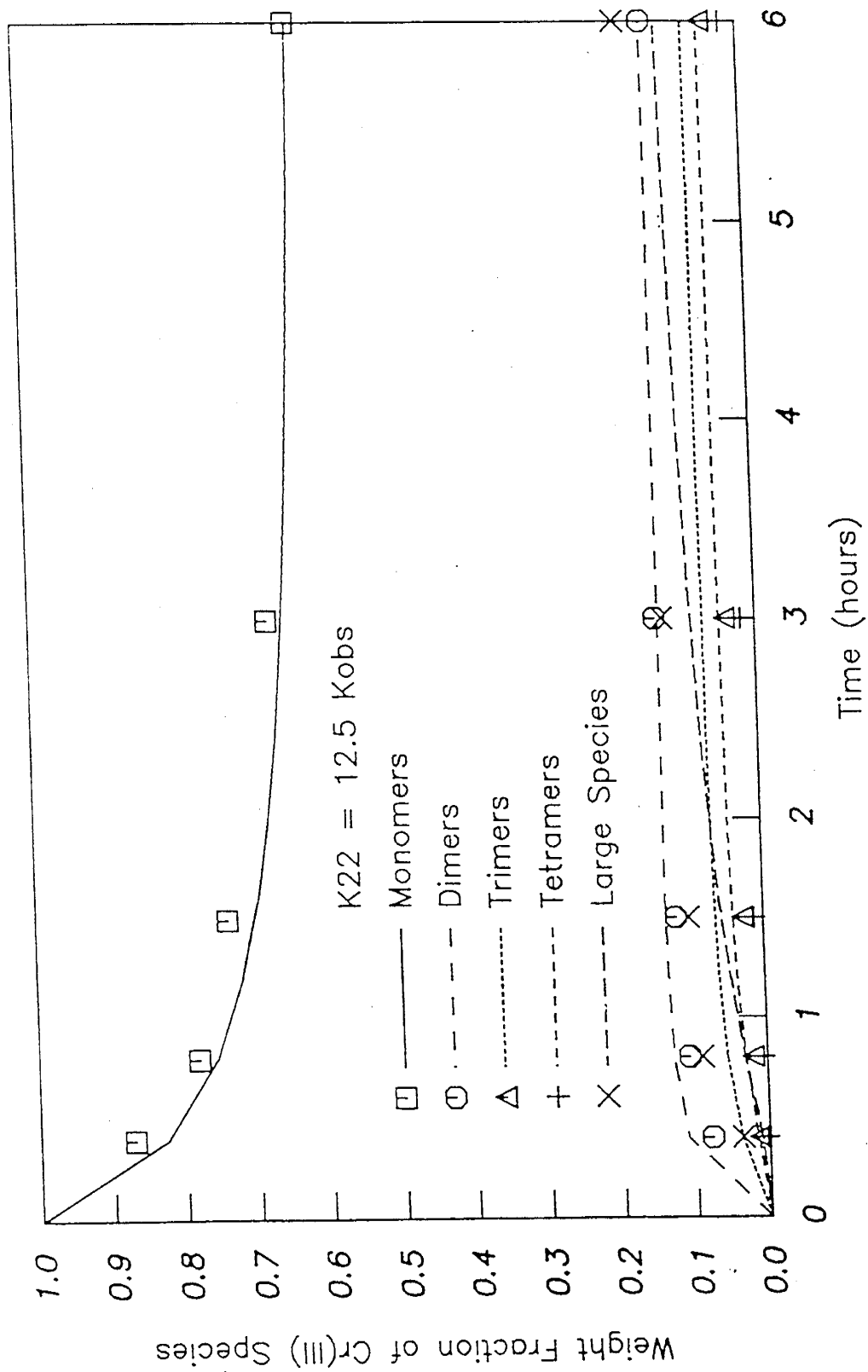


Figure 8.25 Comparison of Stünzi et al. Table II with Dimerization Model Results [see Reference 26]

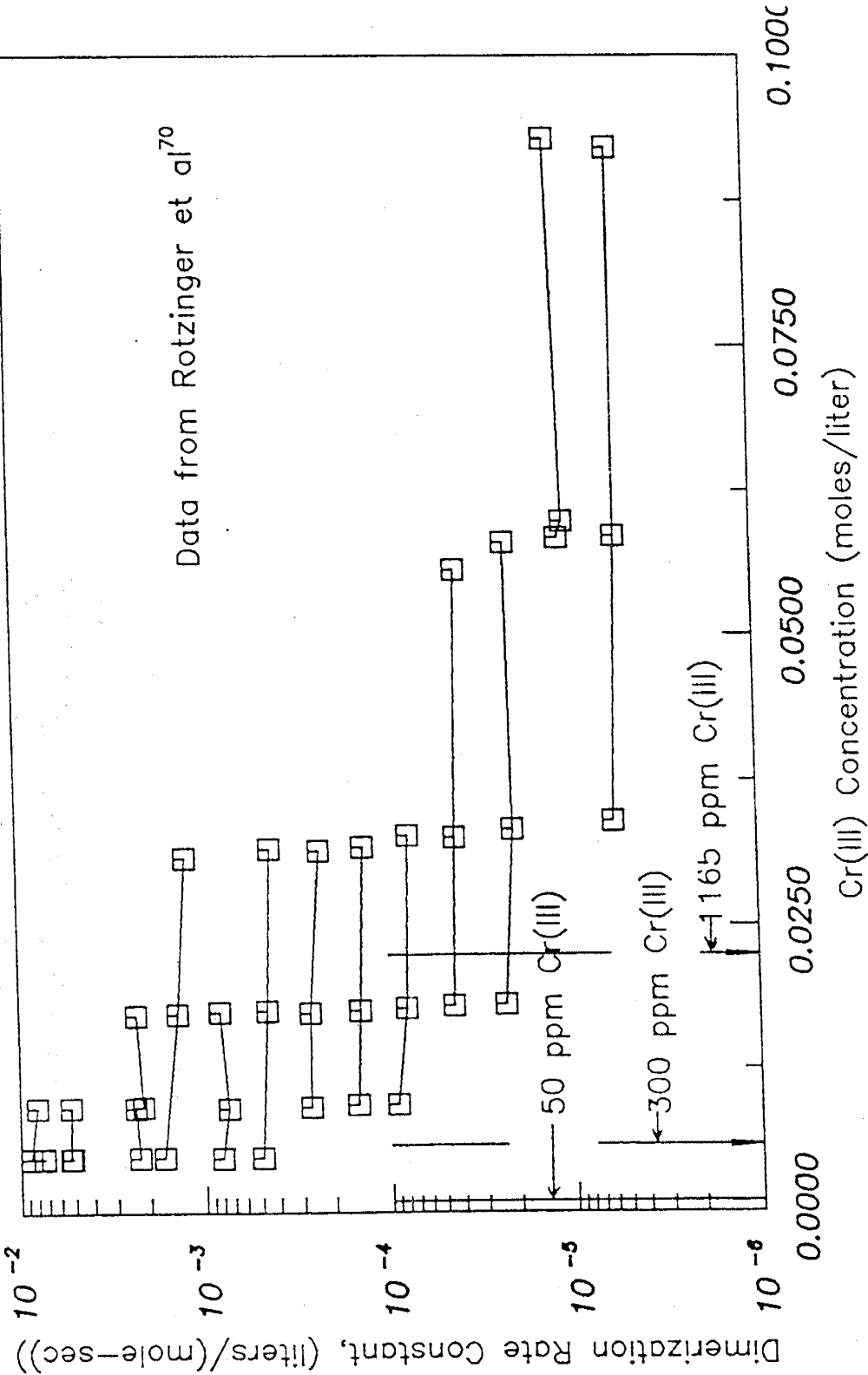


Figure 8.26 Chromium Dimerization Rate as a Function of Chromium Concentration at Different pH's

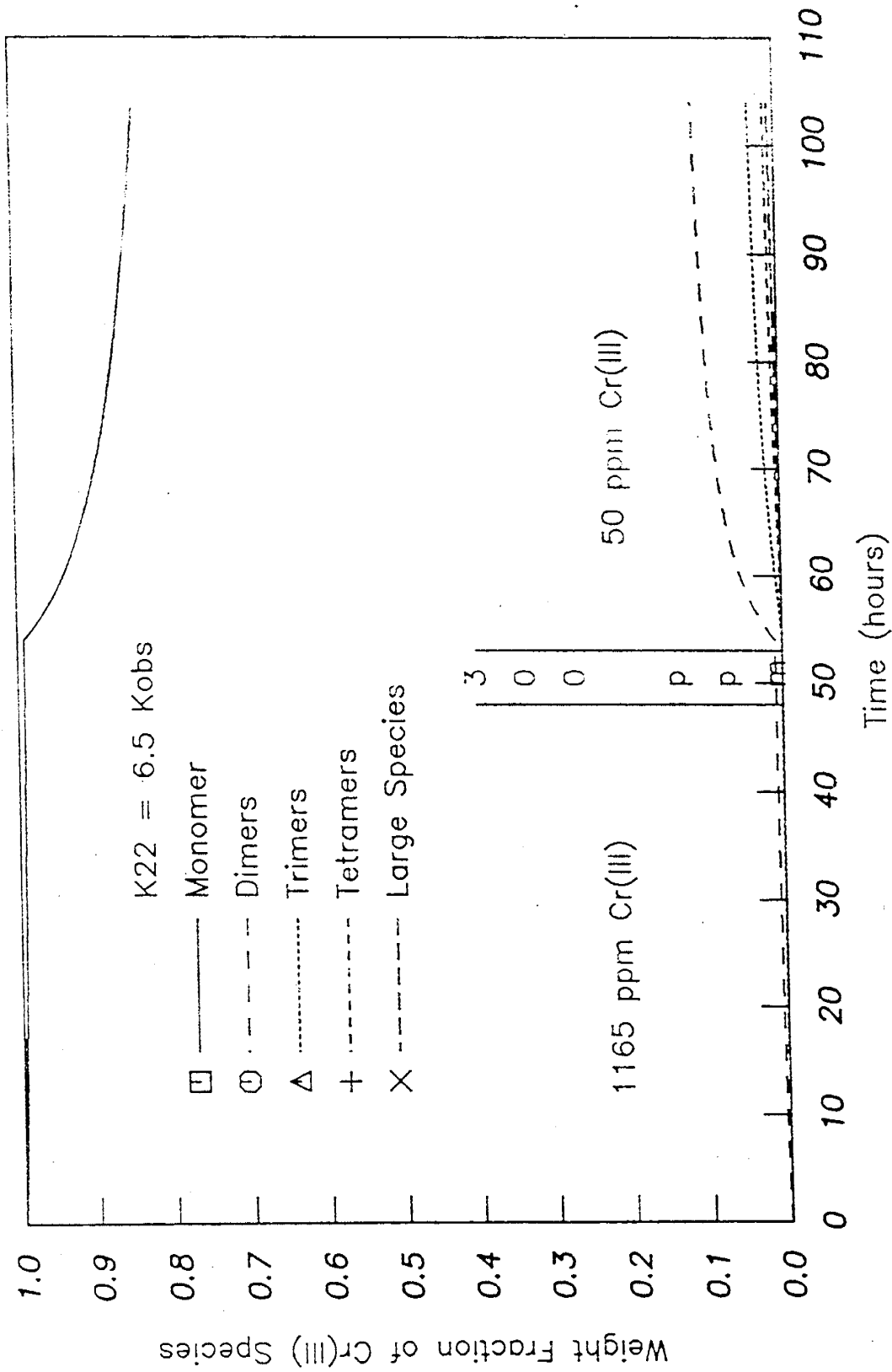


Figure 8.27 Simulated Chromium Oligomer Concentrations for Hejri's Gelling System [see Reference 4]

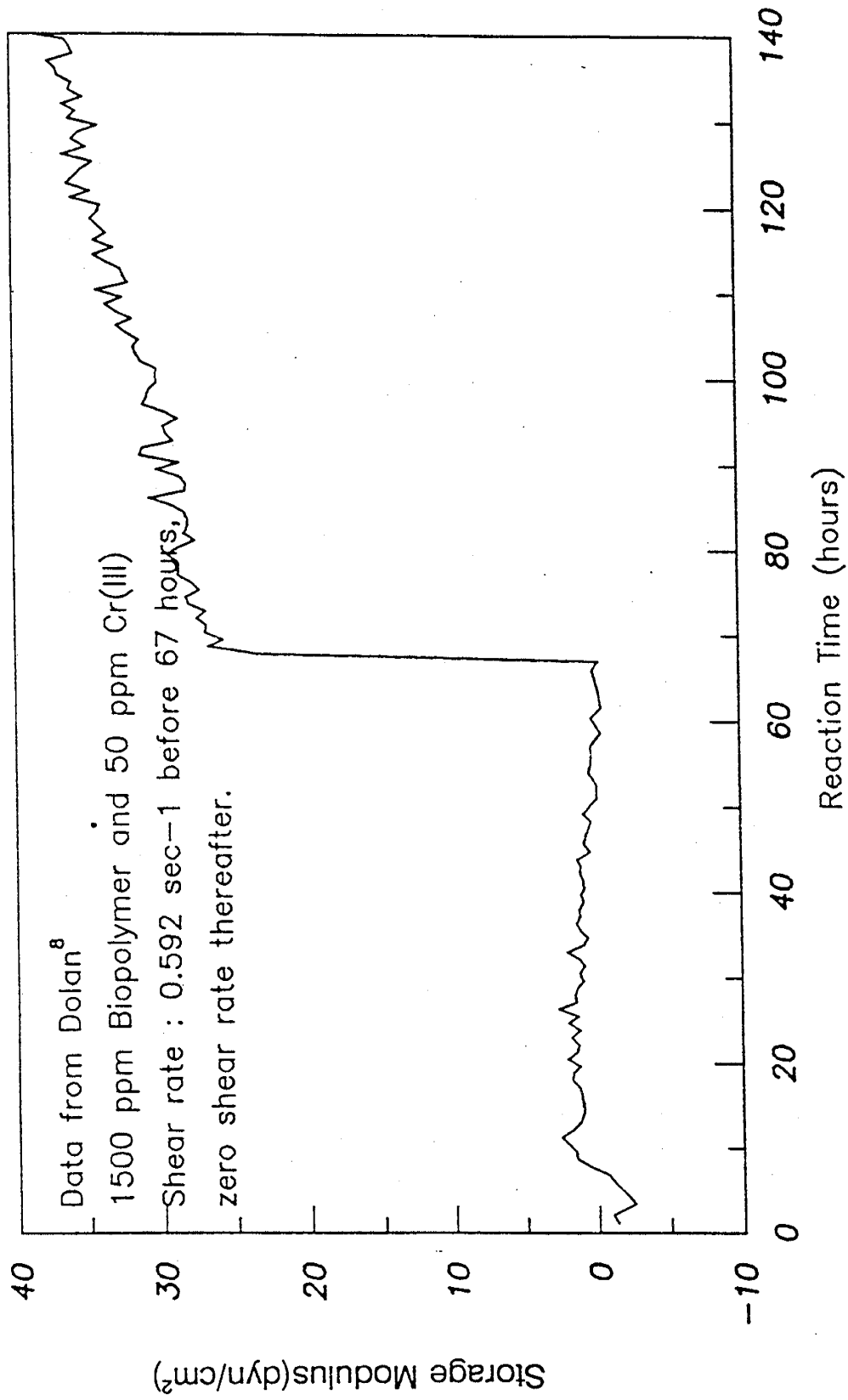


Figure 8.28 Storage Modulus Evolution of Biopolymer/Cr<sup>+3</sup> Solutions Under Variable Shear Rates

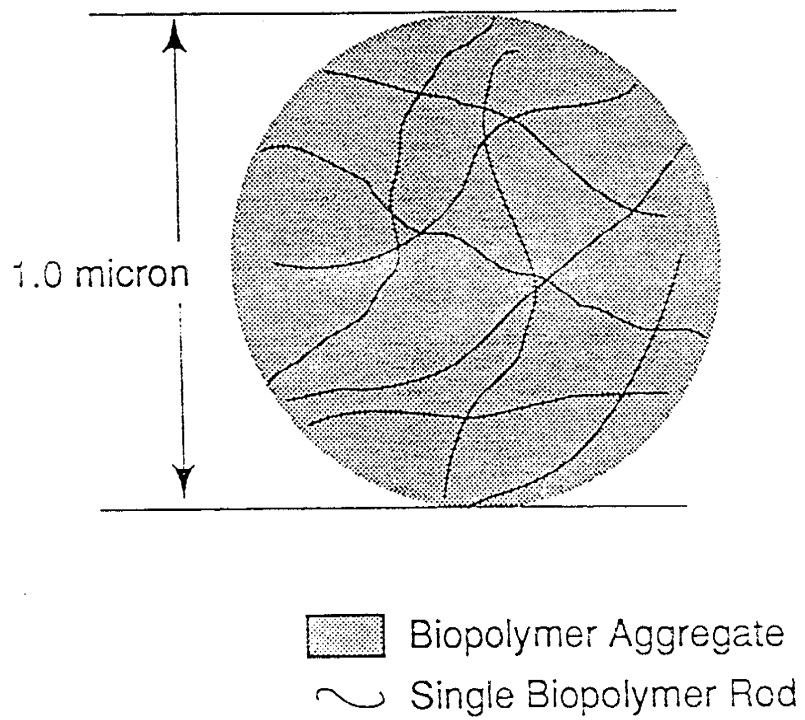


Figure 8.29 Spherical Approximation of a Biopolymer Molecule

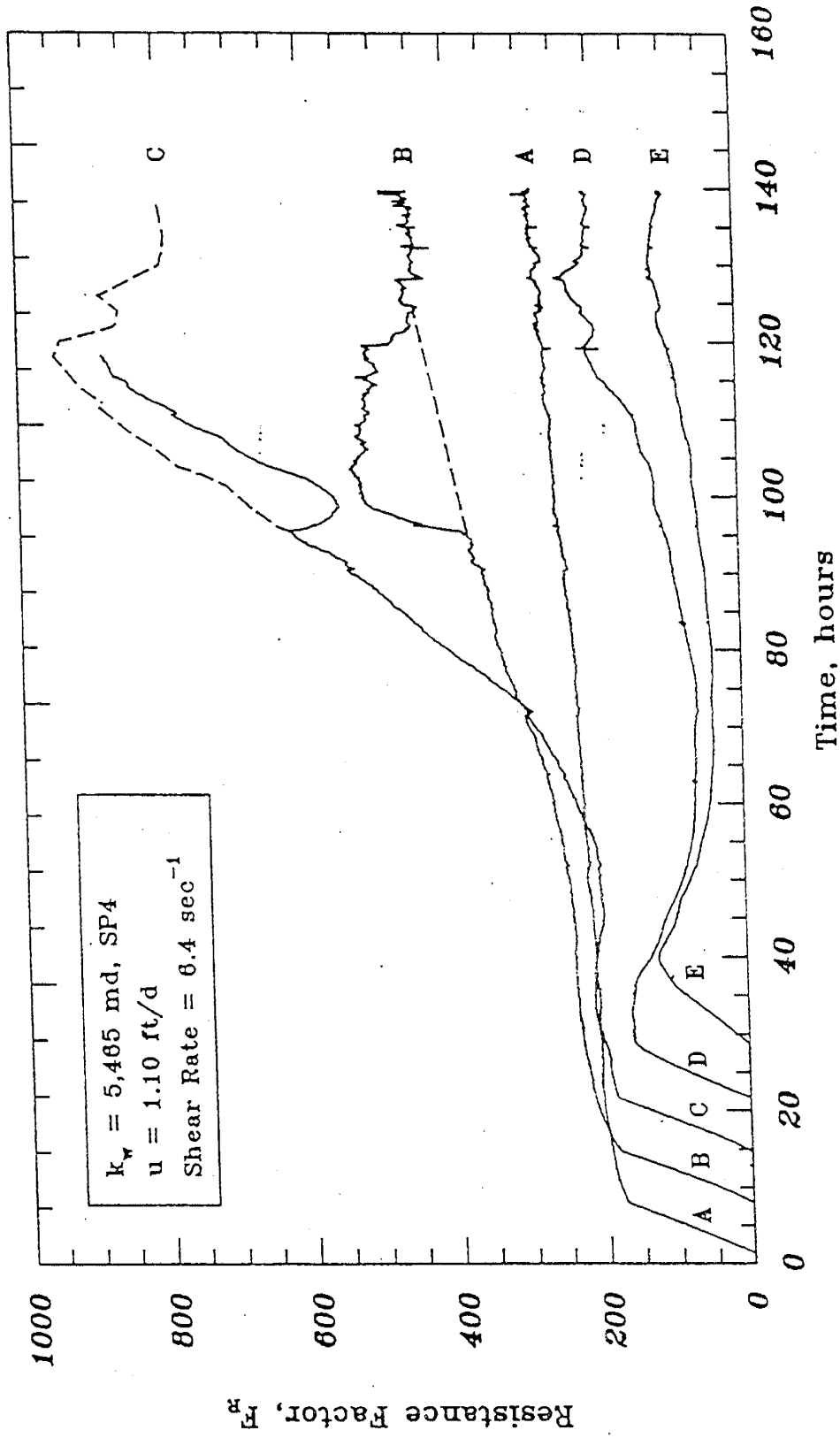


Figure 8.30 Hejri's Displacement Data [see Reference 4]  
 (Sandpack 4,  $V_o = 1.10 \text{ ft/day}$ )

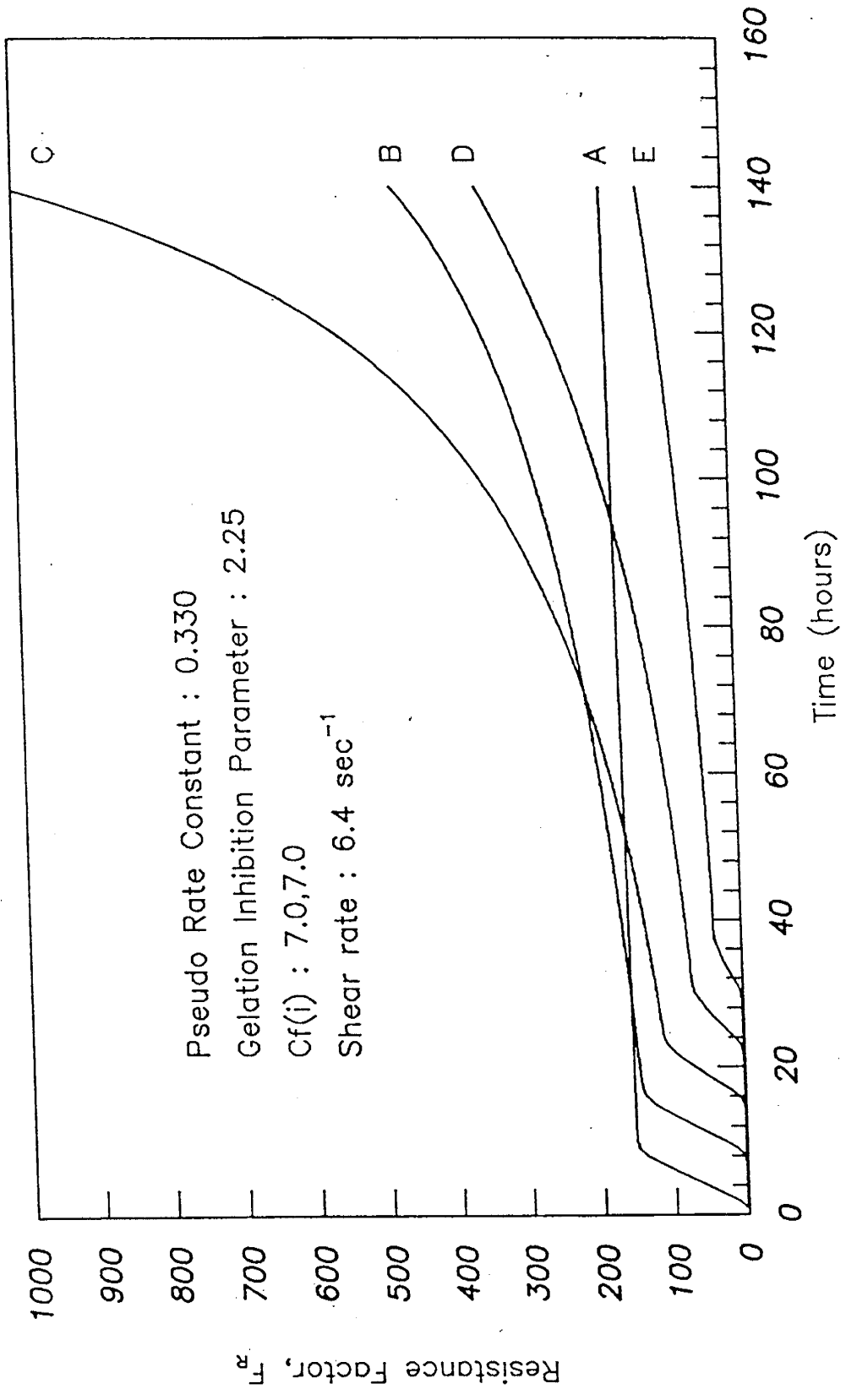


Figure 8.31 Simulated Biopolymer Gelation Run  
(Sandpack 4,  $V_D = 1.10$  ft/day)

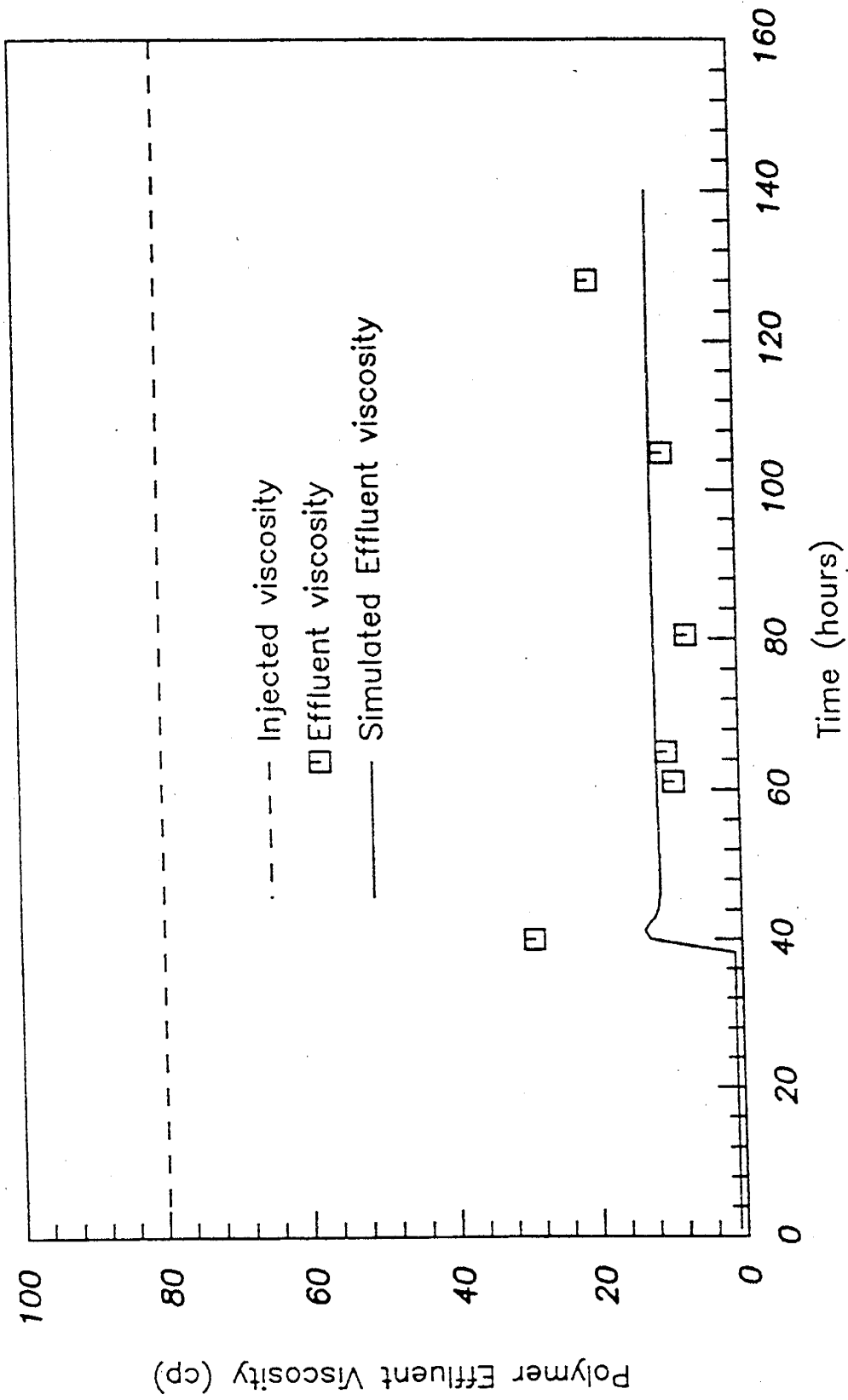


Figure 8.32 Simulated Polymer Effluent Viscosity  
 (Sandpack 4,  $V_D = 1.10$  ft/day)

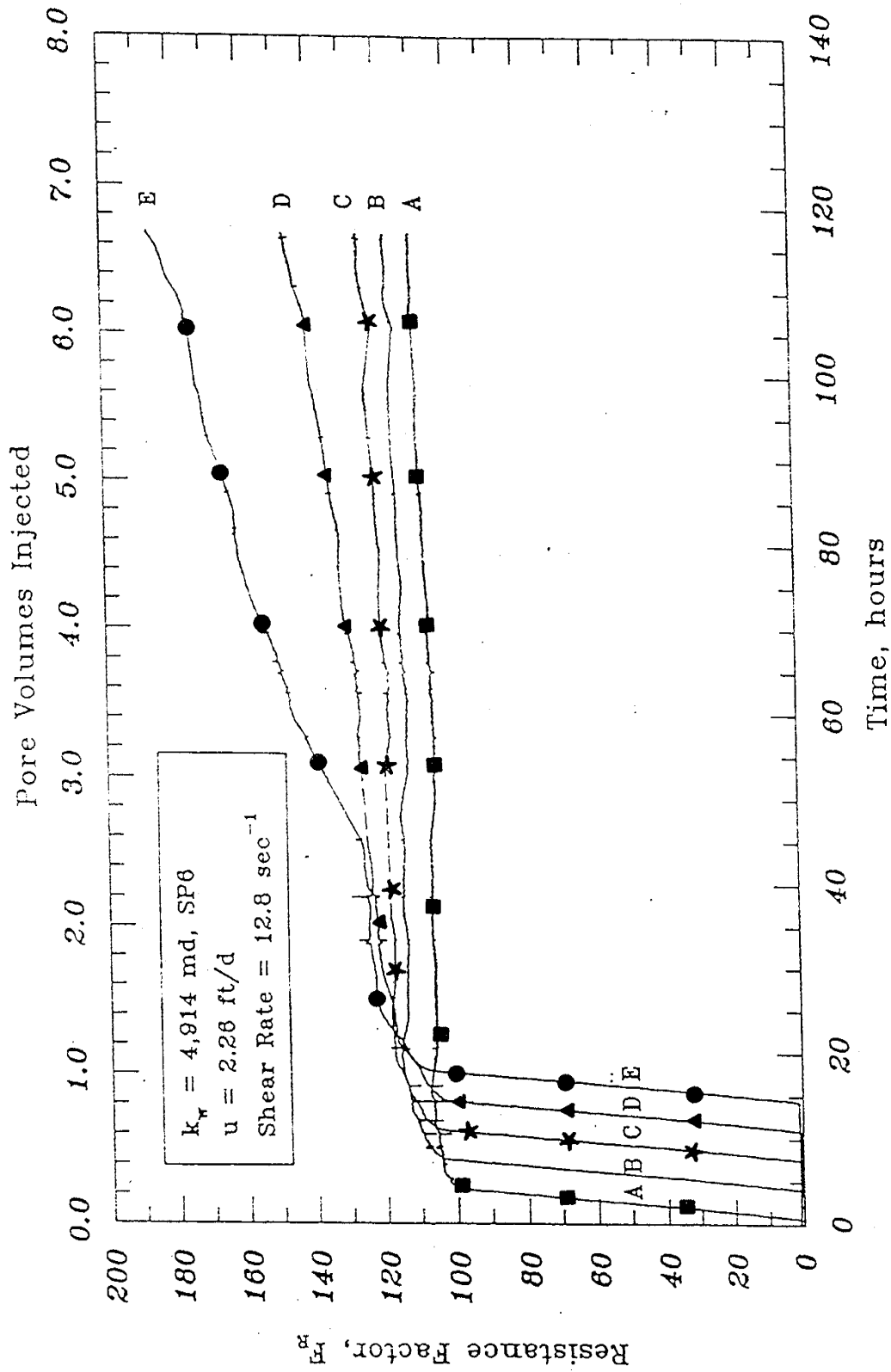


Figure 8.33 Hejri Displacement Data [see Reference 4]  
(Sandpack 6,  $V_0 = 2.26 \text{ ft/day}$ )

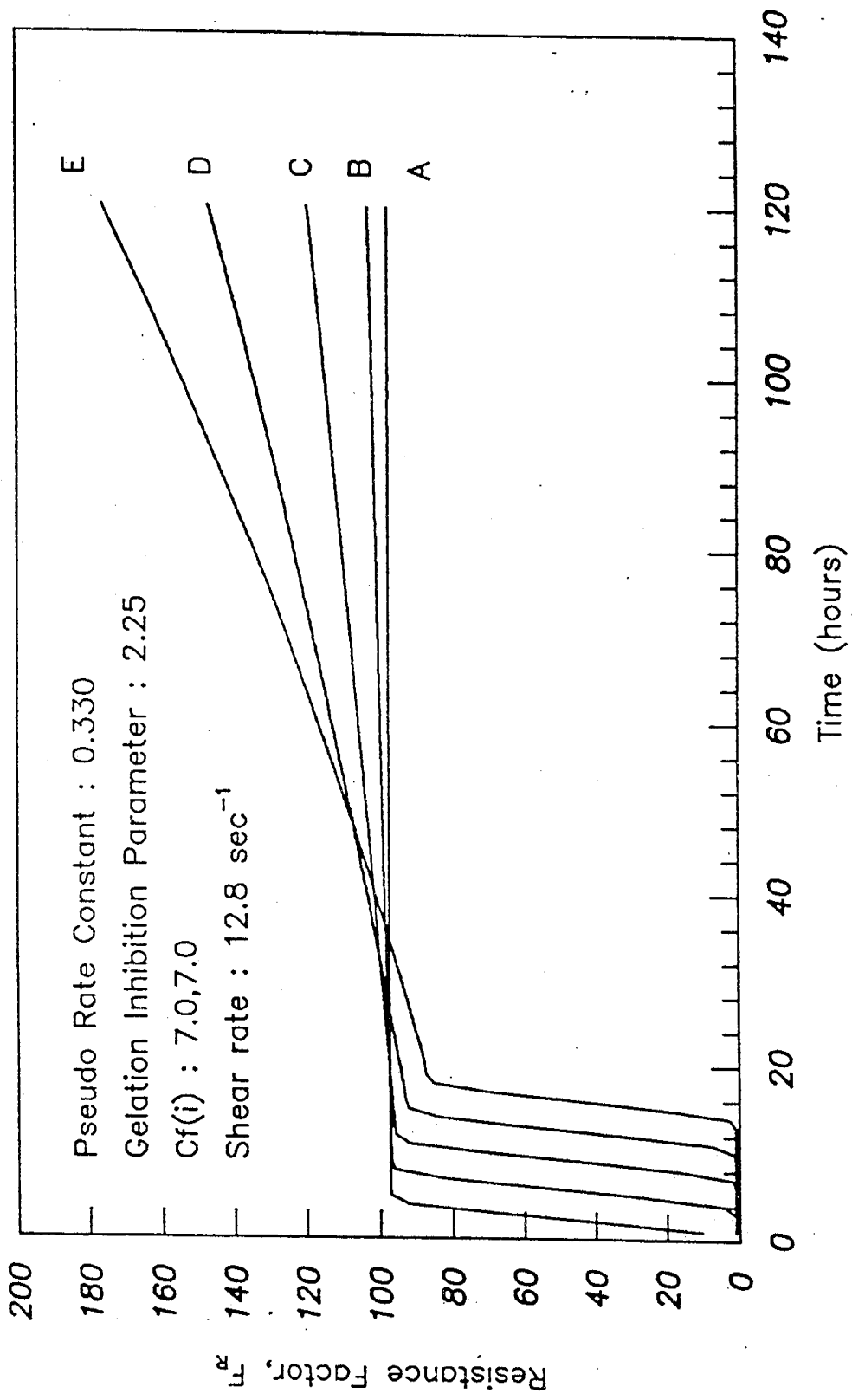


Figure 8.34 Simulated Biopolymer Gelation Run  
 (Sandpack 6,  $V_D = 2.26$  ft/day)

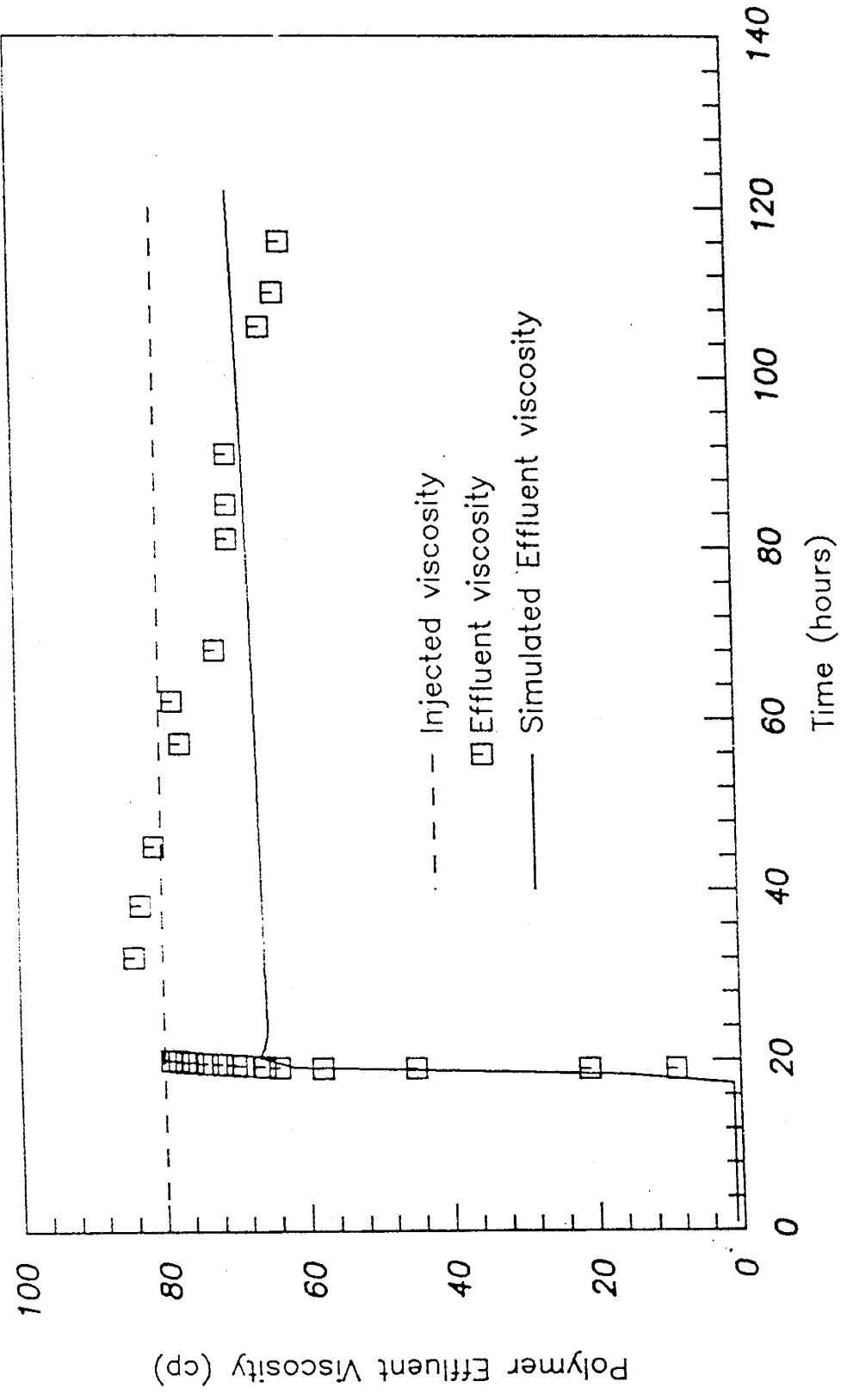


Figure 8.35 Simulated Polymer Effluent Viscosity  
(Sandpack 6,  $V_0 = 2.26$  ft/day)

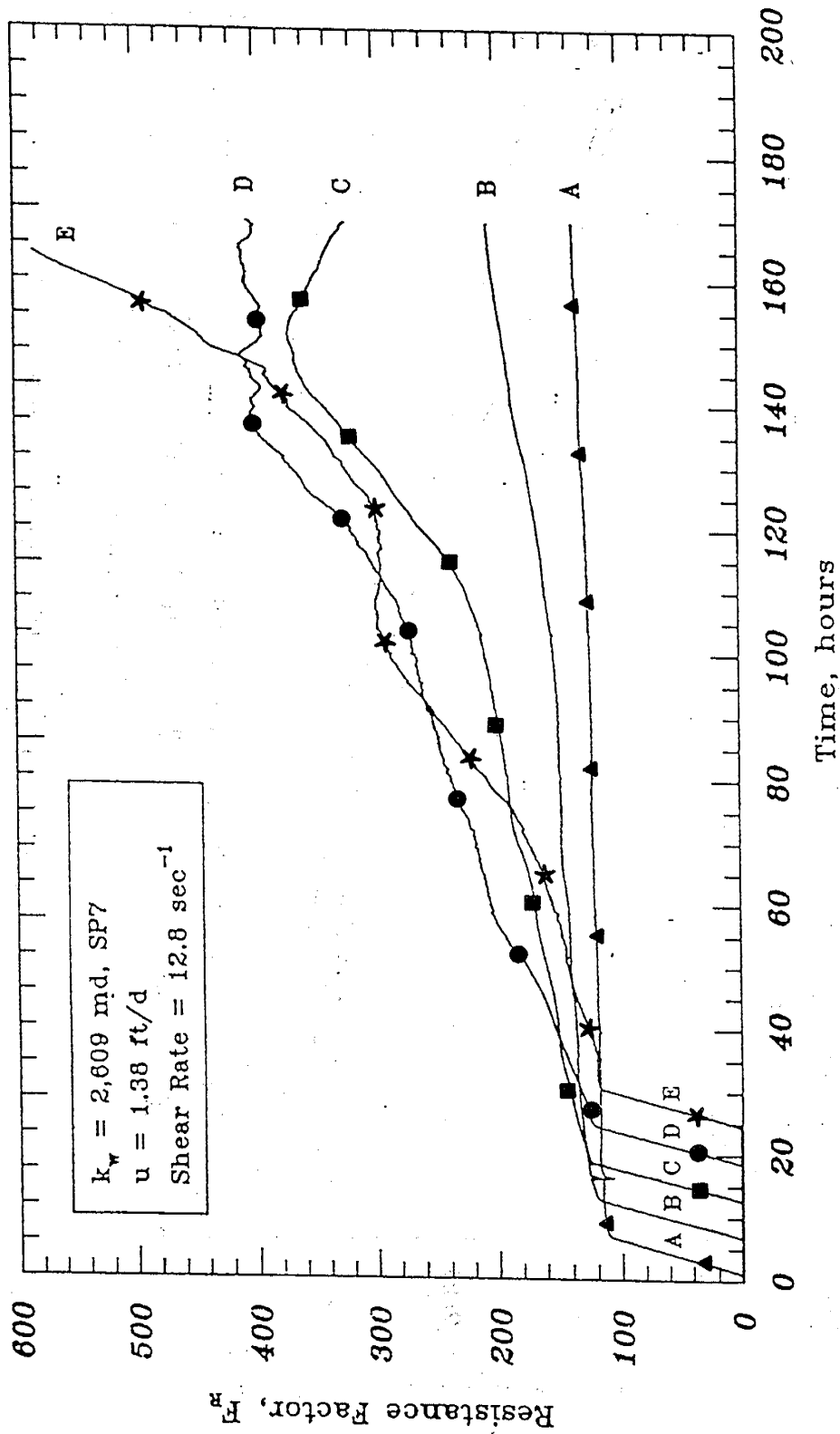


Figure 8.36 Hejri Displacement Data [see Reference 4]  
 (Sandpack 7,  $V_D = 1.38 \text{ ft/day}$ )

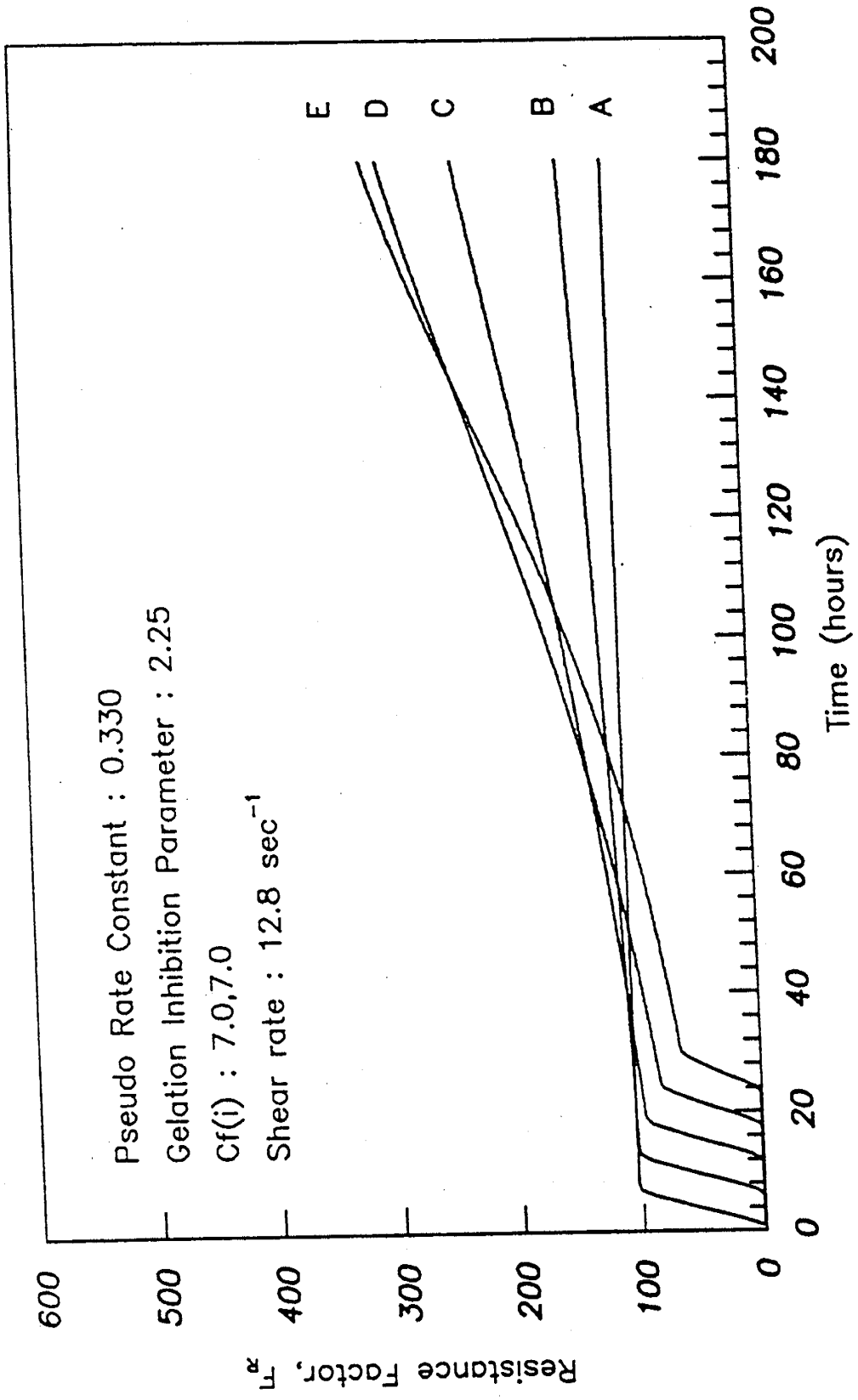


Figure 8.37 Simulated Biopolymer Gelation Run  
 (Sandpack 7,  $V_D = 1.38 \text{ ft/day}$ )

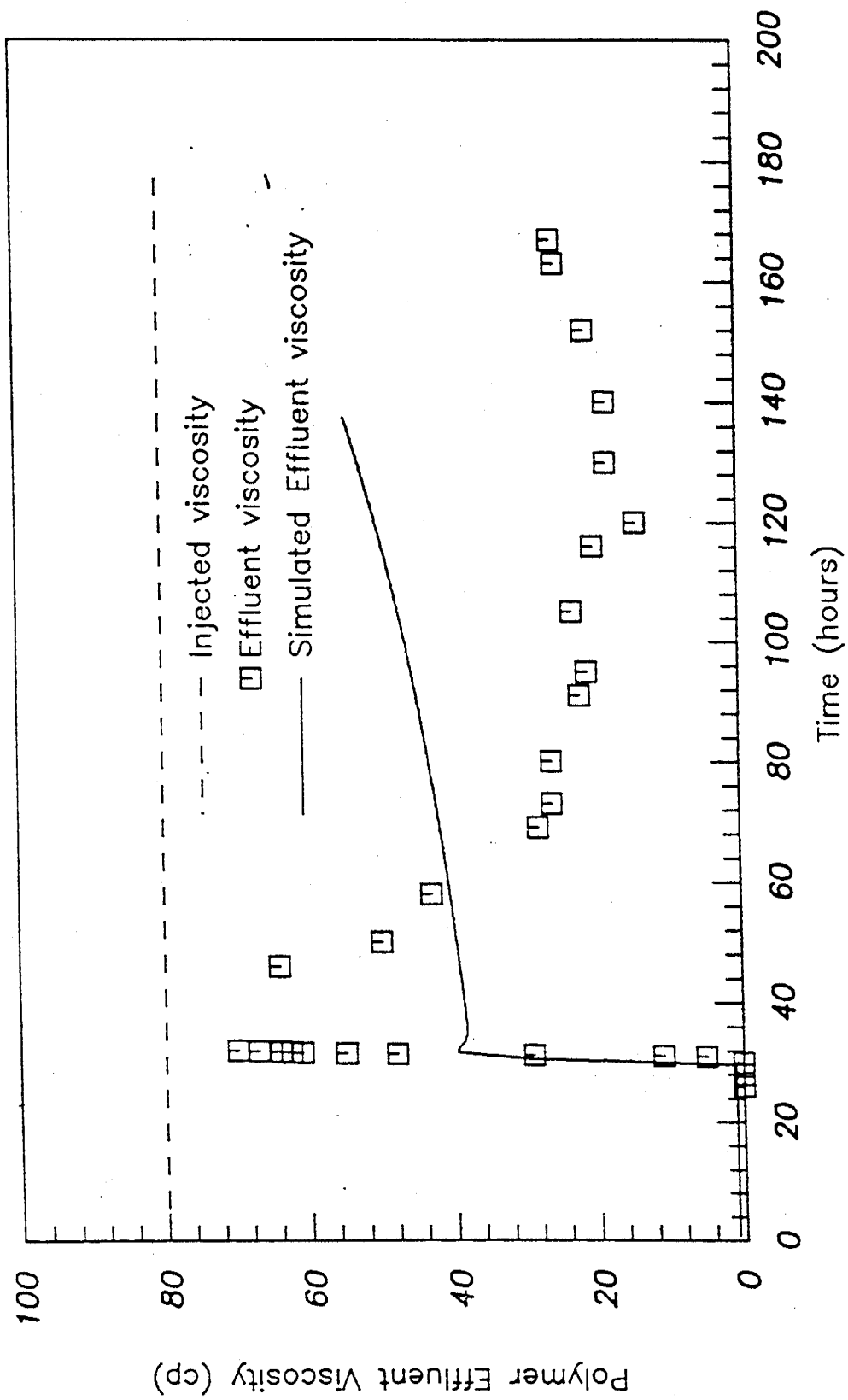


Figure 8.38 Simulated Polymer Effluent Viscosity  
(Sandpack 7,  $V_D = 1.38$  ft/day)

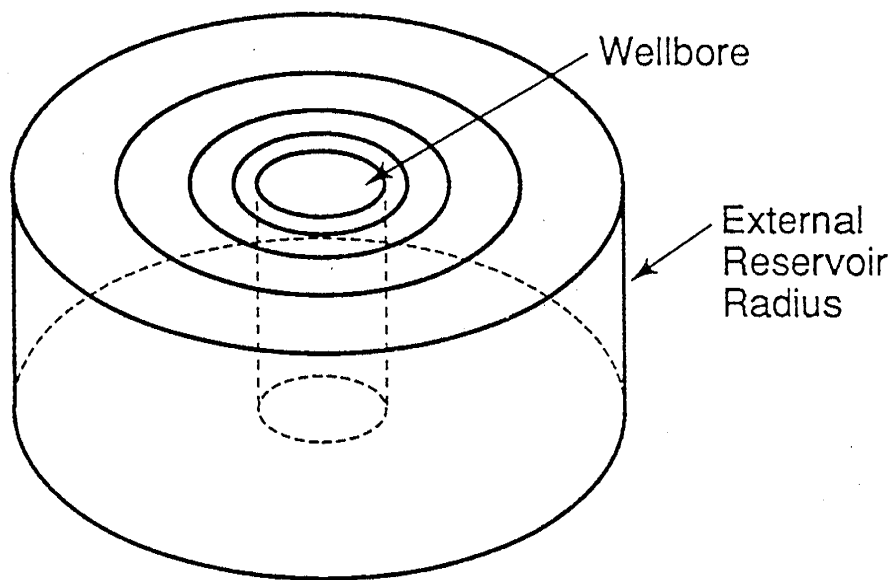


Figure 8.39 Logarithmically Distributed Grid Nodes in Radial Coordinates

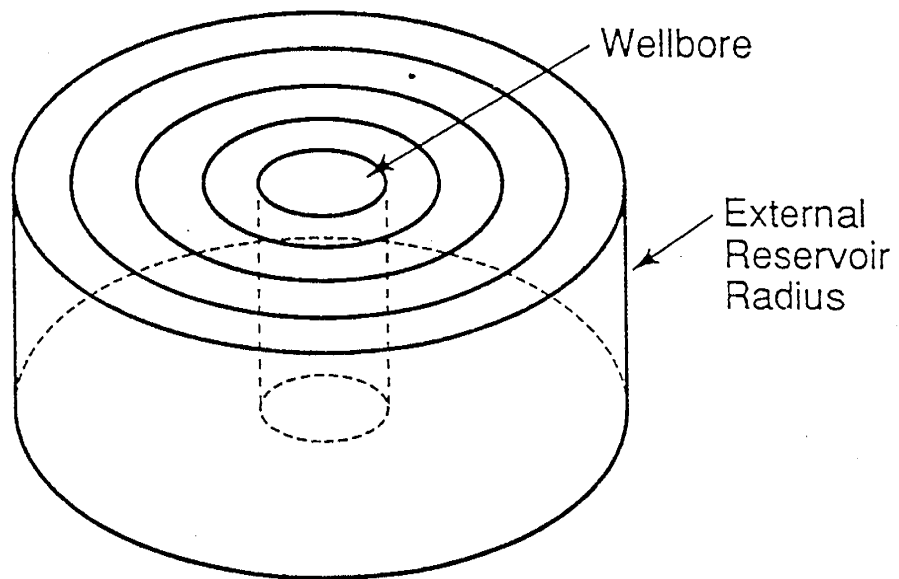


Figure 8.40 Linearly Distributed Grid Nodes in Radial Coordinates

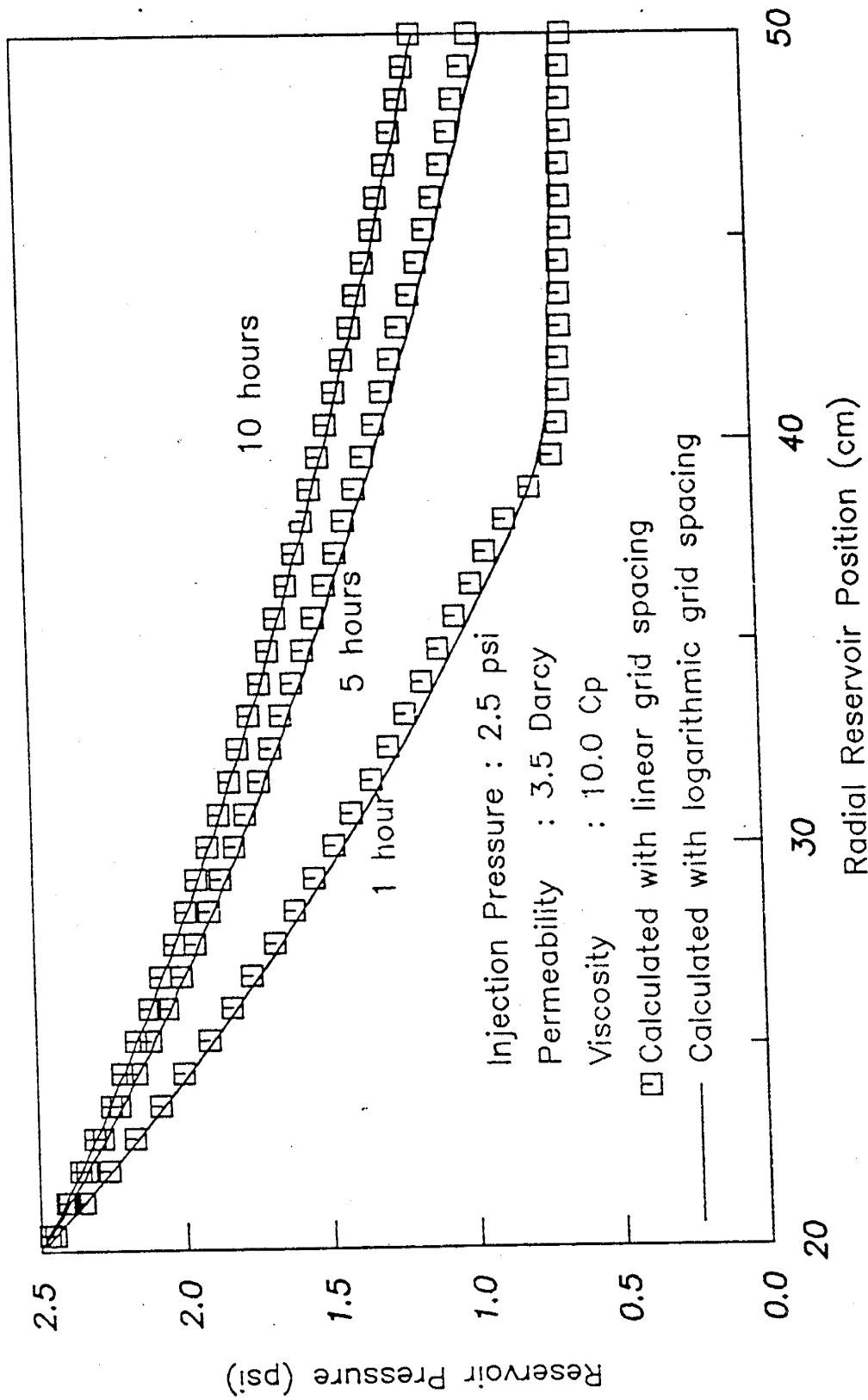


Figure 8.41 Comparison of Reservoir Pressures Near the Wellbore Calculated with Logarithmic and Linear Grid Spacing

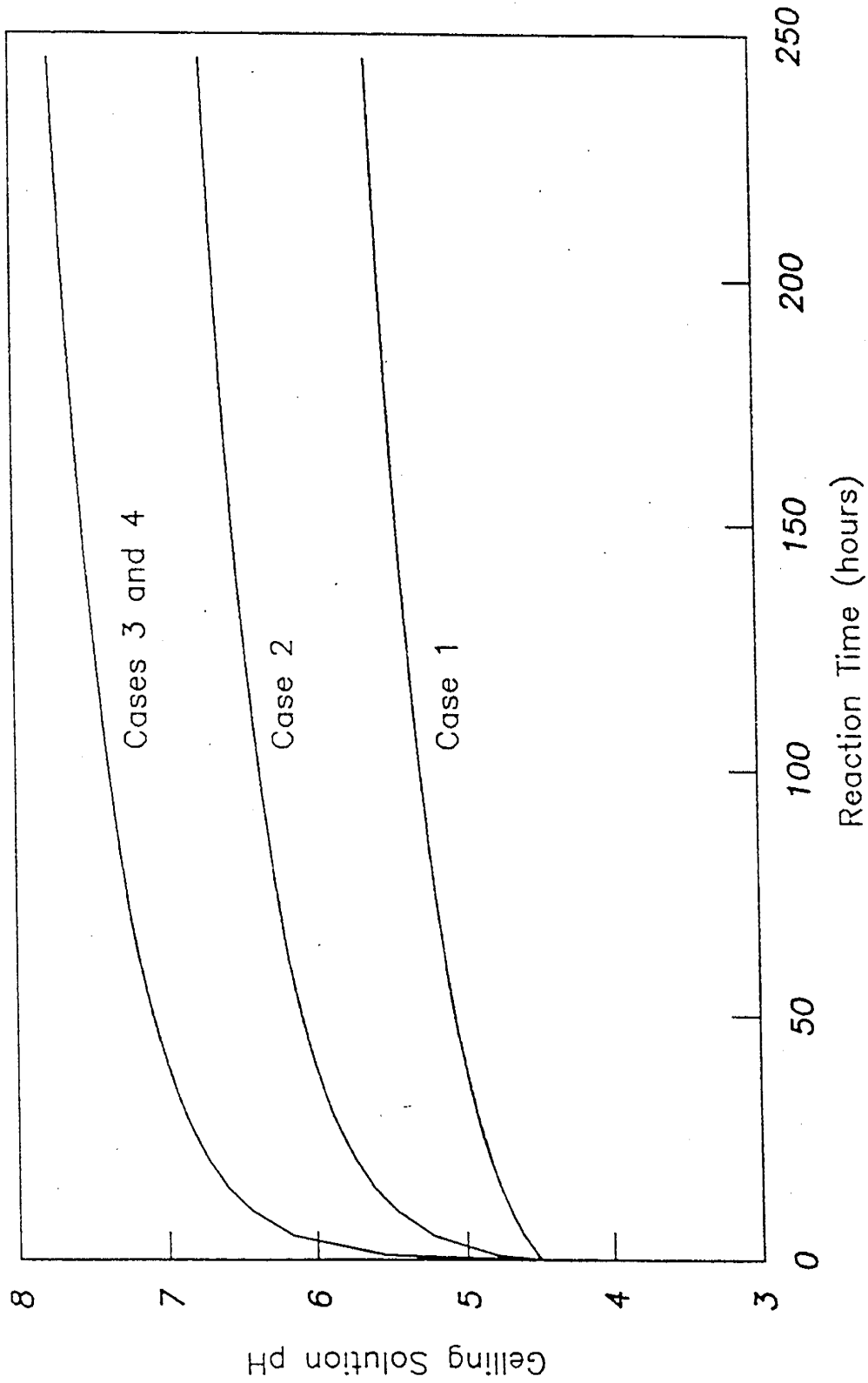


Figure 8.42 pH Trends for Simulation of Radial Reservoir Test Cases

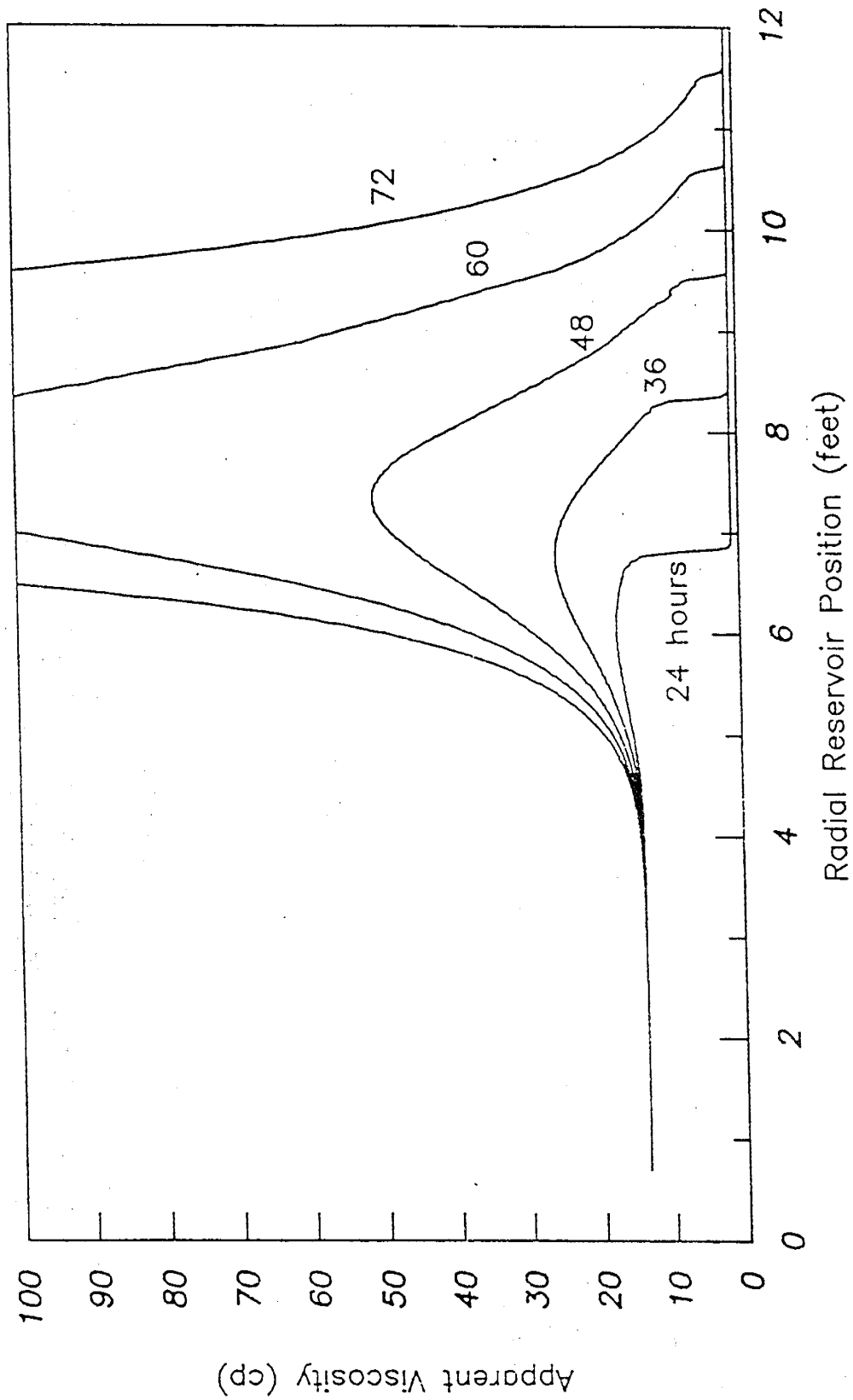


Figure 8.43 Simulated Gelation Run in Radial Geometry  
 (Case 1 : pH from 4.5 to 5.7)

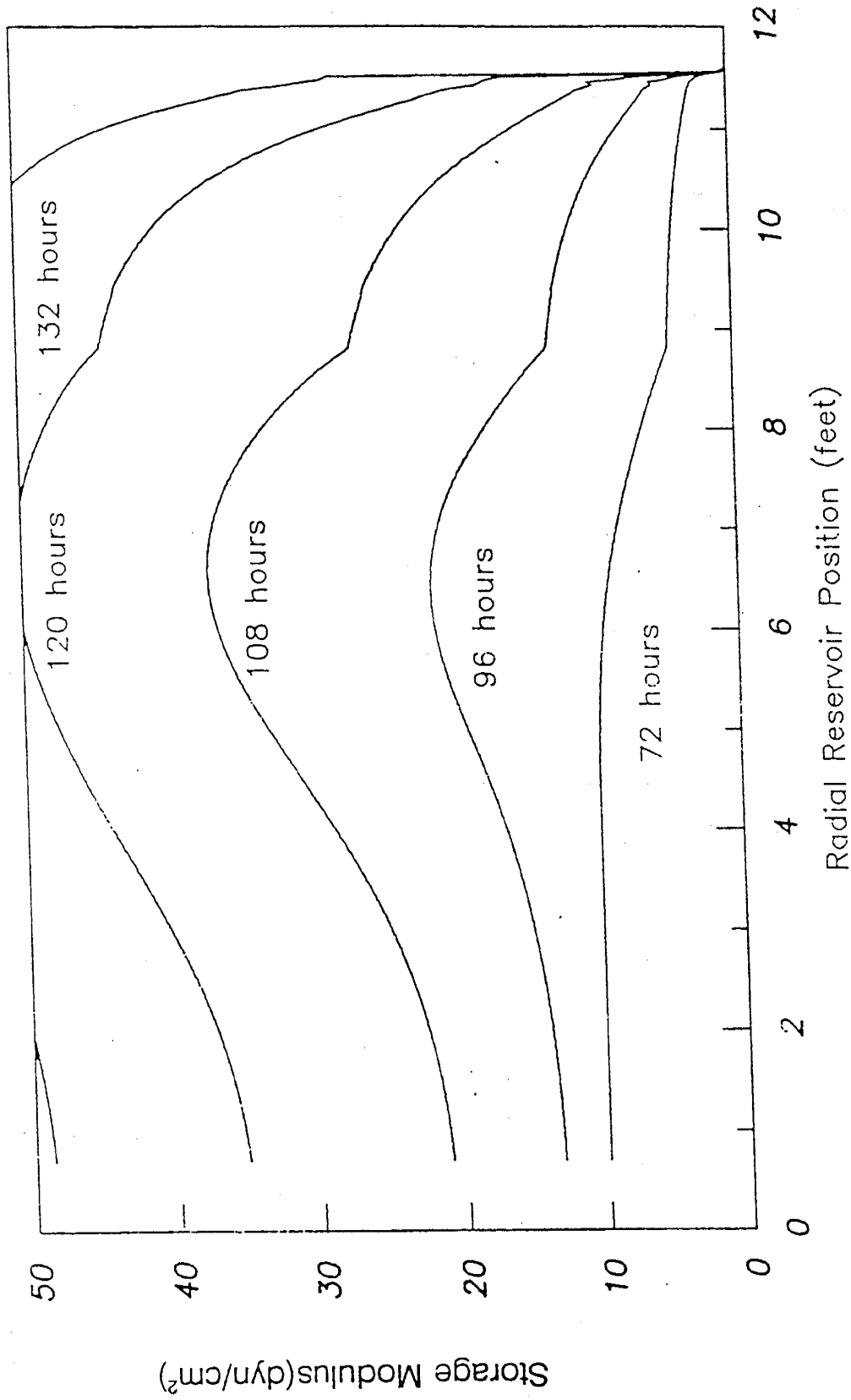


Figure 8.44 Storage Modulus Growth During the Shutin Period  
 (Case 1 : pH from 4.5 to 5.7)

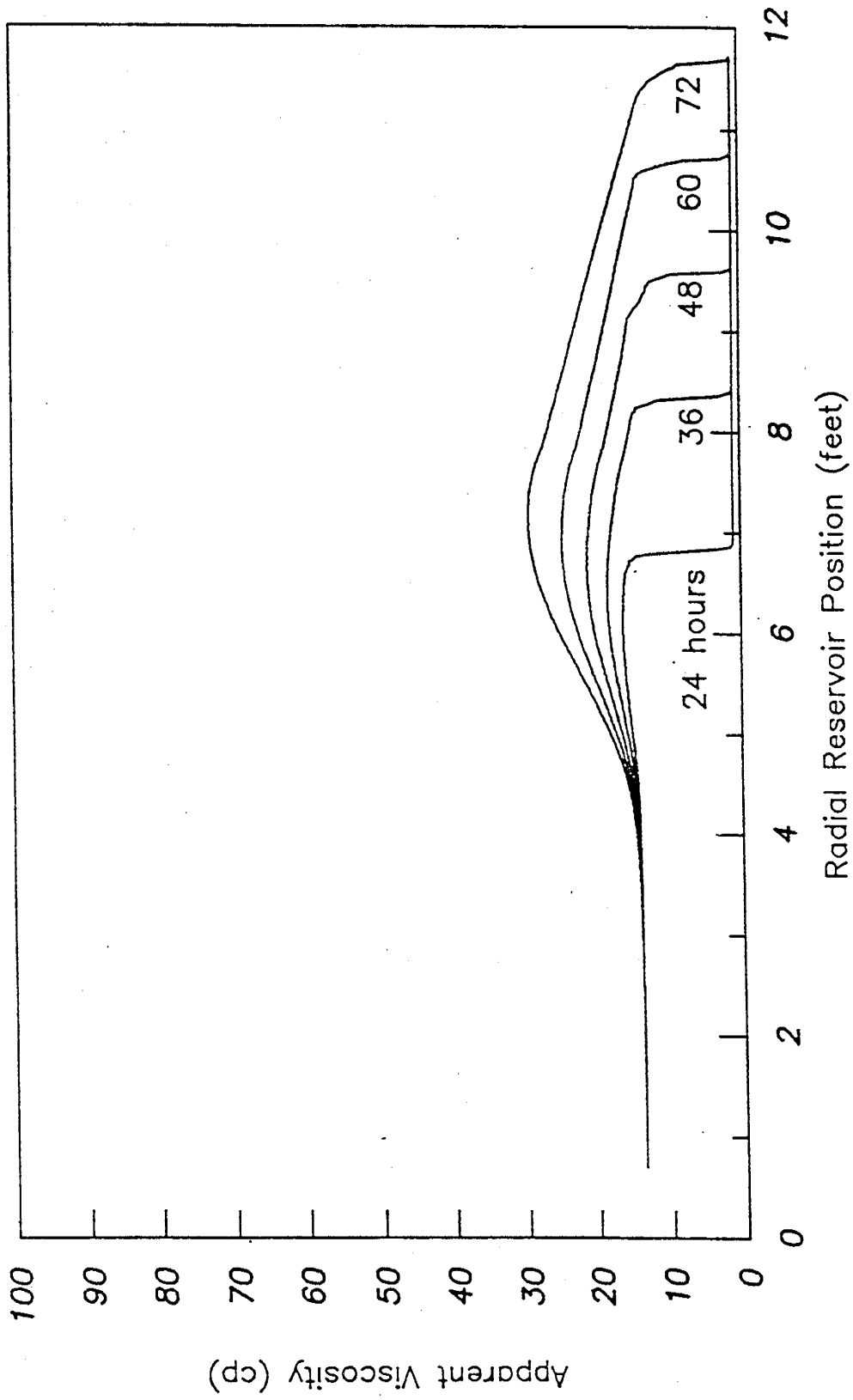


Figure 8.45 Simulated Gelation Run in Radial Geometry  
 (Case 2 : pH from 4.5 to 6.7)

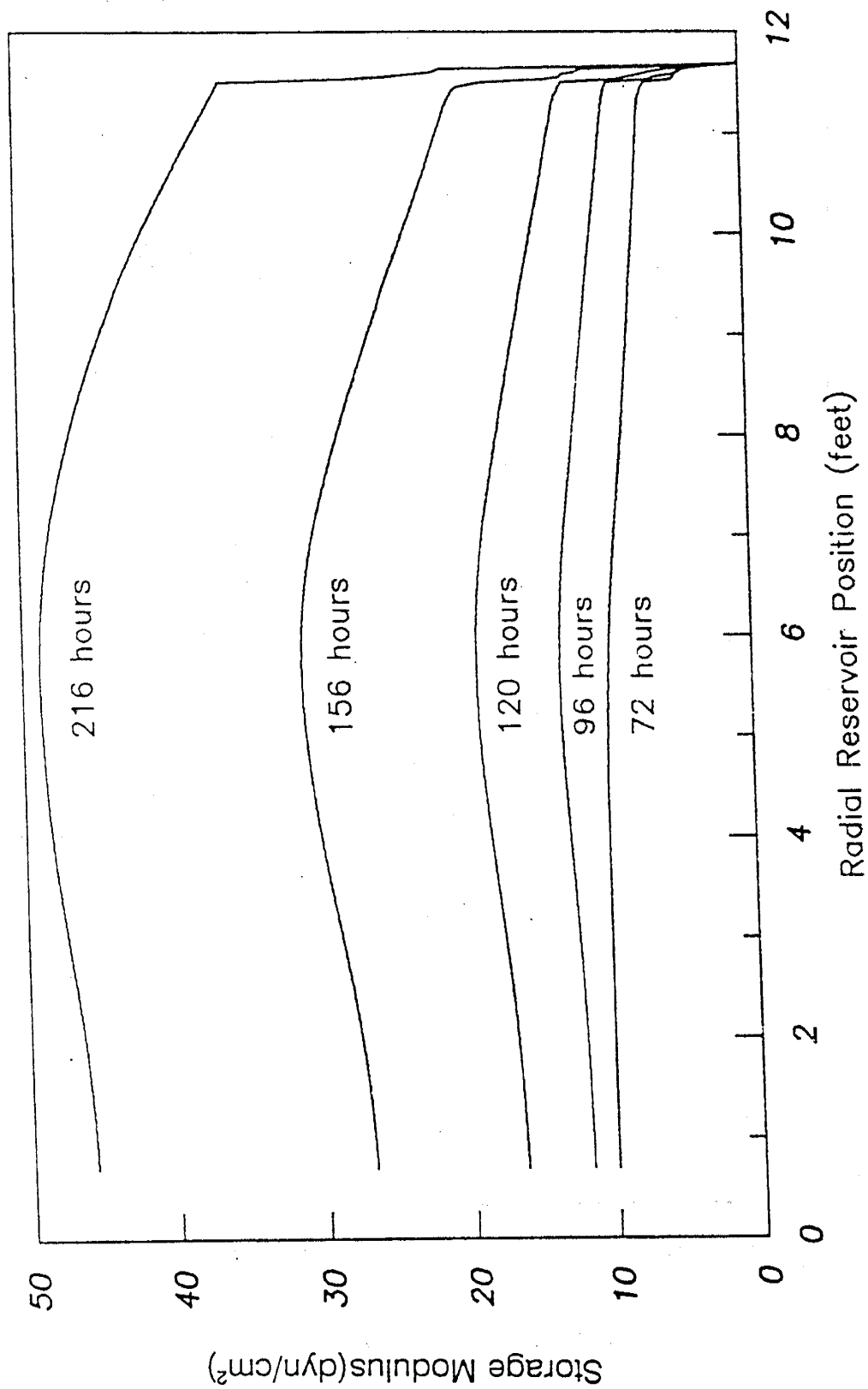


Figure 8.46 Storage Modulus Growth During the Shutin Period  
(Case 2 : pH from 4.5 to 6.7)

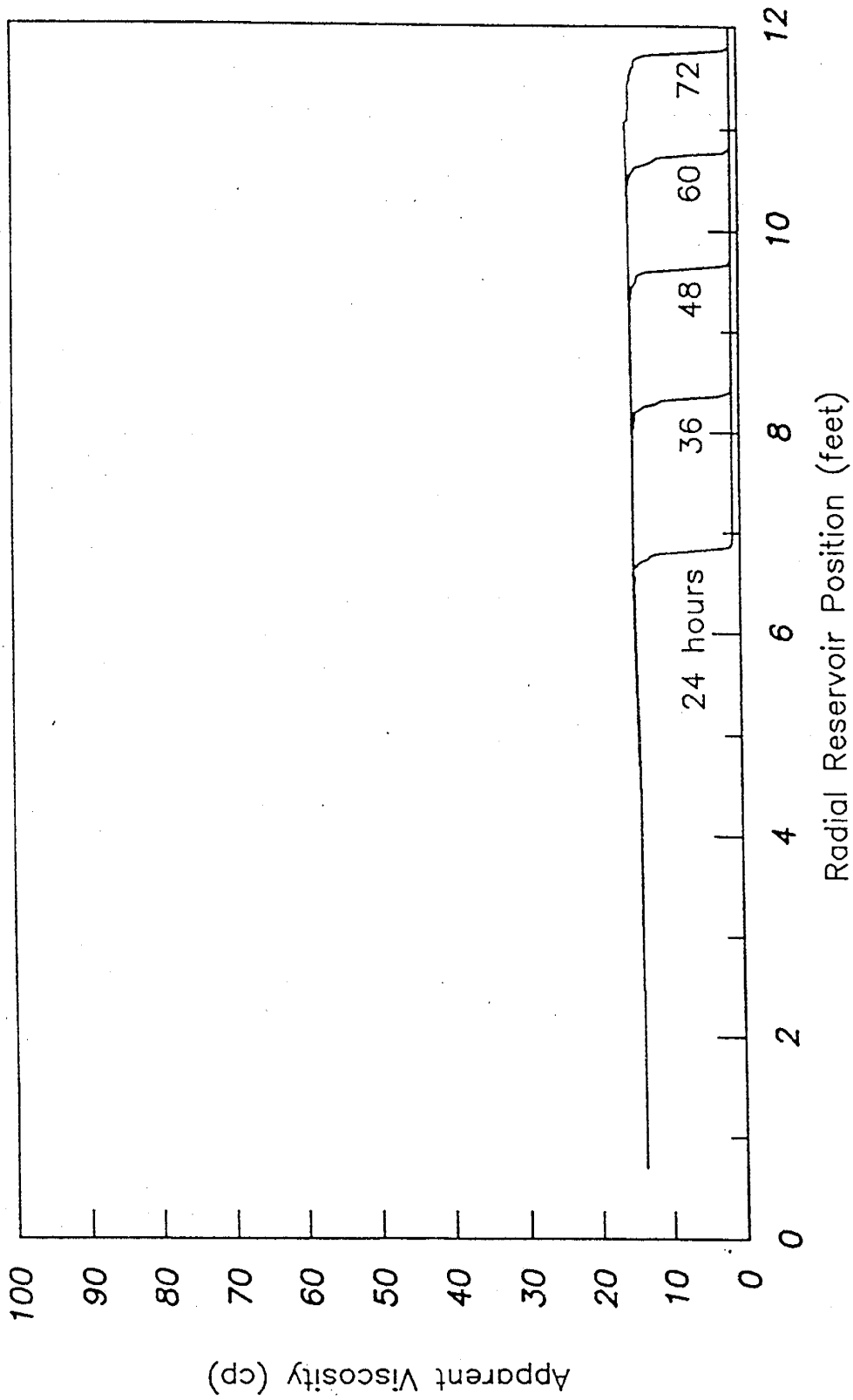


Figure 8.47 Simulated Gelation Run in Radial Geometry  
 (Case 3 : pH from 4.5 to 7.7)

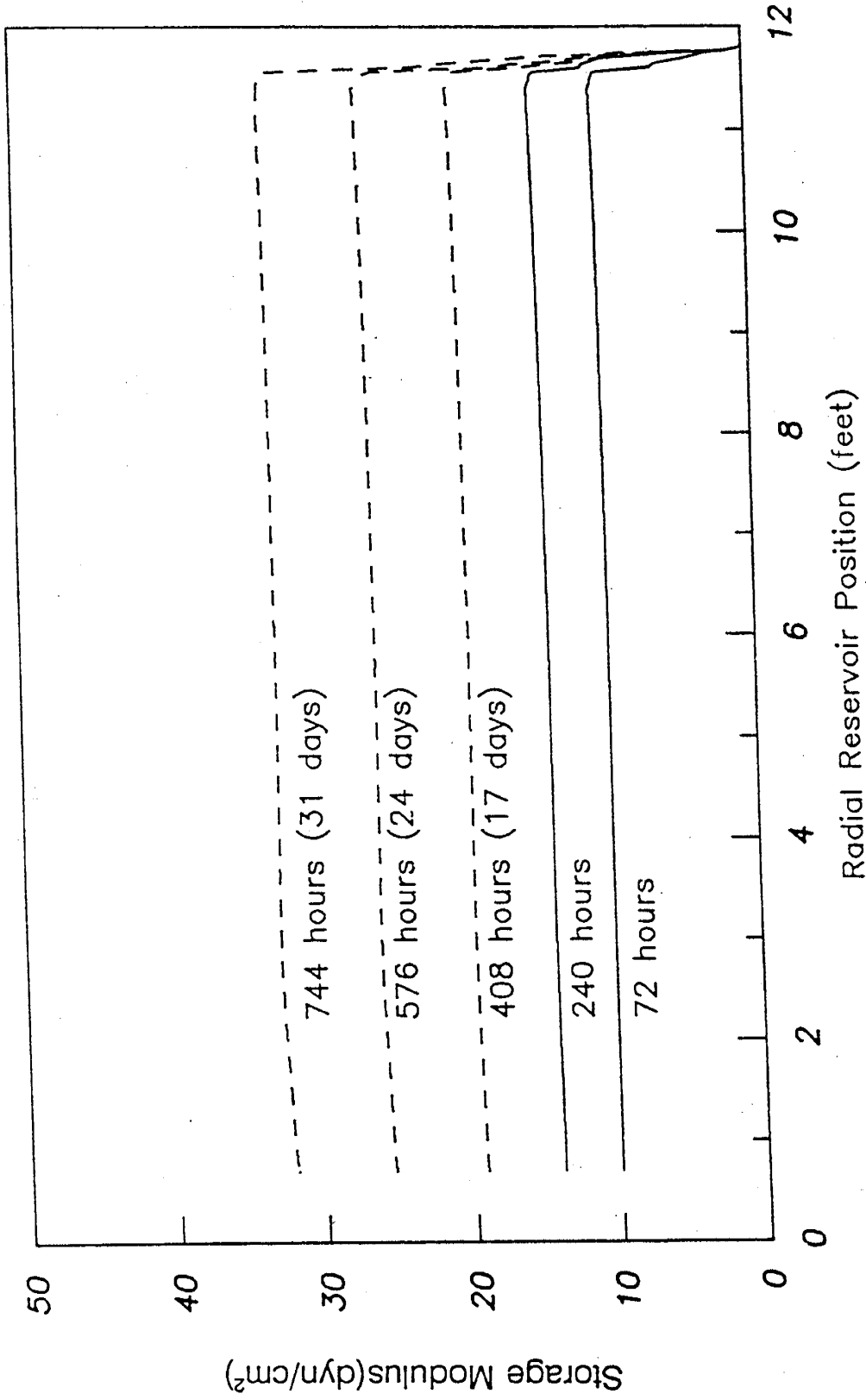


Figure 8.48 Storage Modulus Growth During the Shutin Period  
(Case 3 : pH from 4.5 to 7.7)

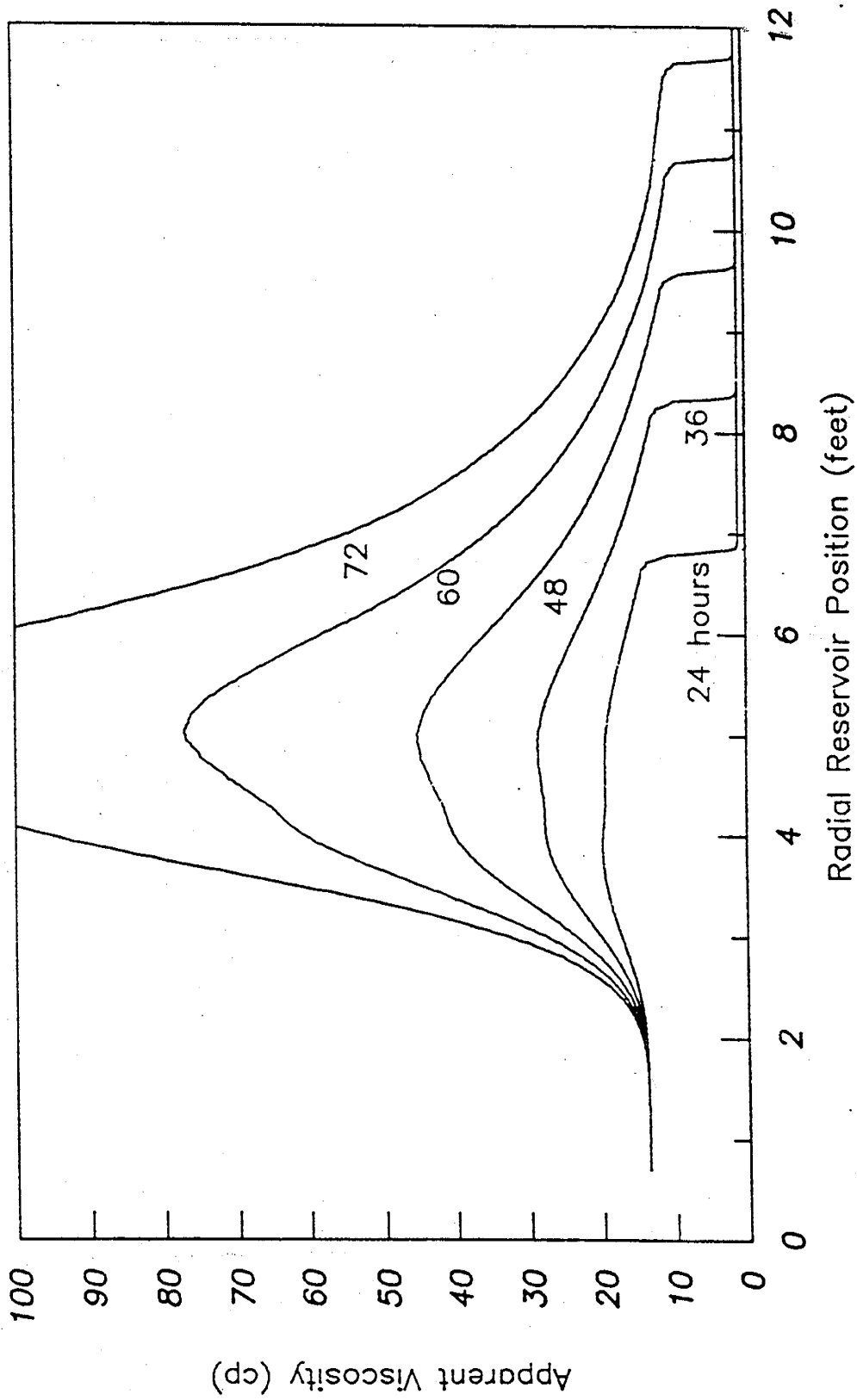


Figure 8.49 Simulated Gelation Run in Radial Geometry  
 (Case 4 : pH from 4.5 to 7.7, 15,000 ppm Thiourea)

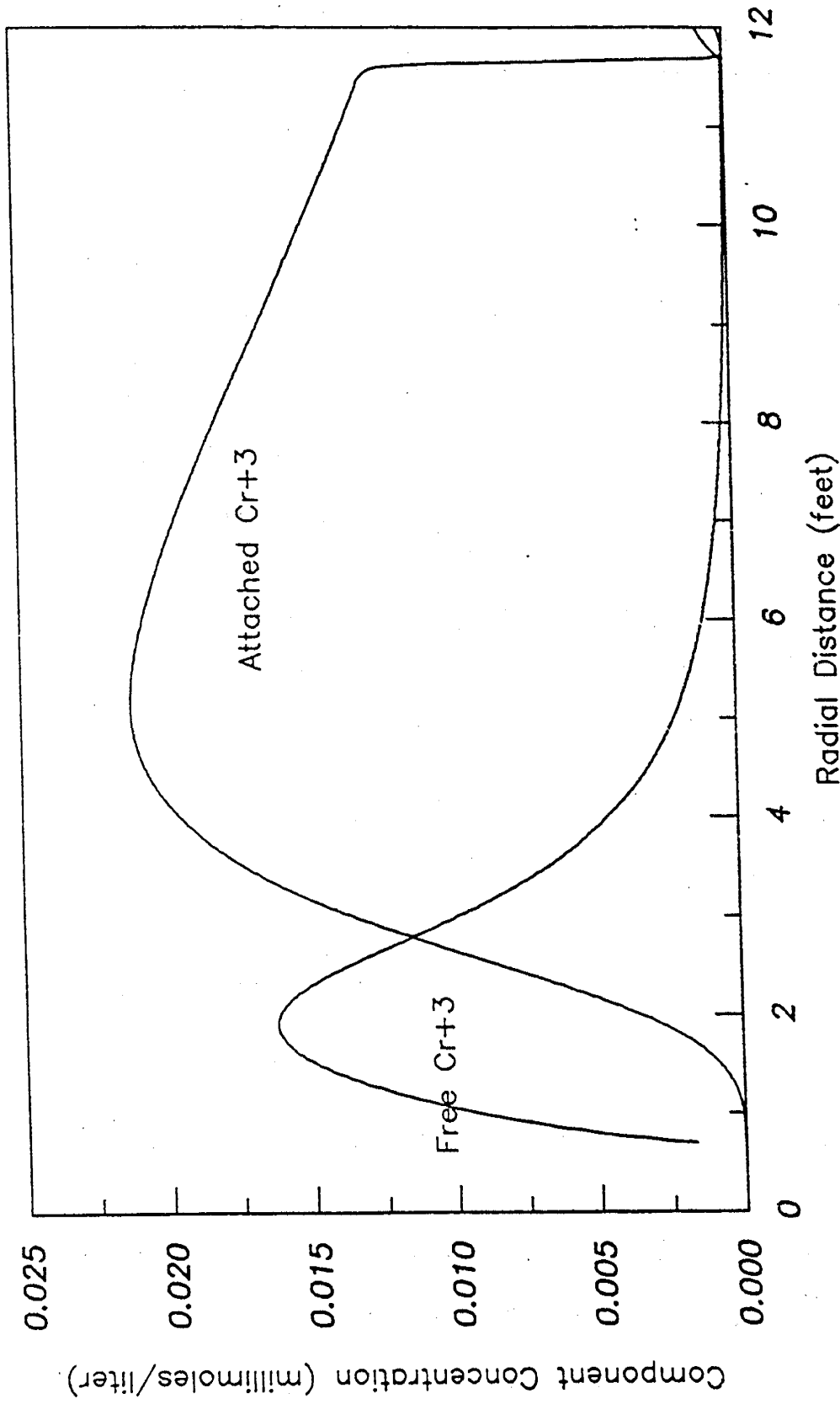


Figure 8.50 Concentrations of Attached and Ionic Cr<sup>+3</sup> after 72 Hours : Case 4

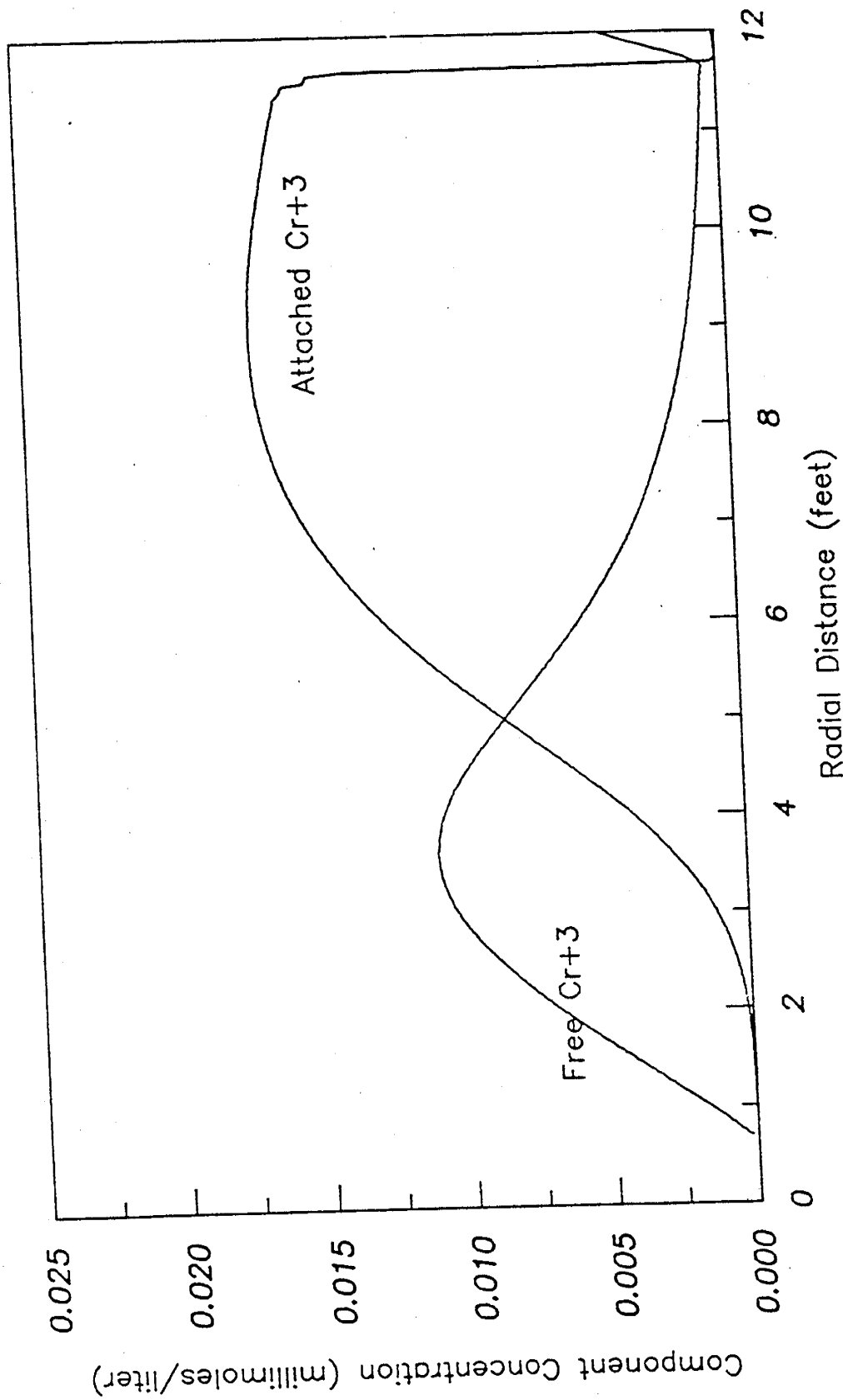


Figure 8.51 Concentrations of Attached and Ionic Cr<sup>+3</sup> after 72 Hours : Case 2

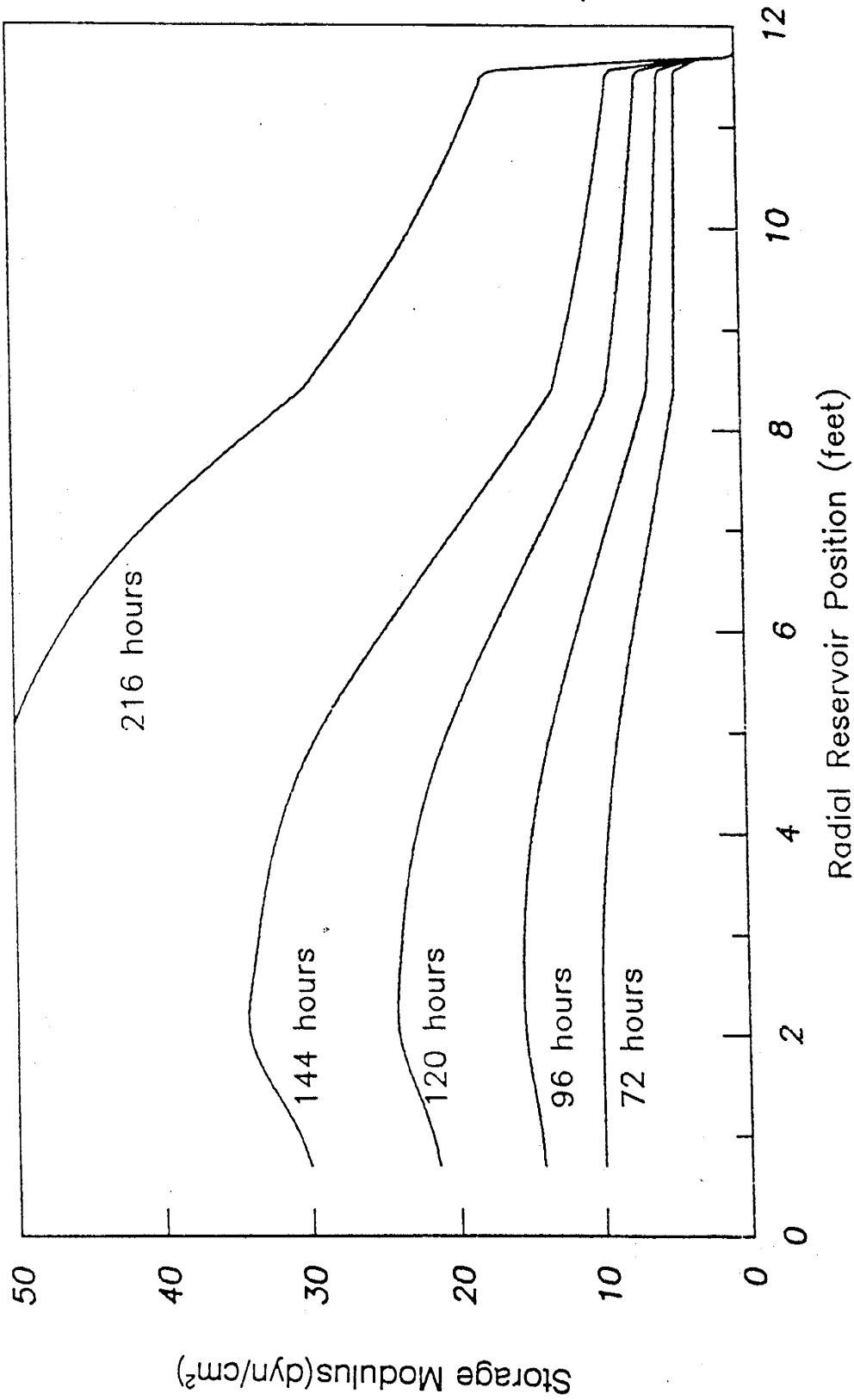


Figure 8.52 Storage Modulus Growth During the Shutin Period  
 (Case 4 : pH from 4.5 to 7.7, 15,000 ppm Thiourea)

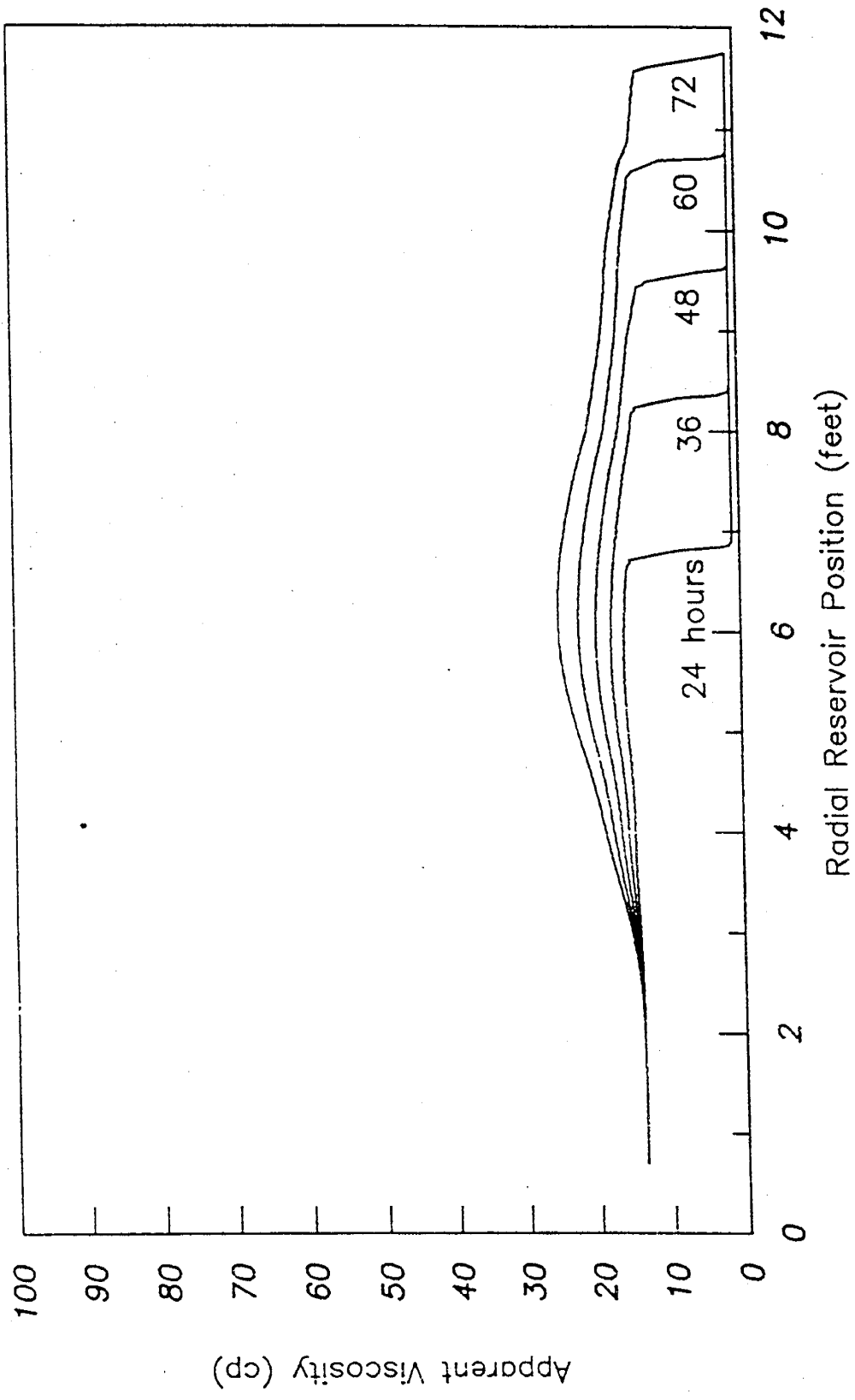


Figure 8.53 Simulated Gelation Run in Radial Geometry  
 (Case 5 : pH from 5.5 to 7.7, 15,000 ppm Thiourea)

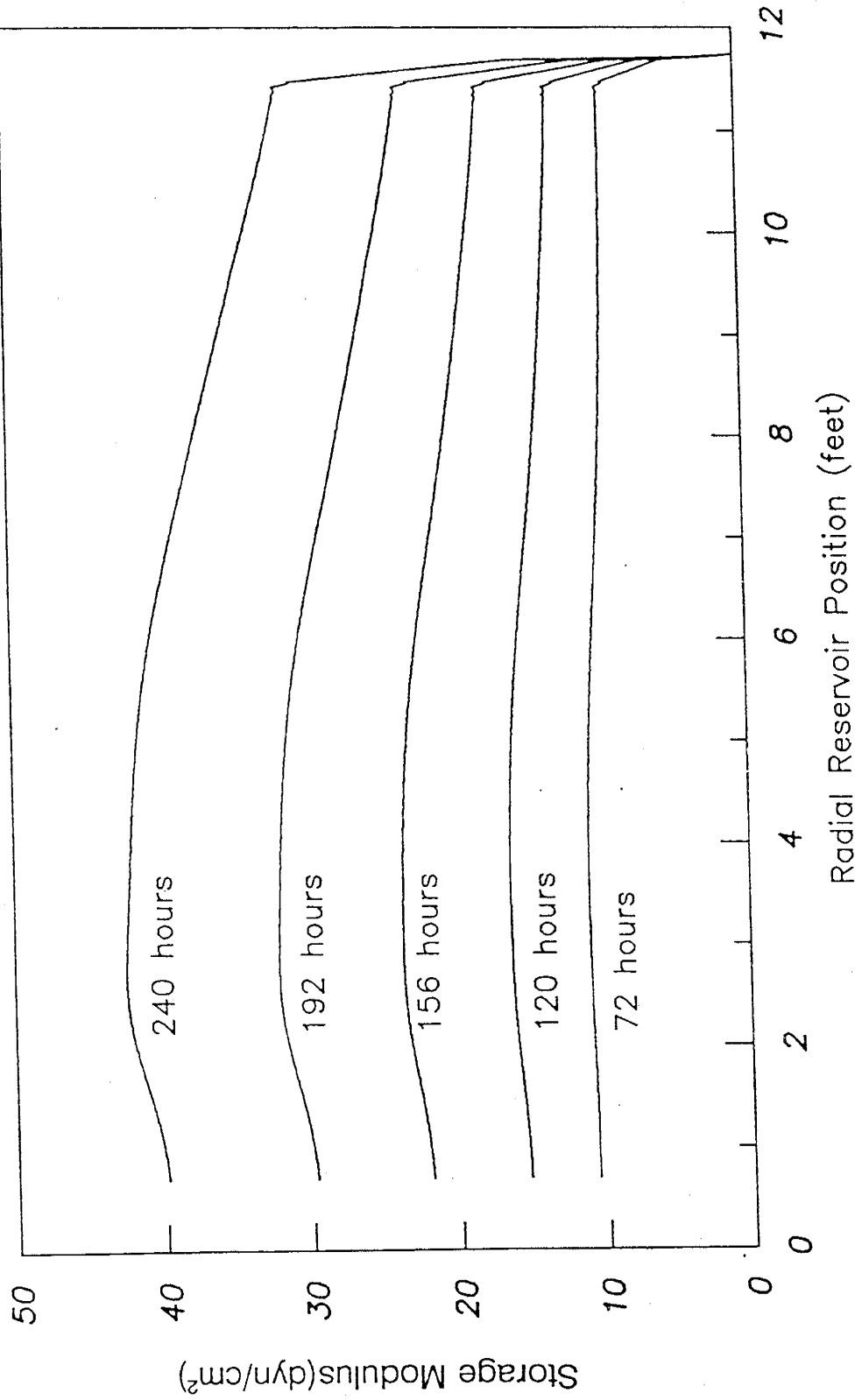


Figure 8.54 Storage Modulus Growth During the Shutin Period  
 (Case 5 : pH from 5.5 to 7.7, 15,000 ppm Thiourea)

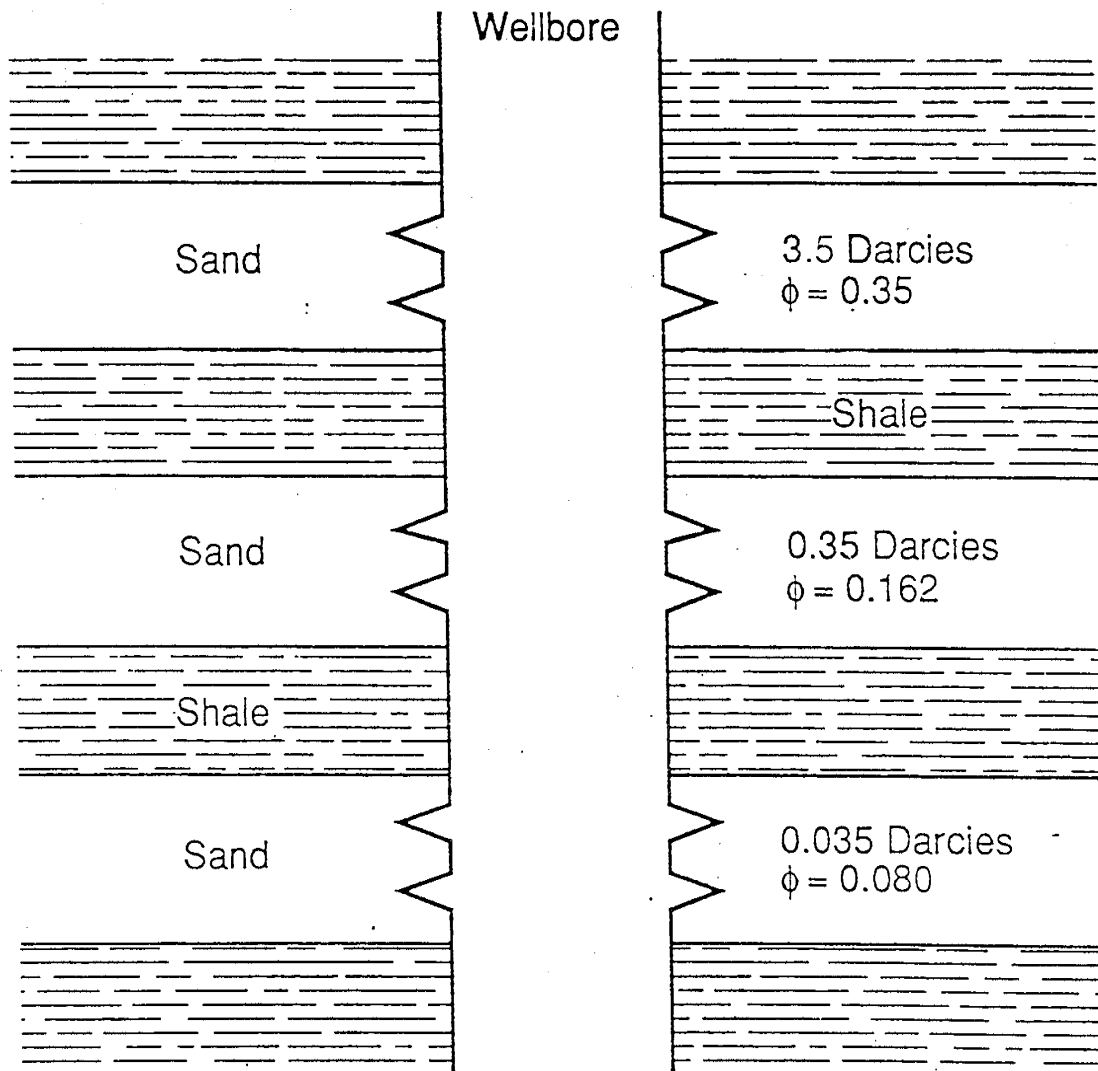


Figure 8.55 Water Injection Well in a Three-Layer Reservoir with Varying Permeability

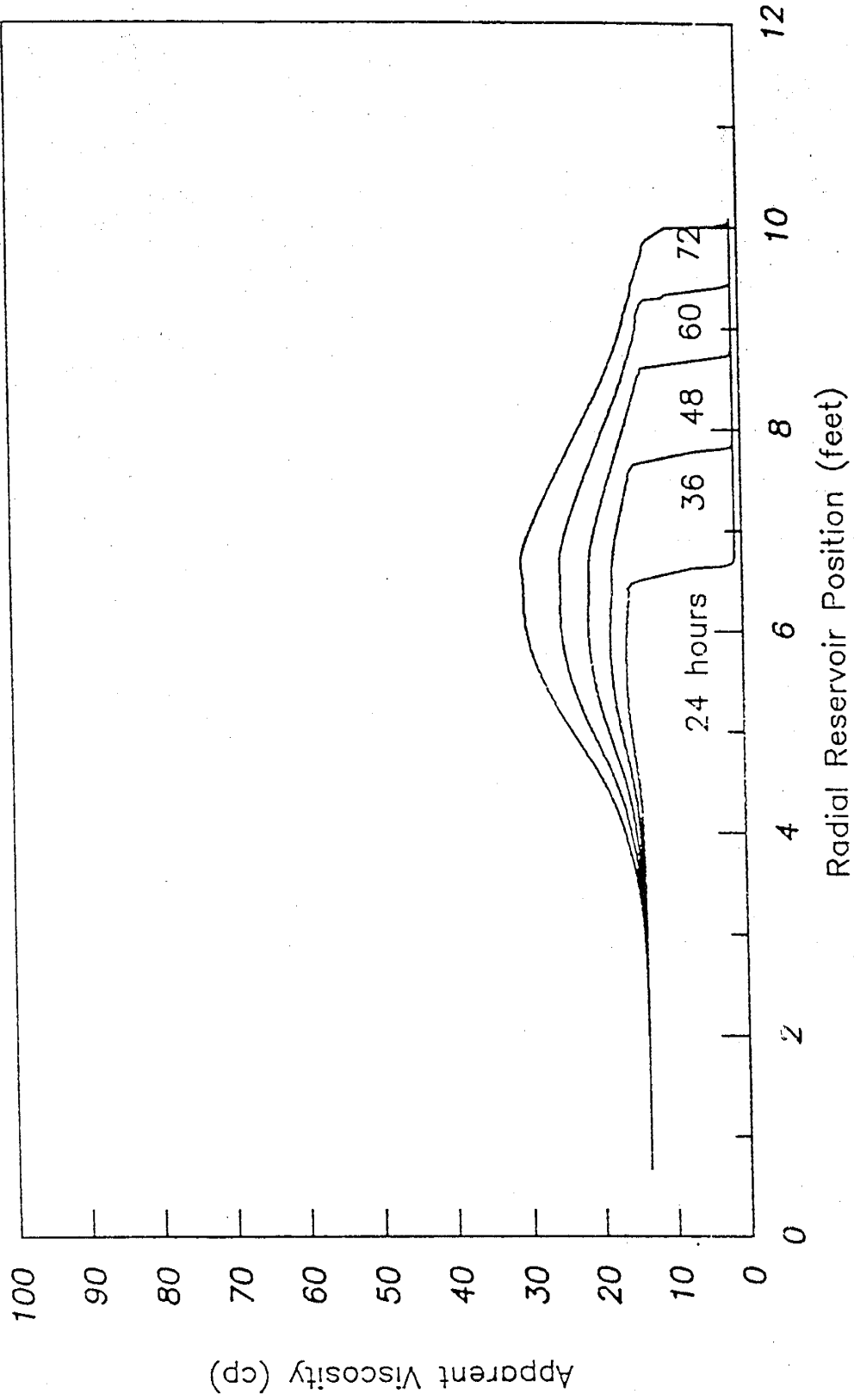


Figure 8.56 Simulated Displacement into a High Permeability Zone (3.5 Darcies) in Radial Geometry

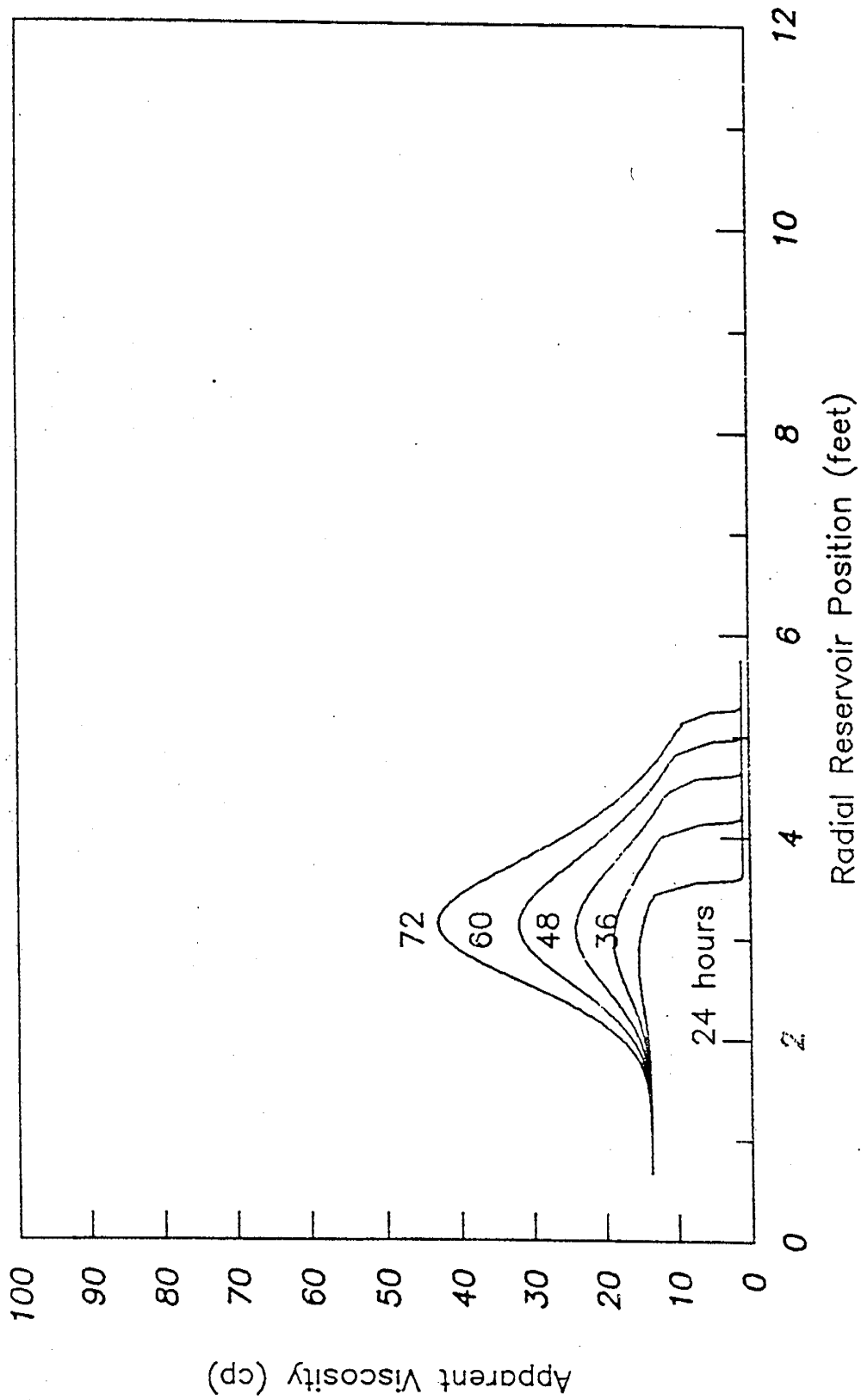


Figure 8.57 Simulated Displacement into a Medium Permeability Zone (0.35 Darcies) in Radial Geometry

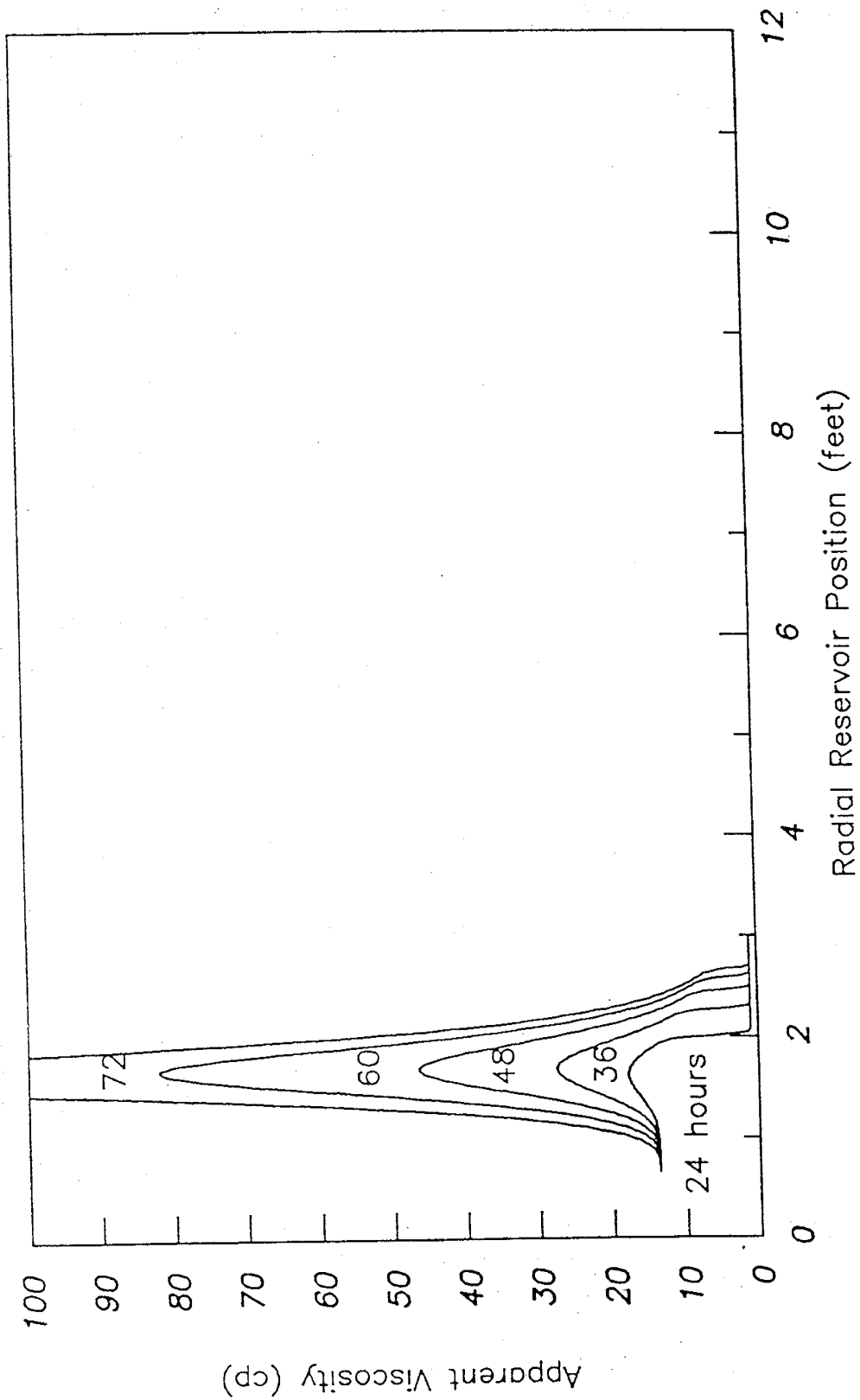


Figure 8.58 Simulated Displacement into a Low Permeability Zone (0.035 Darcies) in Radial Geometry